ESTIMATION OF PHOTOSYNTHETIC LIGHT-USE EFFICIENCY FROM AUTOMATED MULTI-ANGULAR SPECTRORADIOMETER MEASUREMENTS OF COASTAL DOUGLAS-FIR

by

Thomas Hilker

Dipl. Ing. (FH) University of Applied Sciences, Göttingen, 2000
M.Sc. University of Applied Sciences, Stuttgart, 2002

A THESIS SUBMITTED IN PARTIAL FULFILLMENT OF THE
REQUIREMENTS FOR THE DEGREE OF

DOCTOR OF PHILOSOPHY

in

THE FACULTY OF GRADUATE STUDIES

(Forestry)

THE UNIVERSITY OF BRITISH COLUMBIA

(Vancouver)

April 2008

ABSTRACT

Global modeling of gross primary production (GPP) is a critical component of climate change research. On local scales, GPP can be assessed from measuring CO_2 exchange above the plant canopy using tower-based eddy covariance (EC) systems. The limited footprint inherent to this method however, restricts observations to relatively few discrete areas making continuous predictions of global CO_2 fluxes difficult. Recently, the advent of high resolution optical remote sensing devices has offered new possibilities to address some of the scaling issues related to GPP using remote sensing. One key component for inferring GPP spectrally is the efficiency (ε) with which plants can use absorbed photosynthetically active radiation to produce biomass. While recent years have seen progress in measuring ε using the photochemical reflectance index (PRI), little is known about the temporal and spatial requirements for up-scaling these findings continuously throughout the landscape. Satellite observations of canopy reflectance are subject to view and illumination effects induced by the bi-directional reflectance distribution function (BRDF) which can confound the desired PRI signal. Further uncertainties include dependencies of PRI on canopy structure, understorey, species composition and leaf pigment concentration. The objective of this research was to investigate the effects of these factors on PRI to facilitate the modeling of GPP in a continuous fashion. Canopy spectra were sampled over a one-year period using an automated tower-based, multi-angular spectroradiometer platform (AMSPEC), designed to sample high spectral resolution data. The wide range of illumination and viewing geometries seen by the instrument permitted comprehensive modeling of the BRDF. Isolation of physiologically induced changes in PRI yielded a high correlation (r^2=0.82, p<0.05) to EC-measured ε, thereby demonstrating the capability of PRI to model ε throughout the year. The results were extrapolated to the landscape scale using airborne laser-scanning (light detection and ranging, LiDAR) and high correlations were found between remotely-sensed and EC-measured GPP (r^2>0.79, p<0.05). Permanently established tower-based canopy reflectance measurements are helpful for ongoing research aimed at up-scaling ε to landscape and global scales and facilitate a better understanding of physiological cycles of vegetation and serve as a calibration tool for broader band satellite observations.

TABLE OF CONTENTS

LIST OF TABLES

LIST OF FIGURES

ACKNOWLEDGEMENTS

This research was partly funded by a postgraduate scholarship of the German Academic exchange service (DAAD) to myself and a NSERC Discovery grant to N. Coops. Campbell River site flux tower measurements are partly funded by the Canadian Carbon Program through NSERC, BIOCAP Canada and CFCAS. The LiDAR data for this project were acquired by Prof. Benoît St-Onge (Université du Québec à Montréal) funded by NSERC and BIOCAP.

I would like to thank my committee, especially my supervisor Dr. Nicholas Coops for their support and helpful insights. I am especially grateful also to Dr. Andy Black, Zoran Nesic, Dominic Lessard, Rick Ketler, Andrew Sauter and Andrew Hum from UBC, Faculty of Land and Food Systems for their support and assistance in technical design, installation and maintenance of the radiometer platform.

Very special thanks to Dr. Forrest Hall (NASA Goddard Space Flight Center, MD, USA) for many helpful discussions and suggestions, and to Drs. E.M. Middleton, K.F Huemmrich (all NASA, GSFC) Dr. Piers Sellers (NASA, Johnson Space Center, TX, USA) and H.A. Margolis (Université Laval, Quebéc) for their valuable insights and comments. I would also like to thank Dr. John A. Gamon, Dr. Lee Vierling and the SpecNet community for fruitful discussions.

Finally, I would like to thank my wife Marike for her support and understanding throughout the last three years.

DEDICATION

To Marike

CO-AUTHORSHIP STATEMENT

This thesis consists of six scientific papers of which I am the lead author. The initial project overview was proposed by my supervisor, Dr. Nicholas Coops. Technical help was provided for design, construction, setup and maintenance of the described radiometer platform by Dr. Andy Black's group from the Faculty of Land and Food Sytems, UBC, which also provided the biometeorological data for this research. For the scientific journal submissions, I performed all the research, data analyses, and interpretation of the results, and prepared the final manuscripts. Co-authors provided advice on methodology and made editorial comments as required.

1 INTRODUCTION

1.1 The role of carbon in terrestrial ecosystems

Although carbon represents only a small fraction the atmosphere (approximately 0.04%), it is an essential part of life on the Earth as it plays an important role in the structure, biochemistry, and nutrition of all living cells. The exchange of carbon between biosphere, hydrosphere, geosphere and atmosphere is described as the global carbon cycle. In terrestrial ecosystems, forests are one of the most important factors driving carbon cycling (Bolin and Fung, 1992). Covering less than 35% of the Earth's land surface, forests contain more than 80% of the global biomass, storing approximately 500 Gt of carbon (Janzen, 2004). Forest ecosystems sequester CO_2 through the biochemical process of photosynthesis, also known as primary production, defined as the production of biological organic compounds from inorganic materials. Three different types of primary production can be distinguished (Rast, 2001):

- Gross primary production (GPP) refers to the overall rate of fixation of carbon through photosynthesis and quantifies the amount of biomass produced within an ecosystem over a unit of time, regardless of the amount of respiration. This value is also referred to as gross ecosystem production (GEP) or photosynthesis.
- Net primary production (NPP) describes the amount of carbon uptake by an ecosystem after its autotrophic respiration has been discounted.
- Net ecosystem production (NEP) represents the actual rate of accumulation of carbon in the terrestrial biosphere after autotrophic and heterotrophic respiration have been discounted.

Changes in growth and distribution of forests are likely to have a significant impact on atmospheric carbon budgets, because (1) deforestation releases large amounts of carbon into the atmosphere, and (2) changes in climate, for instance through global warming, can alter growth and distribution of trees thereby influencing the amount of carbon being released into or absorbed from the atmosphere (Müller et al., 2007). Studying the interactions between climate and primary production is therefore a key goal of climate change research seeking to improve the understanding of the global dynamics of carbon fluxes between biosphere and atmosphere to quantify potential changes due to increased atmospheric CO_2 concentrations (Comins and McMurtrie 1993, Luo and Reynolds 1999).

1.2 Approaches for monitoring primary production globally

1.2.1 The eddy covariance technique

Among the most commonly applied methods for measuring primary production is the eddy covariance (EC) technique determining NEP from tower measured CO_2 fluxes based on the covariance between fluctuations in vertical wind velocity and CO_2 mixing ratio (Baldocchi, 2003). This can be expressed as

$$F_C = \overline{\rho_a}\,\overline{w's_c'} \qquad (1)$$

where F_c is the carbon flux density, commonly referred to as flux, $\overline{\rho_a}$ is the mean molar density of dry air and $\overline{w's_c'}$ is the covariance between the vertical wind velocity (w) and the mole-mixing ratio of CO_2 (s_c) defined as $s_c = \rho_c/\rho_a$ with ρ_c being the CO_2 density. The prime indicates fluctuations from the average; the overbar indicates that data are being averaged over a certain time interval, usually 30 minutes. While this measurement technique is capable of providing accurate and continuous estimates of ecosystem level NEP (Wofsy et al., 1993, Baldocchi et al., 2001), the area or footprint that can be sampled with EC measurements (also known as the flux footprint) is usually restricted to a few hectares, depending on the height of the flux measurement, terrain, stand height and density (Schmid and Lloyd, 1999, Kljun et al., 2004). Furthermore, EC theory assumes that the environmental conditions are steady within the area observed with the underlying vegetation extending in upwind direction for at least the footprint radius (Baldocchi, 2003). Violation of these assumptions can cause systematic errors in the interpretation of EC measurements (Baldocchi et al., 1988, Foken and Wichura, 1996, Massman and Lee, 2002), which magnify when estimates of NEP are integrated over time (Moncrieff et al., 1996).

In order to characterize NEP for different ecosystems, national and worldwide EC-flux networks have been formed over recent years with the ultimate goal of facilitating the modeling of primary production globally. One such program, established as a nationwide network for Canada is the Canadian Carbon Program (CCP) (previously Fluxnet Canada), consisting of permanent observational flux towers along an east-west national transect, encompassing Canada's most important eco-regions (CCP, 2008). The primary objective of the network is to facilitate continuous, multi-year measurements of CO_2, water, heat fluxes, and in some cases other greenhouse gases, for mature and disturbed forest, and peatland ecosystems thereby providing parameters for ecosystem process and climate models.

1.2.2 Remote sensing

While EC measurements and flux tower networks have greatly improved our understanding of carbon cycling over recent years, tower-based estimates of primary production are restricted to relatively few spatially discrete observations, with major difficulties remaining in extrapolating these measurements across the continuous landscape (Chen et al., 2003, Reichstein et al., 2006). As a complement to the EC technique, satellite-based remote sensing provides spatially continuous observations of the land surface, thereby holding promise to overcome some of the scaling issues related to EC data by predicting plant productivity, in particular GPP, globally and in a continuous mode from space. Broadly defined as the "science and art of obtaining useful information about an object, area or phenomenon through the analysis of data acquired by a device that is not in contact with the object, area, or phenomenon under investigation" (Lillesand and Kiefer, 1979, p1), remote sensing is a key tool for determining and classifying various kinds of vegetation properties such as leaf pigment concentrations (Zarco-Tejada et al., 2002), bio-chemical components (Curran et al., 1989, 2001, Smith et al., 2002), and foliage biomass (Coops et al., 1998). Typically operating in a spectral range of about 400-2500 nm wavelengths, remote sensing of plant physiology is based on the understanding that plant physiological properties are related to the biochemical composition of plant foliage and that this biochemical composition is expressed in the spectral reflectance properties of leaves. For instance, different chemical and structural components are related to distinctive spectral regions of the electromagnetic spectrum (Curran et al., 1989) (Figure 1.1), often in the range of only a few nanometers (Datt et al., 1998, Sims and Gamon, 2002, Gamon et al., 2003) and can be detected using high spectral resolution optical remote sensing instrumentation.

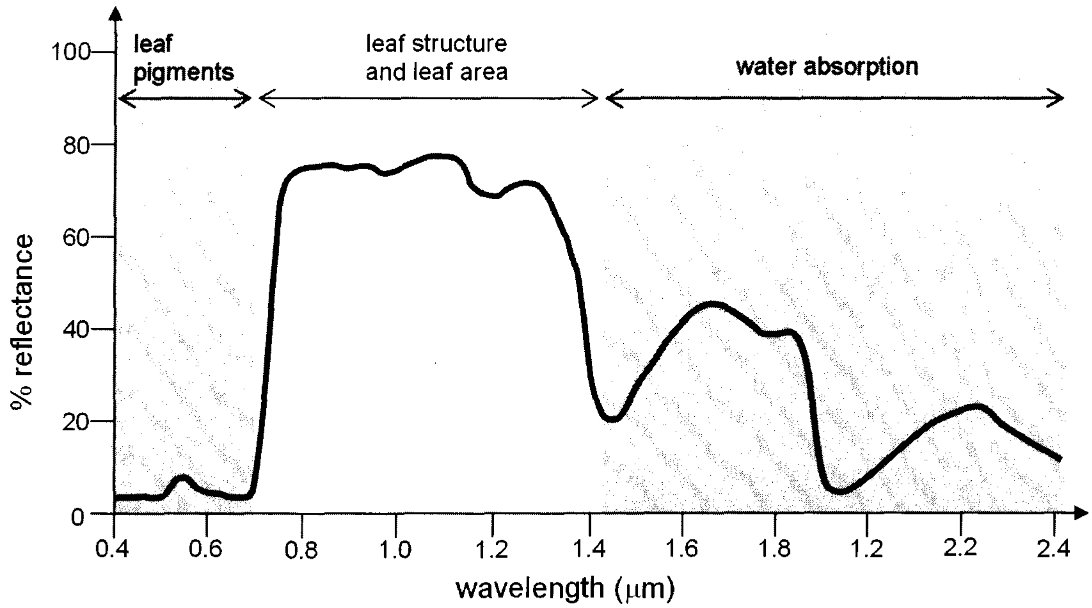

Figure 1.1: Typical spectrum of healthy vegetation with key absorption bands indicated. Figure adapted from Rast, 2001.

Remote sensing based models of primary production often express GPP as (Monteith, 1972, 1977).

$$GPP = PAR \cdot f_{par} \cdot \varepsilon \qquad (2)$$

where PAR is the incident photosynthetically active radiation that can be utilized by plants for the production of biomass (Rast, 2001). The range of PAR coincides with that of the visible light (400-700 nm). During photosynthesis, leaf pigments, such as chlorophylls and carotenoids absorb a fraction of PAR, f_{par}, which is used to procure chemical energy to fix carbon dioxide into carbohydrates and other organic compounds. The magnitude of f_{par} depends on size, density, structure and chemical composition of the canopy, but is also a function of solar position and predominant radiation conditions (i.e. ratio of direct to diffuse radiation) (Daughtry 1983, Myneni and Williams, 1994). Finally, photosynthesis also depends on ε, the efficiency with which the absorbed radiation energy can be utilized for the production of biomass (Monteith 1972, 1977). This light-use efficiency reflects the availability of resources, other than light, required for the photosynthetic reaction: The absorption of photons by leaf pigments, during the first stage of photosynthesis, known as light reactions, releases electrons into an electron transport chain, and these electrons are ultimately used to provide chemical energy in the form of the energy carrier NADPH[1] for the fixation of carbon through a second, light-independent set of reactions. During this light independent reaction, the enzyme RuBisCO[2] captures CO_2 from the atmosphere and three-carbon sugar phosphates are produced, which are then combined with water and CO_2 to form sucrose and starch. Shortage of water, CO_2 (whose availability is determined through stomata opening), or nutrients required to support the formation of the required chemical compounds will limit the photochemical reaction process, resulting in an accumulation of hydrogen ions in the thylakoid space.

To balance absorption of light quanta, and utilization of NADPH, plants regulate the amount of procured energy through a biochemical mechanism called photoprotection to prevent excessive energy levels from causing photo-oxidative damage in leaves (Demmig-Adams, 1990). Accumulation of hydrogen ions in the thylakoid space results in a lowering of its pH-value (Krause and Weis 1991), which induces the rapid epoxidation of a group of leaf pigments called xanthophylls from violaxanthin via intermediate

[1] Nicotinamide adenine dinucleotide phosphate (reduced form)
[2] Ribulose-1,5-bisphosphate carboxylase/oxygenase

antheraxanthin to zeaxanthin (Demmig Adams and Adams, 1996, 2003). Both antheraxanthin and zeaxanthin have photoprotective structures, capable of safely dissipating excessive energy as heat. The reaction is reversed under lower light conditions.

Remotely-sensed inputs of PAR are typically retrieved from top of the atmosphere solar radiance, and modelled as a fraction of the reflected shortwave radiation (Pinker and Ewing, 1985, Sellers et al., 1995, Running et al., 1999), with more recent approaches incorporating the temporal and spatial variability with respect to changing atmospheric conditions. The fraction of absorbed PAR is commonly described using its empirical relationship to the top of the canopy reflectance in the visible and near infrared region (Tucker 1979, Daughtry et al., 1983, Asrar et al., 1984, Sellers, 1985, 1987), generalized to the global scale using radiative transfer models (see Chapter 2 for details).

The most challenging parameter to be determined at a global scale is ε (Running et al., 2004), which in existing GPP models, is often expressed as a biome-specific constant, adjusted through a few globally measurable meteorological variables representing canopy stresses. Numerous studies have highlighted the limitations of this approach, which often fails to adequately describe the spatial and temporal heterogeneity in ε (Turner et al., 2003, 2005, Running et al., 2004, Heinsch et al., 2006, Zhao et al., 2006). More recently, remote sensing research has focused on improving global estimates of GPP by sensing ε from a narrow waveband spectral reflectance feature at the 531nm region (Gamon et al., 1990, 1992, 1993), which is directly related to the xanthophyll pigment conversion induced by photoprotection (Gamon et al., 1990, 1992). While remote sensing of ε holds promise to improve global modeling of GPP significantly, the observed reflectance change is relatively small and therefore difficult to extract in the presence of other factors that can cause variations in spectral reflectance of similar or larger magnitudes (Hall et al., 2008). To reduce the impact of extraneous variations, Gamon et al. (1992, 1993) developed the photochemical reflectance index (PRI), comparing the normalized difference reflectance between the absorption feature at 531 nm (ρ_{531}) and a xanthophyll insensitive reference band at 570 nm (ρ_{570}).

$$PRI = \frac{\rho_{531} - \rho_{570}}{\rho_{531} + \rho_{570}} \tag{3}$$

Originally established for sunflower leaves, an empirical relationship between PRI and ε has since been confirmed over a wide range of species (Peñuelas et al., 1994, 1995, Filella et al., 1996, Gamon and Surfus, 1999). Generalization of this relationship through space and time, however, remains difficult (Barton and North, 2001, Rahman et al., 2001, 2004).

In the temporal domain, challenges are faced by the high variability of ε requiring observations with high temporal resolution, currently achievable only using permanently established ground based instrumentation or geostationary satellites. Additionally, PRI is sensitive to a number of biochemical changes in leaves such as the ratio of chlorophylls to carotenoids, also known as the pigment pool size (Barton and North, 2001), or leaf senescence, which do not necessarily affect ε in the same way as PRI. Finally, spectral reflectance in the PRI wavebands changes also with atmospheric radiation conditions, which, while likely to also affect ε in some way, interfere with the measured xanthophyll related reflectance change at 531 nm. In the spatial domain, PRI is highly sensitive to the view angle, sun geometry, soil background reflectance, leaf angle distribution (at larger view angles), leaf area (Barton and North, 2001), the canopy structure driving shading between and within tree crowns, and species composition. As a result of these difficulties in separating the xanthophyll related reflectance signal from extraneous factors causing variations in PRI reflectance, determination of ε in a spatially and temporally continuous mode from spectral reflectance is a highly complex process which has not yet been satisfactorily developed (Huemmrich et al., 2005).

1.3 Approach and objectives

A possible way of improving the understanding of the relationship between stand level PRI and ε is comparing continuously acquired spectral reflectance data obtained from tower-based measurements with ε acquired from EC measurements at an existing flux-tower site. Eddy covariance and micro-meteorological data allow determination of ε from incoming and absorbed PAR, NEP, and ecosystem respiration using equation (2) and therefore provide a second, independent measurement method. At the same time, both approaches are sampling approximately the same area, or "footprint", thereby minimizing scaling effects. The eddy covariance flux footprint is variable and depends on atmospheric stability, windspeed and measurement height above the canopy (Leclerc and Thurtell, 1990); most daytime measurements, however, originate from a radius of up to 150 m (Blanken et al., 2001, Kljun et al., 2004, Chen et al., 2007a,b) around the tower. The footprint for spectral measurements is stable and depends on setup and instantaneous field of view of the remote sensing instrumentation.

Investigation of plant physiological processes at the stand level requires consideration of multiple viewing geometries, as temporal dynamics require study of diurnal as well as seasonal patterns, and full assessment of stand level photosynthesis from spectral reflectance requires careful observation of leaves, branches, structures, gaps, and understorey to understand how reflectance depends on viewing and illumination geometry (Asner, 1998). Multi-angular observations provide a means to characterize the anisotropy of surface reflectance (Chen et al., 2005), which has been shown to contain information on the structure of vegetated surfaces and shaded parts of the canopy (Chen et al., 2003, Gao and Schaaf, 2003). A multi-angular platform sampling spectra under different view and sun-angles will allow investigating the geometric effects on canopy reflectance thereby facilitating observations of the dependencies between changes in canopy spectra, sun-observer geometry, canopy structure, and shading effects of the canopy. Micro-meteorological data can help to identify stress factors and explain some of the temporal variability observed in canopy spectra throughout the observation period.

A critical component for determining ε from canopy level PRI is the canopy structure, as it not only alters the reflected signal by physically changing its strength (Rahman, 2001, Barton and North, 2001), but also drives the photosynthetic output of individual leaves through its effect on canopy light transmittance (Forseth and Norman, 1991). The capacity of passive remote sensing to quantify structure is limited, since remotely-sensed reflectance largely originates from the top of the canopy, while the contributions of shaded leaves lower in the canopy are harder to quantify (Hall et al., 1992, Chen et al., 2003, Gao et al., 2003). Further, optical remote sensing measures are typically asymptotic with respect to vertically distributed structural attributes such as leaf area, volume, or biomass (Wulder, 1998). Detailed information of the canopy structure can, however, be obtained from airborne laser scanning, or light detection and ranging (LiDAR), an active remote sensing technique, which determines distances to an object or surface using laser pulses. These laser pulses, being emitted from an airborne sensor, are reflected from either the terrain or objects on the terrain (such as trees), thereby allowing measurement of the distance between source and reflector by the time the light beam travels from the sensor to the reflector and back. This technique yields detailed information of the three-dimensional distribution of vegetation canopy components as well as sub-canopy topography, thereby providing high spatial resolution topographic elevation, and accurate estimates of vegetation height, cover density, and other aspects of canopy structure (Lefsky et al., 2005, Coops et al., 2007) with measurement errors typically in the order of less than 1.0 m (Persson et al., 2002, Næsset 1997, 2002, Magnussen and Boudewyn 1998, Næsset and Økland 2002).

The objective of this dissertation was to investigate the factors driving PRI reflectance throughout the year at the stand level from high spectral, spatial and temporal resolution tower-based reflectance measurements of a Douglas-fir (*Pseudotsuga menziesii* var *menziesii* (Mirb.) Franco) dominated forest stand. The goal was to separate these factors from reflectance changes induced by changes in canopy light-use efficiency thereby facilitating year-round direct measurements of ε, and modeling of stand and landscape level GPP using remotely-sensed inputs. First, the current status of modeling GPP from remote sensing is reviewed from existing literature and a discussion of future requirements is undertaken, based on the results of plot scaled field studies, large field experiments and theoretical work (Hilker et al., 2007a, Chapter 2). Second, the stress factors driving ε at the research site are identified using micro-meteorological measurements and eddy-covariance-based data of CO_2 and heat fluxes in combination with LiDAR-modelled fractions of canopy shading (Hilker et al., 2008a, Chapter 3). A non-parametric data mining approach is used to identify the impact of each stress factor over half hourly, daily, and weekly time scales. In a third step, a radiometer platform is developed to facilitate year round observation of canopy reflectance with high spatial, spectral, and temporal resolution (Hilker et al., 2007b, Chapter 4). The platform developed features a motor-driven probe for automated measurements of canopy spectra under a large variety of view and sun angles. In a fourth step, spectral data are then collected over a one-year period and are used to separate the physiologically-induced changes in canopy reflectance from those originating from other factors by modeling the bi-directional reflectance distribution function (BRDF) (Hilker et al., 2008b, Chapter 5). A simple classification approach is used to stratify spectra into homogeneous subsets of observations with respect to both sky conditions and physiological canopy status and BRDF models are subsequently fitted to each stratum. This method allows tracking of ε continuously throughout the year from remotely-sensed inputs. In a fifth step, an approach to model GPP is developed from remote sensing and tower-measured findings are extrapolated vertically and horizontally throughout the canopy using airborne LiDAR data (Hilker et al., 2008c, Chapter 6). Remotely-sensed estimates of GPP are verified using eddy covariance data and a footprint model is used to adjust the spatial scales of both systems. Finally, spectrally derived estimates of ε are compared to the currently common approach, which is modeling ε as a biome specific constant, constrained by a few globally-measured meteorological variables, and the potential and benefits of sensing

ε directly from spectral reflectance are assessed over a one-year time span (Hilker et al., 2008d, Chapter 7).

1.4 References

Asner, G. (1998) Biophysical and Biochemical Sources of Variability in Canopy Reflectance. *Remote Sensing of Environment* **64**,

Asner, G.P. and Warner, A.S. (2003) Canopy Shadow in Ikonos Satellite Observations of Tropical Forests and Savannas. *Remote Sensing of Environment* **87**, 521-533.

Asner, G.P., Bateson, C.A., Privette, J.L., El Saleous, N. and Wessman, C.A. (1998) Estimating Vegetation Structural Effects on Carbon Uptake Using Satellite Data Fusion and Inverse Modeling. *Journal of Geophysical Research-Atmospheres* **103**, 28839-28853.

Asrar, G., Fuchs, M., Kanemasu, E.T. and Hatfield, J.L. (1984) Estimating Absorbed Photosynthetic Radiation and Leaf-Area Index From Spectral Reflectance in Wheat. *Agronomy Journal* **76**, 300-306.

Baldocchi, D. (1988) A Multi-Layer Model for Estimating Sulfur-Dioxide Deposition to a Deciduous Oak Forest Canopy. *Atmospheric Environment* **22**, 869-884.

Baldocchi, D.D. (2003) Assessing the Eddy Covariance Technique for Evaluating Carbon Dioxide Exchange Rates of Ecosystems: Past, Present and Future. *Global Change Biology* **9**, 479-492.

Barton, C.V.M. and North, P.R.J. (2001) Remote Sensing of Canopy Light-use efficiency Using the Photochemical Reflectance Index - Model and Sensitivity Analysis. *Remote Sensing of Environment* **78**, 264-273.

Blanken, P.D., Black, T.A., Neumann, H.H., Den Hartog, G., Yang, P.C., Nesic, Z. and Lee, X. (2001) The Seasonal Water and Energy Exchange Above and Within a Boreal Aspen Forest. *Journal of Hydrology* **245**, 118-136.

Bolin, B. and Fung, I. (1992) Report: The Carbon Cycle Revisited. In D. Ojiama (Ed.) *Modelling the earth system.* Boulder, Colorado, USA

Brakke, T.W. (1994) Specular and Diffuse Components of Radiation Scattered by Leaves. *Agricultural and Forest Meteorology* **71**, 283-295.

Chen, J.M., Liu, J., Leblanc, S.G., Lacaze, R. and Roujean, J.L. (2003) Multi-Angular Optical Remote Sensing for Assessing Vegetation Structure and Carbon Absorption. *Remote Sensing of Environment* **84**, 516-525.

Chen, J.M., Menges, C.H. and Leblanc, S.G. (2005) Global Mapping of Foliage Clumping Index Using Multi-Angular Satellite Data. *Remote Sensing of Environment* **97**, 447-457.

Chen B., Chen, J. M., Mo, G. and Black T. A. (2007a) Comparison of Regional Carbon Flux Estimates from CO_2-Concentration Measurements and Remote Sensing-based Footprint Integration. *Global Biogeochemical Cycle*, (accepted).

Chen B., Black T.A. and Morgenstern K. (2007b) Intra- and Inter- Annual Variability of EC-flux Footprint and its Implications in Carbon Balance Analysis, *Boundary-Layer Meteorology* (submitted).

Comins, H.N. and Mcmurtrie, R.E. (1993) Long-Term Response of Nutrient-Limited Forests to CO_2 Enrichment - Equilibrium Behavior of Plant-Soil Models. *Ecological Applications* **3**, 666-681.

Coops, N.C., Delahaye, A., Pook, E.(1998) Estimation of Eucalypt Forest Leaf Area on the South Coast of New South Wales using Landsat MSS Data. *Australian Journal of Botany* ***45***, 757-769.

Coops, N.C., Hilker, T., Wulder, M.A., St-Onge, B., Newnham, G., Siggins, A. and Trofymow, J.A. (2007) Estimating Canopy Structure of Douglas-Fir Forest Stands From Discrete-Return LiDAR. *Trees-Structure and Function* **21**, 295-310.

Curran, P.J. (1989) Remote Sensing of Foliar Chemistry. *Remote Sensing of Environment* **30**, 271-278.

Curran, P.J., Dungan, J.L. and Peterson, D.L. (2001) Estimating the Foliar Biochemical Concentration of Leaves With Reflectance Spectrometry Testing the Kokaly and Clark Methodologies. *Remote Sensing of Environment* **76**, 349-359.

Datt, B. (1998) Remote Sensing of Chlorophyll A, Chlorophyll B, Chlorophyll A+B, and Total Carotenoid Content in Eucalyptus Leaves. *Remote Sensing of Environment* **66**, 111-121.

Daughtry, C.S.T., Gallo, K.P. and Bauer, M.E. (1983) Spectral Estimates of Solar-Radiation Intercepted by Corn Canopies. *Agronomy Journal* **75**, 527-531.

Demmig-Adams, B. (1990) Carotenoids and Photoprotection in Plants - A Role for the Xanthophyll Zeaxanthin. *Biochemica et Biophysica Acta* ***1020***, 1-24.

Demmig-Adams, B. (2003) Linking the Xanthophyll Cycle With Thermal Energy Dissipation. *Photosynthesis Research* ***76***, 73-80.

Demmig-Adams, B. and Adams, W. W. (1996) The Role of Xanthophyll Cycle Carotenoids in the Protection of Photosynthesis. *Trends in Plant Science* ***1***, 21-26.

Demmig-Adams, B. and Adams, W. W. (2000) Photosynthesis - Harvesting Sunlight Safely. *Nature* ***403***, 371.

Filella, I., Amaro, T., Araus, J.L. and Peñuelas, J. (1996) Relationship Between Photosynthetic Radiation-Use Efficiency of Barley Canopies and the Photochemical Reflectance Index (PRI). *Physiologia Plantarum* **96**, 211-216.

Foken, T. and Wichura, B. (1996) Tools for Quality Assessment of Surface-Based Flux Measurements. *Agricultural and Forest Meteorology* **78**, 83-105.

Forseth, I.N. and Norman, J.M. (1991) Modelling of Solar Irradiance, Leaf Energy Budget, and Canopy Photosynthesis. In Hall, D.O., Scurlock, J.M.O., Bolhar-Nordenkampf, R.C., Leegood, R.C. & Long, S.P. (eds). *Techniques in Photosynthesis and Productivity Research for a Changing Environment*. Chapman & Hall. London.

Gamon, J.A. and Surfus, J.S. (1999) Assessing Leaf Pigment Content and Activity With a Reflectometer. *New Phytologist* **143**, 105-117.

Gamon, J.A., Field, C.B., Bilger, W., Björkman, O., Fredeen, A.L. and Peñuelas, J. (1990) Remote-Sensing of the Xanthophyll Cycle and Chlorophyll Fluorescence in Sunflower Leaves and Canopies. *Oecologia* **85**, 1-7.

Gamon, J.A., Peñuelas, J. and Field, C.B. (1992) A Narrow-Waveband Spectral Index that Tracks Diurnal Changes in Photosynthetic Efficiency. *Remote Sensing of Environment* **41**, 35-44.

Gamon JA, Filella I, Peñuelas J (1993). The Dynamic 531-Nanometer Reflectance Signal: A Survey of Twenty Angiosperm Species. Yamamoto HY , Smith CM (Eds). *Photosynthetic Responses to the Environment.* American Society of Plant Physiologists, Rockville. pp. 172-177.

Gao W. and Schaaf C.B. (2003) Detecting Vegetation Structure Using a Kernel-Based BRDF Model. *Remote Sensing of Environment* ***86***, 198-205

Hall, F.G., Huemmrich, K.F., Goetz, S.J., Sellers, P.J. and Nickeson, J.E. (1992) Satellite Remote-Sensing of Surface-Energy Balance - Success, Failures, and Unresolved Issues in FIFE. *Journal of Geophysical Research-Atmospheres* **97**, 19061-19089.

Hall, F.G., Hilker, T., Coops, N.C., Lyapustin, A., Huemmrich, K.F., Middleton, E.M., Drolet, G.G., Margolis, H.A., Black, T.A. (2008) Can Light-Saturated Reductions in Canopy Photosynthetic Capacity Be Observed From Space? *Remote Sensing of Environment*, accepted

Hilker T., Coops N.C., Wulder, M.A., Black, T.A., Guy, R.D., (2007a) The Use of Remote Sensing in Light-Use Efficiency Based Models of Gross Primary Production: A Review of Current Status and Future Requirements. *Science of the Total Environment*, doi:10.1016/j.scitotenv.2007.11.007

Hilker, T., Coops, N.C., Nesic, Z., Wulder, M.A. and Black, A.T. (2007b), Instrumentation and Approach for Unattended Year Round Tower-based Measurements of Spectral Reflectance. *Computers and Electronics in Agriculture* ***56***, 72-84.

Hilker, T., Coops, N.C., Schwalm, C.R., Jassal, R.S., Black, T.A. and Krishnan, P. (2008a) Effects of Mutual Shading of Tree Crowns on Prediction of Photosynthetic Light-Use Efficiency in a Coastal Douglas-Fir Forest. *Tree Physiology* ***28***, 825-834

Hilker, T., Coops, N.C., Hall, F.G., Black, T.A., Wulder, M.A. Nesic, Z., Krishnan, P. (2008b) Separating Physiologically and Directionally Induced Changes in PRI Using BRDF Models. *Remote Sensing of Environment*, in press

Hilker, T., Coops, N.C., Hall, F.G., Black, T.A., Chen, B., Krishnan, P.,Wulder, M.A., Sellers, P.J., Middleton, E.M., Huemmrich, K.F. (2008c) A Modeling Approach for Up-scaling Gross Ecosystem Production to the Landscape Scale Using Remote Sensing Data. *Journal of Geophysical Research – Biogeosciences*, accepted pend. rev.

Hilker, T., Coops, N.C., Black, T.A. (2008d) Assessing Uncertainties in MODIS Light-Use Efficiency in a Douglas-Fir Stand Using Multi-Angular Spectral Observations and Eddy Covariance Data. *Geophysical Research letters*, in review

Heinsch, F.A., Zhao, M.S., Running, S.W., Kimball, J.S., Nemani, R.R., Davis, K.J., Bolstad, P.V., Cook, B.D., Desai, A.R., Ricciuto, D.M., Law, B.E., Oechel, W.C., Kwon, H., Luo, H.Y., Wofsy, S.C., Dunn, A.L., Munger, J.W., Baldocchi, D.D., Xu, L.K., Hollinger, D.Y., Richardson, A.D., Stoy, P.C., Siqueira, M.B.S., Monson, R.K., Burns, S.P. and Flanagan, L.B. (2006) Evaluation of Remote Sensing Based Terrestrial Productivity From MODIS Using Regional Tower Eddy Flux Network Observations. *IEEE-Transactions on Geoscience and Remote Sensing* **44**, 1908-1925.

Huemmrich, K.F., Middleton, E.M., Drolet, G., Hall, F.G., Margolis, H. and Knox, R.G. (2005) Determining Ecosystem Light-Use Efficiency for Carbon Exchange from Satellite. *Proceedings of SPIE* **5996**

Janzen, H. H. (2004) Carbon Cycling in Earth Systems -A Soil Science Perspective. *Agriculture, Ecosystems and Environment,* ***104***, 399 – 417.

Kljun, N., Calanca, P., Rotachhi, M.W. and Schmid, H.P. (2004) A Simple Parameterization for Flux Footprint Predictions. *Boundary-Layer Meteorology* **112**, 503-523.

Leclerc, M.Y. and Thurtell, G.W. (1990) Footprint Prediction of Scalar Fluxes Using a Markovian Analysis. *Boundary-Layer Meteorology* **52**, 247-258.

Lefsky, M.A., Turner, D.P., Guzy, M. and Cohen, W.B. (2005) Combining LiDAR Estimates of Aboveground Biomass and Landsat Estimates of Stand Age for Spatially Extensive Validation of Modeled Forest Productivity. *Remote Sensing of Environment* **95**, 549-558.

Lillesand, T.M. and Kiefer, R.W. (1979) Remote Sensing and Image Interpretation, John Wiley and Sons, Inc, 1979.

Luo, Y.Q. and Reynolds, J.F. (1999) Validity of Extrapolating Field CO_2 Experiments to Predict Carbon Sequestration in Natural Ecosystems. *Ecology* **80**, 1568-1583.

Magnussen, S., Boudewyn, P. and Wulder, M. (2004) Contextual Classification of Landsat-TM Images to Forest Inventory Cover Types. *International Journal of Remote Sensing* **25**, 2421-2440.

Massman, W.J. and Lee, X. (2002) Eddy Covariance Flux Corrections and Uncertainties in Long-Term Studies of Carbon and Energy Exchanges. *Agricultural and Forest Meteorology* **113**, 121-144.

Moncrieff, J.B., Malhi, Y. and Leuning, R. (1996) The Propagation of Errors in Long-Term Measurements of Land-Atmosphere Fluxes of Carbon and Water. *Global Change Biology* **2**, 231-240.

Monteith, J.L. (1972) Solar-Radiation and Productivity in Tropical Ecosystems. *Journal of Applied Ecology* **9**, 747-766.

Monteith, J.L. (1977) Climate and Efficiency of Crop Production in Britain. *Philosophical Transactions of the Royal Society of London Series B-Biological Sciences* **281**, 277-294.

Müller, C., Eickhout, B., Zaehle, S., Bondeau, A., Cramer, W., Lucht, W (2007) Effects of Changes in CO_2, Climate, and Land Use on the Carbon Balance of the Land Biosphere During the 21st Century. *Journal of Geophysical Research-Biogeosciences* ***112*** (G2) Art. No. G02032.

Myneni, R. and Williams, D. (1994) On the Relationship between F_{APAR} and NDVI. *Remote Sensing of Environment* **49**, 200-211.

Næsset, E. (2002) Predicting Forest Stand Characteristics with Airborne Scanning Laser Using a Practical two-stage Procedure and Field Data. *Remote Sensing of Environment* **80**, 88-99.

Næsset, E. and Řkland, T. (2002) Estimating Tree Height and Tree Crown Properties Using Airborne Scanning Laser in a Boreal Nature Reserve. *Remote Sensing of Environment* **79**, 105-115.

Næsset, E. (1997) Estimating Timber Volume of Forest Stands Using Airborne Laser Scanner Data. *Remote Sensing of Environment* **61**, 246-253.

Peddle, D.R., Hall, F.G. and Ledrew, E.F. (1999) Spectral Mixture Analysis and Geometric-Optical Reflectance Modeling of Boreal Forest Biophysical Structure. *Remote Sensing of Environment* **67**, 288-297.

Peñuelas, J., Filella, I. and Gamon, J.A. (1995) Assessment of Photosynthetic Radiation-Use Efficiency With Spectral Reflectance. *New Phytologist* **131**, 291-296.

Peñuelas, J., Gamon, J.A., Fredeen, A.L., Merino, J. and Field, C.B. (1994) Reflectance Indexes Associated With Physiological-Changes in Nitrogen-Limited and Water-Limited Sunflower Leaves. *Remote Sensing of Environment* **48**, 135-146.

Persson, A., Holmgren, J. and Soderman, U. (2002) Detecting and Masuring Individual Trees Using an Airborne Laser Scanner. *Photogrammetric Engineering & Remote Sensing* **68**, 925-932.

Pinker, R.T. and Ewing, J.A. (1985) Modeling Surface Solar-Radiation - Model Formulation and Validation. *Journal of Climate and Applied Meteorology* **24**, 389-401.

Rahman, A.F., Cordova, V.D., Gamon, J.A., Schmid, H.P. and Sims, D.A. (2004) Potential of MODIS Ocean Bands for Estimating CO_2 Flux From Terrestrial Vegetation: a Novel Approach. *Geophysical Research Letters* **31**,

Rahman, A.F., Gamon, J.A., Fuentes, D.A., Roberts, D.A. and Prentiss, D. (2001) Modeling Spatially Distributed Ecosystem Flux of Boreal Forest Using Hyperspectral Indices From AVIRIS Imagery. *Journal of Geophysical Research-Atmospheres* **106**, 33579-33591.

Rast, M. (2001). SPECTRA – Surface Processes and Ecosystem Changes through Response Analysis. *ESA SP – 1257(5).* ESA The Netherlands. 132pp.

Reichstein M., Papale, D. (2006) On the Use of Eddy Covariance and Optical Remote Sensing Data for Biogeochemical Modeling. *Carbon Fusion International Workshop*, Edinburgh, 2006

Running, S., Baldocchi, D., Turner, D., Gower, S., Bakwin, P. and Hibbard, K. (1999) A Global Terrestrial Monitoring Network Integrating Tower Fluxes, Flask Sampling, Ecosystem Modeling and EOSD Satellite Data. *Remote Sensing of Environment* **70**, 108-127.

Running, S.W., Nemani, R.R., Heinsch, F.A., Zhao, M.S., Reeves, M. and Hashimoto, H. (2004) A Continuous Satellite-Derived Measure of Global Terrestrial Primary Production. *Bioscience* **54**, 547-560.

Schmid, H.P. and Lloyd, C.R. (1999) Spatial Representativeness and the Location Bias of Flux Footprints Over Inhomogeneous Areas. *Agricultural and Forest Meteorology* **93**, 195-209.

Sellers, P.J., Meeson, B.W., Hall, F.G., Asrar, G., Murphy, R.E., Schiffer, R.A., Bretherton, F.P., Dickinson, R.E., Ellingson, R.G., Field, C.B., Huemmrich, K.F., Justice, C.O., Melack, J.M., Roulet, N.T., Schimel, D.S. and Try, P.D. (1995) Remote-Sensing of the Land-Surface for Studies of Global Change - Models, Algorithms, Experiments. *Remote Sensing of Environment* **51**, 3-26.

Sims, D.A. and Gamon, J.A. (2002) Relationships Between Leaf Pigment Content and Spectral Reflectance Across a Wide Range of Species, Leaf Structures and Developmental Stages. *Remote Sensing of Environment* **81**, 337-354.

Smith, M.L. S.V. Ollinger, M.E. Martin, J.D. Aber, R.A. Hallett and C.J. Goodale (2002) Direct Prediction of Above Ground Forest Productivity by Hyperspectral Remote Sensing of Canopy Nitrogen. *Ecological Applications **12***, 1286-1302

Smolander, S. and Stenberg, P. (2001) A Method for Estimating Light Interception by a Conifer Shoot. *Tree Physiology* **21**, 797-803.

Tucker, C. (1979) Red and Photographic Infrared Linear Combinations for Monitoring Vegetation. *Remote Sensing of Environment* **8**, 127-150.

Turner, D.P., Ritts, W.D., Cohen, W.B., Maeirsperger, T.K., Gower, S.T., Kirschbaum, A.A., Running, S.W., Zhao, M.S., Wofsy, S.C., Dunn, A.L., Law, B.E., Campbell, J.L., Oechel, W.C., Kwon, H.J., Meyers, T.P., Small, E.E., Kurc, S.A. and Gamon, J.A. (2005) Site-Level Evaluation of Satellite-Based Global Terrestrial Gross Primary Production and Net Primary Production Monitoring. *Global Change Biology* **11**, 666-684.

Turner, D.P., Urbanski, S., Bremer, D., Wofsy, S.C., Meyers, T., Gower, S.T. and Gregory, M. (2003) A Cross-Biome Comparison of Daily Light-use efficiency for Gross Primary Production. *Global Change Biology* **9**, 383-395.

Weiss, A. and Norman, J.M. (1985) Partitioning Solar-Radiation Into Direct and Diffuse, Visible and Near-Infrared Components. *Agricultural and Forest Meteorology* **34**, 205-213.

Wofsy, S.C., Goulden, M.L., Munger, J.W., Fan, S.M., Bakwin, P.S., Daube, B.C., Bassow, S.L. and Bazzaz, F.A. (1993) Net Exchange of CO_2 in a Mid-latitude Forest. *Science* **260**, 1314-1317.

Wulder, M. (1998) Optical Remote Sensing Techniques for the Assessment of Forest Inventory and Biophysical Parameters. *Progress in Physical Geography, 22,* 449-476.

Zarco-Tejada, P.J., Miller, J.R., Mohammed, G.H., Noland, T.L. and Sampson, P.H. (2002) Vegetation Stress Detection Through Chlorophyll A+B Estimation and Fluorescence Effects on Hyperspectral Imagery. *Journal of Environmental Quality* **31**, 1433-1441.

Zhao, M., Running, S.W. and Nemani, R.R. (2006) Sensitivity of Moderate Resolution Imaging Spectroradiometer (MODIS) Terrestrial Primary Production to the Accuracy of Meteorological Re-Analyses. *Journal of Geophysical Research-Biogeosciences* **111**, Art. No. G01002

2 THE USE OF REMOTE SENSING IN LIGHT-USE EFFICIENCY-BASED MODELS OF GROSS PRIMARY PRODUCTION: A REVIEW OF CURRENT STATUS AND FUTURE REQUIREMENTS[3]

2.1 Introduction

Terrestrial ecosystems absorb approximately 60 Gt of carbon annually through the physiological process of photosynthesis (Janzen, 2004), also referred to as Gross Primary Production (GPP) (Hamilton et al., 2002). Simultaneously, autotrophic and heterotrophic organisms release about the same amount of carbon back into the atmosphere thereby closing the terrestrial carbon cycle. As the estimated annual turnover between the atmosphere and terrestrial ecosystems is approximately 120 Gt, considerably greater than the amount of fossil fuel emissions (5 Gt), small alterations in the terrestrial carbon balance are likely to have a significant impact on atmospheric CO_2 concentrations. As a result, there is a need for a better understanding of the dynamics of carbon fluxes between biosphere and atmosphere to help quantify potential changes due to increased atmospheric CO_2 concentrations (Comins and McMurtrie 1993, Luo and Reynolds 1999). Global monitoring and prediction of GPP over forested and agricultural environments is therefore an ultimate goal of Earth climate change research seeking universal, generic modelling approaches applicable across multiple biomes and a wide variety of vegetation types.

[3] A version of this chapter has been published. Hilker T., Coops N.C., Wulder, M.A., Black, T.A., Guy, R.D. (2007) The Use of Remote Sensing in Light-Use Efficiency-Based Models of Gross Primary Production: A Review of Current Status and Future Requirements. *Science of the Total Environment,* doi:10.1016/j.scitotenv.2007.11.007

Modeling of carbon cycling requires parameterization of the land surface (Hall et al., 1995), which, in a spatially continuous mode and on a regular basis, is only possible using remote sensing. Modeling GPP from remote sensing is largely based on the awareness that plant physiological properties are related to the biochemical composition of plant foliage, and that this composition is reflected in the spectral radiation properties of leaves. Since the launch of the first satellite-based sensors in the 1970s the remote sensing community has been limited in the number and width of the spectral wavebands available, and observation frequencies of existing sensors were incapable of detecting the spatial and temporal variability of primary production of vegetation. Recently, the advent of high spectral resolution optical sensors, capable of detecting changes in leaf-spectral properties with a high temporal frequency (Prince and Goward, 1995) has allowed the scientific community to revisit a number of existing approaches for modeling GPP, and reassess the potential for using remotely-sensed inputs, with the ultimate aim of driving GPP models entirely from satellite-based observations (Running et al., 2004, Rahman et al., 2005). This chapter reviews the current status of determining GPP from remotely-sensed inputs and addresses future requirements for developing remote sensing based models of the terrestrial carbon cycle, specifically on approaches based on the light-use efficiency concept.

2.2 Light-use efficiency based modeling of primary production

One of the most widely applied concepts for modeling GPP is the light-use efficiency approach of Monteith (1972, 1977) (e.g. Prince, 1991, Goetz and Prince, 1999, Heinsch et al., 2002, Turner et al., 2003a,b), which expresses GPP as the product of the absorbed photosynthetically active radiation (PAR) (μmol m^{-2} s^{-1}), defined as absorbed solar radiation between 400-700 nm wavelength, and the efficiency with which the absorbed PAR can be converted into biomass:

$$GPP = PAR \cdot f_{PAR} \cdot \varepsilon \qquad (1)$$

where f_{PAR} represents the fraction of PAR absorbed by the canopy and ε (g MJ^{-1}) is the photosynthetic efficiency term. The light-use efficiency concept is based on the functional convergence theory (Field, 1991) hypothesizing that plants are scaling canopy leaf area and light harvesting by the availability of resources as a result of evolutionary processes in order to optimize their carbon fixation (Goetz et al., 1999). Detailed development and discussion of the underlying concepts behind the light-use efficiency model are described in extensive studies and reviews by Field (1991), Reich et al. (1997) and Goetz and Prince (1999).

The amount of photosynthetically active radiation absorbed by a plant canopy ρ_a is defined as the difference between the PAR incident upon the canopy (Q), the amount of PAR being reflected from the canopy (ρ_r), and PAR being transmitted through the canopy (τ_t) (Beer-Lambert law):

$$\rho_a = Q - \rho_r - \tau_t \qquad (2)$$

For a given time, ρ_r and τ_t are a function of the leaf surface area (Sellers, 1985) parameterized by the leaf area index (LAI) defined as half the total foliage area per unit ground surface area (Chen and Black, 1992). Because of temporal variations in solar irradiance, chlorophyll content (Dawson et al., 2003) and leaf-sun geometry (Chen and Black, 1992) the amount of solar radiation being absorbed by a plant canopy varies diurnally as well as seasonally (Chen, 1996).

ε is determined by the a combination of a large number of environmental stresses restraining the photochemical reaction process, such as nutrition supply, water and temperature, depends on individual vegetation types, and, as a result, varies greatly within space and time (Field and Mooney 1986, Prince and Goward 1996, Turner et al., 2003b). An important biochemical process driving ε is known as photoprotection (Figure 2.1). In situations where plants receive more sunlight than they can actually use, light harvesting is being regulated to balance absorption and utilization of quanta as excessive light energy can cause photo-oxidative damage to the leaf (Demmig-Adams, 1990). The mechanism regulating the use of absorbed light is controlled by a group of leaf pigments named xanthophylls which occur over a broad range of species (Bilger et al., 1989, Bilger and Björkman 1990, Demmig-Adams and Adams, 2000, Demmig-Adams et al., 1998). Under excessive light conditions, the xanthophyll cycle pigment violaxanthin is de-epoxidized rapidly via intermediate antheraxanthin to zeaxanthin and this reaction is reversed when light is limiting. Antheraxanthin, as well as zeaxanthin, have photo-protective structures accepting excessive light energy from the antenna pigments of Photosystem II and safely dissipating it as heat (Demmig-Adams and Adams, 1996). Recently, a second xanthophyll cycle, the lutein cycle, has been discovered (Bungard, 1999), which is believed, within some species, to work in parallel. Photo-protection is also closely related to active emittance of light quanta in leaves, known as chlorophyll fluorescence (Demmig-Adams and Adams, 1996).

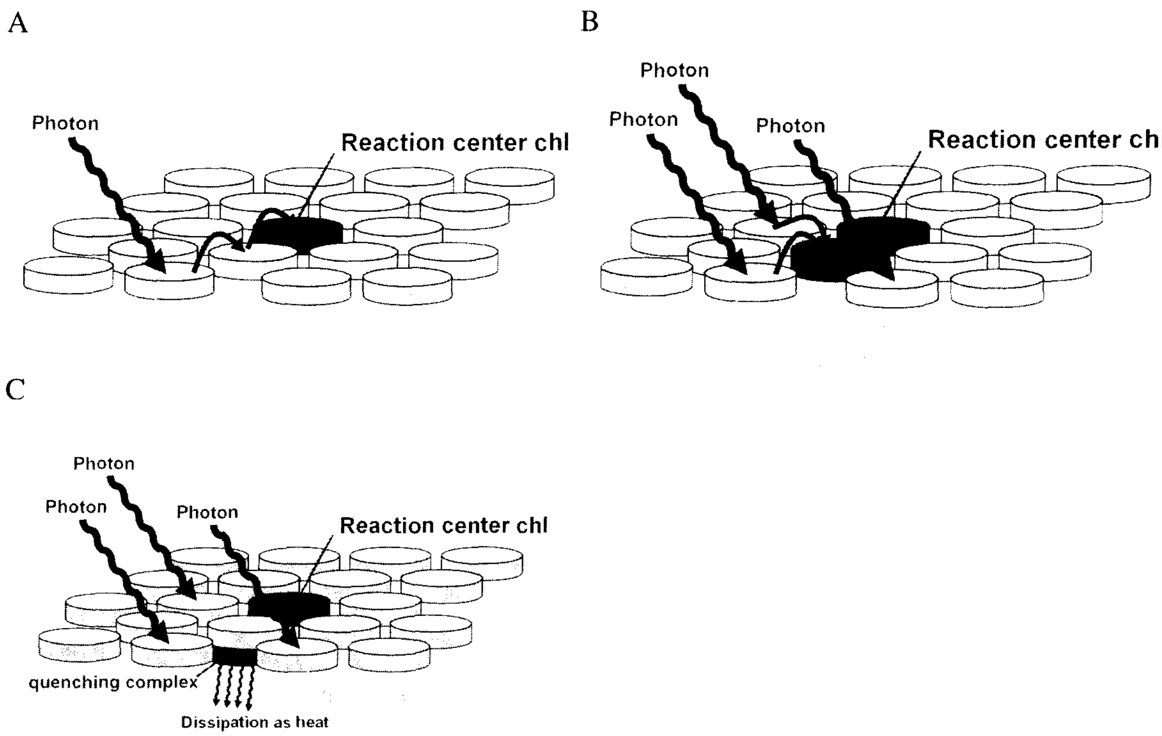

Figure 2.1A-C: Schematic drawing of the photoprotective mechanism inside the light-harvesting complex (LHC) of a leaf. A: Light is harvested by antenna pigments and the energy is transferred to the reaction center. B: In case plants receive more light energy than they can actually use, this excessive energy accumulates inside the LHC (illustrated by the black disk). Excessive radiation energy can potentially cause photo-oxidative damage to the photosynthetic apparatus of the leaf. C: The excessive radiation energy is safely dissipated as heat by means of a quenching complex.

2.3 Current status of determining GPP from remote sensing

2.3.1 Photosynthetically active radiation

While the extraterrestrial radiation budget and its wavelength distribution are well known and relatively constant, the terrestrial reception of PAR is altered by a dynamically changing atmosphere (Van Laake and Sanchez-Azofeifa, 2004). Atmospheric radiative transfer is driven by absorption, molecular (Raleigh) and particle (Mie) scattering effects attenuating the amount of solar radiation received by the earth surface (Szeicz, 1974, Rao, 1984, Baker and Frouin, 1987). Early estimates of broad scaled PAR were obtained from networks of surface pyranometers (Bland and Clayton, 1994, Bland, 1996), allowing long-term time series from well maintained and calibrated instruments. This method, however, is insufficient for global modeling since estimates of PAR are restricted to a few discrete observations (Frouin and Pinker, 1995). Since the launch of the first multispectral satellite sensors, numerous approaches have been developed to infer large scaled PAR from top of the atmosphere solar radiance using optical modeling (Sellers et al., 1995) to allow spatially exhaustive estimates of broadband and shortwave irradiance (Eck and Dye, 1991, Frouin and Gautier, 1992, Pinker and Laszlo, 1992). PAR is thereby often defined as a fraction of the reflected shortwave radiation (e.g. Tarpley, 1979, Gautier et al., 1980, Pinker and Ewing, 1985, Running et al., 1999), which is sufficient for most biological applications (Blackburn and Proctor, 1983, Weiss and Norman, 1985).

Recently, there has been a focus on incorporating the temporal and spatial variability of solar irradiance with respect to changing atmospheric conditions into global estimates of PAR to obtain highly accurate inputs for climate change modeling. Atmospheric conditions are currently assessed on a global scale by the Moderate Resolution Imaging Spectroradiometer (MODIS), on board NASA's EOS (earth observation system) satellites Terra and Aqua. The MODIS Atmospheric Profile products (MOD04–MOD07) consist of total-ozone burden, atmospheric stability, temperature and moisture profiles, and atmospheric water vapour, measured on a daily basis. Even though the atmospheric interactions of solar irradiance are well understood, a standardized product providing regular observations of global PAR is currently not available (Liang et al., 2006); however, techniques to derive accurate estimates of global PAR using MODIS have been developed (Van Laake and Sanchez-Azofeifa, 2004, Liang et al., 2006).

2.3.2 Absorbed photosynthetically active radiation

Approaches to infer the fraction of PAR which is absorbed by the vegetation canopy using remote sensing techniques can be divided into empirical techniques, primarily relying on curve fitting of reflectance measurements, and physical approaches, which attempt to model the relationship between leaf, canopy and stand-level biophysical characteristics and reflected and emitted radiation (Myneni and Williams, 1994, Hall et al., 1995) (Figure 2.2).

2.3.2.1 Empirical determination of absorbed PAR

Empirical approaches are largely based on spectral vegetation indices (SVI) which are linear and non-linear combinations of discrete spectral bands, seeking to maximize the sensitivity of the index to the canopy characteristic requested while minimizing the sensitivity to the unknown and unwanted canopy characteristics (Hall et al., 1995). Starting in the early 1980s, numerous studies have shown substantial evidence of a close relationship between f_{PAR} and top of the canopy reflectance measurements in the visible and near infrared region (Tucker 1979, Daughtry et al., 1983, Asrar et al., 1984), and theoretical work (Sellers, 1985, 1987) has given this relationship a solid basis as a measure of the solar photosynthetically active radiation absorbed by the canopy. Various linear and non-linear relationships between satellite-derived SVIs and f_{PAR} have been found for different vegetation types and climatic conditions (e.g., Asrar et al., 1984, Badhwar et al., 1986, Fassnacht and Gower, 1997) with the most popular SVI being the Normalized Difference Vegetation Index (NDVI), defined as

$$NDVI = \frac{\rho_{NIR} - \rho_{Red}}{\rho_{NIR} + \rho_{Red}} \qquad (3)$$

where ρ_{NIR} and ρ_{Red} are the reflectance in the near infrared and red, respectively (Tucker, 1979). SVIs have also been used to follow seasonal dynamics of vegetation using temporal profile analysis (Badhwar and Henderson, 1981, Henderson and Badhwar, 1984), and, when seasonally integrated, have been shown to be correlated with above-ground net primary production (NPP, defined as the difference between GPP and plant respiration) on an annual basis (Goward and Dye, 1987, Waring et al., 2006).

While the body of evidence supporting these relationships is impressive (Myneni and Williams, 1994), a direct conversion of satellite spectral reflectance to surface f_{PAR} over larger areas is difficult, since empirical relationships are site and sampling condition dependent, sensor-specific, change in space and time and generally are unsuitable for application to large areas or in different seasons (Goward and Huemmrich, 1992, Huemmrich and Goward, 1997, Gobron et al., 1997). Major factors influencing empirical estimates of f_{PAR} using SVIs are vegetation spectral properties, pixel heterogeneity, background reflectance, solar zenith and view zenith angle, vegetation shadow fractions, atmospheric scattering and bi-directional reflectance effects (Li and Strahler, 1985, Myneni and Williams, 1994). Some of these factors can be mitigated using more advanced indexing techniques such as the enhanced vegetation index (EVI) (Huete et al., 2002, 2006), which seek to enhance the vegetation signal with improved sensitivity in high biomass regions thereby de-coupling canopy background signals and reducing atmospheric influences. However, broad scaled direct application of vegetation indices remains challenging (e.g. Running and Nemani, 1988).

An empirical solution to the directional reflectance problem, resulting in the first globally available LAI and f_{PAR} product as a monthly 1x1° dataset, was the FASIR (Fourier Adjusted, Solar zenith angle corrected, Interpolated and Reconstructed) approach of Sellers et al. (1994) and Los et al. (1994), based on data from the spaceborne Advanced Very High Resolution Radiometer (AVHRR) sensor (Tucker et al., 1986). FASIR accounts for the effects caused by varying illumination conditions using heuristic corrective methods to obtain spatially continuous multi-year datasets of surface variables, primarily for use in global climate models (Hall et al., 1995). Further (semi-physical) algorithms for the modeling of global LAI have also been reported by Price (1993).

2.3.2.2 Physical models for determination of absorbed PAR

Since the mid-1980's there has been an increase in the development of physical approaches to determining f_{PAR}, due partly to global diagnostic studies using satellite data (Tucker and Sellers, 1986), plot scale field studies (Asrar et al., 1984, Tucker et al., 1981), large field experiments (Sellers et all., 1992, Hall et al, 1992, Sellers et al., 1997, Running et al., 1999) and theoretical work (Myneni et al, 1992, Hall et al, 1990, Sellers

1985, 1987, Sellers et al,. 1992, Sellers et al., 1996a,b). This research formed the basis for physical models of canopy reflectance, transferring reflectance and biophysical property relationships from the leaf level, where they can be easily measured and related to leaf composition and structure, to the pixel level, where leaf optics interact with canopy structure, understorey characteristics, background reflectance, view and illumination geometry to produce a complicated relationship among pixel-level reflectance, stand structural, biophysical and leaf-optical properties (Hall et al., 1995). The understanding gained from these models is then used to develop algorithms to relate biophysical characteristics to reflectance measurements at the landscape and global levels (Hall et al., 1995). Modeling efforts that have addressed this problem are numerous, and can be placed into four general classes (Goel, 1988): 1) turbid medium models, describing the interaction of photons in the atmosphere-vegetation-soil medium (e.g. Myneni et al., 1997), 2) geometric optical models (e.g. Li and Strahler, 1985), 3) hybrid combinations of 1) and 2) (e.g. Li et al, 1995), and 4) complex computer simulation models (e.g. Goel et al., 1991). The model parameters either depend on physical properties directly (i.e. canopy structure and vegetation type) or can be obtained from mathematical inversion of reflectance measurements (e.g. Wanner et al., 1995), allowing the estimation of both leaf and canopy parameters in a predictive mode, thereby overcoming the need for parameterisation required in the use of regressive semi-empirical models (Privette et al., 1996, Bicheron and Leroy 1999). Over the last decade, models allowing for parameter acquisition from mathematical inversion have arisen as the most promising technique for retrieving f_{PAR} (Meroni et al., 2004) and several studies have been successfully conducted for crop and forested environments (e.g. Gao, 1994, Goel and Grier, 1988, Myneni et al., 1997). The accuracy of such estimations is dependent on the model employed, the type and quality of remote sensing data and the inversion procedure used (Jacquemoud et al., 2000).

One of the most prominent examples of a radiative transfer based global f_{PAR} model is the LAI/f_{PAR} product used in MODIS, providing 8-day averaged global LAI and f_{PAR} data at a 1x1 km spatial resolution. The algorithm uses photon transport theory to estimate both the radiation regime within the vegetation canopy and the radiant exitance, based on the architecture of individual plants and the entire canopy, optical properties of vegetation elements and soil atmospheric conditions (Knyazikhin, 1999, Myneni et al., 1989). The MODIS algorithm requires a land cover classification (also derived from MODIS data) to model the radiative transfer over larger areas. Canopy transmittance, reflectance, and absorptance are elements of a look-up table (LUT), distinguishing between biome types, each of which represents a pattern of the architecture of an individual tree (leaf normal orientation, stem-trunk-branch area fractions, leaf and crown size) and the entire canopy (trunk distribution, topography), as well as patterns of spectral reflectance and transmittance of other vegetation elements. Soil type and understorey are also biome specific, and can vary continuously within given biome-dependent ranges. Information on the leaf canopy spectral properties from MODIS and structural attributes from the LUT are then used to retrieve LAI and f_{PAR} (Knyazikhin et al., 2003). A full description of the MODIS f_{PAR} LAI product can be obtained from Knyazikhin et al. (1998, 2003), reviewed by Myneni et al. (2002).

2.3.3 Photosynthetic light-use efficiency

Whilst determination of f_{PAR} has matured over a number of years, the estimation of ε using remote sensing techniques emerged only in the past decade, encouraged by the advent of fine resolution spectral measurement devices allowing tracking of subtle changes in canopy reflectance using narrow wavebands in the visible and near infrared region. In general, approaches inferring ε from remote sensing can be classified into either indirect techniques, seeking to determine ε from environmental stresses, or direct approaches, trying to predict ε by measuring chlorophyll fluorescence and changes in leaf spectral reflectance resulting from photoprotection (Figure 2.2).

2.3.3.1 Determination of photosynthetic efficiency from environmental stresses

Stress factors driving photosynthetic efficiency are numerous and their detection over larger areas is relatively difficult due to the high temporal and spatial variability inherent to site and meteorological conditions. Remote sensing of stresses has mostly focussed on water, nitrogen and temperature related conditions. While more severe stresses, manifesting in symptoms such as chlorosis, defoliation or degradation of canopies, can be sensed using time series of broad-band SVIs based on reflectance in the visible and near infrared region (Liu and Kogan, 1996), these stresses are exceptional and such techniques cannot be applied to sense more moderate stress situations or early stages of severe stresses where the plants' response is much less apparent (Baret et al., 2007).

Remote sensing of soil moisture related stress factors includes passive microwave systems (e.g. Prevot et al, 2003, Wigneron et al., 2003) and combinations of simultaneous measurements in the visible, near infrared, and thermal infrared bands. While microwave systems have shown good correspondence to soil moisture content, existing instruments lack adequate spatial and temporal resolution for sufficiently detailed estimates of water related vegetation stresses (Deshayes et al., 2006). Spectral measurements, combining SVI based estimates of the vegetation status with thermal radiation (temperature vegetation index – TVX (Prihodko and Goward, 1997)) predict soil moisture content from the difference between soil temperature and vegetation canopy temperature. This technique has been successfully used to determine plant water deficit (Lopez et al., 1991), water balance (Duchemin et al., 1999), and latent heat fluxes (Vidal et al., 1994) on local scales, however, application over larger areas remains complex (Prince and Goward, 1996), as 1) the difference between soil temperature and vegetation canopy temperature is not only a function of soil moisture but is also dependent on the incident solar radiation load and 2) the moisture content of sub-surface layers cannot be determined using this technique (Prince and Goward, 1995).

Like soil water related stresses, the understanding of nitrogen cycling and nitrification in forest ecosystems has greatly improved over recent decades, however the ability to characterize spatial patterns using remote sensing is limited (Ollinger et al., 2002) as derivation of stress maps is complex (Guerif and Duke, 2000). Early studies on the use of remote sensing for nitrogen stress quantification were based on empirical relationships using SVIs sensitive to the leaf chlorophyll content (Peñuelas et al., 1994, Bausch and Duke, 1996). More recent approaches suggest the use of hyperspectral imagery for direct prediction of foliage nitrogen content from narrow waveband reflectance (Wessman et al., 1988, Martin and Aber 1997). Ollinger et al. (2002) presented a method to derive foliage nitrogen using data from NASA's Airborne Visible and Infra-Red Imaging Spectrometer (AVIRIS). A first study successfully applying spaceborne instrumentation was reported by Smith et al. (2003) using EO1-Hyperion satellite data. While the results from these hyperspectral approaches are encouraging, application over larger areas presents challenges to data analysis (Liu et al., 2006), as narrow waveband reflectance measurements are highly sensitive to atmospheric scattering and directional reflectance effects.

Arguably, the first stress based model for prediction of global ε was the Global Production Efficiency Model (GLO-PEM) of Prince and Goward (1995) based on the AVHRR Land Pathfinder dataset providing 10-day averages of daily global observations. GLO-PEM uses a TVX based approach to estimate water related stresses for a normalized solar zenith angle (Goward and Prince 1995, Nemani and Running, 1989). Estimates of atmospheric saturation deficit (D) are modeled from combinations of air temperature and atmospheric water vapour, derived from thermal infrared observations in two different wavebands. A similar approach of a global model predicting primary production was presented by Field et al. (1995) which uses estimates of ε based on the CASA model (Carnegie Ames Stanford Approach) introduced by Potter et al. (1993) and calibrated using AVHRR data.

More recently, global estimation of ε from environmental stresses is undertaken using the MODIS GPP product (MOD17), which estimates GPP from 8-day averages of f_{PAR}, PAR and ε (Heinsch et al., 2002). The MOD17 algorithm models ε using a look-up table containing biome specific information about the maximum light-use efficiency ε_{max}, scaled daily minimum temperature (T_{Min}) and water vapour pressure (D) for maximum and minimum ε of each biome type (Running et al., 2000, Turner et al., 2003a). The biome specific constant ε_{max} is adjusted using 1°x1.25° estimates of T_{Min} and D, derived from GCMs (e.g. Potter et al., 1993, Sellers et al., 1996a, 1996b) to account for the limiting effects of climatic variables on ε (Heinsch et al., 2002, Turner et al., 2003a),

$$\varepsilon = \varepsilon_{\max} \cdot T_{Min} \cdot D \qquad (4)$$

For a full description of the MODIS GPP algorithm see Heinsch et al. (2002).

2.3.3.2 Direct estimation of photosynthetic efficiency

Thus far estimation of ε has been via environmental stresses. In the past decade research has focussed on the direct estimation of ε, as this technique not only offers the potential to determine the combined effect of vegetation stresses, but also includes information about the degree to which these stresses are limiting photosynthesis (Adams and Demmig-Adams, 1996).

Remote estimation of chlorophyll fluorescence includes both passive (Carter et al., 1990) and laser-induced active methods (Rosema et al., 1998, Corp et al., 2006). Active fluorescence measurements use laser pulses to manipulate the level of photosynthetic activity and to measure the corresponding changes in the chlorophyll fluorescence yield (e.g. Kolber et al., 2005). These pulse-modulated measuring systems, probe the yield of chlorophyll fluorescence under steady-state illumination (*Fs*) and during a short saturating flash delivered at close range (1–100 mm), and have been successfully used for measuring photosynthesis (Adams et al., 1999, Rascher et al., 2000). However, their application is mostly restricted to individual leaves in accessible canopies (Ananyev et al., 2005), with a few notable exceptions (e.g. Cecchi et al., 1994).

Evidence of a solar induced fluorescence signal superimposed on leaf reflectance signatures has been reported by various studies (Buschmann and Lichtenthaler, 1977, 1999, Peñuelas et al., 1995, Gitelson et al., 1999) and the effects of solar induced chlorophyll flurorescence emissions on the apparent spectral reflectance have been investigated using radiative transfer modeling (Zarco-Tejada et al., 2000). Chlorophyll fluorescence from passive remote sensing systems provides a potential for broad scaled assessment of ε (Corp et al., 2006), however, its application is technically challenging as under natural sunlight illumination chlorophyll fluorescence emitted by the vegetation represents less than 3% of the reflected light in the near infrared part of the electromagnetic spectrum (Moya et al., 2004). Consequently, passive sensing of chlorophyll fluorescence is possible only using sub-nanometer reflectance bands in the red and near infrared regions (often 690 and 760 nm) where solar radiation is not abundant as a result of atmospheric absorption (Fraunhofer lines) (Meroni and Colombo, 2006). The intended launch of a spaceborne fluorescence sensor by the European Space Agency (ESA) as part the FLEX (fluorescence experiment) mission may provide new opportunities to exploit this method for estimation of global ε from space.

Determining ε using the photoprotective mechanism in leaves is based on observation of changes in leaf spectral reflectance resulting from the epoxidation state of the xanthophyll cycle. These changes manifest in two narrow waveband absorption features at 505 and at 531 nm and can be quantified using SVIs, such as the Photochemical Reflectance Index (PRI), defined as (Gamon et al., 1990),

$$PRI = \frac{\rho_{531} - \rho_{570}}{\rho_{531} + \rho_{570}} \tag{5}$$

comparing the reflectance at 531 nm (ρ_{531}) to a xanthophyll-insensitive reference band at 570nm (ρ_{570}). Originally established for sunflower leaves, the empirical relationship between PRI and ε has been confirmed over a wide range of species (Peñuelas et al., 1994, 1995, Filella et al., 1996, Gamon and Surfus, 1999) thereby demonstrating the potential use of this method for global estimation of ε. Up-scaling of these findings from leaf to canopy, regional and global levels, however remains challenging. First, the temporal dynamics existing in plant photosynthesis, require the observation of vegetation status under multiple illumination and viewing conditions and these observations are then, even more than in the case of f_{PAR}, subject to bi-directional reflectance and scattering effects (Los et al., 2005) overlapping with the desired reflectance signal (Huemmrich et al., 2005). Second, airborne or spaceborne sensors can only provide snapshots in time determined by a given aircraft or satellite overpass (Sims et al., 2005), however, the temporal and spatial requirements for these observations to be representative of the physiological status of plant canopies are not well understood (Hall et al., 1995). Third, the relationship between PRI and ε is species dependent and also changes with age, canopy structure, disturbances and LAI (Rahman et al., 2001), making a spatial extrapolation of empirical findings difficult.

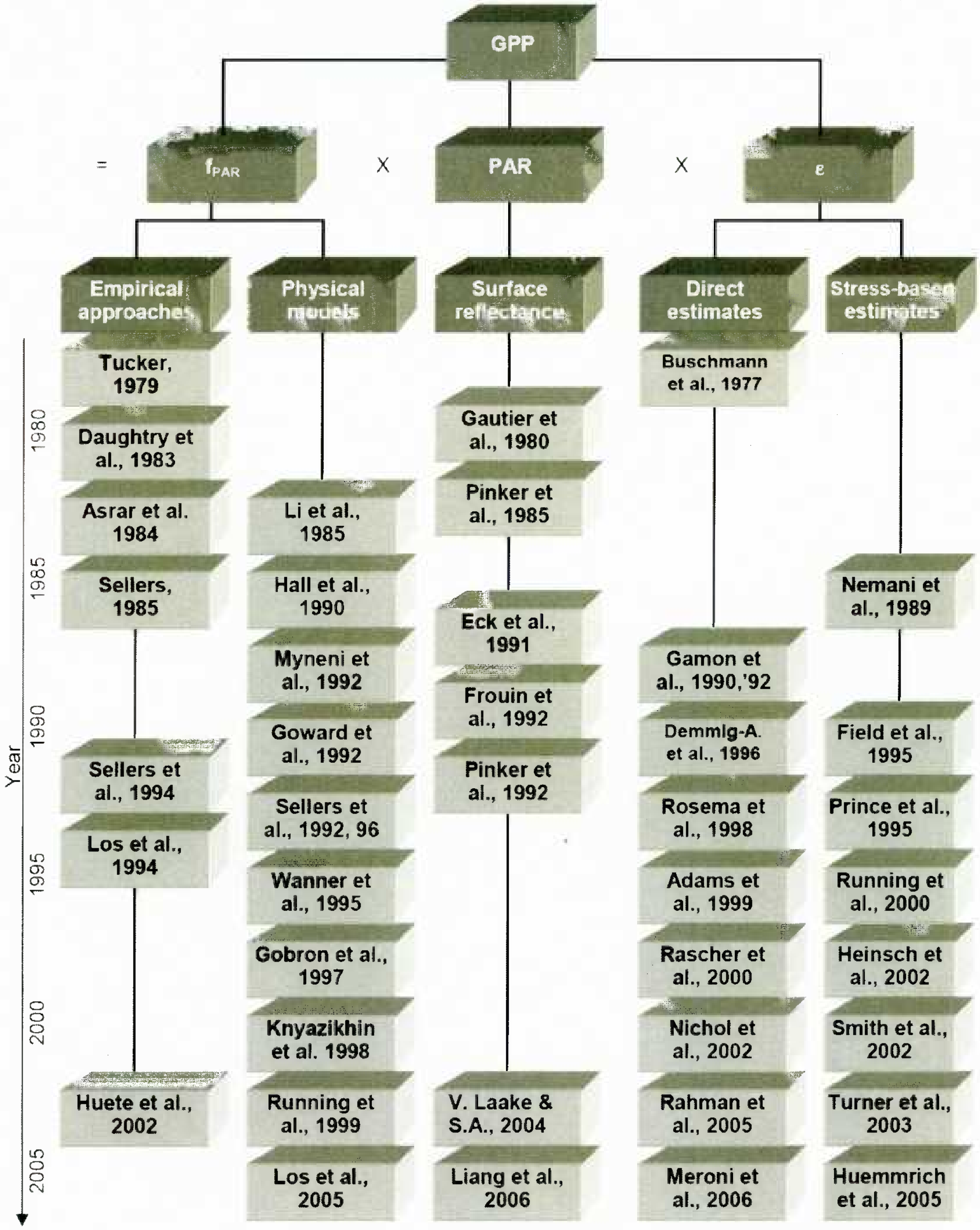

Figure 2.2: Illustration of approaches to assess GPP from remote sensing. PAR is generally derived from Top of Atmosphere (ToA) reflectance, techniques inferring f_{PAR} from remote sensing can be divided into empirical approaches and physical models. ε can either be determined directly or indirectly through stress factors. Some examples of key literature to each approach are given.

Recent efforts to further the understanding of the temporal and spatial dynamics involved, include near surface observations using transect measurements (Sims et al., 2006), permanently established tower-based observations of forest canopies (Leuning et al., 2006), and airborne measurements (Nichol et al., 2000, 2002, Chen and Vierling, 2006, Rahman et al., 2001). A spaceborne assessment of ε was introduced by Drolet et al. (2005), successfully using backscatter reflectance data from MODIS Aqua over the Canadian boreal forest with a spatial resolution of 1 km^2.

2.4 Validation approaches

Validation and operationalization of the light-use efficiency approach is currently underway at a number of spatial and temporal scales. At the stand level, eddy covariance data (EC) exhibit a key role for studying the temporal and spatial variability of GPP (Turner et al., 2006). EC measurements facilitate continuous estimates of net carbon accumulation, also referred to as net ecosystem production (NEP), from flux towers measuring CO_2 mixing ratios of up and down-moving eddies (Baldocchi, 2003), thereby using the covariance between the vertical velocity (w) and the mole-mixing ratio of CO_2 (sc) to estimate carbon fluxes (F_c),

$$F_C = \overline{\rho_a}\,\overline{w's_c'} \qquad (6)$$

where $\overline{\rho_a}$ is the mean molar density of dry air and $\overline{w's_c'}$ is the covariance between the vertical velocity (w) and the mole-mixing ratio of CO_2 (s_c). The spatial scale of an EC flux tower is about 1 km^2 (Kljun et al., 2004) and the temporal resolution is given by the integration of high frequency data, usually at a half-hourly basis (Morgenstern et al., 2004). GPP can be determined from EC data by adding estimates of ecosystem respiration (R) to measured NEP values, and ε can be obtained from additional measurements of f_{PAR} and PAR using radiation sensors above and below the canopy (Humphreys et al., 2006). Remotely-sensed estimates of stand level GPP have been correlated with EC flux data from ground-based (Cheng et al., 2006, Sims et al., 2006), tower-based (Filella et al., 1996, Stylinski et al., 2002), airborne (Nichol et al., 2000, 2002) and spaceborne platforms (Running et al., 1999, Drolet et al., 2005, Coops et al., 2007). Also, to bridge the spatial gap existing between near surface and airborne remote sensing platforms, Chen and Vierling (2006) tested a tethered balloon mounted platform to evaluate canopy reflectance of a grassland conifer forest ecotone. Networking approaches, such as the recently established SpecNet initiative (Gamon et al., 2006) attempt to link these observations with existing global flux-tower sites to further the understanding of relationships existing between biophysical processes and spectral reflectance data, thereby trying to overcome the fundamental scale mismatch between estimates obtained from eddy flux and remote sensing (Running et al., 1999, Rahman et al., 2001, Cheng et al., 2006, Gamon et al., 2006). Other objectives of this network are the exploration of temporal matters, derivation of flux components and the validation of satellite data products (Gamon et al., 2006).

At the landscape level, verification of GPP estimates has been undertaken in various broad-scaled field studies comparing ground-based estimates to remotely-sensed data. One of the first projects designed to coordinate data collected by satellites, aircraft, and ground instruments in order to improve the understanding of carbon and water cycles, was FIFE (First ISLSCP (International Satellite Land Surface Climatology Project) Field Experiment), undertaken in the prairies of central Kansas from 1987 through 1989 (e.g. Hall et al., 1991, 1992, Sellers and Hall., 1992, Walthall, et al., 1993). The objectives of FIFE were to improve the understanding of interactions between the atmosphere and the vegetated land surface and to investigate the use of satellite observations to infer climatologically significant land surface parameters (Sellers and Hall., 1992). While remotely-sensed estimates of f_{PAR} were found to be accurate within a range of 10%, key issues identified for remote sensing of photosynthesis were stress related factors such as soil moisture and saturation deficit (Hall et al., 1992, Charpentier and Groffman, 1992).

One of the largest projects aiming to improve our understanding of terrestrial carbon cycling and other biosphere-atmosphere interactions was the Boreal-Ecosystem-Atmosphere Study (BOREAS), undertaken between 1993 and 1997. Specifically designed to bridge a wide range of spatial scales (e.g. Kharouk et al., 1995, Sellers et al., 1995, 1997, Potter et al., 1999, Goetz et al., 1999), BOREAS integrated repeated leaf scale, flux-tower, airborne, and spaceborne observations to investigate issues of up-scaling local observations to landscape levels (1000x1000 km) (Sellers et al., 1997). The study, located at multiple boreal forest sites in Saskatchewan and Manitoba (Canada), substantially improved the use of remote sensing for definition of vegetation structure and land cover for assessment of the surface–atmosphere exchange of mass and energy, nature and variability of surface albedo and radiation budgets, and the regional carbon balance (Gamon et al., 2004).

Most recently, validation of the MODIS GPP product was undertaken using the BigFoot approach, scaling field observations to global, satellite-based estimates of GPP. BigFoot relied on ground measurements, EC flux tower data, remotely sensed data, and ecosystem process models to represent CO_2 fluxes for different biome types. Nine BigFoot study sites spanned eight major biomes, from desert to tundra, to tropical forest (Running et al., 1999). Validation of the MODIS GPP product was mainly undertaken in the form of time series comparisons between GPP estimated from eddy covariance flux tower data and GPP from MODIS for one or more 1 km^2 cells surrounding the tower (Turner et al., 2003a,b, Xiao et al., 2004). While some of these comparisons have shown reasonable agreement between tower-based estimates of CO_2 fluxes and MODIS land cover products, numerous limitations were found and issues identified for further research: The largest error associated with the land cover classification is the simplifying assumption that each 1x1 km pixel only contains a single land cover class (Heinsch et al., 2006). This assumption generally fails to reflect the spatial heterogeneity in land cover, stand age, soil type and canopy structure for most biomes (Goulden et al., 1996). The use of a simple lookup table approach to determine ε from biome-specific parameters which do not vary in space and time (Running et al., 2000, Heinsch et al., 2002, Turner et al., 2003a), and distinguish only between 11 different vegetation types (Turner et al., 2003a, Heinsch et al., 2006) has been identified as the weak point of the GPP product as it greatly simplifies the existing spatial and temporal variability in ε. In addition, assigning values of ε on the basis of biome type assumes between-biome variability to be greater than within biome variability, which is often not realistic (Goetz and Prince, 1996, Landsberg et al., 1997). A further serious limitation is the degree to which the GCM derived inputs represent realistic estimates of climate variables because of the coarse scale of the GCM model outputs (~100 km) (Turner et al., 2003a,b). These issues, together with errors related to propagation from other underlying MODIS products (Heinsch et al., 2006), have been identified as potential sources of the differences found between satellite-based GPP estimates and field measurements for some biomes (Running et al., 1999, Coops et al., 2007).

2.5 Requirements and direction for future studies

The ability to acquire primary production from remotely-sensed data has increased considerably over the last few decades. However, from the reviewed literature, it is apparent that accurate modeling of GPP over large areas remains an active area of research with issues remaining to be solved at the leaf, stand, and landscape levels.

2.5.1 Leaf level

Arguably, the use of remote sensing for detecting photosynthesis at the leaf level is relatively well established, however many gaps remain in our understanding of the biochemical mechanisms that invoke and relax photo-protection and chlorophyll fluorescence. To date, an energy dependent component, likely induced by low pH values in the thylakoid membrane of the chloroplast (Demmig-Adams and Adams, 1996) and an energy independent component, relaxing only very slowly after more severe stress situations such as droughts or winter stress, have been identified (Adams et al., 1999). While the energy dependent component is reasonably well understood, less is known about the processes driving the energy independent component (Demmig and Winter, 1988). Additionally, the role of the lutein cycle (Bungard et al., 1999) in photosynthetic efficiency is largely unexplored. Comprehensive understanding of these biochemical mechanisms driving the photochemical reaction process across a wide range of species is a key requirement for up-scaling leaf-level estimates to stand and global levels.

2.5.2 Stand level

At the stand level, uncertainty remains in understanding the temporal dynamics involved in photosynthetic efficiency and the contributions of shaded and sunlit parts of the canopy (Demmig-Adams et al., 1998). To improve the understanding of stand level GPP, modeling requires observation of vegetation canopies in a continuous mode and under varying illumination and environmental conditions. Accurate algorithms are required to distinguish the reflectance signals obtained from such observations between physiologically and physically induced components. The application of bi-directional reflectance distribution functions (BRDF) (e.g. Wanner et al., 1995, Li and Strahler, 1995) can help in this regard. Separation of reflectance signals however, is not trivial, as the high physiologically induced variability in canopy reflectance especially with respect to ε makes acquisition of BRDF-parameters from inversion of semi-empirical algorithms difficult (Los et al., 2005).

Possible ways to address these issues include spectral measurements from permanently established, near surface remote sensing devices, facilitating intensive and continuous studies of canopy level reflectance. At present, relatively few spectral datasets have been acquired using radiometers mounted on canopy cranes (Mariscal et al., 2004) or towers (Leuning et al., 2006). Future research would benefit from integrated, tower-based approaches to intensify measures of reflectance properties and temporal variability of GPP at networked sites, which can then be linked directly to CO_2 fluxes determined using the eddy covariance technique. Based on physical reflectance properties studied at the stand level using near surface remote sensing, mathematical models can be developed which, when calibrated from high resolution satellite platforms on a daily and fully spatial basis, may facilitate detailed estimates of photosynthetic flux from space. Hence, the success for estimating carbon fluxes at broader levels will heavily depend on our understanding of the dynamics and interrelations of spectral reflectance obtained at the stand scale.

2.5.3 Landscape level

At the landscape scale, research focused on the complex interactions between the biosphere and atmosphere targeting issues of up-scaling from site observations to ecoregion, biome, and global levels is underway and must be actively pursued, with major challenges evident in the areas of modelling and minimising signal distortions, due to both the atmosphere and directional reflectance effects. Our understanding of bi-directional reflectance, radiative transfer modeling, and interactions between reflectance and forest stand structure has benefited greatly from multi-angle instruments, including the POLDER (Polarization and Directionality of Earth Reflectance) (Deschamps et al., 1994) and MISR (Multi-angle Imaging Spectrometer) (e.g. Lyapustin et al., 2007) sensors, specifically designed to address BRDF characteristics of the Earth surface from space (Leroy et al., 1997, Gamon et al., 2006). However, several challenges related to atmospheric effects remain, primarily caused by water vapour and aerosols, as these, even though they are well understood, are difficult to correct due to their high temporal and spatial variability (Hall et al., 1995).

Direct approaches regarding global prediction of ε from remote sensing, using both xanthophyll-related pigment changes in the visible spectrum and fluorescence measurements in the near infrared region show promise to facilitate precise estimation of ε over large areas thereby overcoming a number of issues related to indirect approaches using stress related factors. Global estimation of vegetation stresses, however, provides valuable information that can help understanding the observed physiological responses of plant canopies. Satellite sensors providing high spectral and spatial resolution hold promise to facilitate acquisition of detailed stress maps of plant canopies which will allow mutual validation of ε acquired from direct and indirect approaches in a spatially comprehensive mode.

Currently, there is an absence of spaceborne sensors available with wavebands narrow enough to obtain reflectance measurements specifically in the PRI region. EO1-Hyperion was the first hyperspectral sensor in space with a contiguous spectral bandwidth of 10 nm. However, being designed as a demonstration instrument, this sensor is limited in its signal to noise ratio and calibration accuracy (Datt et al., 2003, Khurshid et al., 2006). The MODIS sensor provides wavebands close to the PRI region (Drolet et al., 2005), however, initial results indicate that the approach at this stage does not sufficiently account for the spatial heterogeneity of the landscape. Additionally, there is a lack of algorithms available for processing the full suite of MODIS water bands over land surfaces which limits the routine application of the approach. Future generation satellite sensors, data processing streams, and resultant data products can combine to help address and eventually overcome these issues.

The large area characterization of primary production depends on comprehensive testing and continued efforts of land surface validation, requiring coordinated scientific networking to meaningfully combine findings and results representative of a range of spatial scales. Networking approaches such as the Fluxnet community have greatly improved our knowledge on interactions of plant physiological responses to changing environmental conditions in the past. Intensified and networked research efforts are required for improved understanding of physically and physiologically induced reflectance properties of various vegetation types to facilitate modeling of GPP estimates representative of large areas. The ability to characterize GPP over a range of scales will greatly benefit from interdisciplinary communication and networking for both development of algorithms and product validation.

2.6 References

Adams, W.W., Demmig-Adams, B., Logan, B.A., Barker, D.H. and Osmond, C.B. (1999) Rapid Changes in Xanthophyll Cycle-Dependent Energy Dissipation and Photosystem Ii Efficiency in Two Vines, *Stephania Japonica* and *Smilax Australis*, Growing in the Understory of an Open Eucalyptus Forest. *Plant Cell and Environment* **22**, 125-136.

Ananyev, G., Kolber, Z.S., Klimov, D., Falkowski, P.G., Berry, J.A., Rascher, U., Martin, R. and Osmond, B. (2005) Remote Sensing of Heterogeneity in Photosynthetic Efficiency, Electron Transport and Dissipation of Excess Light in *Populus Deltoides* Stands Under Ambient and Elevated CO_2 Concentrations, and in a Tropical Forest Canopy, Using a New Laser-Induced Fluorescence Transient Device. *Global Change Biology* **11**, 1195-1206.

Asrar, G., Fuchs, M., Kanemasu, E.T. and Hatfield, J.L. (1984) Estimating Absorbed Photosynthetic Radiation and Leaf-Area Index From Spectral Reflectance in Wheat. *Agronomy Journal* **76**, 300-306.

Badhwar, G.D. and Henderson, K.E. (1981) Estimating Development Stages of Corn From Spectral Data - an Initial Model. *Agronomy Journal* **73**, 748-755.

Badhwar, G.D., Macdonald, R.B. and Mehta, N.C. (1986) Satellite-Derived Leaf-Area-Index and Vegetation Maps as Input to Global Carbon-Cycle Models - a Hierarchical Approach. *International Journal of Remote Sensing* **7**, 265-281.

Baker, K.S. and Frouin, R. (1987) Relation Between Photosynthetically Available Radiation and Total Insolation at the Ocean Surface Under Clear Skies. *Limnology and Oceanography* **32**, 1370-1377.

Baldocchi, D.D. (2003) Assessing the Eddy Covariance Technique for Evaluating Carbon Dioxide Exchange Rates of Ecosystems: Past, Present and Future. *Global Change Biology* **9**, 479-492.

Baret, F., Houles, V. and Guerif, M. (2007) Quantification of Plant Stress Using Remote Sensing Observations and Crop Models: the Case of Nitrogen Management. *Journal of Experimental Botany* **58**, 869-880.

Barton, C.V.M. and North, P.R.J. (2001) Remote Sensing of Canopy Light-Use Efficiency Using the Photochemical Reflectance Index - Model and Sensitivity Analysis. *Remote Sensing of Environment* **78**, 264-273.

Bausch, W.C. and Duke, H.R. (1996) Remote Sensing of Plant Nitrogen Status in Corn. *Transactions of the ASAE* **39**, 1869-1875.

Bicheron, P. and Leroy, M. (1999) A Method of Biophysical Parameter Retrieval at Global Scale by Inversion of a Vegetation Reflectance Model. *Remote Sensing of Environment* **67**, 251-266.

Bilger, W. and Björkman, O. (1990) Role of the Xanthophyll Cycle in Photoprotection Elucidated by Measurements of Light-Induced Absorbency Changes, Fluorescence and Photosynthesis in Leaves of *Hedera-Canariensis*. *Photosynthesis Research* **25**, 173-185.

Bilger, W., Björkman, O. and Thayer, S.S. (1989) Light-Induced Spectral Absorbance Changes in Relation to Photosynthesis and the Epoxidation State of Xanthophyll Cycle Components in Cotton Leaves. *Plant Physiology* **91**, 542-551.

Blackburn, W.J. and Proctor, J.T.A. (1983) Estimating Photosynthetically Active Radiation From Measured Solar Irradiance. *Solar Energy* **31**, 233-234.

Bland, W.L. (1996) Uncertainty of Daily Insolation Estimates From a Mesoscale Pyranometer Network. *Journal of Atmospheric and Oceanic Technology* **13**, 255-261.

Bland, W.L. and Clayton, M.K. (1994) Spatial Structure of Solar-Radiation in Wisconsin. *Agricultural and Forest Meteorology* **69**, 75-84.

Bungard, R.A., Ruban, A.V., Hibberd, J.M., Press, M.C., Horton, P. and Scholes, J.D. (1999) Unusual Carotenoid Composition and a New Type of Xanthophyll Cycle in Plants. *Proceedings of the National Academy of Sciences of the United States of America* **96**, 1135-1139.

Buschmann, C. and Lichtenthaler, H.K. (1999) Contribution of Chlorophyll Fluorescence to the Reflectance of Leaves in Stressed Plants as Determined With the Viraf-Spectrometer. *Zeitschrift Für Naturforschung C-A Journal of Biosciences* **54**, 849-855.

Buschmann, C. and Lichtenthaler, H.K. (1977) Hill-Activity and P700 Concentration of Chloroplasts Isolated From Radish Seedlings Treated With Beta-Indoleacetic Acid, Kinetin or Gibberellic-Acid. *Zeitschrift Für Naturforschung C-a Journal of Biosciences* **32**, 798-802.

Carter, C.D., King, G.B. and Laurendeau, N.M. (1990) Laser-Induced Fluorescence Measurements of OH in Laminar $C_2H_6/O_2/N_2$ Flames at High-Pressure. *Combustion Science and Technology* **71**, 263-273.

Cecchi, G., Mazzinghi, P., Pantani, L., Valentini, R., Tirelli, D. and Deangelis, P. (1994) Remote-Sensing of Chlorophyll-a Fluorescence of Vegetation Canopies .1. Near and Far-Field Measurement Techniques. *Remote Sensing of Environment* **47**, 18-28.

Charpentier, M.A. and Groffman, P.M. (1992) Soil-Moisture Variability Within Remote-Sensing Pixels. *Journal of Geophysical Research-Atmospheres* **97**, 18987-18995.

Chen, J.M. and Black, T.A. (1992) Defining Leaf-Area Index for Non-Flat Leaves. *Plant Cell and Environment* **15**, 421-429.

Chen, J.M. and Cihlar, J. (1996) Retrieving Leaf Area Index of Boreal Conifer Forests Using Landsat-TM Images. *Remote Sensing of Environment* **55**, 153-162.

Chen, X.X. and Vierling, L. (2006) Spectral Mixture Analyses of Hyperspectral Data Acquired Using a Tethered Balloon. *Remote Sensing of Environment* **103**, 338-350.

Cheng, Y.F., Gamon, J.A., Fuentes, D.A., Mao, Z.Y., Sims, D.A., Qiu, H.L., Claudio, H., Huete, A. and Rahman, A.F. (2006) A Multi-Scale Analysis of Dynamic Optical Signals in a Southern California Chaparral Ecosystem: a Comparison of Field, AVIRIS and MODIS Data. *Remote Sensing of Environment* **103**, 369-378.

Comins, H.N. and McMurtrie, R.E. (1993) Long-Term Response of Nutrient-Limited Forests to CO_2 Enrichment - Equilibrium Behavior of Plant-Soil Models. *Ecological Applications* **3**, 666-681.

Coops, NC, Black, TA, Jassal, RS, Trofymow, JA, Morgenstern, K. (2007) Comparison of MODIS, Eddy Covariance Determined and Physiologically Modeled Gross Primary Production (GPP) in a Douglas-Fir Forest Stand. *Remote Sensing of Environment* **107**, 385-401.

Corp, L.A., Middleton, E.M., Mcmurtrey, J.E., Campbell, P.K.E. and Butcher, L.M. (2006) Fluorescence Sensing Techniques for Vegetation Assessment. *Applied Optics* **45**, 1023-1033.

Datt, B., Mcvicar, T.R., Van Niel, T.G., Jupp, D.L.B. and Pearlman, J.S. (2003) Preprocessing EO-1 Hyperion Hyperspectral Data to Support the Application of Agricultural Indexes. *IEEE-Transactions on Geoscience and Remote Sensing* **41**, 1246-1259.

Daughtry, C.S.T., Gallo, K.P. and Bauer, M.E. (1983) Spectral Estimates of Solar-Radiation Intercepted by Corn Canopies. *Agronomy Journal* **75**, 527-531.

Dawson, T.P., North, P.R.J., Plummer, S.E. and Curran, P.J. (2003) Forest Ecosystem Chlorophyll Content: Implications for remotely-sensed Estimates of Net Primary Productivity. *International Journal of Remote Sensing* **24**, 611-617.

Demmig-Adams, B. and Adams, W.W. (2000) Photosynthesis - Harvesting Sunlight Safely. *Nature* **403**, 371-372

Demmig-Adams, B., Moeller, D.L., Logan, B.A. and Adams, W.W. (1998) Positive Correlation Between Levels of Retained Zeaxanthin Plus Antheraxanthin and Degree of Photoinhibition in Shade Leaves of *Schefflera Arboricola* (Hayata) Merrill. *Planta* **205**, 367-374.

Demmig, B. and Winter, K. (1988) Characterization of 3 Components of Non-Photochemical Fluorescence Quenching and Their Response to Photo-Inhibition. *Australian Journal of Plant Physiology* **15**, 163-177.

Demmig-Adams, B. (1990) Carotenoids and Photoprotection in Plants - a Role for the Xanthophyll Zeaxanthin. *Biochimica et Biophysica Acta* **1020**, 1-24.

Demmig-Adams, B. and Adams, W.W. (1996) The Role of Xanthophyll Cycle Carotenoids in the Protection of Photosynthesis. *Trends in Plant Science* **1**, 21-26.

Deschamps, P.Y., Breon, F.M., Leroy, M., Podaire, A., Bricaud, A., Buriez, J.C. and Seze, G. (1994) The Polder Mission - Instrument Characteristics and Scientific Objectives. *IEEE- Transactions on Geoscience and Remote Sensing* **32**, 598-615.

Deshayes, M., Guyon, D., Jeanjean, H., Stach, N., Jolly, A. and Hagolle, O. (2006) The Contribution of Remote Sensing to the Assessment of Drought Effects in Forest Ecosystems. *Annals of Forest Science* **63**, 579-595.

Drolet, G.G., Huemmrich, K.F., Hall, F.G., Middleton, E.M., Black, T.A., Barr, A.G. and Margolis, H.A. (2005) A MODIS-Derived Photochemical Reflectance Index to Detect Inter-Annual Variations in the Photosynthetic Light-Use Efficiency of a Boreal Deciduous Forest. *Remote Sensing of Environment* **98**, 212-224.

Dubayah, R. and Loechel, S. (1997) Modeling Topographic Solar Radiation Using Goes Data. *Journal of Applied Meteorology* **36**, 141-154.

Duchemin, B., Guyon, D. and Lagouarde, J.P. (1999) Potential and Limits of NOAA-AVHRR Temporal Composite Data for Phenology and Water Stress Monitoring of Temperate Forest Ecosystems. *International Journal of Remote Sensing* **20**, 895-917.

Eck, T.F. and Dye, D.G. (1991) Satellite Estimation of Incident Photosynthetically Active Radiation Using Ultraviolet Reflectance. *Remote Sensing of Environment* **38**, 135-146.

Fassnacht, K.S. and Gower, S.T. (1997) Interrelationships Among the Edaphic and Stand Characteristics, Leaf Area Index, and Aboveground Net Primary Production of Upland Forest Ecosystems in North Central Wisconsin. *Canadian Journal of Forest Research-Revue Canadienne De Recherche Forestiere* **27**, 1058-1067.

Field C. and Mooney, H.A. (1986) The Photosynthesis-Nitrogen Relationship in Wild Plants. In: T.Givnish, Editor. On the Economy of Plant Form and Function. *Cambridge Univ. Press, Cambridge, U.K.* 22-55.

Field, C.B. (1991) Ecological Scaling of Carbon Gain to Stress and Resource Availability. In: Integrated Responses of Plants to Stress (eds. Mooney, HA Winner, SE Pell, EJ). *Academic Press, San Diego, CA* 35-65.

Field, C.B., Jackson, R.B. and Mooney, H.A. (1995) Stomatal Responses to Increased CO_2 - Implications From the Plant to the Global-Scale. *Plant Cell and Environment* **18**, 1214-1225.

Filella, I., Amaro, T., Araus, J.L. and Peñuelas, J. (1996) Relationship Between Photosynthetic Radiation-Use Efficiency of Barley Canopies and the Photochemical Reflectance Index (PRI). *Physiologia Plantarum* **96**, 211-216.

Frouin, R. and Pinker, R.T. (1995) Estimating Photosynthetically Active Radiation (PAR) at the Earths Surface From Satellite-Observations. *Remote Sensing of Environment* **51**, 98-107.

Gamon, J.A., Field, C.B., Bilger, W., Björkman, O., Fredeen, A.L. and Peñuelas, J. (1990) Remote-Sensing of the Xanthophyll Cycle and Chlorophyll Fluorescence in Sunflower Leaves and Canopies. *Oecologia* **85**, 1-7.

Gamon, J.A., Huemmrich, K.F., Peddle, D.R., Chen, J., Fuentes, D., Hall, F.G., Kimball, J.S., Goetz, S., Gu, J., Mcdonald, K.C., Miller, J.R., Moghaddam, M., Rahman, A.F., Roujean, J.L., Smith, E.A., Walthall, C.L., Zarco-Tejada, P., Hu, B., Fernandes, R. and Cihlar, J. (2004) Remote Sensing in Boreas: Lessons Learned. *Remote Sensing of Environment* **89**, 139-162.

Gamon, J.A., Peñuelas, J. and Field, C.B. (1992) A Narrow-Waveband Spectral Index That Tracks Diurnal Changes in Photosynthetic Efficiency. *Remote Sensing of Environment* **41**, 35-44.

Gamon, J.A., Rahman, A.F., Dungan, J.L., Schildhauer, M. and Huemmrich, K.F. (2006) Spectral Network (SpecNet) - What Is It and Why Do We Need It? *Remote Sensing of Environment* **103**, 227-235.

Gamon, J.A. and Surfus, J.S. (1999) Assessing Leaf Pigment Content and Activity With a Reflectometer. *New Phytologist* **143**, 105-117.

Gao, W. (1994) Atmosphere-Biosphere Exchange Flux of Carbon-Dioxide in a Tallgrass Prairie Modeled With Satellite Spectral Data. *Journal of Geophysical Research-Atmospheres* **99**, 1317-1327.

Garcia-Plazaola, J.I., Hormaetxe, K., Hernandez, A., Olano, J.M. and Becerril, J.M. (2004) The Lutein Epoxide Cycle in Vegetative Buds of Woody Plants. *Functional Plant Biology* **31**, 815-823.

Gautier, C., Diak, G. and Masse, S. (1980) A Simple Physical Model to Estimate Incident Solar-Radiation at the Surface From Goes Satellite Data. *Journal of Applied Meteorology* **19**, 1005-1012.

Gautier, C. and Frouin, R. (1992) Net Surface Solar Irradiance Variability in the Central Equatorial Pacific During 1982-1985. *Journal of Climate* **5**, 30-55.

Gitelson, A.A., Buschmann, C. and Lichtenthaler, H.K. (1999) The Chlorophyll Fluorescence Ratio F-735/F-700 as an Accurate Measure of the Chlorophyll Content in Plants. *Remote Sensing of Environment* **69**, 296-302.

Gobron, N., Pinty, B. and Verstraete, M.M. (1997) Theoretical Limits to the Estimation of the Leaf Area Index on the Basis of Visible and Near-Infrared Remote Sensing Data. *IEEE- Transactions on Geoscience and Remote Sensing* **35**, 1438-1445.

Goel, N.S. Models of Vegetation Canopy Reflectance and Their Use in Estimation of Biophysical Parameters from Reflectance Data. *Remote Sensing Reviews* **4**, 1-212.

Goel, N.S. and Grier, T. (1988) Estimation of Canopy Parameters for Inhomogeneous Vegetation Canopies From Reflectance Data .3. Trim - a Model for Radiative-Transfer in Heterogeneous 3-Dimensional Canopies. *Remote Sensing of Environment* **25**, 255-293.

Goel, N.S., Rozehnal, I. and Thompson, R.L. (1991) A Computer-Graphics Based Model for Scattering From Objects of Arbitrary Shapes in the Optical-Region. *Remote Sensing of Environment* **36**, 73-104.

Goel, N.S., Strebel, D.E. and Thompson, R.L. (1984) Inversion of Vegetation Canopy Reflectance Models for Estimating Agronomic Variables .2. Use of Angle Transforms and Error Analysis as Illustrated by Suits Model. *Remote Sensing of Environment* **14**, 77-111.

Goel, N.S. and Thompson, R.L. (1984) Inversion of Vegetation Canopy Reflectance Models for Estimating Agronomic Variables. *Remote Sensing of Environment* **16**, 69-85.

Goetz, S.J. and Prince, S.D. Modelling Terrestrial Carbon Exchange and Storage: Evidence and Implications of Functional Convergence in Light-Use Efficiency. *Advances in Ecological Research* **28,** 57-92.

Goetz, S.J., Prince, S.D., Goward, S.N., Thawley, M.M., Small, J. and Johnston, A. (1999) Mapping Net Primary Production and Related Biophysical Variables With Remote Sensing: Application to the Boreas Region. *Journal of Geophysical Research-Atmospheres* **104**, 27719-27734.

Goulden, M.L., Munger, J.W., Fan, S.M., Daube, B.C. and Wofsy, S.C. (1996) Exchange of Carbon Dioxide by a Deciduous Forest: Response to Interannual Climate Variability. *Science* **271**, 1576-1578.

Goward S.N. and Dye (1987) Evaluating North American Net Primary Productivity with Satellite Observations . *Adv. Space Res.* **7**, 165-174.

Goward, S.N. and Huemmrich, K.F. (1992) Vegetation Canopy PAR Absorptance and the Normalized Difference Vegetation Index - an Assessment Using the Sail Model. *Remote Sensing of Environment* **39**, 119-140.

Goward, S.N., Tucker, C.J. and Dye, D.G. (1985) North-American Vegetation Patterns Observed With the NOAA-7 Advanced Very High-Resolution Radiometer. *Vegetatio* **64**, 3-14.

Guerif, M. and Duke, C.L. (2000) Adjustment Procedures of a Crop Model to the Site Specific Characteristics of Soil and Crop Using Remote Sensing Data Assimilation. *Agriculture Ecosystems & Environment* **81**, 57-69.

Hall, F.G., Huemmrich, K.F., Goetz, S.J., Sellers, P.J. and Nickeson, J.E. (1992) Satellite Remote-Sensing of Surface-Energy Balance - Success, Failures, and Unresolved Issues in FIFE. *Journal of Geophysical Research-Atmospheres* **97**, 19061-19089.

Hall, F.G., Huemmrich, K.F. and Goward, S.N. (1990) Use of Narrow-Band Spectra to Estimate the Fraction of Absorbed Photosynthetically Active Radiation. *Remote Sensing of Environment* **32**, 47-54.

Hall, F.G., Sellers, P.J., Strebel, D.E., Kanemasu, E.T., Kelly, R.D., Blad, B.L., Markham, B.J., Wang, J.R. and Huemmrich, F. (1991) Satellite Remote-Sensing of Surface-Energy and Mass Balance - Results From FIFE. *Remote Sensing of Environment* **35**, 187-199.

Hall, F.G., Townshend, J.R. and Engman, E.T. (1995) Status of Remote-Sensing Algorithms for Estimation of Land-Surface State Parameters. *Remote Sensing of Environment* **51**, 138-156.

Hamilton, J.G., Delucia, E.H., George, K., Naidu, S.L., Finzi, A.C. and Schlesinger, W.H. (2002) Forest Carbon Balance Under Elevated CO_2. *Oecologia* **131**, 250-260.

Heinsch, F.A., Reeves, M., Votava, P., Kang, S., Milesi, C., Zhao, M., Glassy, J., Jolly, W.M., Loehman, R., Bowker, C.F., Kimball, J.S., Nemani, R.R. and Running, S.W. (2002) User's Guide GPP and NPP (MOD17A2/A3) Products NASA MODIS Land Algorithm. Website, accessed April 07. Available at: http://www.ntsg.umt.edu/modis/MOD17UsersGuide.pdf.

Heinsch, F.A., Zhao, M.S., Running, S.W., Kimball, J.S., Nemani, R.R., Davis, K.J., Bolstad, P.V., Cook, B.D., Desai, A.R., Ricciuto, D.M., Law, B.E., Oechel, W.C., Kwon, H., Luo, H.Y., Wofsy, S.C., Dunn, A.L., Munger, J.W., Baldocchi, D.D., Xu, L.K., Hollinger, D.Y., Richardson, A.D., Stoy, P.C., Siqueira, M.B.S., Monson, R.K., Burns, S.P. and Flanagan, L.B. (2006) Evaluation of Remote Sensing Based Terrestrial Productivity From MODIS Using Regional Tower Eddy Flux Network Observations. *IEEE-Transactions on Geoscience and Remote Sensing* **44**, 1908-1925.

Henderson, K.E. and Badhwar, G.D. (1984) An Initial Model for Estimating Soybean Development Stages From Spectral Data. *Remote Sensing of Environment* **14**, 55-63.

Huemmrich, K.F. and Goward, S.N. (1997) Vegetation Canopy Par Absorptance and NDVI: an Assessment for Ten Tree Species With the Sail Model. *Remote Sensing of Environment* **61**, 254-269.

Huemmrich, K.F., Privette, J.L., Mukelabai, M., Myneni, R.B. and Knyazikhin, Y. (2005) Time-Series Validation of MODIS Land Biophysical Products in a Kalahari Woodland, Africa. *International Journal of Remote Sensing* **26**, 4381-4398.

Huete, A., Didan, K., Miura, T., Rodriguez, E.P., Gao, X. and Ferreira, L.G. (2002) Overview of the Radiometric and Biophysical Performance of the MODIS Vegetation Indices. *Remote Sensing of Environment* **83**, 195-213.

Huete, A.R., Didan, K., Shimabukuro, Y.E., Ratana, P., Saleska, S.R., Hutyra, L.R., Yang, W.Z., Nemani, R.R. and Myneni, R. (2006) Amazon Rainforests Green-up With Sunlight in Dry Season. *Geophysical Research Letters* **33**,

Humphreys, E.R., Black, T.A., Morgenstern, K., Cai, T.B., Drewitt, G.B., Nesic, Z. and Trofymow, J.A. (2006) Carbon Dioxide Fluxes in Coastal Douglas-Fir Stands at Different Stages of Development After Clearcut Harvesting. *Agricultural and Forest Meteorology* **140**, 6-22.

Jacquemoud, S. (1993) Inversion of the Prospect + Sail Canopy Reflectance Model From AVIRIS Equivalent Spectra - Theoretical-Study. *Remote Sensing of Environment* **44**, 281-292.

Jacquemoud, S., Bacour, C., Poilve, H. and Frangi, J.P. (2000) Comparison of Four Radiative Transfer Models to Simulate Plant Canopies Reflectance: Direct and Inverse Mode. *Remote Sensing of Environment* **74**, 471-481.

Janzen, H.H. (2004) Carbon Cycling in Earth Systems - a Soil Science Perspective. *Agriculture Ecosystems & Environment* **104**, 399-417.

Kergoat, L., Lafont, S., Douville, H., Berthelot, B., Dedieu, G., Planton, S. and Royer, J.F. (2002) Impact of Doubled CO_2 on Global-Scale Leaf Area Index and Evapotranspiration: Conflicting Stomatal Conductance and LAI Responses. *Journal of Geophysical Research-Atmospheres* **107**, Kharouk, V.I., Middleton, E.M., Spencer, S.L., Rock, B.N. and Williams, D.L. (1995) Aspen Bark Photosynthesis and its Significance to Remote-Sensing and Carbon Budget Estimates in the Boreal Ecosystem. *Water Air and Soil Pollution* **82**, 483-497.

Khurshid, K.S., Staenz, K., Sun, L.X., Neville, R., White, H.P., Bannari, A., Champagne, C.M. and Hitchcock, R. (2006) Preprocessing of EO-1 Hyperion Data. *Canadian Journal of Remote Sensing* **32**, 84-97.

Kljun, N., Calanca, P., Rotachhi, M.W. and Schmid, H.P. (2004) A Simple Parameterisation for Flux Footprint Predictions. *Boundary-Layer Meteorology* **112**, 503-523.

Knyazikhin Y., J. Glassy, J. L. Privette, Y. Tian, A. Lotsch, Y. Zhang, Y. Wang, J. T. Morisette, P.Votava, R.B. Myneni, R. R. Nemani and S. W. Running (1999) MODIS Leaf Area Index (LAI) and Fraction of Photosynthetically Active Radiation Absorbed by Vegetation (f_{PAR}) Product (MOD15) Algorithm Theoretical Basis Document, http://eospso.gsfc.nasa.gov/atbd/modistables.html.

Knyazikhin, Y., Martonchik, J.V., Myneni, R.B., Diner, D.J. and Running, S.W. (1998) Synergistic Algorithm for Estimating Vegetation Canopy Leaf Area Index and Fraction of Absorbed Photosynthetically Active Radiation From MODIS and MISR Data. *Journal of Geophysical Research-Atmospheres* **103**, 32257-32275.

Knyazikhin, Y., Yang, W., Dong, H., Bin, T., Shabanov, N. and Myneni, R. (2003) MODIS LAI and f_{PAR} Product on Global, Regional and Local Scales Fall Meeting 2003 of the American Geophysical Union.

Kolber, Z., Klimov, D., Ananyev, G., Rascher, U., Berry, J. and Osmond, B. (2005) Measuring Photosynthetic Parameters at a Distance: Laser Induced Fluorescence Transient (LIFT) Method for Remote Measurements of Photosynthesis in Terrestrial Vegetation. *Photosynthesis Research* **84**, 121-129.

Kvifte, G., Hegg, K. and Hansen, V. (1983) Spectral Distribution of Solar-Radiation in the Nordic Countries. *Journal of Climate and Applied Meteorology* **22**, 143-152.

Landsberg, J.J., Prince, S.D., Jarvis, P.G., McMutrie, R.E. and Luxmore, R. (1997) Energy conversion and use in forests: The analysis of forest production in terms of utilization efficiency. In: Use of Remote Sensing for Modeling of Forest Productivity (Ed. by H.L. Gholz, K. Nakane (Editor), H. Shimoda (Editor). *Kluwer Academic Publishing, The Hague,* 273-298.

Leroy, M., Deuze, J.L., Breon, F.M., Hautecoeur, O., Herman, M., Buriez, J.C., Tanre, D., Bouffies, S., Chazette, P. and Roujean, J.L. (1997) Retrieval of Atmospheric Properties and Surface Bi-directional Reflectances Over Land From Polder/Adeos. *Journal of Geophysical Research-Atmospheres* **102**, 17023-17037.

Leuning, R., Hughes, D., Daniel, P., Coops, N.C. and Newnham, G. (2006) A Multi-Angle Spectrometer for Automatic Measurement of Plant Canopy Reflectance Spectra. *Remote Sensing of Environment* **103**, 236-245.

Li, X.W. and Strahler, A.H. (1985) Geometric-Optical Modeling of a Conifer Forest Canopy. *IEEE-Transactions on Geoscience and Remote Sensing* **23**, 705-721.

Li, X.W., Strahler, A.H. and Woodcock, C.E. (1995) A Hybrid Geometric Optical-Radiative Transfer Approach for Modeling Albedo and Directional Reflectance of Discontinuous Canopies. *IEEE-Transactions on Geoscience and Remote Sensing* **33**, 466-480.

Liang, S.L., Zheng, T., Liu, R.G., Fang, H.L., Tsay, S.C. and Running, S. (2006) Estimation of Incident Photosynthetically Active Radiation From Moderate Resolution Imaging Spectrometer Data. *Journal of Geophysical Research-Atmospheres* **111**,

Liu, W.T. and Kogan, F.N. (1996) Monitoring Regional Drought Using the Vegetation Condition Index. *International Journal of Remote Sensing* **17**, 2761-2782.

Liu, X., Smith, W.L., Zhou, D.K. and Larar, A. (2006) Principal Component-Based Radiative Transfer Model for Hyperspectral Sensors: Theoretical Concept. *Applied Optics* **45**, 201-209.

Lopez, S., Gonzalez, F., Llop, R. and Cuevas, J.M. (1991) An Evaluation of the Utility of NOAA AVHRR Images for Monitoring Forest-Fire Risk in Spain. *International Journal of Remote Sensing* **12**, 1841-1851.

Los, S.O., Justice, C.O. and Tucker, C.J. (1994) A Global 1-Degrees-by-1-Degrees NDVI Data Set for Climate Studies Derived From the Gimms Continental NDVI Data. *International Journal of Remote Sensing* **15**, 3493-3518.

Los, S.O., North, P.R.J., Grey, W.M.F. and Barnsley, M.J. (2005) A Method to Convert AVHRR Normalized Difference Vegetation Index Time Series to a Standard Viewing and Illumination Geometry. *Remote Sensing of Environment* **99**, 400-411.

Luo, Y.Q. and Reynolds, J.F. (1999) Validity of Extrapolating Field CO_2 Experiments to Predict Carbon Sequestration in Natural Ecosystems. *Ecology* **80**, 1568-1583.

Lyapustin, A., Wang, Y., Kahn, R., Xiong, J., Ignatov, A., Wolfe, R., Wu, A., Holben, B. and Bruegge, C. (2007) Analysis of MODIS-MISR Calibration Differences Using Surface Albedo Around Aeronet Sites and Cloud Reflectance. *Remote Sensing of Environment* **107**, 12-21.

Mariscal, M.J., Martens, S.N., Ustin, S.L., Chen, J.Q., Weiss, S.B. and Roberts, D.A. (2004) Light-Transmission Profiles in an Old-Growth Forest Canopy: Simulations of Photosynthetically Active Radiation by Using Spatially Explicit Radiative Transfer Models. *Ecosystems* **7**, 454-467.

Martin, M.E. and Aber, J.D. (1997) High Spectral Resolution Remote Sensing of Forest Canopy Lignin, Nitrogen, and Ecosystem Processes. *Ecological Applications* **7**, 431-443.

Meroni, M. and Colombo, R. (2006) Leaf Level Detection of Solar Induced Chlorophyll Fluorescence by Means of a Subnanometer Resolution Spectroradiometer. *Remote Sensing of Environment* **103**, 438-448.

Meroni, M., Colombo, R. and Panigada, C. (2004) Inversion of a Radiative Transfer Model With Hyperspectral Observations for Lai Mapping in Poplar Plantations. *Remote Sensing of Environment* **92**, 195-206.

Monteith, J.L. (1977) Climate and Efficiency of Crop Production in Britain. *Philosophical Transactions of the Royal Society of London Series B-Biological Sciences* **281**, 277-294.

Monteith, J.L. (1972) Solar-Radiation and Productivity in Tropical Ecosystems. *Journal of Applied Ecology* **9**, 747-766.

Morgenstern, K., Black, T.A., Humphreys, E.R., Griffis, T.J., Drewitt, G.B., Cai, T.B., Nesic, Z., Spittlehouse, D.L. and Livingstone, N.J. (2004) Sensitivity and Uncertainty of the Carbon Balance of a Pacific Northwest Douglas-Fir Forest During an El-Niño La-Niña Cycle. *Agricultural and Forest Meteorology* **123**, 201-219.

Moya, I., Camenen, L., Evain, S., Goulas, Y., Cerovic, Z.G., Latouche, G., Flexas, J. and Ounis, A. (2004) A New Instrument for Passive Remote Sensing 1. Measurements of Sunlight-Induced Chlorophyll Fluorescence. *Remote Sensing of Environment* **91**, 186-197.

Myneni, R.B., Asrar, G. and Hall, F.G. (1992) A 3-Dimensional Radiative-Transfer Method for Optical Remote-Sensing of Vegetated Land Surfaces. *Remote Sensing of Environment* **41**, 105-121.

Myneni, R.B., Hoffman, S., Knyazikhin, Y., Privette, J.L., Glassy, J., Tian, Y., Wang, Y., Song, X., Zhang, Y., Smith, G.R., Lotsch, A., Friedl, M., Morisette, J.T., Votava, P., Nemani, R.R. and Running, S.W. (2002) Global Products of Vegetation Leaf Area and Fraction Absorbed Par From Year One of MODIS Data. *Remote Sensing of Environment* **83**, 214-231.

Myneni, R.B., Nemani, R.R. and Running, S.W. (1997) Estimation of Global Leaf Area Index and Absorbed Par Using Radiative Transfer Models. *IEEE-Transactions on Geoscience and Remote Sensing* **35**, 1380-1393.

Myneni, R.B., Ross, J. and Asrar, G. (1989) A Review on the Theory of Photon Transport in Leaf Canopies. *Agricultural and Forest Meteorology* **45**, 1-153.

Myneni, R.B. and Williams, D.L. (1994) On the Relationship Between F_{APAR} and NDVI. *Remote Sensing of Environment* **49**, 200-211.

Nemani, R.R. and Running, S.W. (1989) Estimation of Regional Surface-Resistance to Evapotranspiration From NDVI and Thermal-IR AVHRR Data. *Journal of Applied Meteorology* **28**, 276-284.

Nichol, C.J., Huemmrich, K.F., Black, T.A., Jarvis, P.G., Walthall, C.L., Grace, J. and Hall, F.G. (2000) Remote Sensing of Photosynthetic-Light-Use Efficiency of Boreal Forest. *Agricultural and Forest Meteorology* **101**, 131-142.

Nichol, C.J., Lloyd, J., Shibistova, O., Arneth, A., Roser, C., Knohl, A., Matsubara, S. and Grace, J. (2002) Remote Sensing of Photosynthetic-Light-Use Efficiency of a Siberian Boreal Forest. *Tellus Series B-Chemical and Physical Meteorology* **54**, 677-687.

Ollinger, S.V., Smith, M.L., Martin, M.E., Hallett, R.A., Goodale, C.L. and Aber, J.D. (2002) Regional Variation in Foliar Chemistry and N Cycling Among Forests of Diverse History and Composition. *Ecology* **83**, 339-355.

Peñuelas, J., Filella, I. and Gamon, J.A. (1995) Assessment of Photosynthetic Radiation-Use Efficiency With Spectral Reflectance. *New Phytologist* **131**, 291-296.

Peñuelas, J., Gamon, J.A., Fredeen, A.L., Merino, J. and Field, C.B. (1994) Reflectance Indexes Associated With Physiological-Changes in Nitrogen-Limited and Water-Limited Sunflower Leaves. *Remote Sensing of Environment* **48**, 135-146.

Pinker, R.T. and Ewing, J.A. (1985) Modeling Surface Solar-Radiation - Model Formulation and Validation. *Journal of Climate and Applied Meteorology* **24**, 389-401.

Pinker, R.T. and Laszlo, I. (1992) Modeling Surface Solar Irradiance for Satellite Applications on a Global Scale. *Journal of Applied Meteorology* **31**, 194-211.

Prihodko L, Goward SN (1997). Estimation of Air Temperature from Remotely-Sensed Surface Observations. *Remote Sensing of Environment* **60**, 335-346.

Potter, C.S., Coughlan, J.C. and Brooks, V. (1999) Investigations of Boreas Spatial Data in Support of Regional Ecosystem Modeling. *Journal of Geophysical Research-Atmospheres* **104**, 27771-27788.

Potter, C.S., Randerson, J.T., Field, C.B., Matson, P.A., Vitousek, P.M., Mooney, H.A. and Klooster, S.A. (1993) Terrestrial Ecosystem Production - A Process Model-Based on Global Satellite and Surface Data. *Global Biogeochemical Cycles* **7**, 811-841.

Prevot, L., Chauki, H., Troufleau, D., Weiss, M., Baret, F. and Brisson, N. (2003) Assimilating Optical and Radar Data Into the Stics Crop Model for Wheat. *Agronomie* **23**, 297-303.

Price, J.C. (1993) Estimating Leaf-Area Index From Satellite Data. *IEEE-Transactions on Geoscience and Remote Sensing* **31**, 727-734.

Prince, S.D. (1991) Satellite Remote-Sensing of Primary Production - Comparison of Results for Sahelian Grasslands 1981-1988. *International Journal of Remote Sensing* **12**, 1301-1311.

Prince, S.D. and Goward, S.N. (1996) Evaluation of the NOAA/NASA Pathfinder AVHRR Land Data Set for Global Primary Production Modelling. *International Journal of Remote Sensing* **17**, 217-221.

Prince, S.D. and Goward, S.N. (1995) Global Primary Production: a Remote Sensing Approach. *Journal of Biogeography* **22**, 815-835.

Privette, J.L., Emery, W.J. and Schimel, D.S. (1996) Inversion of a Vegetation Reflectance Model With NOAA AVHRR Data. *Remote Sensing of Environment* **58**, 187-200.

Rahman, A.F., Gamon, J.A., Fuentes, D.A., Roberts, D.A. and Prentiss, D. (2001) Modeling Spatially Distributed Ecosystem Flux of Boreal Forest Using Hyperspectral Indices From AVIRIS Imagery. *Journal of Geophysical Research-Atmospheres* **106**, 33579-33591.

Rahman, A.F., Sims, D.A., Cordova, V.D. and El-Masri, B.Z. (2005) Potential of MODIS EVI and Surface Temperature for Directly Estimating Per-Pixel Ecosystem C Fluxes. *Geophysical Research Letters* **32**,

Rao, C.R.N. (1984) Photosynthetically Active Components of Global Solar-Radiation - Measurements and Model Computations. *Archives for Meteorology Geophysics and Bioclimatology Series B-Theoretical and Applied Climatology* **34**, 353-364.

Rascher, U., Liebig, M. and Luttge, U. (2000) Evaluation of Instant Light-Response Curves of Chlorophyll Fluorescence Parameters Obtained With a Portable Chlorophyll Fluorometer on Site in the Field. *Plant Cell and Environment* **23**, 1397-1405.

Reich, P.B., Walters, M.B. and Ellsworth, D.S. (1997) From Tropics to Tundra: Global Convergence in Plant Functioning. *Proceedings of the National Academy of Sciences of the United States of America* **94**, 13730-13734.

Rosema, A., Snel, J.F.H., Zahn, H., Buurmeijer, W.F. and Van Hove, L.W.A. (1998) The Relation Between Laser-Induced Chlorophyll Fluorescence and Photosynthesis. *Remote Sensing of Environment* **65**, 143-154.

Running, S.W., Baldocchi, D.D., Turner, D.P., Gower, S.T., Bakwin, P.S. and Hibbard, K.A. (1999) A Global Terrestrial Monitoring Network Integrating Tower Fluxes, Flask Sampling, Ecosystem Modeling and Eos Satellite Data. *Remote Sensing of Environment* **70**, 108-127.

Running, S.W. and Nemani, R.R. (1988) Relating Seasonal Patterns of the AVHRR Vegetation Index to Simulated Photosynthesis and Transpiration of Forests in Different Climates. *Remote Sensing of Environment* **24**, 347-367.

Running, S.W., Nemani, R.R., Heinsch, F.A., Zhao, M.S., Reeves, M. and Hashimoto, H. (2004) A Continuous Satellite-Derived Measure of Global Terrestrial Primary Production. *Bioscience* **54**, 547-560.

Running, S.W., Queen, L. and Thornton, M. (2000) The Earth Observing System and Forest Management. *Journal of Forestry* **98**, 29-31.

Sellers, P.J. (1985) Canopy Reflectance, Photosynthesis and Transpiration. *International Journal of Remote Sensing* **6**, 1335-1372.

Sellers, P.J. (1987) Canopy Reflectance, Photosynthesis, and Transpiration .2. The Role of Biophysics in the Linearity of Their Interdependence. *Remote Sensing of Environment* **21**, 143-183.

Sellers, P.J. and Hall, F.G. (1992) FIFE in 1992 - Results, Scientific Gains, and Future-Research Directions. *Journal of Geophysical Research-Atmospheres* **97**, 19091-19109.

Sellers, P.J., Hall, F.G., Kelly, R.D., Black, A., Baldocchi, D., Berry, J., Ryan, M., Ranson, K.J., Crill, P.M., Lettenmaier, D.P., Margolis, H., Cihlar, J., Newcomer, J., Fitzjarrald, D., Jarvis, P.G., Gower, S.T., Halliwell, D., Williams, D., Goodison, B., Wickland, D.E. and Guertin, F.E. (1997) Boreas in 1997: Experiment Overview, Scientific Results, and Future Directions. *Journal of Geophysical Research-Atmospheres* **102**, 28731-28769.

Sellers, P.J., Heiser, M.D. and Hall, F.G. (1992) Relations Between Surface Conductance and Spectral Vegetation Indexes at Intermediate (100 m^2 to 15 km^2) Length Scales. *Journal of Geophysical Research-Atmospheres* **97**, 19033-19059.

Sellers, P.J., Los, S.O., Tucker, C.J., Justice, C.O., Dazlich, D.A., Collatz, G.J. and Randall, D.A. (1996) A Revised Land Surface Parameterization (SiB2) for Atmospheric GCMS. 2. The Generation of Global Fields of Terrestrial Biophysical Parameters From Satellite Data. *Journal of Climate* **9**, 706-737.

Sellers, P.J., Meeson, B.W., Hall, F.G., Asrar, G., Murphy, R.E., Schiffer, R.A., Bretherton, F.P., Dickinson, R.E., Ellingson, R.G., Field, C.B., Huemmrich, K.F., Justice, C.O., Melack, J.M., Roulet, N.T., Schimel, D.S. and Try, P.D. (1995) Remote-Sensing of the Land-Surface for Studies of Global Change - Models, Algorithms, Experiments. *Remote Sensing of Environment* **51**, 3-26.

Sellers, P.J., Randall, D.A., Collatz, G.J., Berry, J.A., Field, C.B., Dazlich, D.A., Zhang, C., Collelo, G.D. and Bounoua, L. (1996) A Revised Land Surface Parameterization (SiB2) for Atmospheric GCMs .1. Model Formulation. *Journal of Climate* **9**, 676-705.

Sellers, P.J., Tucker, C.J., Collatz, G.J., Los, S.O., Justice, C.O., Dazlich, D.A. and Randall, D.A. (1994) A Global 1-Degrees-by-1-Degrees NDVI Data Set for Climate Studies .2. The Generation of Global Fields of Terrestrial Biophysical Parameters From the NDVI. *International Journal of Remote Sensing* **15**, 3519-3545.

Sims, D.A., Luo, H.Y., Hastings, S., Oechel, W.C., Rahman, A.F. and Gamon, J.A. (2006) Parallel Adjustments in Vegetation Greenness and Ecosystem CO_2 Exchange in Response to Drought in a Southern California Chaparral Ecosystem. *Remote Sensing of Environment* **103**, 289-303.

Sims, D.A., Rahman, A.F., Cordova, V.D., Baldocchi, D.D., Flanagan, L.B., Goldstein, A.H., Hollinger, D.Y., Misson, L., Monson, R.K., Schmid, H.P., Wofsy, S.C. and Xu, L.K. (2005) Midday Values of Gross CO_2 Flux and Light-use efficiency During Satellite Overpasses Can Be Used to Directly Estimate Eight-Day Mean Flux. *Agricultural and Forest Meteorology* **131**, 1-12.

Smith, M.L., Martin, M.E., Plourde, L. and Ollinger, S.V. (2003) Analysis of Hyperspectral Data for Estimation of Temperate Forest Canopy Nitrogen Concentration: Comparison Between an Airborne (AVIRIS) and a Spaceborne (Hyperion) Sensor. *IEEE-Transactions on Geoscience and Remote Sensing* **41**, 1332-1337.

Stylinski, C.D., Gamon, J.A. and Oechel, W.C. (2002) Seasonal Patterns of Reflectance Indices, Carotenoid Pigments and Photosynthesis of Evergreen Chaparral Species. *Oecologia* **131**, 366-374.

Szeicz, G. (1974) Solar-Radiation for Plant-Growth. *Journal of Applied Ecology* **11**, 617-636.

Tarpley, J.D. (1979) Estimating Incident Solar-Radiation at the Surface From Geostationary Satellite Data. *Journal of Applied Meteorology* **18**, 1172-1181.

Tucker, C.J. (1986) Maximum Normalized Difference Vegetation Index Images for Sub-Saharan Africa for 1983-1985. *International Journal of Remote Sensing* **7**, 1383-1384.

Tucker, C.J. (1979) Red and Photographic Infrared Linear Combinations for Monitoring Vegetation. *Remote Sensing of Environment* **8**, 127-150.

Tucker, C.J., Fung, I.Y., Keeling, C.D. and Gammon, R.H. (1986) Relationship Between Atmospheric CO_2Variations and a Satellite-Derived Vegetation Index. *Nature* **319**, 195-199.

Tucker, C.J., Jones, W.H., Kley, W.A. and Sundstrom, G.J. (1981) A 3-Band Hand-Held Radiometer for Field Use. *Science* **211**, 281-283.

Tucker, C.J., Justice, C.O. and Prince, S.D. (1986) Monitoring the Grasslands of the Sahel 1984-1985. *International Journal of Remote Sensing* **7**, 1571-1581.

Tucker, C.J. and Sellers, P.J. (1986) Satellite Remote-Sensing of Primary Production. *International Journal of Remote Sensing* **7**, 1395-1416.

Turner, D.P., Ritts, W.D., Cohen, W.B., Gower, S.T., Zhao, M.S., Running, S.W., Wofsy, S.C., Urbanski, S., Dunn, A.L. and Munger, J.W. (2003) Scaling Gross Primary Production (GPP) Over Boreal and Deciduous Forest Landscapes in Support of MODIS GPP Product Validation. *Remote Sensing of Environment* **88**, 256-270.

Turner, D.P., Urbanski, S., Bremer, D., Wofsy, S.C., Meyers, T., Gower, S.T. and Gregory, M. (2003) A Cross-Biome Comparison of Daily Light-Use Efficiency for Gross Primary Production. *Global Change Biology* **9**, 383-395.

Van Laake, P.E. and Sanchez-Azofeifa, G.A. (2005) Mapping PAR Using MODIS Atmosphere Products. *Remote Sensing of Environment* **94**, 554-563.

Van Laake, P.E. and Sanchez-Azofeifa, G.A. (2004) Simplified Atmospheric Radiative Transfer Modelling for Estimating Incident PAR Using MODIS Atmosphere Products. *Remote Sensing of Environment* **91**, 98-113.

Vidal, A., Pinglo, F., Durand, H., Devauxros, C. and Maillet, A. (1994) Evaluation of a Temporal Fire Risk Index in Mediterranean Forests From NOAA Thermal Ir. *Remote Sensing of Environment* **49**, 296-303.

Walthall, C.L., Kim, M., Williams, D.L., Meeson, B.W., Agbu, P.A., Newcomer, J.A. and Levine, E.R. (1993) Data Sets for Modeling - a Retrospective Collection of Bi-directional Reflectance and Forest Ecosystems Dynamics Multi-sensor Aircraft Campaign Data Sets. *Remote Sensing of Environment* **46**, 340-346.

Wanner, W., Li, X. and Strahler, A.H. (1995) On the Derivation of Kernels for Kernel-Driven Models of Bi-directional Reflectance. *Journal of Geophysical Research-Atmospheres* **100**, 21077-21089.

Waring, R.H., Coops, N.C., Fan, W. and Nightingale, J.M. (2006) MODIS Enhanced Vegetation Index Predicts Tree Species Richness Across Forested Ecoregions in the Contiguous USA. *Remote Sensing of Environment* **103**, 218-226.

Weiss, A. and Norman, J.M. (1985) Partitioning Solar-Radiation Into Direct and Diffuse, Visible and Near-Infrared Components. *Agricultural and Forest Meteorology* **34**, 205-213.

Wessman, C.A., Aber, J.D., Peterson, D.L. and Melillo, J.M. (1988) Remote-Sensing of Canopy Chemistry and Nitrogen Cycling in Temperate Forest Ecosystems. *Nature* **335**, 154-156.

Wiegand, C.L., Richardson, A.J., Escobar, D.E. and Gerbermann, A.H. (1991) Vegetation Indexes in Crop Assessments. *Remote Sensing of Environment* **35**, 105-119.

Wigneron, J.P., Calvet, J.C., Pellarin, T., Van De Griend, A.A., Berger, M. and Ferrazzoli, P. (2003) Retrieving Near-Surface Soil Moisture From Microwave Radiometric Observations: Current Status and Future Plans. *Remote Sensing of Environment* **85**, 489-506.

Xiao, X.M., Zhang, Q.Y., Braswell, B., Urbanski, S., Boles, S., Wofsy, S., Berrien, M. and Ojima, D. (2004) Modeling Gross Primary Production of Temperate Deciduous Broadleaf Forest Using Satellite Images and Climate Data. *Remote Sensing of Environment* **91**, 256-270.

Zarco-Tejada, P.J., Miller, J.R., Mohammed, G.H. and Noland, T.L. (2000) Chlorophyll Fluorescence Effects on Vegetation Apparent Reflectance: I. Leaf-Level Measurements and Model Simulation. *Remote Sensing of Environment* **74**, 582-595.

3 EFFECTS OF MUTUAL SHADING OF TREE CROWNS ON PREDICTION OF PHOTOSYNTHETIC LIGHT-USE EFFICIENCY IN A COASTAL DOUGLAS-FIR FOREST[4]

3.1 Introduction

Global modelling of plant photosynthesis, also known as gross primary production (GPP) is a critical component of climate change research because it determines the amount of atmospheric CO_2 being absorbed by terrestrial ecosystems (Hamilton et al., 2002, Janzen 2004). Existing models often express GPP as a product of photosynthetically active radiation (PAR), defined as solar radiation between 400-700 nm wavelength, the fraction of PAR being absorbed by the plant canopy (f_{PAR}), and the efficiency (ε) with which the absorbed energy can used to produce to biomass (Monteith 1972, 1977):

$$GPP = \varepsilon \cdot f_{PAR} \cdot PAR \qquad (1)$$

Our ability to globally measure f_{PAR} and PAR using satellite remote sensing has increased significantly in recent years; the determination of ε over space and time, however, remains challenging (Running et al., 2004, Hall et al., 2006). Physiologically, ε is determined by a large number of environmental stresses, some of which may only have temporary effects on photosynthesis (photo-inhibition), while others can cause longer term reductions affecting GPP even after the actual stress event has ended (Adams et al., 1999, Adams et al., 2002). Consequently, ε is highly variable and differs among sites,

[4] A version of this chapter has been published. Hilker, T., Coops, N.C., Schwalm, C.R., Jassal, R.S., Black, T.A., Krishnan, P. (2008) Effects of Mutual Shading of Tree Crowns on Prediction of Photosynthetic Light Use Efficiency in a Coastal Douglas-Fir Forest. *Tree Physiology* ***28***, 825-834

species and individuals (Demmig-Adams et al., 1998). The complexity inherent to ε can be a serious limitation to modelling GPP (Running et al., 2004) and as a result, a better understanding of the relationship between stress factors and photosynthesis is needed to permit reliable estimates of GPP over larger areas.

Existing satellite-based measures of GPP incorporate ε either explicitly or implicitly from environmental stresses, typically focussing on a few globally measurable meteorological variables. In temperate climates, the prevailing atmospheric sky condition, driven by cloudiness, water vapour content or smog, is a key factor influencing photosynthesis (Turner et al., 2003, Lagergren et al., 2006, Schwalm et al., 2006) as it controls the amount and type (direct or diffuse) of radiation incident on a plant canopy. The influence of radiation on GPP is twofold: (1) light can be a limiting factor to photosynthesis in itself, in which case a maximum of absorbed solar energy is used to produce photosynthate; and (2) the over-abundance of light can trigger a photo-protective reaction, down-regulating ε (Demmig-Adams et al., 1990, 1996).

A common approach to describe radiation regimes is the ratio of direct to diffuse radiation (Q) available from instrumentation at flux tower sites (Turner et al., 2003, Schwalm et al., 2006). In a forest canopy, however, the amount of radiation effectively received by a tree crown is not only dependent on atmospheric conditions, but is also largely affected by canopy structure which drives mutual shading between and within individual tree crowns. These shading effects may produce significant shifts in the effective proportion of direct to diffuse radiation (Q_E) received, especially in the morning and late afternoon hours when solar elevation angles are low (Li and Strahler 1992).

Consequently, shading of forest canopies drives the amount of energy incident on trees, and may therefore have a significant impact on ε. Additionally, the capacity of leaves to thermally dissipate excessive radiation energy varies within the canopy (vertically and horizontally) as shaded leaves are much more susceptible to photo-inhibition than sunlit leaves (Demmig Adams 1998). Finally, shading effects are a major component of the surface conductance of canopy foliage through stomatal aperture (Brooks et al., 1997) which in turn controls the availability of CO_2 required for the photosynthetic reaction. While the effects of mutual shading on canopy illumination have been acknowledged in several studies (Li and Strahler 1992, Li et al., 1995), the resulting effect on ε has been largely ignored.

In this study, we introduce a new approach to assess mutual shadowing of forest canopies (hereafter canopy shadow fraction, σ_c) and its effect on ε using airborne laser scanning (referred to as Light Detection and Ranging-LiDAR). Canopy shading is modeled over a six-year period (May 1, 2000 and August 31, 2006) and is used to calculate Q_E incident on a Douglas-fir (*Pseudotsuga menziesii* var *menziesii* (Mirb.) Franco) dominated forest stand. Shadow proportions are combined with several meteorological variables to assess the relative explanatory power for variance in ε observed over different time scales using regression tree analysis. The results are then compared to a second set of regressions based on meteorological variables alone (i.e., not considering σ_c). In addition, the potential of up-scaling canopy shading and modeling it as a function of structure and stand age to facilitate application over larger areas is demonstrated for clear-cut, young growth, intermediate, and mature forest stands.

3.2 Methods

3.2.1 Research site

The study area is a Canadian Carbon Program (CCP) site (hereafter DF49 site), located on the eastern side of Vancouver Island, British Columbia, Canada (49°52 N, 125°20, elevation 300m). The site is located within the dry maritime Coastal Western Hemlock biogeoclimatic subzone (CWHxm), characterized by cool summers and mild winters with occasional drought during late summer (mean annual precipitation = 1500 mm and mean annual temperature = 8.5°C, Humphreys et al., 2006). The site consists of 80% Douglas-fir, 17% western red cedar (*Thuja plicata* Donn *ex* D. Don) and 3% western hemlock (*Tsuga heterophylla* (Raf.) Sarg.) (Morgenstern et al., 2004, Humphreys et al., 2006). The soil is a humo-ferric podzol with a gravelly sandy loam texture which is overlain by a surface organic layer ranging from 1 to 10 cm in depth.

3.2.2 Flux tower data

3.2.2.1 CO_2 flux and heat flux measurements

Continuous, half-hourly fluxes of CO_2 and water vapor were measured above the canopy using the eddy covariance (EC) technique (Morgenstern et al., 2004, Humphreys et al., 2006) for the 2000 – 2006 growing seasons (defined as days of year (DOY) 105 to 288). Net ecosystem exchange (NEE) was calculated as the sum of half-hourly fluxes of CO_2, and the rate of change in CO_2 storage in the air column between the ground and the EC measurement level (42 m), measured with a three-axis sonic anemometer-thermometer

(SAT, Model R3, Gill Instruments Ltd., Lymington, UK) and a closed-path CO_2/H_2O infrared gas analyzer (IRGA) (model LI-6262, LI-COR Inc., Lincoln, NE). Incident and reflected PAR were measured with upward and downward looking quantum sensors (Model 190 SZ, LI-COR), installed above and below the canopy. Gaps in data of less than two hours were filled by linear interpolation. Half-hourly measures of daytime GPP were derived from:

$$GPP = NEP + R_d \qquad (2)$$

where NEP = -NEE and R_d is daytime ecosystem respiration (Morgenstern et al., 2004, Jassal et al., 2007). Light-use efficiency was calculated from (1) with PAR measured directly by the downward looking quantum sensor and half-hourly f_{PAR} being modelled from incident and reflected PAR above and below the canopy ($\rho_1(\theta)$ and $\rho_2(\theta)$, respectively), solar zenith angle (θ) and the effective leaf area (LAI_e) (Chen, 1996):

$$f_{PAR} = (1-\rho_1(\theta)) - (1-\rho_2(\theta))e^{(-G_t(\theta)LAI_e/\cos\theta)} \qquad (3)$$

where $G_t(\theta)$ is the projection coefficient for total PAR transmission, assumed to be a constant of 0.5 (Chen, 1996, Chen et al., 2006) and LAI_e = 4.3 is derived from ground-based methods (Chen et al., 2006) and a clumping index for the needle-leaf forest of 0.45 (Chen, 1996). Sensible (H) and latent heat (λE) fluxes were calculated as described by Humphreys et al. (2006), and Jassal et al. (2007).

3.2.2.2 *Weather measurements*

Incident diffuse PAR was measured using a "sunshine sensor" (model BF3, Delta-T Devices Ltd., Burwell, UK) and upwelling ($L\uparrow$) and downwelling ($L\downarrow$) thermal infrared radiation (defined as radiation with a wavelength λ > 4000nm) were determined from pyrgeometers (model CNR1 Kipp & Zonen B.V., Delft, The Netherlands) above the canopy. Above-canopy air temperature (T_{Air}) and relative humidity were derived from temperature and humidity probes (HMP45CF, Vaisala Oyj, Helsinki, Finland) housed in aspirated shields (model 076B radiation shield, Met-One Instruments Inc., Grants Pass, OR) (Humphreys et al., 2006). Atmospheric pressure deficit (D) was computed from T_{Air} and relative humidity (Buck 1981).

Half-hourly means of soil water content in the 0–0.6 m soil layer (Θ_{60}) were derived from water content reflectometers (Model CS-615, Campbell Scientific Inc., Logan, UT, USA) at two locations and four depths between 2 and 100 cm and 11 stations of time domain reflectometry (TDR) probes (Hook and Livingston 1996). Soil water content–soil matric potential relationships were determined on intact soil cores from 0–60 cm layers in the laboratory with a pressure plate apparatus. The resulting field capacity and permanent wilting point were 0.25 and 0.10 m^3 m^{-3}, respectively (Coops et al., 2007).

3.2.3 LiDAR data

LiDAR is an airborne remote sensing technology that determines distances to an object or surface with laser pulses. First pulse returns are reflected from the highest surface (e.g., tree canopies), whereas last hit returns are reflected from the lowest points in the landscape, most often the terrain surface. LiDAR data were acquired on June 8 2004, by Terra Remote Sensing (Sidney, BC, Canada) with a ground return density of 0.7 hit per m^2 and a footprint diameter (spot size) of 0.19 m. Classification of LiDAR data into either ground or non-ground returns was carried out with Terrascan v. 4.006 software (Terrasolid, Helsinki, Finland) (Kraus and Pfeifer 1998).

3.2.4 Modelling shadow fractions within the canopy

3.2.4.1 Model development

Canopy shading was computed in two steps. First, non-ground LiDAR returns were extracted and used to generate a three-dimensional forest canopy surface model (CSM) (spatial resolution is 30cm) at a radius of 500 m around the tower to approximate the eddy flux footprint (Blanken et al., 2001, Kljun et al., 2004). This CSM was assumed to be representative and constant over the entire six year period, as the structure of the coniferous forest was not expected to change significantly during this time (Klinka et al., 1991). Second, the generated CSM was used to simulate σ_c per half hour time step based on a hillshade algorithm (ArcGIS, Esri Inc. Redlands, California, USA). Hillshades are panchromatic rasters that model the illumination conditions for a given surface based on sun position (Reda and Andreas 2004) and are commonly used in spatial mapping (Van Den Eeckhaut 2005). Assuming clear sky conditions, canopy shadow fractions can be computed from hillshades as the proportion of sunlit to shaded pixels derived from binary classification. In the case of a canopy surface, σ_c is likely to overestimate shadowing effects, as the CSM describes the canopy as a totally opaque surface, whereas tree canopies are translucent. To mitigate this effect, a weighting, or transparency, factor (p) was introduced, reducing the effective amount of shading within the canopy. The transparency factor was defined corresponding to the probability of canopy gaps P at a given solar zenith angle (θ) (Chen 1996),

$$P(\theta) = \exp\left[\frac{-G_t(\theta)LAI_e}{\cos\theta}\right] \tag{4}$$

where LAI_e and $G_t(\theta)$ were used in conformity with Eqn. 3. To verify modelled σ_c, digital images were acquired from the 45 m flux tower in 24 directions around the mast (horizontal offset between each picture was 11.5°, beginning at 313° to avoid blocking by the tower) at a constant vertical zenith angle of 118° with a digital camera (DSC T7, Sony Inc.) under clear sky conditions. Image histograms were computed and a simple threshold defined to classify pixels as either sunlit or shaded. A hillshade for the same half hour interval was computed and the shadow fractions were compared.

3.2.4.2 Implementing shadow fractions in the canopy radiation regime

The ratio of direct to diffuse PAR (Q) (without considering σ_c) is defined as:

$$Q = \frac{\rho_{total} - \rho_{diffuse}}{\rho_{diffuse}} \tag{5}$$

where ρ_{total} and $\rho_{diffuse}$ are total and diffuse incident PAR, respectively. Mutual shading of tree crowns affects Q incident on a leaf by increasing the diffuse and decreasing the direct radiation component, hence the effective amount of direct PAR incident on the canopy ($\rho_{E_{direct}}$) can be obtained from $\rho_{direct}(1 - p\sigma_c)$, where $p\sigma_c$ is the weighted shadow fraction. The amount of effective diffuse radiation ($\rho_{E_{diffuse}}$) is then calculated from $\rho_{total} - \rho_{E_{direct}}$ and both terms substituted in (5) yield Q_E as:

$$Q_E = \frac{\rho_{E_{direct}}}{\rho_{E_{diffuse}}} = \frac{\rho_{E_{direct}}}{\rho_{total} - \rho_{E_{direct}}} = \frac{(\rho_{total} - \rho_{diffuse}) \cdot (1 - p\sigma_c)}{\rho_{total} - ((\rho_{total} - \rho_{diffuse}) \cdot (1 - p\sigma_c))} \quad (6)$$

3.2.5 Assessing the explanatory power of Q_E with respect to variations in ε

3.2.5.1 Regression tree analysis

The impact of σ_c on ε was assessed by means of regression tree analysis. Regression trees are a non-parametric data mining approach and can be considered as a sequence of binary nodes (yes/no queries) splitting dependent variables using optimal predictor variables based on least squares (Melendez et al., 2006). The relative importance of each predicting variable in explaining variations in the response variable is assessed by a linearly scaled dimensionless score between 0 (= not important) and 100 (=most important). All regression trees in this study were computed based on a 10-fold cross validation, with a maximum tree depth of 16 and a minimum splitable node size of 10. Tree pruning was set to the minimum cross validation error (Witten and Frank 2005).

3.2.5.2 Relative assessment of explanatory power over different time scales

Regression trees were used to assess the explanatory power of Q_E with respect to variations in ε, relative to additional predictor variables including T_{Air}, $L\downarrow$, $L\uparrow$, H, λE, Θ_{60} and D (Schwalm et al., 2006). As all these variables vary diurnally and seasonally

(Figure 3.1a-l), the proportion of variation in ε explained was expected to change with the temporal scale observed. To investigate these changes, four regression trees were constructed for half hourly (non-water-stressed and water-stressed), daily and weekly time intervals (hereafter referred to as regression trees A1-A4):

A1. Regression tree analysis for half hourly variations of ε:

$$\varepsilon = f\left(Q_E, T_{Air}, L\downarrow, L\uparrow, \lambda E, H, \Theta_{60}, D\right)$$

A2. Regression tree analysis for half hourly variations of ε under water stress situations using values acquired with $\Theta_{60}<0.1$:

$$\varepsilon_{\theta<0.1} = f\left(Q_{E,\Theta<0.1}, T_{Air,\Theta<0.1}, L\downarrow_{\Theta<0.1}, L\uparrow_{\Theta<0.1}, \lambda E_{\Theta<0.1}, H_{\Theta<0.1}, D_{\Theta<0.1}\right)$$

A3. Regression tree analysis investigating daily averaged data:

$$\bar{\varepsilon}_{day} = f\left(\overline{Q_{E\ day}}, \overline{T_{Air\ day}}, \overline{L\downarrow_{day}}, \overline{L\uparrow_{day}}, \overline{\lambda E_{day}}, \overline{H_{day}}, \overline{\Theta_{60\ day}}, \overline{D_{day}}\right)$$

A4. Regression tree analysis investigating weekly averaged data:

$$\bar{\varepsilon}_{week} = f\left(\overline{Q_{E\ week}}, \overline{T_{Air\ week}}, \overline{L\downarrow_{week}}, \overline{L\uparrow_{week}}, \overline{\lambda E_{week}}, \overline{H_{week}}, \overline{\Theta_{60\ week}}, \overline{D_{week}}\right)$$

($\bar{\varepsilon}_{day}$ and $\bar{\varepsilon}_{week}$ were computed as the ratio of summed totals divided by the relevant time frame). The benefit of considering σ_c for explaining variations in ε was assessed in a second analysis, with the same time intervals, settings and input variables, but substituting Q_E with Q that is, not considering σ_c (named regression trees B1-B4).

3.2.6 Investigating the potential of up-scaling shadow fractions

3.2.6.1 Assessing potential of modelling shadow fractions from stand parameters

Although LiDAR data can be used to estimate canopy shading over small areas, large area coverage of LiDAR is relatively expensive. Thus, it is important to determine if broader spatial estimates of σ_c can be developed from more easily measurable parameters, such as solar position and stand type. To assess the potential of modelling shadow fractions from stand parameters, we computed σ_c for three additional stands adjacent to DF49 (a clear-cut, a young growth forest planted in 1990, and an intermediate, 38-year-old stand, (Figure 3.2) and compared σ_c at half-hourly and daily time steps.

3.2.7 Assessing the potential of including σ_c in satellite-based GPP products

The standard GPP algorithm of the moderate resolution imaging spectroradiometer (MODIS) utilises 8-day means of f_{PAR}, PAR and ε, where ε is a biome-specific constant, representing the optimal potential of a vegetation type for converting PAR to biomass (Turner et al., 2003, Running et al., 2004), which is adjusted using daily estimates of D to account for water/humidity related stress factors, and minimum daily air temperature (T_{Min}) to account for thermal stresses (Heinsch et al., 2003). We assessed the potential of improving MODIS based predictions of ε by including shadow fractions as an additional explanatory variable:

$$\varepsilon_{MODIS} = \varepsilon_{\max} \cdot f\left(T_{Min\,day}, \overline{D}_{day}, \overline{\sigma}_{c\ day}\right)$$

where $T_{Min\,day}$ is minimum daily temperature and $\overline{\sigma}_{c\,day}$ is mean daily shadow fraction. The explanatory power of this regression tree (named A5) was then compared with the current approach (named regression tree B5), expressing ε as:

$$\varepsilon_{MODIS} = \varepsilon_{\max} \cdot f\left(T_{Min\,day}, \overline{D}_{day}\right)$$

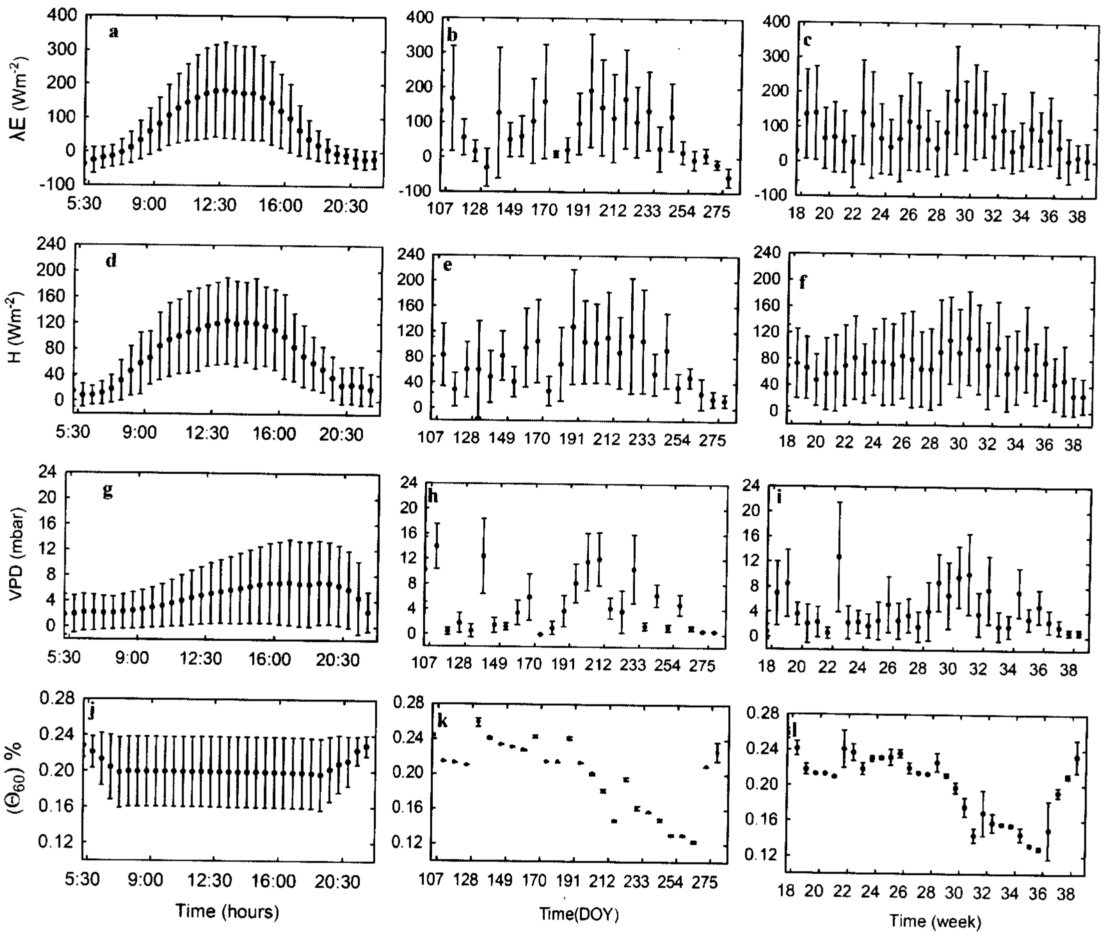

Figure 3.1A-L: Half hourly, daily and weekly averages (abscissa) with standard deviations for λE, H, D and Θ_{60} (ordinate) for the year 2005. Data are shown for the growing season (DOY 105 -288) only. For daily estimates, only every 7th day is displayed.

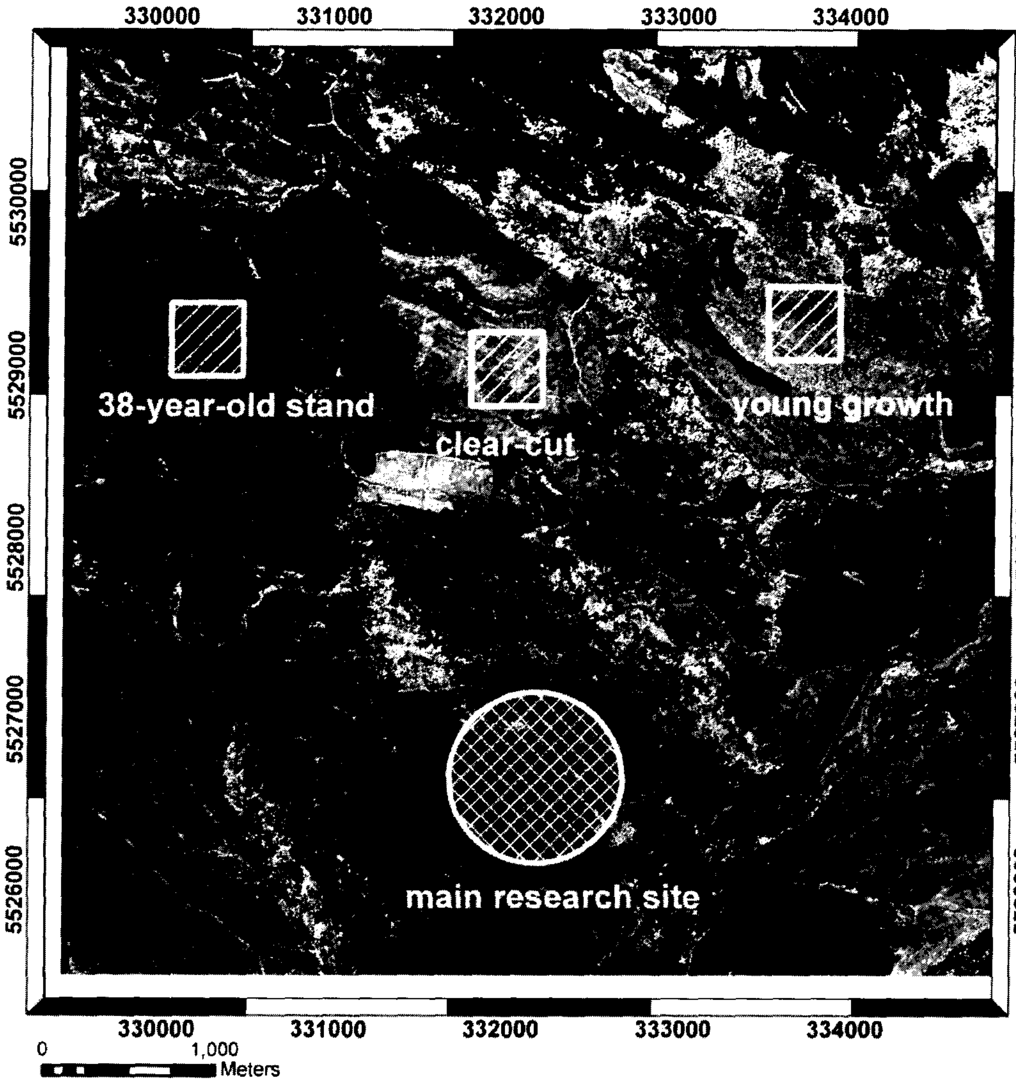

Figure 3.2: Selected sites for acquisition of shadow fractions using LiDAR drawn over a Quickbird panchromatic satellite image (ground resolution: 0.61 m). Coordinates are projected in UTM Zone 10. The circular shape for this site was used to approximate the footprint of the eddy covariance measurements.

3.3 Results

3.3.1 Modelling shadow fractions

Figure 3.3a illustrates the CSM for the DF49 site derived from LiDAR observations. Photographic-estimated shadow fractions and those modeled from hillshades were significantly correlated (r^2 = 0.7, p<0.05, N=24) (Figure 3.3b) with CSM shadow fractions ranging between 10% - 90% and shading obtained from digital photography varying between 20 - 80%. Figures 3.4a-c illustrate how the computed shadow fractions vary over a growing season at different time scales. Half hourly means showed up to 99% mutual shading at sunrise and sunset and between 58% - 77% at solar noon. Daily and weekly means ranged between 65% and 95% with minimum values reached at summer solstice. Radiation use efficiency varied between 0.05 and 4.0 g C MJ^{-1}, and was lowest in the afternoon hours and highest in the early mornings (Figures 3.5a-b), especially under cloudy conditions.

3.3.2 Regression tree analysis

3.3.2.1 Regression trees

A schematic representation of a regression tree computed for weekly averaged data (regression tree A4) is shown in Figure 3.6 and illustrates how the algorithm splits the dependent variable (ε) into homogeneous subsets based on thresholding. The success of splitting is used to assess the importance of each predictive variable. For example, tower-based, weekly estimates of ε were largely explained by $\overline{Q_E}_{week}$, $\overline{\Theta_{60}}_{week}$ and $\overline{L\downarrow}_{week}$.

A B

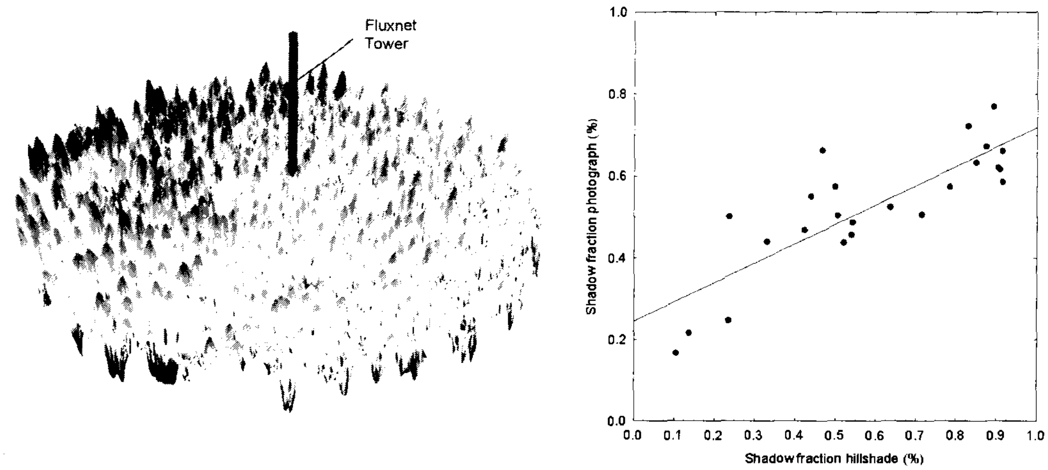

Figure 3.3: A-B A: LiDAR derived canopy structure model at a radius of 1 km around the tower. The height of the tower (center) is overdrawn in this diagram for illustration purposes. Figure B: Correlation between photographically derived shadow fraction (red channel) vs. shadow fraction modelled using hillshade analysis (r^2=0.7, p<0.05). The threshold value separating shadow from light in the digital images is selected independently from the one of the hillshade model, thus a direct comparison of absolute values has to be handled cautiously. Each data point represents an observation at one rotation angle and the dotted line represents the 1:1 line.

A B C

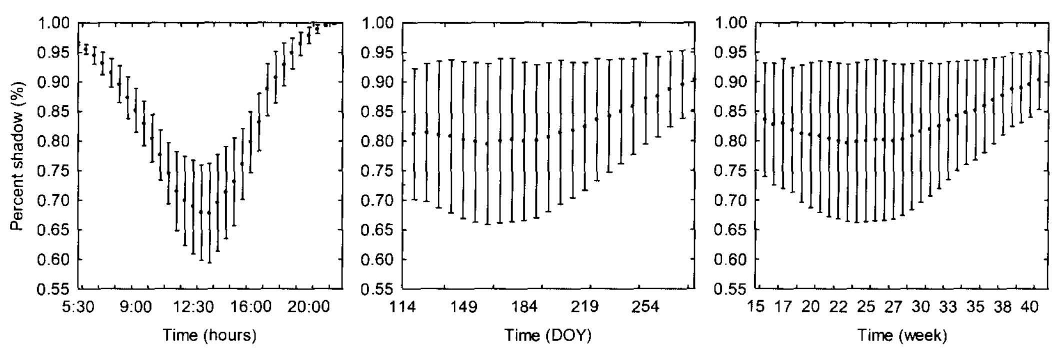

Figure 3.4 Half hourly (A), daily (B) and weekly (C) averages (abscissa) with standard deviations of the computed shadow fractions for 2005. Data are shown for the growing season (DOY 105 -288) only. For daily estimates, only every 7th day is displayed.

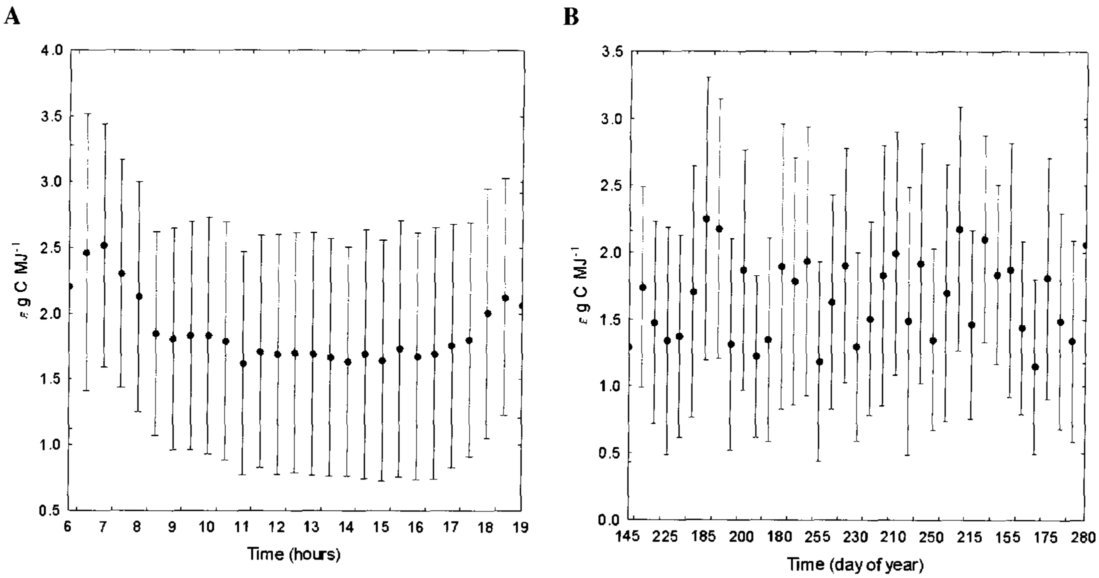

Figure 3.5A-B: Half hourly (A) and daily (B) averages (abscissa) with standard deviations of ε between 2000 and 2006. Data are shown for the growing season (DOY 105 -288) only. For daily estimates, only every 5th day is displayed. The dots represent the mean *ε* values for half hourly and daily averages, respectively. The error bars represent the standard deviations from these mean values.

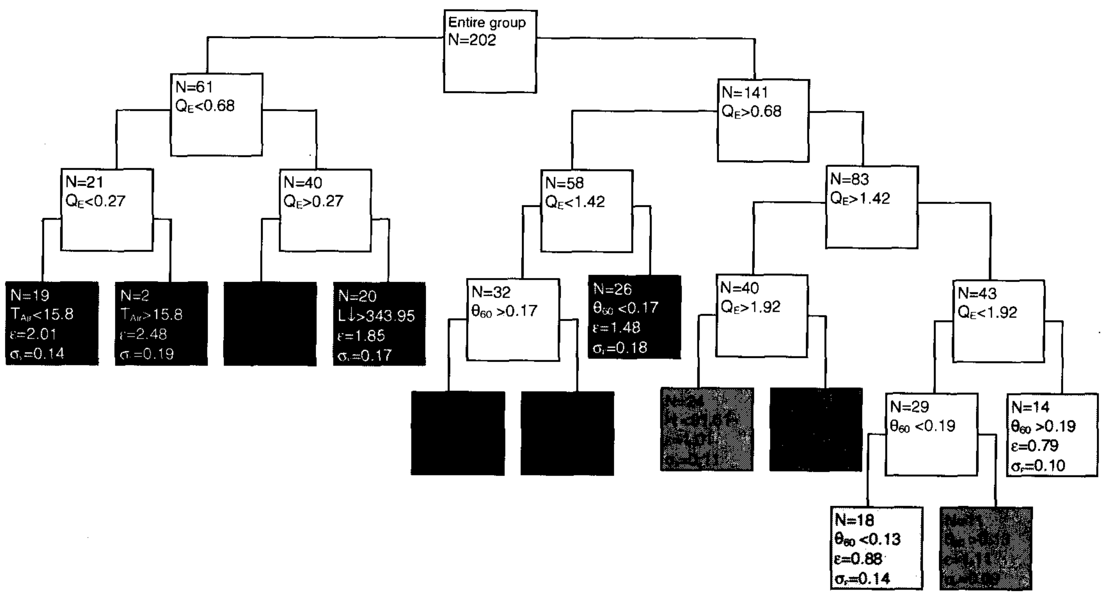

Figure 3.6: Example of a regression tree for weekly averaged estimates of *ε*. Shading of the terminal nodes corresponds to light-use efficiency (low = bright, high= dark). Relative importance of variables for weekly estimates were Q_E=100, $L\downarrow$=6.9, Θ_{60}=8.7, T_{Air}= 3.1, λE=3.9, $L\uparrow$=2.9, D=1.5 and H=1.4.

3.3.2.2 *Explanatory power of regression trees over different time scales*

Regression trees A1-A4 are shown in Figure 3.7. The amount of variance explained by these models varied between 86% and 97% with the explanatory power being highest for half hourly data, followed by daily, weekly and half-hourly-stressed observations (A2). Root mean squared error (RMSE) ranged between 0.0025 g C MJ^{-1} (half-hourly) and 0.000025 g C MJ^{-1} (weekly), respectively. Regression trees B1-B4 explained between 70% and 87% of variations in ε and the explanatory power was highest for half hourly, followed by daily and weekly averaged values. (Figure 3.7). Minimum and maximum RMSE were 0.0256 g C MJ^{-1} and 0.0009 g C MJ^{-1} for half hourly and weekly means, respectively.

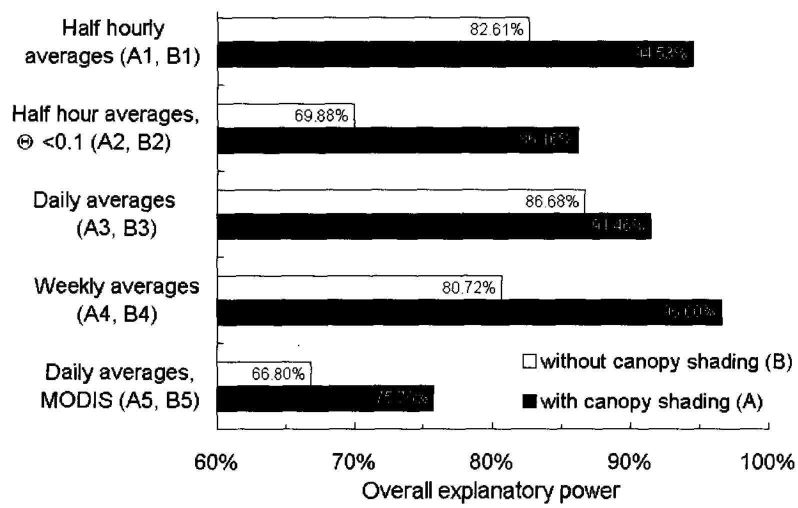

Figure 3.7: Proportion of variation explained using regression tree analysis for half hourly, half hourly drought stressed (Θ_{60}<0.1), daily and weekly averaged data considering shadow fractions (A1-A4) and not considering shadow fractions (B1-B4). The regression trees for the MODIS algorithm explain variations in ε using T_{Air}, T_{Min}, D and σ_c (A5) and T_{Air}, T_{Min} and D (B5).

The variation explained in daily estimates of ε based on the MODIS parameters ($\overline{T_{Air\,day}}, T_{Min\,day}, \overline{D}_{day}$) including $\overline{\sigma_{c\,day}}$ (A5) was 76%, compared with 67% for the model that did not consider canopy shading (Figure 3.7).

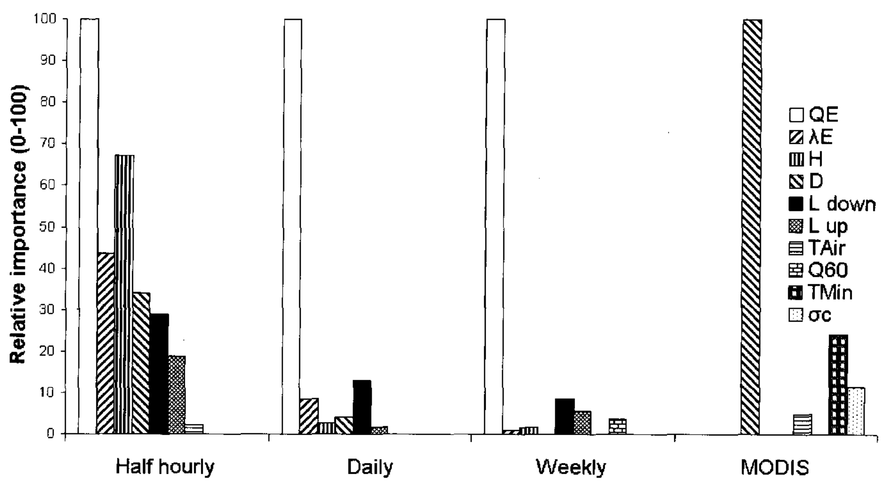

Figure 3.8: Relative importance of predictor variables over half hourly, daily and weekly time frames as computed using regression tree analysis. The predictive power is scaled on a range between 0 (insignificant) and 100 (most significant predictor).

3.3.2.3 Relative importance of predicting variables

The relative importance of explanatory variables varied with time scales (Figure 3.8) as half hourly means of ε were largely explained by Q_E, H, λE and D, whereas daily and weekly means were explained by fewer variables and depended almost exclusively on Q_E. Variations in half-hourly estimates of ε under water stress conditions (Θ_{60}<0.10) (regression tree A2) were largely explained by λE, H, D, $L\uparrow$. Figure 3.8 also shows the relative importance of predicting variables for the MODIS-like ε-term (regression tree

A5, based on $\overline{T_{Air}}_{day}, T_{Min\,day}, \overline{D}_{day}$ and $\overline{\sigma_c}_{day}$). This analysis explained variations in ε largely by D and $T_{Min\,day}$.

3.3.3 Potential of modelling shadow fractions

The daily patterns of σ_c, computed at half-hour intervals for the clear-cut, young, and intermediate forest, and the DF49 site, illustrate the large effect that shading has on mature forest stands (i.e. DF49), while the impact is reduced in younger stands with smaller crowns (Figure 3.9). Shadow fractions for the clear-cut site are negligible, except at very low sun-angles. Figures 3.10a and 3.10b demonstrate an approach of modeling Q_E over the four stands examined based on half-hourly and daily estimates of Q. For the clear-cut site, a linear 1:1 relationship was observed, indicating that the effect of canopy shading on Q_E is minimal. The more structured stands, however, revealed a strong, non-linear relationship between Q and Q_E, with the effective diffuse radiation component being highest in the most mature stand (DF49).

3.4 Discussion and conclusions

This study investigated the importance of mutual canopy shading for explaining variations in ε. Mutual shading was predicted with a three-dimensional canopy structure model derived from LiDAR. Significant correlations found between the modeled canopy shadow and digital photographs indicate that the LiDAR based approach successfully described differences in canopy shading in forest stands.

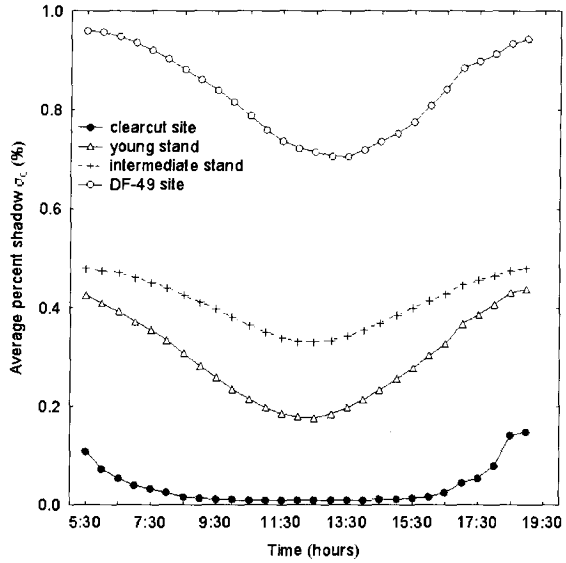

Figure 3.9: Daily averaged canopy shading for the clear-cut site, the young growth stand, the 38-year-old stand and the DF49 site (all sites are Douglas-fir dominated).

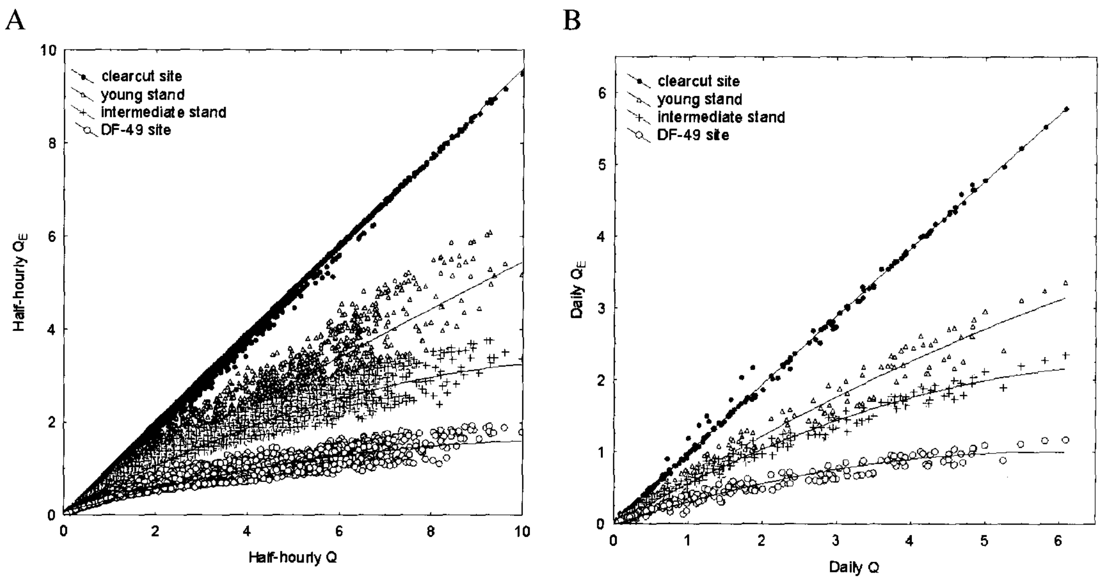

Figure 3.10 A-B 3.10A: Relationship between the simple ratio of direct over diffuse radiation (Q), versus the shadow fraction corrected ratio of direct over diffuse radiation (Q_E) for the clear-cut site(r=0.99, p<0.05), the young growth stand(r=0.98, p<0.05), the 38-year-old stand(r=0.98, p<0.05) and the DF49 site(r=0.96, p<0.05) (all Douglas-fir dominated) as half-hourly estimates. Figure 3.10b: Relationship between the simple ratio of direct over diffuse radiation (Q), versus the shadow fraction corrected ratio of direct over diffuse radiation (Q_E) for the clear-cut site (r=0.99, p<0.05), the young growth stand (r=0.99, p<0.05), the 38-year-old stand(r=0.98, p<0.05) and the DF49 site (r=0.97, p<0.05) (all Douglas-fir dominated) as daily estimates.

Regression tree analysis based on $Q_E, T_{Air}, L\downarrow, L\uparrow, \lambda E, H, \Theta_{60}$ and D explained a significant amount of the variation in ε. Results of previous studies (Turner et al., 2003, Schwalm et al., 2006) indicating that the type and amount of incident PAR are the most important parameters for explaining variations in ε were confirmed over all observed time intervals. Light-use efficiency observations were within the range of published values. Schwalm et al. (2006) investigated ε over an east west transect across Canada, and found ε was highest in grasslands (daily median 3.68 g C MJ^{-1}), with significantly lower values in forested stands (0.83 g C MJ^{-1}). The median value for ε at the study site (DF49) was 1.63 g C MJ^{-1} (Schwalm et al., 2006). Chen et al. (1999) calculated daily ε for a mature deciduous forest with values ranging from 0.05 to 6.0 g C MJ^{-1}, values above 3, however, were rare (n<10 in both 1994 and 1996) and strongly related to air temperature. Turner et al. (2003) analyzed daily and monthly ε at a coniferous boreal forest stand deriving values between 0.1 and 3.1 g C MJ^{-1}. Similar values were found by Nichol et al. (2002) based on midday half-hourly EC measurements obtained under clear sky conditions at a Siberian site during the winter–spring transition.

A general increase in ε of between 6 and 33% during cloudy periods was observed by Alton et al. (2007) who compared several diverse stands under varying sky conditions. Hollinger et al. (1994) and Gu et al. (2002) found increases in ε of between 50% and 180% under cloudy conditions in temperate forests, and Schwalm et al. (2006) reported increases in ε of up to 300%. In our study, differences in ε between cloudy and sunny periods (assuming a threshold (cloudy/non-cloudy) of Q_E= 1) ranged between 100% and 300% (Figure 3.4) with the largest differences found for half hourly time periods, and smallest changes at weekly time scales, most likely due to averaging effects reducing the overall variability of ε (Schwalm et al., 2006). Despite its clear patterns over the course of a year (Figure 3.1j-l), Θ_{60} played only a minor role in explaining variations in ε, again in agreement with Schwalm et al. (2006). Vapour pressure deficit played an important role for explaining variations in ε only for the MODIS regression trees, most likely because of its correlation to irradiance, which is otherwise not expressed in this regression tree. Although T_{Air} was reported to have a significant impact on ε (e.g. Chen et al., 1999, Makela et al., 2006, Schwalm et al., 2006), we found little variation potentially caused by the temperate climatic conditions found at the study site, with temperature values rarely approaching extreme situations, and measurements being restricted to the growing season.

Unlike other statistical methods such multiple regression, decision trees are specifically designed to deal with collinear datasets, consequently, correlation among predicting variables was expected and allowed. For instance, T_{Air} is likely to be correlated to $L\downarrow, L\uparrow$ and H, as all of these variables are indicative of thermal radiation energy. In this study H had the highest explanatory power over shorter time intervals while $L\downarrow$ was a more appropriate variable at longer time scales. Likewise, λE proved a more direct predictor for humidity related stresses over shorter time intervals, whereas D explained larger amounts of variation in ε over daily and weekly time scales.

The regression tree analysis based on D, T_{Min}, T_{Air} and σ_c (A5) confirms that the ε-term used in the MODIS algorithm can explain most of the variations in photosynthetic efficiency, however, the performance is well below the regression trees based on additional measurements of variables $L\downarrow, L\uparrow, \lambda E, H, \Theta_{60}$ (A1-A4, Figure 3.6-3.7). This outcome may account for some of the differences observed between satellite and field based observations of ε (Turner et al., 2003, Martel et al., 2005). The relative importance of D for explaining variations in ε reflects its significant role in photosynthetic production, whereas the relatively low impact of both temperature-related variables can be explained by the temperate climatic conditions at the site.

The enhanced performance of models considering mutual canopy shading (A1-A5) suggests that mutual shading is an important component of ε and that broader spatial estimates of GPP can be improved by considering shadow fractions when estimating the effective amount of radiation energy incident on a forest canopy. Mutual canopy shading can be potentially modeled as a function of stand properties (Figure 3.9-3.10); however, further analysis is needed to confirm the behavior and influence of these relationships over a range of sites and forest compositional and structural types. Figure 3.9 suggests that canopy shadow is most important in older, more structurally diverse stands, as the total area shaded increases with increasing stand age and is more distinct over the course of a day.

Precise estimation of ε is an essential requirement for up-scaling GPP to landscape and global levels using global productivity models (Running et al., 1999). Consideration of σ_c in calculations of incident radiation energy can be a valuable addition to ongoing efforts to modelling ε over large areas from space (Heinsch et al., 2006, Davi et al., 2006, Turner et al., 2006, Ichii et al., 2007, Zhang et al., 2007). Further analysis is needed to confirm this outcome across a range of sites and stand types. For instance, σ_c may be of less importance for stand types with lower LAI values or canopy height.

3.5 References

Adams, W.W., Demmig-Adams, B., Rosenstiel, T. N., Brightwell, A.K. and Ebbert, V. (2002) Photosynthesis and Photoprotection in Overwintering Plants. *Plant Biology* **4**, 545-557.

Adams, W.W., Demmig-Adams, B., Logan, B.A., Barker, D.H and Osmond, C.B. (1999) Rapid Changes in Xanthophyll Cycle-Dependent Energy Dissipation and Photosystem II Efficiency in two Vines, *Stephania japonica* and *Smilax australis*, Growing in the Understory of an Open Eucalyptus Forest. *Plant Cell and Environment* **22**, 125-136.

Alton, P.B., North, P.R. and Los, S.O. (2007) The impact of Diffuse Sunlight on Canopy Light-Use Efficiency, Gross Photosynthetic Product and Net Ecosystem Exchange in Three Forest Biomes. *Global Change Biology* **13**, 776-787.

Blanken, P.D., Black, T.A., Yang, P.C, Neumann, H.H., Nesic and Z. Staebler, R. (2001) Energy Balance and Canopy Conductance of a Boreal Aspen Forest: Partitioning Overstory and Understory Components, *Journal of Hydrology* **245**, 118-136

Brooks, J.R., Flanagan, L.B., Varney, G.T. and Ehleringer, J.R. (1997) Vertical Gradients in Photosynthetic Gas Exchange Characteristics and Refixation of Respired CO_2 within Boreal Forest Canopies. *Tree Physiology* **17**, 1-12.

Buck, A.L. (1981) New Equations for Computing Vapor Pressure and Enhancement Factor. *J. Appl. Meteorol.* **20**, 1527-1532.

Chen, J. (1996) Evaluation of Vegetation Indices and a Modified Simple Ratio for Boreal Applications. *Canadian Journal of Remote Sensing* **22**, 229-242.

Chen, W.J., Black, T.A., Yang, P.C., Barr, A.G., Neumann, H.H., Nesic, Z., Blanken, P.D., Novak, M.D., Eley, J., Ketler, R.J. and Cuenca, R. (1999) Effects of Climatic Variability on the Annual Carbon Sequestration by a Boreal Aspen Forest. *Global Change Biol* **5**, 41–53

Chen, J.M., Govind, A., Sonnentag, O., Zang, Y.Q. Barr, A.G. and Amiro, B. (2006) Leaf Area Index Measurements at Fluxnet-Canada Forest Sites. *Agricultural and Forest Meteorology* **140**, 257-268.

Coops, N.C., Black, T.A., Jassal, R.S., Trofymow, J.A. and Morgenstern, K. (2007) Comparison of MODIS, Eddy Covariance Determined and Physiologically Modelled Gross Primary Production (GPP) in a Douglas-Fir forest stand. *Remote Sensing of Environment* **107**, 385-401

Coops N.C., Waring, R.H. and Landsberg, J.J. (1998) Assessing Forest Productivity in Australia and New Zealand Using a Physiologically-Based Model Driven with Averaged Monthly Weather Data and Satellite-Derived Estimates of Canopy Photosynthetic Capacity. *Forest Ecology and Management* **104**, 113-127

Davi, H., Dufrene, E., Francois, C., Le Maire, G., Loustau, D., Bosc, A. Rambal, S., Granier, A. and Moors, E. (2006) Sensitivity of Water and Carbon Fluxes to Climate Changes from 1960 to 2100 in European Forest Ecosystems. *Agricultural and Forest Meteorology* **141**, 35-56.

De'ath, G. and Fabricius, K.E. (2000) Classification and Regression Trees: A Powerful yet Simple Technique for Ecological Data Analysis. *Ecology* **81**, 3178-3192.

Demmig-Adams, B. (1990) Carotenoids and Photoprotection in Plants - A Role for the Xanthophyll Zeaxanthin. *Biochemica et Biophysica Acta* **1020**, 1-24.

Demmig-Adams, B. (1998) Survey of Thermal Energy Dissipation and Pigment Composition in Sun and Shade Leaves. *Plant and Cell Physiology* **39**, 474-482.

Demmig-Adams, B. and Adams, W.W. (1996) The Role of Xanthophyll Cycle Carotenoids in the Protection of Photosynthesis. *Trends in Plant Science* **1**, 21-26.

Goetz S.J. and Prince, S.D. (1996) Remote Sensing of Net Primary Production in Boreal Forest Stands. *Agricultural and Forest Meteorology* **78**, 149-17

Goetz, S.J. and Prince, S.D. (1999) Modelling Terrestrial Carbon Exchange and Storage: Evidence and Implications of Functional Convergence in Light-Use Efficiency. *Advances in Ecological Research* **28**, 57-92.

Gu, L.H., Baldocchi, D., Verma, S.B., Black, T.A., Vesala, T., Falge, E.M. and Dowty, R.R. (2002) Advantages of Diffuse Radiation for Terrestrial Ecosystem Productivity. *Journal of Geophysical Research-Atmospheres* **107**, Art. No. 4050.

Hall, F.G., De Colstoun, E.B., Collatz, G.J., Landis, D., Dirmeyer, P., Betts, A., Huffman, G.J., Bounoua, L. and Meeson, B. (2006) ISLSCP Initiative II Global Data Sets: Surface Boundary Conditions and Atmospheric Forcings for Land-Atmosphere Studies. *Journal of Geophysical Research-Atmospheres* **111**: Art. No. D22S01

Hamilton, J.G., Delucia, E. H., George, K., Naidu, S. L., Finzi, A. C. and Schlesinger, W.H. (2002) Forest carbon balance under elevated CO_2. *Oecologia* **131**, 250-260.

Heinsch, F.A., Reeves, M., Bowker, C.F., Votava, P., Kang and S. Milesi, C. (2003) User's Guide: GPP and NPP (MOD17A2/A3) products. NASA MODIS Land Algorithm. Version 2.0. Available online at: http://www.ntsg.umt.edu/modis/MOD17UsersGuide.pdf

Heinsch, F.A., Zhao, M.S., Running, S.W., Kimball, J.S., Nemani, R.R., Davis, K.J., Bolstad, P.V., Cook, B.D., Desai, A.R., Ricciuto, D.M., Law, B.E, Oechel, W.C., Kwon, H., Luo, H.Y, Wofsy, S.C., Dunn, A.L., Munger, J.W., Baldocchi, D.D., Xu, L.K., Hollinger, D.Y., Richardson, A.D., Stoy, P.C, Siqueira, M.B.S., Monson, R.K., Burns, S.P. and Flanagan, L.B. (2006) Evaluation of Remote sensing based Terrestrial Productivity from MODIS Using Regional Tower Eddy Flux Network Observations. *IEEE-Transactions on Geoscience and Remote Sensing* **44**, 1908-1925.

Hollinger, D.Y., Kelliher, J.B., Byers, J.N., Hunt, J.E., McSeveny, T.M. and Weir, P.L. (1994) Carbon-dioxide Exchange Between an Undisturbed Old-Growth Temperate Forest and the Atmosphere. *Ecology* **75**, 134-150.

Hook, W.R. and Livingston, N.J. (1996) Errors in Converting Time Domain Reflectometry Measurements of Propagation Velocity to Estimates of Soil Water Content. *Soil Science Society of America Journal* **60**, 35-41.

Humphreys, E.R., Black, T.A., Morgenstern, K., Cai, T.B., Drewitt, G.B., Nesic, Z. and Trofymow, J.A. (2006) Carbon Dioxide Fluxes in Coastal Douglas-Fir Stands at Different Stages of Development After Clearcut Harvesting. *Agricultural and Forest Meteorology* **140**, 6-22.

Ichii, K., Hashimoto, H., White, M.A., Potters, C., Hutyra, L.R., Huete, A.R., Myneni, R.B. and Nemanis, R.R. (2007) Constraining Rooting Depths in Tropical Rainforests Using Satellite Data and Ecosystem Modelling for Accurate Simulation of Gross Primary Production Seasonality. *Global Change Biology* **13**, 67-77.

Janzen, H.H. (2004) Carbon Cycling in Earth Systems - A soil Science Perspective. *Agriculture, Ecosystems and Environment* **104**, 399 - 417

Jassal, R.S., Black, T.A., Cai, T.B., Morgenstern, K., Li, Z., Gaumont-Guay, D. and Nesic, Z. (2007) Components of Ecosystem Respiration and an Estimate of Net Primary Productivity of an Intermediate-aged Douglas-Fir Stand. *Agricultural and Forest Meteorology* **144**, 44-57

Klinka, K., Pojar J. and Meidinger, D.V. (19910 Revision of Biogeoclimatic Units of Coastal British-Columbia. *Northwest Science* **65**, 32-47.

Kljun N., Kastner-Klein, P., Fedorovich, E. and Rotach, M.W. (2004) Evaluation of Lagrangian Footprint Model Using Data from Wind Tunnel Convective Boundary Layer. *Agricultural and Forest Meteorology* **127**, 189-201.

Kraus, K. and Pfeifer, N. (1998) Determination of Terrain Models in Wooded Areas with Airborne Scanner Data. *ISPRS Journal of Photogrammetry and Remote Sensing* **54**, 193-203.

Lagergren, F., Grelle, A., Lankreijer, H., Molder, M. and Lindroth, A. (2006) Current Carbon Balance of the Forested Area in Sweden and Its Sensitivity to Global Change as Simulated by Biome-BGC. *Ecosystems* **9**, 894-908.

Li, X., Strahler, A.H. and Woodcock, C.E. (1995) A hybrid Geometric Optical-Radiative Transfer Approach for Modelling Albedo and Directional Reflectance of Discontinuous Canopies. *IEEE-Transactions on Geoscience and Remote Sensing* **33**, 466-480

Li, X. and Strahler, A.H. (1992) Geometric-Optical Bi-directional Reflectance Modeling of the Discrete Crown Vegetation Canopy: Effect of Crown Shape and Mutual Shadowing. *IEEE-Transactions on Geoscience and Remote Sensing* **30**, 276-292.

Makela, A., Kolari, P., Karimaki, J., Nikinmaa, E., Peramaki, M. and Hari, P. (2006) Modelling Five Years of Weather-Driven Variation of GPP in a Boreal Forest. *Agricultural and Forest Meteorology* **139**, 382-398.

Martel, M.C., Margolis, H.A., Coursolle, C., Bigras, F., Heinsch, F.A. and Running, S.W. (2005) Decreasing Photosynthesis at Different Spatial Scales During the Late Growing Season on a Boreal Cutover. *Tree Physiology* **25**, 689-699.

Melendez, K.V., Jones, D.L. and Feng, A.S. (2006) Classification of Communication Signals of the Little Brown Bat. *Journal of the Acoustical Society of America* **120**, 1095-1102.

Monteith, J.L. (1972) Solar-Radiation and Productivity in Tropical Ecosystems. *Journal of Applied Ecology* **9**, 747-766.

Monteith, J.L. (1977) Climate and Efficiency of Crop Production in Britain. *Philosophical Transactions of the Royal Society of London Series B-Biological Sciences* **281**, 277-294.

Morgenstern, K., Black, T.A., Humphreys, E.R., Drewitt, T.J., Griffis, G.B, Cai, T.B., Nesic, Z., Spittlehouse, D.L. and Livingstone, N.J. (2004) Sensitivity and Uncertainty of the Carbon Balance of a Pacific Northwest Douglas-Fir Forest During an El-Niño La-Niña Cycle. *Agricultural and Forest Meteorology* **123**, 201-219.

Nichol, C.J., Lloyd, J., Shibistova, O., Arneth, A., Roser, C. Knohl, A., Matsubara, S. and Grace, J. (2002) Remote Sensing of Photosynthetic Light-Use Efficiency of a Siberian Boreal Forest. *Tellus Series B-Chemical and Physical Meteorology* **54**, 677-687.

Prince S.D. (1991) Satellite Remote-Sensing of Primary Production - Comparison of Results for Sahelian Grasslands 1981-1988. *International Journal of Remote Sensing* **12**, 1301-11.

Reda I. and Andreas, A. (2004) Solar Position Algorithm for Solar Radiation Applications. *Solar Energy* **76,** 577-589

Running, S.W., Nemani, R., Heinsch, F., Zhao, M., Reeves, M. and Hashimoto, H. (2004) A Continuous Satellite-Derived Measure of Global Terrestrial Primary Production. *BioScience* **54**, 547-560.

Running, S.W., Baldocchi, D.D., Turner, D.P, Gower, S.T., Bakwin, P.S., Hibbard, K.A. (1999) A Global Terrestrial Monitoring Network Integrating Tower Fluxes, Flask Sampling, Ecosystem Modelling and Eos Satellite Data. *Remote Sensing of Environment* **70**, 108-127.

Schwalm, C.R., Black, T.A. Amiro, B.D., Arain, M.A. Barr, A.G., Bourque, C., Dunn, A.L., Flanagan, L.B. Giasson, M.A., Lafleur, P., Margolis, H.A., McCaughey, J.H., Orchansky, A.L., Wofsy, S. (2006) Photosynthetic light-use efficiency of three biomes across an east-west continental-scale transect in Canada. *Agricultural and Forest Meteorlogy* **140**, 269-286.

Turner, D.P., Ritts, W.D. , Zhao, M.S., Kurc, S.A., Dunn, A.L., Wofsy, S.C., Small, E.E. and Running, S.W. (2006) Assessing Interannual Variation in MODIS-Based Estimates of Gross Primary Production. *IEEE-Transactions on Geoscience and Remote Sensing* **44**, 1899-1907.

Turner, D.P., Urbanski, S., Bremer, D., Wofsy, S.C., Meyers, T., Gower, S. T. and Gregory, M. (2003) A Cross-Biome Comparison of Daily Light-Use Efficiency for Gross Primary Production. *Global Change Biology* **9**, 383-395.

Van Den Eeckhaut M., Poesen, J., Verstraeten, G., Vanackera, V., Moeyersonsc, J., Nyssena, J. and van Beek, L.P.H. (2005) The Effectiveness of Hillshade Maps and Expert Knowledge in Mapping Old Deep-Seated Landslides. *Geomorphology* **67**, 351-363.

Witten, I.H. and Frank, E. (2005) Data Mining: Practical machine learning tools and techniques, Morgan Kaufmann, Second ed. San Francisco, CA, 525 pp.

Zhang, L., Wylie, B., Loveland, T., Fosnight, E., Tieszen, L.L., Ji, L. and Gilmanov, T. (2007) Evaluation and Comparison of Gross Primary Production Estimates for the Northern Great Plains Grasslands. *Remote Sensing of Environment* **106**, 173-189.

4 INSTRUMENTATION AND APPROACH FOR UNATTENDED YEAR ROUND TOWER-BASED MEASUREMENTS OF SPECTRAL REFLECTANCE[5]

4.1 Introduction

Phyto-pigments, consisting of chlorophylls, carotenoids, and anthocyanins, are among the most important organic compounds on earth, as they absorb solar radiation, and hence are the ultimate source of energy for the terrestrial biome. As a result, an increased understanding of pigment concentration and distribution within stands, across ecosystems and biomes is an essential requirement for assessing primary productivity and carbon budgets globally. As all phyto-pigments absorb light in distinctive ways (see examples in Figure 4.1), and this absorption is detectable in the reflectance spectra of leaves (Datt, 1998, Sims and Gamon, 2002) and plant canopies (Zarco-Tejada et al., 2002, Stone et al., 2003), spectroscopy can be used as a tool for their quantification. Typically, spectral sensors record reflectance in a range of wavelengths between 400 and 2500 nm, with leaf-pigment absorption most common in the visible part of the spectrum (400-700 nm).

In recent years, one group of carotenoids in particular, named xanthophylls, has been the focus of attention as these pigments control the light-use efficiency (ε) of plants by safely dissipating excessive radiation energy through a fast alteration of the xanthophyll cycle pigment violaxanthin to zeaxanthin via the intermediate antheraxanthin (Demmig-Adams, 1990, Demmig-Adams and Adams, 1996, 2000, Demmig-Adams et al., 1998). ε

---

[5] A version of this chapter has been published. Hilker, T., Coops, N.C., Nesic, Z., Wulder, M.A. and Black, A.T. (2007), Instrumentation and Approach for Unattended Year Round Tower-Based Measurements of Spectral Reflectance. *Computers and Electronics in Agriculture* **56**, 72-84.

is an essential input variable for modeling carbon uptake by plants, termed gross primary production (GPP), from spectral reflectance and is utilized in different modeling approaches such as Monteith (1972, 1977) or the Carnegie, Stanford, Ames Approach (CASA) described in Field et al. (1995).

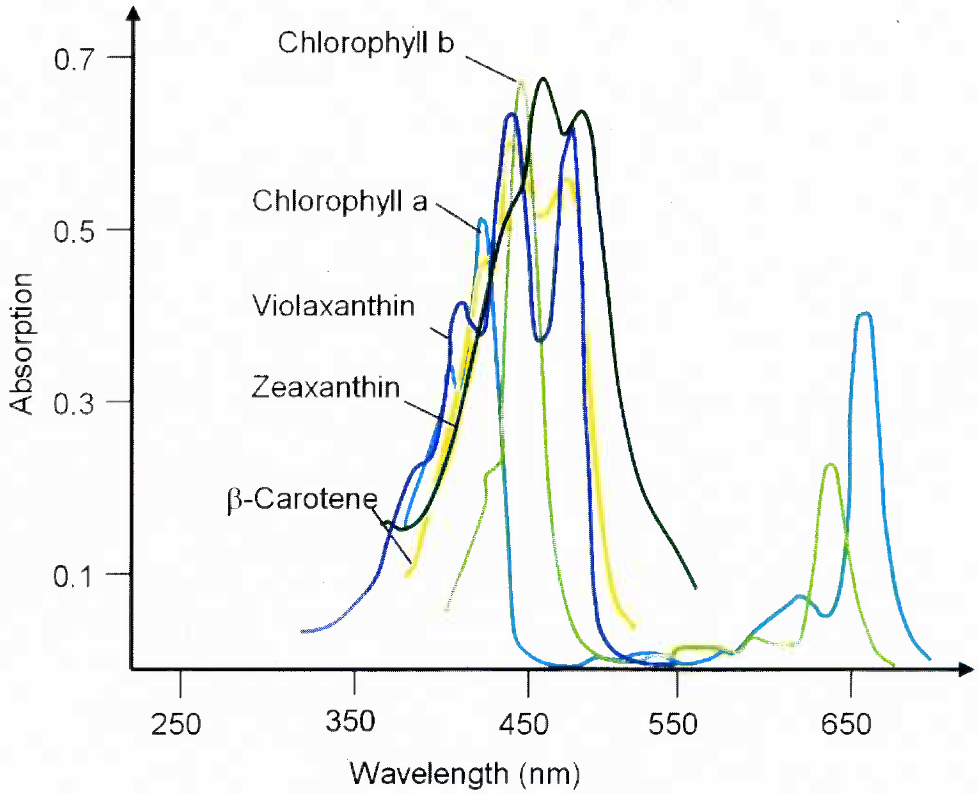

Figure 4.1: Leaf-pigment absorption features (Adapted from Purves et al., 1994).

In order to be able to detect pigment absorption features in the visible part of the electromagnetic spectrum, spectral measurements require 1) a high spectral resolution of only a few nanometers, and 2) a high signal-to-noise ratio, both of which have become readily available with easily portable field instrumentation only during recent years. Additionally, a number of physiological processes associated with leaf-pigments, such as photosynthesis, are highly dynamic (Demmig-Adams and Adams, 1996, 2000) and may vary diurnally as well as seasonally, as plants quickly respond to rapidly changing environmental conditions. As a result, conventional spaceborne sensors often fail to detect and track subtle changes in the visible reflectance, thus only providing detection of broad spectral features at isolated temporal snapshots determined by the satellite's overpass (Sims et al., 2005).

While carbon fluxes can be determined on local scales through CO_2 exchange measurements using the eddy covariance technique (Baldocchi, 2003), one of the major challenges remains the up-scaling of those measurements to landscape, regional and global levels. Remote sensing can help to address these issues by linking carbon fluxes to spectral reflectance data of various spatial scales from near surface remote sensing (e.g. Gamon et al., 2006a) to airborne (Vierling et al., 2006) and satellite platforms (Rahman et al., 2005, Drolet et al., 2006). Network approaches, such as the recently established SpecNet initiative (Gamon et al., 2006b), aim to link such measurements to carbon fluxes globally. Tower-based spectral measurements can be a valuable addition to these efforts as they principally provide reflectance information comparable to simultaneously recorded eddy flux data.

This chapter describes the development of a fully automated, tower-based, spectro-radiometer platform designed for high temporal frequency acquisition of narrow waveband reflectance between 400-1100 nm to estimate changes in plant pigment concentration in real time. The platform is named AMSPEC (Automated Multi-angular Spectroradiometer for Estimation of Canopy reflectance). The system is designed to be installed on existing eddy flux towers, at heights usually between 10 and 30 m above the canopy. AMSPEC is equipped with a motor-driven probe pointing at the forest canopy to automatically measure spectra in a near 360° observation area around the tower (Figure 4.2), while a second probe is pointing upwards for simultaneous measurements of solar irradiance to account for different sky and illumination conditions. Simultaneous measurements of irradiance and reflectance are desirable especially for automated approaches as they allow acquisition of spectral reflectance with minimal user interfacing (no re-calibration is required for changing sky conditions). This chapter discusses the instrument's hardware and software components as well as the results of a 6-month field test.

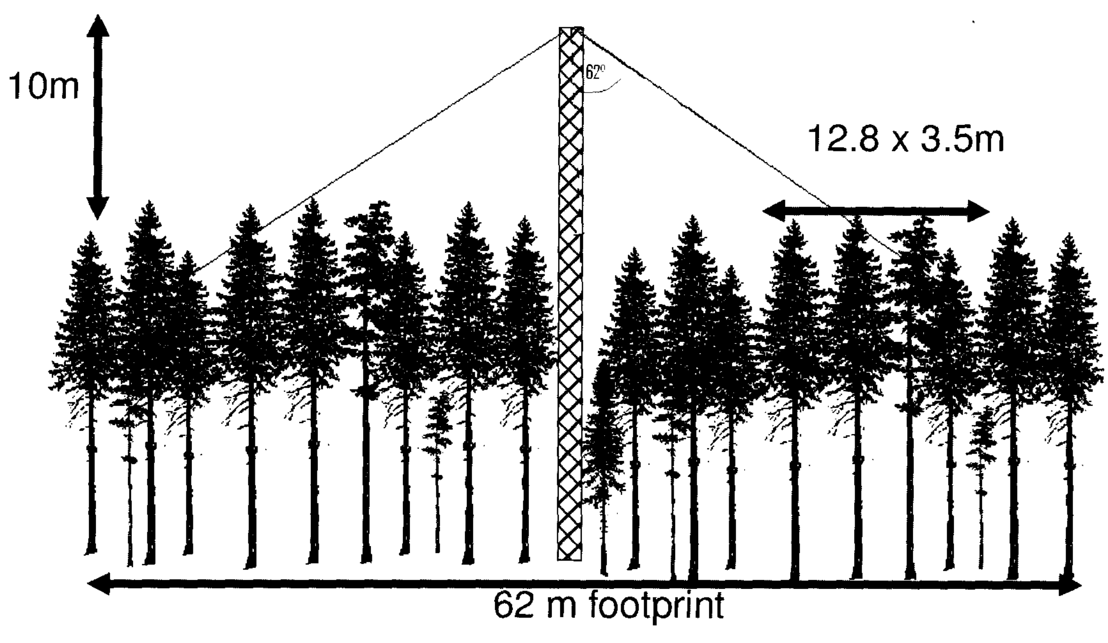

Figure 4.2: Observation area and AMSPEC-setup on flux-tower

4.2 Methods

4.2.1 Components and installation

AMSPEC features two major modules, one located on the tower and another one on the ground. The tower module consists of: 1) a Unispec-DC spectroradiometer (PP-Systems, Amesbury, MA, USA), 2) a CR10X datalogger (Campbell Scientific Inc., Logan, Utah, USA), and 3) a sensor unit equipped with a motor to move the radiometer's probe. The tower equipment is mounted as two separate units on the mast, one for the electronics, containing the radiometer and the datalogger, and the other housing the sensor unit.

The ground module consists of a personal computer linked to a data-server located at the University of British Columbia (UBC) via a mobile phone connection. Tower- and ground-based devices communicate using a 100 m-long serial communication cable. An overview of AMSPEC's components and their interrelations is shown in Figure 4.3.

4.2.1.1 Tower module

a) Spectro-Radiometer

The Unispec-DC has 256 contiguous bands with a sampling interval of a full width half maximum (FWHM) spectral response of 3nm and a nominal range of operation between 350 and 1200 nm. It is equipped with two channels for measuring both solar irradiance and canopy reflectance simultaneously. Each channel is driven by a microcontroller which incorporates a curved grating that focuses the dispersed light across a fixed 256-

element photodiode array. Relevant technical specifications for the Unispec-DC are given in Table 4.1.

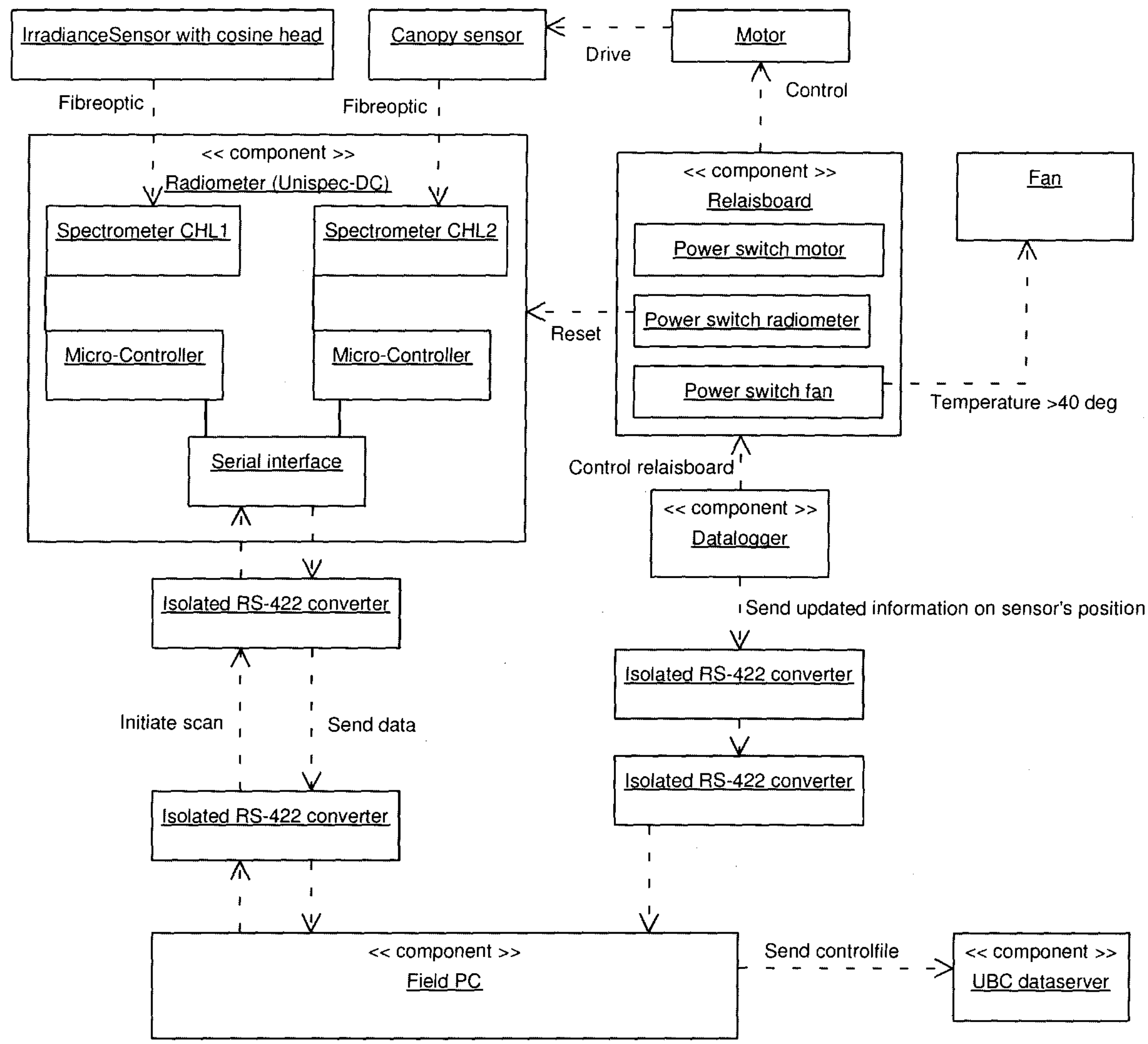

Figure 4.3: Components of AMSPEC shown as Unified Modeling Language (UML) consistent code

Parameter	Performance
Sensor	**400-1100 nm**
Resolution (σ)	**3.0 nm**
Pixel size diode array's	**3.1-3.4 nm (dependent on the wavelength)**
Repeatability	**0.1 nm**
Synchronization accuracy	**Approx. 20 µs**
Integration time	**4 ms -3280 ms**
Averaging number of scans	**1000@ 4ms (less for longer I.T.)**
Operation temperature	**0-40°C**
Scan time	**Approx 2-6 s**

Table 4.1: Technical specifications of the Unispec-DC dual channel spectro-radiometer

As both channels measure absolute values of light intensity, the reflectance can be determined from dividing the radiance by the solar irradiance after consideration of the difference in each channels' sensitivity to light and the instrument's dark current. Differences in light sensitivity are due to the individual photodiodes and foreoptics used and can be corrected through a cross-calibration approach by measuring the reflectance of a standardized reference target (Gamon et al., 2006a):

$$\rho = \frac{\rho_{canopy}}{\rho_{irradiance}} \frac{\rho'_{irradiance}}{\rho'_{control}} \qquad (1)$$

where ρ_{canopy} is the measured radiance of the canopy sensor, $\rho_{irradiance}$ is the simultaneously measured, cosine-corrected irradiance, $\rho'_{control}$ is the measured radiance of the control surface and $\rho'_{irradiance}$ is irradiance at the time $\rho'_{control}$ was taken. For calibration purposes a 5" x 5" standardized reference panel (PP-Systems, Amesbury, MA, USA) was used to calibrate the instrument prior to installation and during its operation on the tower.

Dark current (*dc*) is by definition an electrical current generated by thermal electrons in the photocathode of optical instruments (Bock, 1998) and has to be subtracted from the instrument's optical signal to obtain corrected reflectance data. As the UniSpec-DC does not provide an internal shutter mechanism to automatically correct for dc, the acquired data need to be corrected in a post processing step using manual measurements taken with both sensors completely covered from light. Due to its definition, dc was expected to be highly correlated to sensor temperature which would allow an indirect determination using a built-in sensor thermometer.

b) Datalogger

The datalogger controls the power supply for both the radiometer and the motor unit via a relay-board. The power for the radiometer is turned off once every 24 hours for a short time (10 seconds) to reset the instrument and ensure it remains operational in case of unexpected software failure. To prevent the system from overheating, the CR10X also controls a fan installed in the upper part of the electronic box, when temperatures exceed 40°C.

c) Sensor module

The sensor unit consists of a motor with a shaft and two probes which are connected via 600 μm fibreoptics cables (length: 2m each) to each channel of the radiometer. The probe for measuring solar irradiance is termed the irradiance sensor, and the other pointing at the canopy to measure reflected canopy radiance is termed the canopy sensor (Figure 4.4).

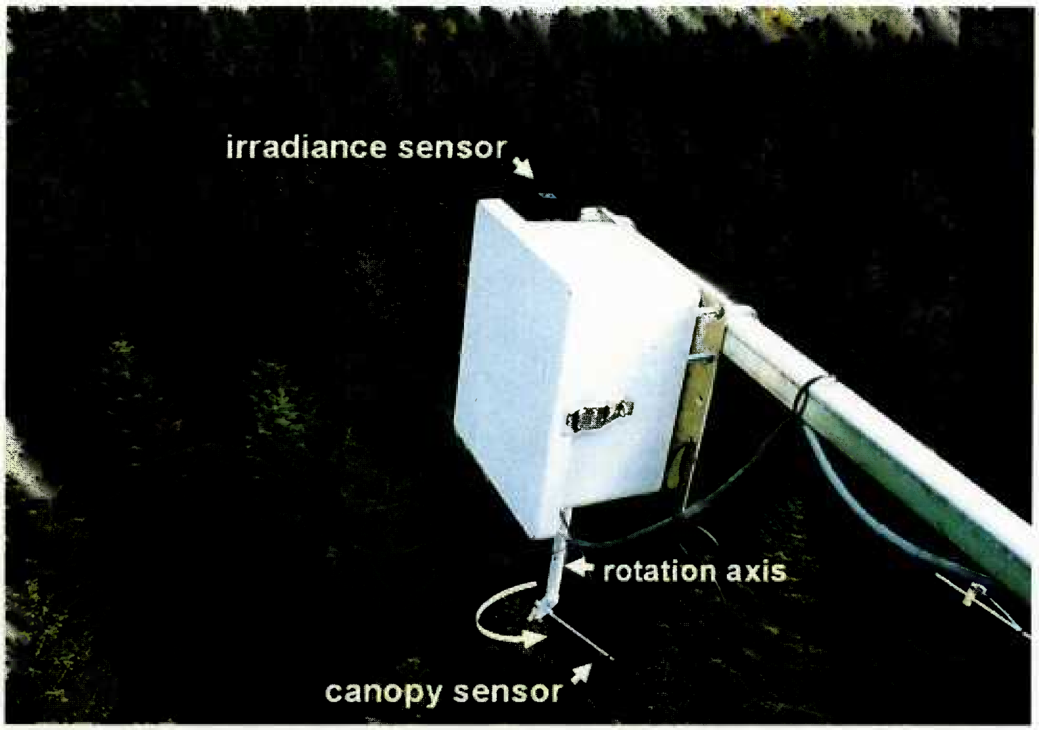

Figure 4.4: Illustration of system at research site

The upward pointing sensor, equipped with a cosine receptor suitable for sky-irradiance measurements (PP-Systems, Amesbury, MA, USA), is fixed on the highest point of the radiometer sensor-box to prevent any obstruction of the view (Figure 4.4). The canopy sensor is attached to the motor via the shaft, facilitating a near 360° observation area around the tower. The motor is controlled by the datalogger and is rotated 11.5° every 30 seconds, completing a full rotation within 15 minutes. At the end of each scan, the sensor is returned to its original position. A potentiometer attached to the shaft of the motor enables the datalogger to measure the exact position of the probe. The view zenith angle of the canopy sensor is flexible and currently set to 62° to optimize the measurement of the leaf area from spectral reflectance under clumped canopy conditions (Chen and Black, 1991). The probe's instantaneous field of view (IFOV) is 20°.

4.2.1.2 Ground component

The ground based PC unit controls the radiometer via a custom software interface described in Section 4.2.2. Two independent serial communication ports are employed, one for sending the scan-command to the radiometer and receiving the measurement results from both channels in response, and another one for tracking the instrument's exact location from the datalogger every time the canopy sensor has moved into a new position. To communicate with the unit on the tower, the RS-232 communication standard of computer's serial port is converted to RS-422 using an optically isolated RS-422 converter (B&B electronics, Ottawa, IL, USA), as RS-232 communication is limited in the length of cable usable to exchange information.

4.2.2 Software components

Two software programs have been developed, one controlling the radiometer (named UnispecController) and the other one summarizing the datafiles created over the day (FieldCheck) to send them as control information to the UBC data-server.

a) UnispecController

UnispecController has been developed in Visual C++ 7.1. Figure 4.5 shows a flow chart, illustrating the functionality of the software. The program is scheduled to launch automatically after system startup, and initially opens the first serial port, connects to, and initializes the radiometer by sending an encoded sequence of characters, describing channel initialization, baud rate, integration time, and number of scans to average. After this initial sequence is transmitted, the radiometer is ready for operation. To track the exact position of the canopy sensor, the second serial port is opened to receive the location information from the datalogger.

Scans are initiated by the software at fixed time intervals (events) adjustable through a parameter file. At each event, a character code is sent to the radiometer, which in turn executes the command and, in response, returns the resulting measurements to the computer. A control mechanism ensures that 256 numbers, one for each spectral band, is received, otherwise the corrupted dataset is deleted from storage and the radiometer's cache memory is refreshed. If the subsequent measurements are still corrupted, for instance due to an unexpected software failure of the radiometer, the system will automatically reset the instrument after a number of attempts (currently set to 10).

Spectral information, the actual radiometer position, and the system time for each scan are stored in a data-vector. An update of the sensor's location is sent from the datalogger every time the canopy sensor has finished repositioning. Every 15 minutes, all data are written to the computer's hard-drive and stored as 8 bit unsigned characters under a unique filename of the format YYMMDDQQ, where QQ is the 2 digit running number for the respective quarter-hour interval. To ensure data compatibility with measurements at other sites, all time measurements are made in Greenwich Mean Time (GMT).

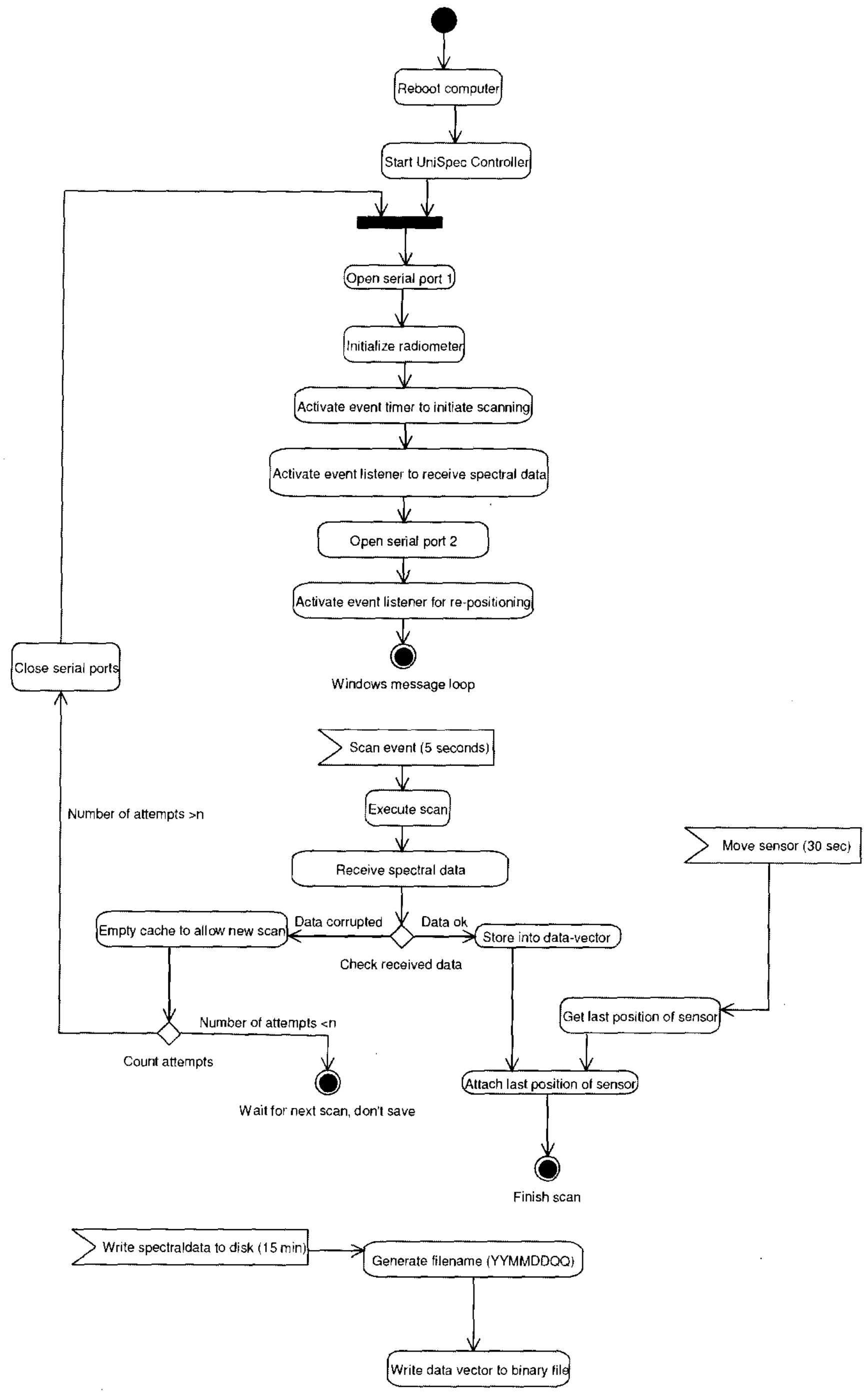

Figure 4.5: Flow chart radiometer control software

b) FieldCheck

The FieldCheck routine, written in MATLAB 5 (MathWorks Inc., Natick, MA, USA), automatically commences at midnight local time daily to calculate a statistical summary of the previous day's data. Arithmetic mean and maximum reflectance-ratio are determined for each 2-hour interval of the day, in the four cardinal directions, and stored in a binary file, which then gets transferred to UBC via a mobile phone connection. The file is designed to provide a summary overview of the previous day's conditions to ensure the instrument is working as intended. In a final step, all data files collected on that day are moved into a folder of the format YYMMDD for retrieval during regular field visits.

To operate the system a series of Microsoft® Windows® events is automatically scheduled, for starting and stopping the radiometer control software, summarizing data files, and the overnight computer reboot. The radiometer software works until shortly before midnight Pacific Standard Time (PST), when the MATLAB routine is initiated to summarize the data files and move them into daily folders. Additionally, a backup routine is invoked, copying all data files to an external drive. The computer reboots itself 3 hours after midnight (PST) to reset the machine, coincident to the radiometer on the tower being reset by the datalogger.

4.2.3 Field test

AMSPEC was installed at a field site where ongoing measurements are being undertaken as part of the Fluxnet-Canada initiative to collect information on CO_2 exchange between atmosphere and forest (Baldocchi et al., 2001). The site is a 57-year-old second growth conifer forest, located 10 km south west of Campbell River on Vancouver Island, BC, Canada (49°52 N, 125°20 W), at an elevation of about 300 m above sea level (Morgenstern, 2004). Douglas-Fir (*Pseudotsuga menziesii* var *menziesii* (Mirb.) Franco) is the dominant tree species in this area with secondary species including western red-cedar (*Thuja plicata* Donn *ex* D. Don) (17%) and western hemlock (*Tsuga heterophylla* (Raf.) (Sarg.)) (3%) (Morgenstern et al., 2004). The radiometer is mounted on a 45m tall, 51 cm triangular open-lattice type tower (Morgenstern, 2004) at a height of about 9 m above the canopy.

The view area (Figure 4.6) observed by the instrument varies slightly with height of installation above canopy and terrain slope while looking in different directions, however, at this site, the outer diameter is about 62 m at canopy height (Figure 4.3, Figure 4.6), while the elliptic instantaneous view area of the probe has a major axis of 17.9 m and a minor axis of 3.5 m (at canopy height). The small portion not seen by the instrument is due to obstruction from the open lattice tower and depends on how the instrument is mounted on the tower and the tower size (e.g. scaffold tower, vs. open lattice tower).

The sampling area for the eddy covariance measurements or flux-footprint depends on atmospheric stability (Leclerc and Thurtell, 1990), and can range from a few hectares to a few square-kilometres (Schmid, 1994). However, the area to which flux measurements are most sensitive, also referred to as peak footprint, is much smaller and covers a radius of only 100-300 m (Blanken et al., 2001, Kljun et al., 2004). Using AMSPEC, about 10-20% of this area can be sampled, which, under stable atmospheric conditions, can be assumed to be representative of the entire footprint, due to stand homogeneity inherent to flux tower sites (Baldocchi, 2003).

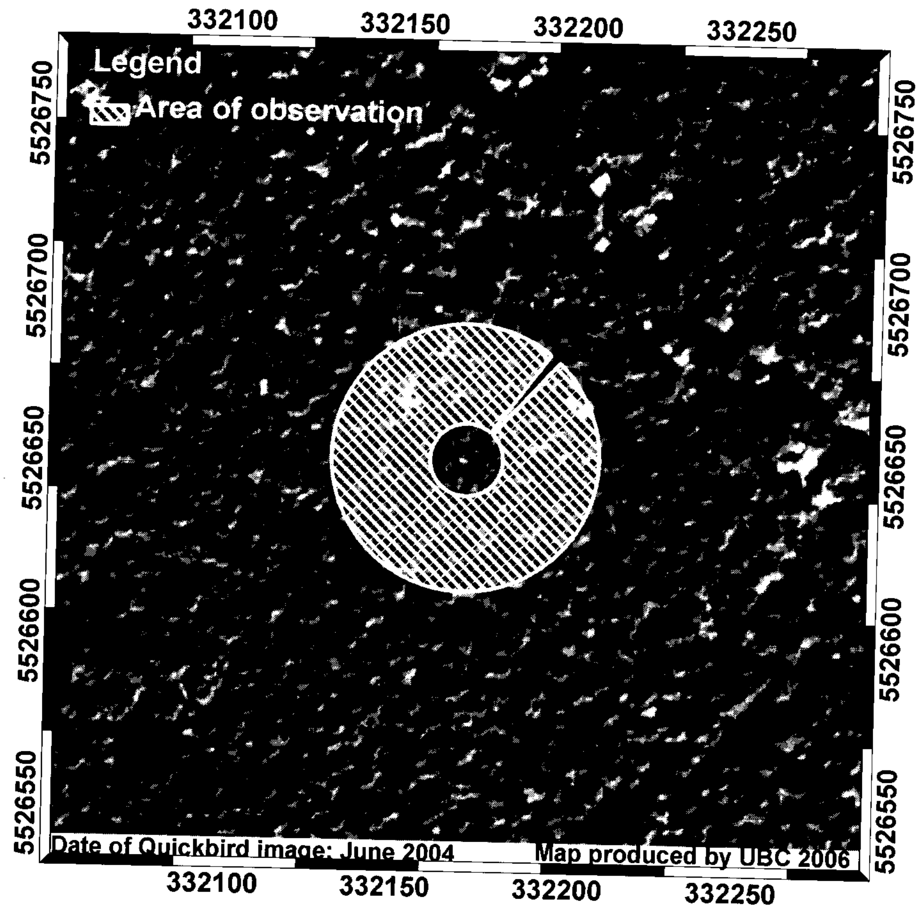

Figure 4.6: AMSPEC's footprint over backdrop of QuickBird (0.6 m x 0.6 m spatial resolution panchromatic imagery). The missing area in the North-West is due to obstruction by the open lattice tower.

4.3 Results and Discussion

4.3.1 Instrument operation

Since installation, AMSPEC has been operating for 6 months (November 2005 – May 2006). In that time the instrument has compiled nearly 2 million spectral datasets. System failure rate to date has been 3%, excluding a downtime due to a defective motor in March 2006 accounting for 21 additional days. The failure rate is well within the range of classical methods of GPP assessment, such as the eddy covariance technique, for which data gaps of 17-50% were reported, which do, however, also include gaps in nighttime data (Wilson and Baldocchi, 2001, Falge et al., 2001, Monson et al., 2002, Hui et al., 2004).

4.3.2 Multi-angular observations

Figure 4.7a shows a set of sample spectra recorded under clear sky conditions on May 3rd, 2006 at 20:00 GMT (12:00 PST) over 15 minutes covering all view angles from 11.5-345° in 30 steps of 11.5° each. The large variation in reflectance, especially in the near infrared region (NIR) of the spectrum, is principally due to different viewing directions, as radiation gets largely scattered by canopy architecture when not observing single leaves, but rather heavily structured tree crowns. A similar kind of spectral pattern can be obtained when looking at a fixed location over the course of one day from sunrise to sunset. Under cloudy conditions, the directional effect is much less as the radiation regime is dominated by diffuse radiation, yet still abundant. Figure 4.7b shows a spectrum for one full rotation recorded under cloudy conditions on April, 26th 2006 at 21:00 GMT (13:00 PST)

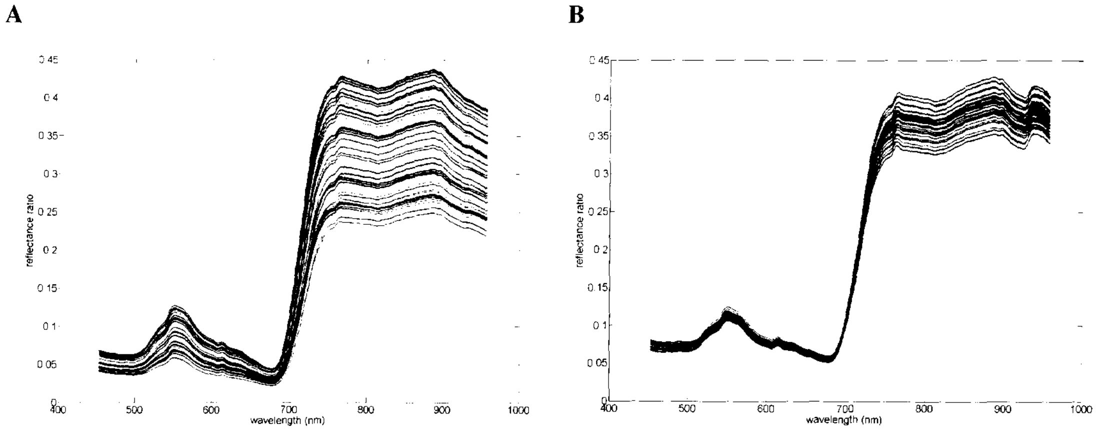

Figure 4.7: Variation in canopy spectra due to different viewing directions a) under clear sky conditions (May, 5th 2006, 12:00 PST) and b) under cloudy conditions (April, 26th 2006, 13:00 PST)

The range of seasonal variability collected by AMSPEC can be seen by the example given in Figure 4.8. The graph shows daily reflectance spectra recorded during the commencement of the growing season, between April 4th 2006 and May 15th 2006, at solar noon facing north. Besides the tree canopy undergoing dramatic physiological changes over this period of time, the variation is also largely due to the differences in solar elevation. The daily maximum solar elevation during the described period varied between 46.70° and 58.76°.

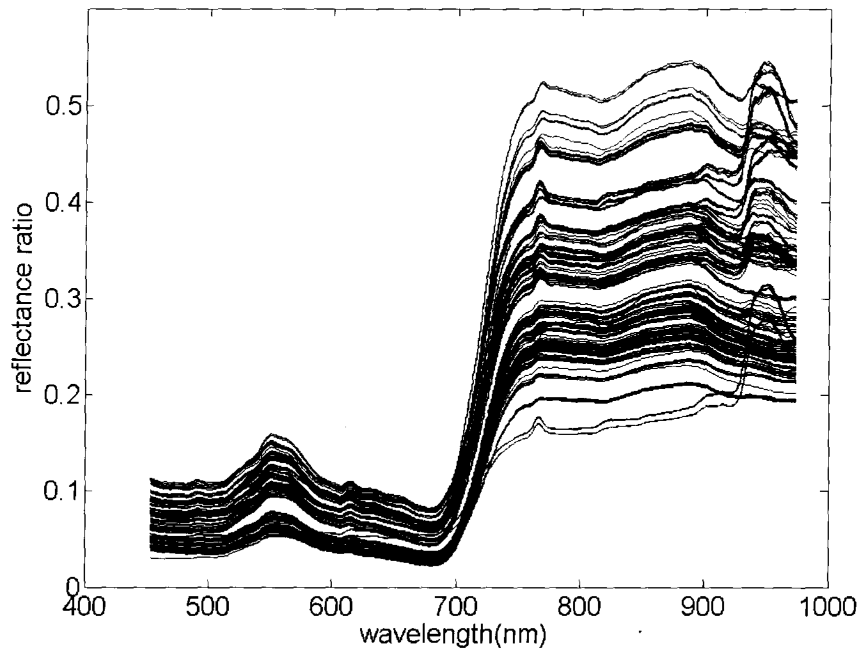

Figure 4.8: Variation in canopy spectra due to seasonal dependencies between April 6th and May 15th 2006 looking north.

Multi- angular spectral data represent canopy level dependencies, capturing leaves, branches, structures, gaps, and understorey (Asner, 1998) and include a number of valuable information that cannot be obtained from nadir measurements alone. Hall et al. (1992) showed that reflected solar radiance from nadir measurements originates mostly from sunlit leaves only, as radiative signals from shaded leaves are relatively weak, yet shaded leaves can contribute a significant part to a plant's photosynthesis. Chen et al. (2003) demonstrated that the information from shaded leaves is contained in the variation pattern of sunlit leaves if similar measurements are made over a wider range of view zenith angles, suggesting that a full assessment of plant physiological properties from spectral reflectance is only possible under multiple viewing directions. Studies of the interaction of radiation with vegetation canopies and the underlying soil surface have shown that multi-angular measurements are potentially rich in information on vegetation structure, especially when the observer's direction is close to coincidence with the sun direction (Jupp and Strahler 1990, Chen and Leblanc 1997, Goel et al., 1997). This phenomenon is also referred to as hotspot effect (Grant et al., 2003) and is a prominent feature in remote sensing. Additionally, multi-angular observations allow the determination of leaf pigment concentration under various illumination conditions (Demmig Adams and Adams, 1996, Adams et al., 1999). The current vertical zenith angle of 62° is optimized to facilitate studies of effective leaf area index (LAI_e) (Chen and Black, 1991, Chen et al., 2005) and the fraction of the photosynthetically active radiation (f_{PAR}) (Chen, 1996), both essential for modeling GPP (Monteith, 1972, Field et al., 1995).

A way to minimize and correct for the directional impacts on spectra inherent to off-nadir observations is through fitting a bi-directional reflectance distribution function (BRDF) which describes the complex radiation regimes of canopy surfaces. In ongoing research, our approach is to employ a combination of kernels based on a number of site observations and empirical modeling to correct for existing directional effects. Kernel based BRDF models describe reflectance regimes as linear superposition of a set of basic BRDF shapes (Wanner et al., 1995) and have been applied, for instance, in the AMBRALS model employed in the MODIS satellite products (Lucht et al., 2000). The modeling approach for the described field site will include a radiative transfer model to describe the branch architecture within the tree crowns, as well as a detailed canopy surface model, derived from three-dimensional laser scanning (LiDAR - Light Detection and Ranging), to describe the fraction of sunlit to shaded crowns and overall brightness for each given AMSPEC reflectance spectra.

4.3.3 Dark current

To verify the long term dependency of dark current and sensor temperature, nighttime measurements recorded at solar midnight were compared to temperature values of the same time period. The result is shown in Figure 4.9 ($r^2 = 0.71$, $p<0.05$). The abscissa describes the sensor temperature measured inside the Unispec DC, while the ordinate contains the integrated reflectance data (=sum over all 256 channels obtained at solar midnight) over the first five months of operation.

Despite dc measurements being obtained without a shutter mechanism using nighttime data only, the figure reveals the general dependency between temperature and dc allowing for interpolation of manually taken dc measurements before, within and after the described operation period.

4.4 Conclusion

The AMSPEC system described in this chapter is suitable for unattended, high frequency, long term observation and tracking of diurnal and seasonal variations of plant physiological processes under various weather and illumination conditions. The number of spectral datasets that may be collected in a given period of time allows detailed studies, even of short term processes, such as variation of light-use efficiency and photosynthesis. The spatial resolution, determined by the sensor's instantaneous field of view (IFOV), vertical view angle, and height of installation above canopy, is sufficiently fine to study the spectral response of only a few individual tree-crowns.

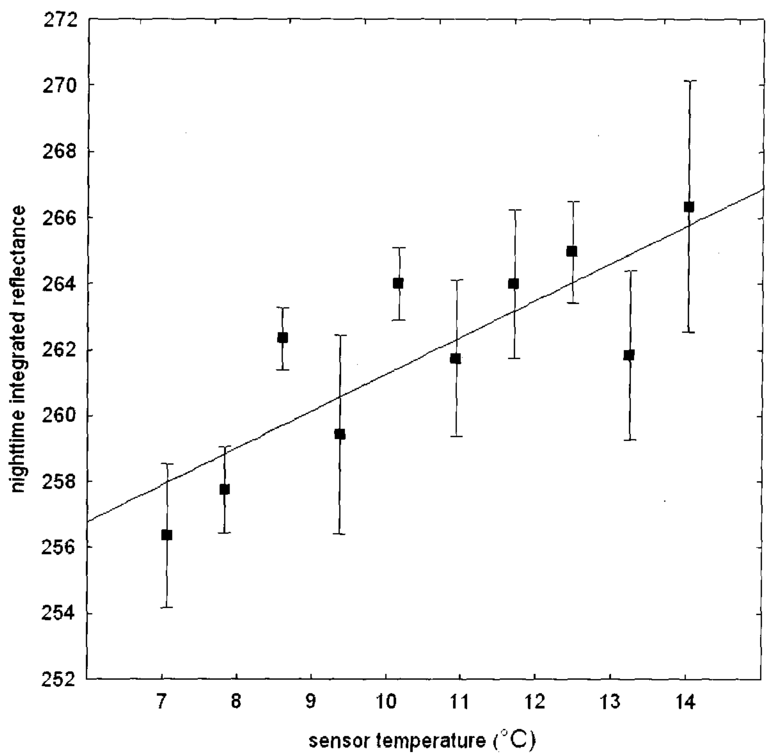

Figure 4.9: Dependency between midnight integrated radiation data (=sum of dc over all 256 bands, grouped into 10 different classes) and sensor temperature. (r^2=0.71, p<0.05). To reduce the existing background radiation at night, the integrated reflectance data were grouped by temperature and averaged into 10 classes (standard errors as shown in the graph).

The collected dataset also allows detailed studies of the forest canopy under multiple view angles, as spectra are available under a large variety of different observer- and sun-angles. Additionally, the relatively small viewing area facilitates intensive studies of the canopy structure including ratios of sunlit to shaded leaves, depth, and composition of tree crowns, by using either ground-based methods or automated tools such as LiDAR (Lim et al., 2003). The large variation of view- and solar zenith angles, however, also makes the correction of BRDF an essential requirement when trying to detect physiologically induced changes in spectra.

The installation on existing flux towers allows direct comparison of radiometric measurements with CO_2 fluxes, obtained from eddy covariance measurements. This characteristic makes it highly suitable as tool for the SpecNet network (Gamon, 2002, Gamon et al., 2006b) designed to extend the capabilities of the existing flux-tower network (Baldocchi et al., 2001) by linking spectral reflectance data with gas exchange measurements (Gamon et al., 2006b).

The development of systems, such as the one described in this chapter can help to improve the understanding of diurnal and seasonal variations in vegetation absorption due to pigment concentrations as well as obtain a more detailed understanding of the viewing geometry which will ultimately lead to improved detection of changing vegetation characteristics from satellites.

4.5 References

Adams, W.W., Demmig-Adams, B., Logan, B.A., Barker, D.H., Osmond, C.B., (1999) Rapid Changes in Xanthophyll Cycle Dependent Energy Dissipation and Photosystem II Efficiency in two Vines, *Stephania japonica* and *Smilax australis*, Growing in the Understory of an open Eucalyptus forest. *Plant, Cell and Environment* **1999**, 125-136.

Asner, G.P., (1998) Biophysical and Biochemical Sources of Variability in Canopy Reflectance. *Remote Sensing of Environment* **64**, 234-253.

Baldocchi, D., Falge, E., Gu, L.H., Olson, R., Hollinger, D., Running, S., Anthoni, P., Bernhofer, C., Davis, K., Evans, R., Fuentes, J., Goldstein, A., Katul, G., Law, B., Lee, X.H., Malhi, Y., Meyers, T., Munger, W., Oechel, W., U, K.T.P., Pilegaard, K., Schmid, H.P., Valentini, R., Verma, S., Vesala, T., Wilson, K., Wofsy, S., (2001) Fluxnet: A New Tool to Study the Temporal and Spatial Variability of Ecosystem-Scale Carbon Dioxide, Water Vapor, and Energy Flux Densities. *Bulletin of the American Meteorological Society* **82**, 2415-2434.

Baldocchi, D.D., (2003). Assessing the Eddy Covariance Technique for Evaluating Carbon Dioxide Exchange Rates of Ecosystems: Past, Present and Future. *Global Change Biology* **9**, 479-492.

Blanken, P.D., Black, T.A., Yang, P.C., Neumann, H.H., Nesic, Z., Staebler R., (2001) Energy Balance and Canopy Conductance of a Boreal Aspen Forest: Partitioning Overstory and Understory Components, *Journal of Hydrology* **245**, 118-136

Bock, R.K., (1998) Dark current. Website. Accessed 10/2006 at http://rd11.web.cern.ch/RD11/rkb/PH14pp/node40.html

Chen, J.M., Black, T.A. (1991) Measuring Leaf Area Index of Plant Canopies with Branch Architecture. *Agricultural and Forest Meteorology* **57**, 1-12.

Chen J.M., (1996) Canopy Architecture and Remote Sensing of the Fraction of Photosynthetically Active Radiation Absorbed by Boreal Conifer Forests. *IEEE-Transactions on Geoscience and Remote Sensing* **34**, 1353-1368

Chen, J.M., Liu, J., Leblanc, S.G., Lacaze, R. and Roujean, J.L. (2003) Multi-Angular Optical Remote Sensing for Assessing Vegetation Structure and Carbon Absorption. *Remote Sensing of Environment* **84**, 516-525.

Chen J.M., Menges C.H., Leblanc S.G., (2005) Global Mapping of Foliage Clumping Index Using Multi-Angular Satellite Data. *Remote Sensing of Environment* **97**, 447-457

Datt, B., (1998) Remote Sensing of Chlorophyll a, Chlorophyll B, Chlorophyll A+B, and Total Carotenoid Content in Eucalyptus Leaves. *Remote Sensing of Environment* **66**, 111-121.

Demmig-Adams, B. (1990) Carotenoids and Photoprotection in Plants - A Role for the Xanthophyll Zeaxanthin. *Biochimica Et Biophysica Acta* **1020**, 1-24.

Demmig-Adams, B., Adams, W. W. (1996) The Role of Xanthophyll Cycle Carotenoids in the Protection of Photosynthesis. *Trends in Plant Science* **1**, 21-26.

Demmig-Adams, B., Adams, W.W. (2000) Photosynthesis - Harvesting Sunlight Safely. *Nature* **403**, 371-374.

Demmig-Adams, B., Moeller, D.L., Logan, B.A., Adams, W.W. (1998) Positive Correlation Between Levels of Retained Zeaxanthin Plus Antheraxanthin and Degree of Photoinhibition in Shade Leaves of Schefflera Arboricola, Hayata. Merrill. *Planta* **205**, 367-374.

Drolet G.G., Huemmrich K.F., Hall F.G., Middleton E.M., Black T.A., Barr A.G., Margolis H.A. (2005). A MODIS-derived Photochemical Reflectance Index to Detect Inter-Annual Variations in the Photosynthetic Light-Use Efficiency of a Boreal Deciduous Forest. *Remote Sensing of Environment* **98**, 212-224.

Falge, E., Baldocchi, D., Olson, R., Anthoni, P., Aubinet, M., Bernhofer, C., Burba, G., Ceulemans, G., Clement, R., Dolman, H., Granier, A., Gross, P., Grunwald, T., Hollinger, D., Jensen, N.O., Katul, G., Keronen, P., Kowalski, A., Lai, C.T., Law, B.E., Meyers, T., Moncrieff, J., Moors, E., Munger, J.W., Pilegaard, K., Rannik, U., Rebmann, C., Suyker, A., Tenhunen, J., Tu, K., Verma, S., Vesala, T., Wilson, K., Wofsy, S. (2001) Gap Filling Strategies for Long Term Energy Flux Datasets. *Agricultural and Forest Meteorology* **107**, 71-77.

Field C.B., Randerson J.T, Malmstrom C.M. (1995) Global Net Primary Production – Combining Ecology and Remote Sensing. *Remote Sensing of Environment* **51**, 74-88.

Grant, I.F., Bréon , F.M., Leroy, M.M. (2003) First Observation of the Hot Spot from Space at Sub-Degree Angular Resolution using POLDER data. *International Journal of Remote Sensing* **24**, 1103 – 1110.

Gamon, J.A., (2002). SpecNet: Proposal for an NCEAS Working Group. *Website*. Accessed 06/2006 at http://specnet.info/

Gamon, J.A., Cheng, Y, Claudio, H., MacKinney, L. Sims, D.A., (2006a) A Mobile Tram System for Systematic Sampling of Ecosystem Optical Properties. *Remote Sensing of Environment* **103**, 246-254.

Gamon, J.A.,Rahman, A.F., Dungan J.L., Schildhauer M., Huemmrich K.F. (2006b) Spectral Network (SpecNet) - What is it and why do we need it? *Remote Sensing of Environment* **103**, 227-235.

Goel N.S., Qin W.H., Wang B.Q. (1997) On the Estimation of Leaf Size and Crown Geometry for Tree Canopies from Hotspot Observations. *Journal of Geophysical Research - Atmospheres* **102**, 29543-29554

Hall, F.G., Huemmrich, K.F., Goetz, S.J., Sellers P.J., Nickeson, J.E (1992). Satellite Remote Sensing of Surface Energy Balance: Success, Failures, and Unresolved Issues in FIFE. *Journal of Geophysical Research* **97**, 19061–19089.

Hui, D.F., Wan, S.Q., Su, B., Katul, G., Monson, R., Luo, Y.Q. (2004) Gap-Filling Missing Data in Eddy Covariance Measurements Using Multiple Imputation (Mi) for Annual Estimations. *Agricultural and Forest Meteorology* **121**, 93-111.

Kljun N, Kastner-Klein P., Fedorovich E., Rotach, M.W. (2004) Evaluation of Lagrangian Footprint Model Using Data from Wind Tunnel Convective Boundary Layer. *Agricultural and Forest Meteorology* **127**, 189-201.

Leclerc, M.Y. and Thurtell, G.W. (1990) Footprint Prediction of Scalar Fluxes Using a Markovian Analysis. *Boundary-Layer Meteorology* **52**, 247–258

Lim, K., Treitz, P., Wulder, M., St-Onge, B., Flood, M. (2003). LiDAR Remote Sensing of Forest Structure. *Progress in Physical Geography* **27**, 88-106.

Lucht W., Schaaf C.B., Strahler A.H. (2000) An Algorithm for the Retrieval of Albedo from Space Using Semi-Empirical BRDF models. *IEEE-Transactions on Geoscience and Remote Sensing* **38**, 977-998

Monson, R.K., Turnipseed, A.A., Sparks, J.P., Harley, P.C., Scott-Denton, L.E., Sparks, K., Huxman, T.E. (2002) Carbon Sequestration in a High-Elevation, Subalpine Forest. *Global Change Biology* **8**, 459-478.

Monteith, J.L. (1972) Solar-Radiation and Productivity in Tropical Ecosystems. *Journal of Applied Ecology* **9**, 747-766.

Monteith, J.L. (1977) Climate and Efficiency of Crop Production in Britain. *Philosophical Transactions of the Royal Society of London. Series B-Biological Sciences* **281**, 277-294.

Morgenstern, K., Black, T.A., Humphreys, E.R., Griffis, T.J., Drewitt, G.B., Cai, T.B., Nesic, Z., Spittlehouse, D.L., Livingstone, N.J. (2004) Sensitivity and Uncertainty of the Carbon Balance of a Pacific Northwest Douglas-Fir Forest During an El-Niño La-Niña Cycle. *Agricultural and Forest Meteorology* **123**, 201-219.

Purves W.K., Orians, G.H., Heller, H.R., Heller, H.C. (1994) Life: The Science of Biology, 4th Edition, Sinauer Associates

Rahman A.F., Sims D.A., Cordova V.D. (2005) Potential of MODIS EVI and surface temperature for directly estimating per-pixel ecosystem C fluxes. *Geophysical Research Letters* **32**: Art. No. L19404.

Rast, M., 2001. SPECTRA – Surface Processes and Ecosystem Changes through Response Analysis. *ESA SP* **1257**, 5 . ESA The Netherlands. 132pp

Schmid H.P. (1994) Source Areas for Scalars and Scalar Fluxes. *Boundary Layer Meteorology* **67**, 293–318.

Sims, D.A., Gamon, J.A. (2002) Relationships Between Leaf-pigment Content and Spectral Reflectance Across a Wide Range of Species, Leaf Structures and Developmental Stages. *Remote Sensing of Environment* **81**, 337-354.

Sims, D.A., Rahman, A.F., Cordova, V.D., Baldocchi, D.D., Flanagan, L.B., Goldstein, A.H., Hollinger, D.Y., Misson, L., Monson, R.K., Schmid, H.P., Wofsy, S.C., Xu, L.K. (2005). Midday Values of Gross CO_2 Flux and Light-use efficiency During Satellite Overpasses Can Be Used to Directly Estimate Eight-Day Mean Flux. *Agricultural and Forest Meteorology* **131**, 1-12.

Smith, M., Martin, M., Plourde, L., Ollinger, S. (2003) Analysis of Hyperspectral Data for Estimation of Temperate Forest Canopy Nitrogen Concentration: Comparison Between Airborne (AVIRIS) and a Spaceborne, Hyperion Sensor. *IEEE-Transactions on Geoscience and Remote Sensing* **41**, 1332-1337.

Stone, C., Chisholm, L.A., McDonald, S. (2003). Spectral Reflectance Characteristics of Pinus Radiata Needles Affected by Dothistroma Needle Blight. *Canadian Journal of Botany-Revue Canadienne De Botanique* **81**, 560-569.

Strahler, A., Jupp, D. (1990) Modelling Bi-directional Reflectance of Forests and Woodlands Using Boolean Models and Geometric Optics. *Remote Sensing of Environment* **34**, 153-166.

Vierling, L.A., Fersdahl, M., Chen, X., Li, Z., Zimmerman, P. (2006). The Short Wave Aerostat-Mounted Imager (SWAMI): A novel Platform for Acquiring Remotely-Sensed Data from a Tethered Balloon. *Remote Sensing of Environment* **103** , 255-264.

Wanner W., Li, X., Strahler, A.H. (1995). On the Derivation of Kernels for Kernel Driven Models of Bi-Directional Reflectance, *Journal of Geophysical Research* **100**, 21077-21089

Wilson, K.B., Baldocchi, D.D. (2001) Comparing Independent Estimates of Carbon Dioxide Exchange Over 5 Years at a Deciduous Forest in the Southeastern United States. *Journal of Geophysical Research-Atmospheres* **106**, 34167-34178.

Zarco-Tejada, P.J., Miller, J.R., Mohammed, G.H., Noland, T.L., Sampson, P.H. (2002) Vegetation Stress Detection Through Chlorophyll A+B Estimation and Fluorescence Effects on Hyperspectral Imagery. *Journal of Environmental Quality* **31**, 1433-1441.

5 SEPARATING PHYSIOLOGICALLY AND DIRECTIONALLY INDUCED CHANGES IN PRI USING BRDF MODELS[6]

5.1 Introduction

Plant physiological processes, governing biosphere-atmosphere interactions, are highly dynamic and can vary significantly over space and time as plants respond to rapidly changing environmental conditions. As a result, study of such processes requires careful consideration of the spatial and temporal dynamics involved (Hall et al., 1995). A prominent example of such a process is the photosynthetic light-use efficiency (ε), which describes the efficiency with which a plant can use absorbed solar radiation energy for the production of biomass (Monteith, 1972, 1977) thereby driving (amongst other factors) the amount of carbon accumulation in terrestrial ecosystems (Monteith et al., 1977, Field, 1991, Goetz et al., 1999). Determined by any of a large number of environmental stresses restraining the photochemical reaction process, such as nutrition supply, water, and temperature, ε depends on vegetation types and varies greatly over space and time (Field and Mooney 1986, Prince and Goward 1995, Turner et al., 2003). Whilst recent years have seen considerable progress detecting ε using high spectral resolution remote sensing instrumentation at the leaf, canopy, and stand scales, the angular, spatial, spectral and temporal requirements for up-scaling such observations to landscape and global levels using satellite remote sensing remain less well understood (Hall et al., 1995, Xiao et al., 2004).

[6] A version of this chapter has been published. Hilker, T., Coops, N.C., Hall, F.G., Black, T.A., Wulder, M.A. Nesic, Z., Krishnan, P. (2008) Separating Physiologically and Directionally Induced Changes in PRI using BRDF Models. *Remote Sensing of Environment*, in press

One way to investigate scaling requirements for modeling ecosystem processes from satellite-derived land surface parameters is to study relationships between canopy reflectance and plant physiological processes at the stand level, using permanently established tower-based remote sensing devices, allowing continuous observation of the canopy surface with high spatial and spectral resolution observations (Leuning et al., 2006, Chapter 4). Knowledge obtained from such studies may then be used to develop models for up-scaling reflectance parameters to landscape and global scales.

Investigation of plant physiological processes at the stand level requires consideration of multiple viewing geometries, as 1) temporal dynamics require study of diurnal as well as seasonal patterns, and 2) full assessment of stand-level photosynthesis from spectral reflectance requires careful observation of leaves, branches, structures, gaps, and understorey to understand how reflectance depends on viewing and illumination geometry (Asner, 1998). This information, however, is not easily obtained from nadir measurements alone (Strahler and Jupp 1990, Chen and Leblanc 1997, Goel and Grier, 1988). For instance, canopy radiance from nadir measurements originates mostly from sunlit leaves only, as radiative signals from shaded leaves are relatively weak, even though shaded leaves contribute a significant part to a plant's overall photosynthesis (Hall et al., 1992). Multi-angular observations provide a means to characterize the anisotropy of surface reflectance (Chen et al., 2005), which has been shown to contain information on the structure of vegetated surfaces and shaded parts of the canopy (Chen et al., 2003, Myneni et al., 2002, Gao et al., 2003). These multi-angular observations, however, are subject to directional reflectance effects that can confound the desired signal used for extraction of canopy information (Los et al., 2005). These effects can be described in terms of geometric and volumetric scattering effects (Jupp, 1998). The volumetric effect, driven by the canopy structure, including leaf angle distribution and total leaf area, leads to changes in path length and extinction, while the geometric effect relates to individual canopy shapes (Roujean et al., 1992, Jupp, 1998) causing scenes to appear darker or brighter depending on the amount of shadow cast as seen by an observer (Privette et al., 1994, Lucht et al., 2000).

One possible way to model these directional reflectance effects is using a bi-directional reflectance distribution function (BRDF), which describes how land surface reflectance varies with view zenith, solar zenith and azimuth angle (Barnsley et al., 1997, Gao et al., 2003, Los et al., 2005). Several different approaches exist to modeling BRDF, of which the semi-empirical kernel representation is the most common (Roujean et al., 1992 Wanner et al., 1995). Kernel based BRDF models represent angular reflectance distribution as linear superposition of a set of basic BRDF shapes based on relative sun position and simple measures of the canopy structure (Wanner et al., 1995). Their simple character allows acquisition of model parameters from mathematical inversion of relatively few reflectance observations, thereby facilitating applications over a wide range of spatial scales. An underlying assumption for these observations, however, is that the physiological status of the observed canopy is constant, which does not hold for narrow waveband reflectance, used to track short term changes in physiological vegetation properties. As a result, modeling BRDF is problematic (Los et al., 2005), as the observed reflectance measurements are an integrated function of both changes in geometrically induced illumination conditions and physiologically induced changes in leaf spectral reflectance.

In this chapter, we develop and apply an approach to separate directional and physiologically induced reflectance effects from canopy spectra estimates by stratifying observations according to environmental conditions, which, assuming that physiology follows environmental factors, should also stratify the dataset according to physiological states (Los et al., 2005). Once developed, the approach is applied using tower-based spectral reflectance observations of a Douglas-fir (*Pseudotsuga menziesii* var *menziesii* (Mirb.) Franco) dominated forest stand in British Columbia, Canada. Within each stratified set of observations, variations in canopy reflectance status are observed using reflectance obtained from a platform-mounted multi-angular spectroradiometer over a full year with physiologically induced reflectance changes separated from directional effects using a kernel driven BRDF model.

5.2 Methods

5.2.1 Research area

The study area is a Canadian Carbon Program flux tower site, located between Courtenay and Campbell River on Vancouver Island, British Columbia, Canada (49°52'7.8" N, 125°20'6.3" W) at 350 m above sea level. The coniferous forest consists of 80% Douglas-fir, 17% western red cedar (*Thuja plicata* Donn *ex* D. Don) and 3% western hemlock (*Tsuga heterophylla* (Raf.) Sarg.) (Morgenstern et al., 2004) and is considered second-growth planted in 1949, after harvesting of the original stand (Goodwin, 1937). The understorey consists mainly of salal (*Gaultheria shallon* Pursh.), Oregon grape

(*Berberis nervosa* Pursh), vanilla-leaf deer foot (*Achlys triphylla* (Smith) DC), various ferns and mosses (Morgenstern et al., 2004). A 1998 site survey found that the stand density was 1100 stems ha^{-1}, and tree height was 30-35 m, and the average diameter at breast height (DBH) was 29 cm. Chen et al. (2006) found that the leaf area index (LAI) was 7.3 m^2 m^{-2} based on measurements using TRAC and LAI-2000.

The site is among the most productive in Canada, with harvest rotation cycles as short as 60 years (Morgenstern et al., 2004). The soil is a humo-ferric podzol with a gravelly sandy loam texture and a surface organic layer ranging from 1 to 10 cm in depth. The total soil C content to 1 m is 11.5 kg Cm^{-2}, of which 2.5 kg Cm^{-2} is in the surface organic layer (Drewitt et al., 2002, Morgenstern et al., 2004). The research area is part of the dry maritime Coastal Western Hemlock biogeoclimatic subzone (*CWHxm*) with an average annual precipitation of 1500 mm and mean annual temperature of 8.5°C (Humphreys et al., 2006). This subzone is characterized by a maritime climate with typically cool summers and mild winters, but can experience significant drought conditions during late summer and early autumn. Year-round eddy covariance flux measurements have been made since 1997 and the site (referred to as DF49) was part of the Fluxnet-Canada Research Network from 2002 to 2007 (Morgenstern et al., 2004, Margolis et al., 2006).

5.2.2 Eddy covariance data

Continuous, half-hourly fluxes of CO_2 and water vapor were measured above the canopy between April 1st 2006 and March 31st 2007 using the eddy covariance (EC) technique (Morgenstern et al., 2004, Humphreys et al., 2006). EC fluxes were measured with a three-axis sonic anemometer-thermometer (SAT, R3, Gill Instruments Ltd., Lymington, UK) and a closed-path CO_2/H_2O infrared gas analyzer (IRGA) (LI-6262, LI-COR Inc., Lincoln, NE, USA). Net ecosystem exchange (NEE) was calculated as the sum of the half-hourly fluxes of CO_2 and the rate of change in CO_2 storage in the air column between the ground and the EC-measurement level (42m). Incident and reflected photosynthetically active radiation (PAR [μmol m^{-2} s^{-1}]), defined as the photon flux between 400-700 nm wavelength, were measured using up and downward looking quantum sensors (model 190 SZ, LI-COR Inc.), installed above and below the canopy and diffuse PAR was measured using a "sunshine sensor" (model BF3, Delta-T Devices Ltd., Burwell, UK). Wind speed related gaps in CO_2 fluxes of less than 2 h were filled using linear interpolation. Half-hourly measurements of gross primary production (GPP) were calculated using,

$$GPP = NEP + R_d \qquad (1)$$

where NEP is the daytime net ecosystem production (NEP=-NEE) and R_d is the daytime ecosystem respiration (Morgenstern et al., 2004), calculated using the annual exponential relationship between nighttime NEE and soil temperature at 5-cm depth after applying a logarithmic transformation to correct for heteroscedasticity (Black et al., 1996, Goulden et al., 1997). Gaps in GPP were filled using a Michaelis-Menten GPP versus PAR relationship fitted to daytime data when air temperature $T_{Air} > -1$ °C (see Morgenstern et al., 2004, Jassal et al., 2007). Half hourly ε was calculated from GPP using the light-use efficiency term of Monteith (1972, 1977):

$$\varepsilon = \frac{GPP}{PAR \cdot f_{PAR}} \qquad (2)$$

where PAR is the half-hour PAR incident upon the canopy and f_{PAR} represents the half-hour fraction of PAR being absorbed by the plant canopy. f_{PAR} was determined from the ratio of incident to reflected total PAR measured above and below the canopy ($\rho_1(\theta)$ and $\rho_2(\theta)$), respectively, the solar zenith angle (θ) at the time of measurement and the effective leaf area to account for clumping effects (LAI$_e$ [m^2m^{-2}])(Chen 1996):

$$f_{PAR} = (1-\rho_1(\theta)) - (1-\rho_2(\theta))e^{(G_t(\theta)LAI_e/\cos\theta)} \qquad (3)$$

where $G_t(\theta)$ is the projection coefficient for total PAR transmission approximated being a constant of 0.5 (Chen, 1996, Chen et al., 2006) and LAI$_e$ was defined for the mature evergreen forest as a constant 4.3 throughout the study period assuming a clumping index of 0.45 (Chen et al., 2006). A complete description of the EC data and processing methods applied can be found in Morgenstern et al. (2004), Humphreys et al. (2006), and Jassal et al. (2007).

5.2.3 Remotely-sensed data

Canopy reflectance measurements were obtained from an automated multi-angular spectroradiometer platform (named AMSPEC) installed at a height of 45m (≈10m above the tree canopy) on the open-lattice 50-cm triangular flux-tower (Chapter 4). The instrument features a motor-driven probe that allows observations in a 330° view area around the tower. The probe rotates in 11.5° intervals every 30 seconds, thereby completing a full rotation every 15 minutes. A potentiometer attached to the shaft of the motor facilitates exact measurement of the probe's position. At the end of each sweep, the sensor is returned to its original position. The spectroradiometer used is a Unispec-

DC (PP Systems, Amesbury, MA, USA) featuring 256 contiguous bands with a nominal band spacing of 3 nm and a nominal range of operation between 350 and 1200 nm. To allow sampling under varying sky conditions, canopy reflectance is obtained from simultaneous measurements of solar irradiance and radiance, sampled every 5 seconds from sunrise to sunset. The upward pointing probe is equipped with a cosine receptor (PP-Systems) to correct sky irradiance measurements for varying solar altitudes. The downward looking probe measures canopy radiance at a zenith angle of 62° to account for canopy clumping (Chen and Black, 1991). The probe's instantaneous field of view (IFOV) is 20°. The outer diameter of the instrument's footprint is approximately 62 m at canopy height, while the elliptic instantaneous view area of the probe has a major axis of about 17.9 m and a minor axis of around 3.5 m (Figure 5.1). No observations were made between an azimuth of 220° and 250° (defined from geodetic north) due to obstruction by the tower. Reflectance measurements used for this analysis were collected continuously between April 1st 2006 and March 31st 2007. A complete technical description of the instrument, its setup and calibration can be found in Chapter 4.

The sampling area for the eddy covariance measurements or flux-footprint depends on windspeed and atmospheric conditions (Leclerc and Thurtell, 1990), and can range from a few hectares to a few square-kilometres (Schmid and Lloyd, 1999). However, the area to which flux measurements are most sensitive, also referred to as peak footprint, is much smaller and covers a radius of only 100-300 m (Blanken et al., 2001, Kljun et al., 2004). Using the radiometer platform, about 10-20% of this area can be sampled, which can be assumed to be representative of the entire footprint, due to stand homogeneity of this flux tower site and as a result, spectral measurements obtained from AMSPEC are directly comparable to EC-flux data (Chapter 4).

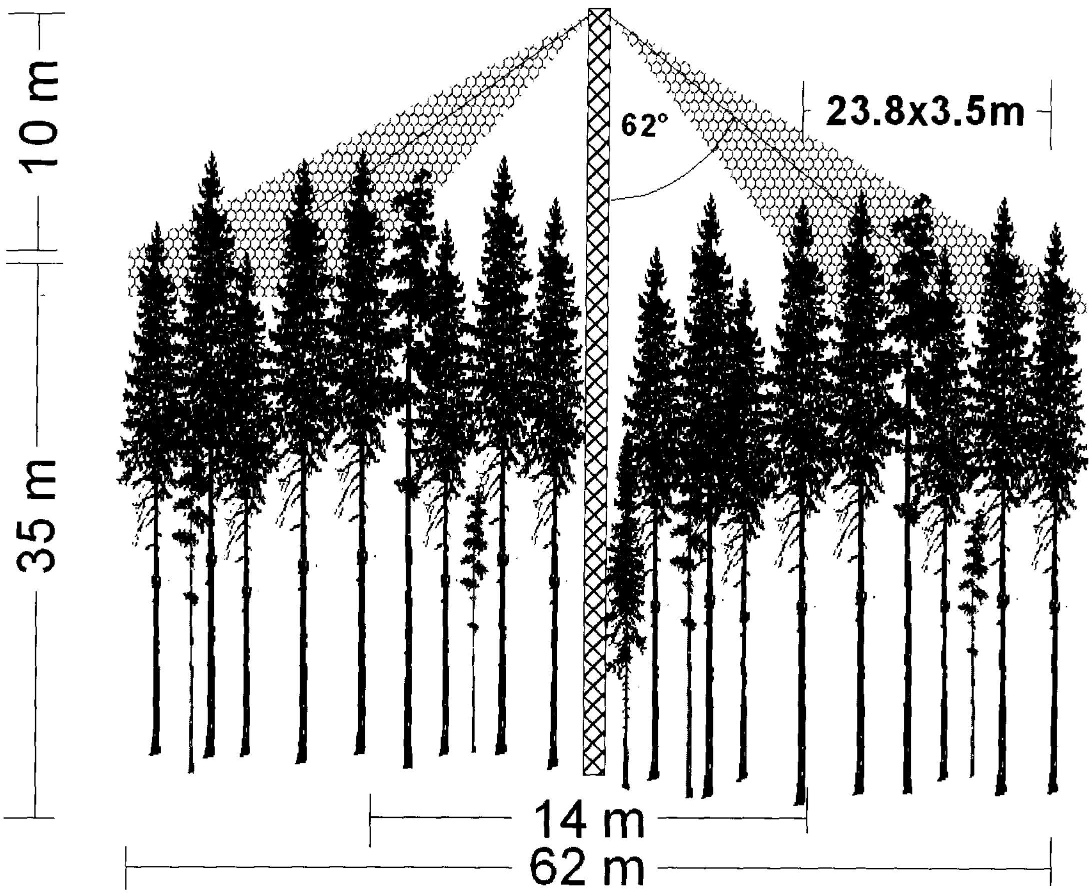

Figure 5.1: Area of observation of tower-based spectroradiometer and technical setup (Chapter 4). The footprint area varies slightly with individual tree height and differences in terrain height. The vertical zenith angle is 62°, the approximate footprint size is 62m (diameter).

5.2.4 Inferring ε from remote sensing

One way to infer ε from remotely-sensed observations is narrow waveband detection of the epoxidation state of a group of leaf-pigments named xanthophylls, responsible for balancing absorption and utilization of light quanta in order to prevent oxidative damage to the photosynthetic apparatus in leaves (Demmig-Adams and Adams, 1996, Demmig-Adams and Adams, 2000). Under excessive radiation conditions the xanthophyll cycle pigment violaxanthin is de-epoxidized rapidly via intermediate antheraxanthin to zeaxanthin, both of which dissipate radiation energy safely as heat, with the reaction reversed when light is limiting (Demmig-Adams and Adams, 1998). These pigment changes manifest in a narrow waveband (difference) absorption feature centered at 531 nm (Gamon et al., 1993) and hence can be quantified in leaves, canopies and stands as the Photochemical Reflectance Index (PRI), (Gamon et al., 1992, 1993, Peñuelas et al., 1995),

$$PRI = \frac{\rho_{531} - \rho_{570}}{\rho_{531} + \rho_{570}} \tag{4}$$

comparing the reflectance at 531 nm (ρ_{531}) to a xanthophyll-insensitive reference band at 570nm (ρ_{570}). Originally established for sunflower leaves, the empirical relationship between PRI and ε has been confirmed over a wide range of species (Peñuelas et al., 1994, 1995, Filella et al., 1997, Gamon and Surfus, 1999). Generalization of this correlation for application at the stand level and beyond, however, remains difficult (Barton and North, 2001, Rahman et al., 2001, 2004) as PRI is highly sensitive to view-angle, soil background reflectance, leaf angle distribution (at larger view angles) and leaf area (Barton and North, 2001).

For this study, high temporal frequency observations of PRI were calculated from AMSPEC data using linear interpolation of the closest wavebands available for 530 nm (529.4 nm and 532.7 nm) and 570 nm (568.8 nm and 572.1 nm), respectively for all solar altitudes > 10° (as derived from the time of measurement, Reda and Andreas, 2004) between April 1st 2006 and March 31st, 2007.

5.2.5 Modeling the bi-directional reflectance distribution of PRI

5.2.5.1 BRDF notation

Semi-empirical kernel driven models for the BRDF of vegetated land surfaces typically consist of a linear combination of three kernels describing isotropic, geometric and volumetric scattering effects (Roujean et al., 1992). Isotropic scattering refers to the reflectance properties of an isotropic, Lambertian surface, and, assuming random leaf distribution, can be seen as aggregate property of the sum of leaves, while geometric scattering describes scattering effects due to crown shape (Roujean et al., 1992). Volumetric scattering models dispersion effects due to vertical and horizontal distribution of vegetation elements inside the tree canopy. A series of different mathematical kernels can be selected to optimize BRDF models for various kinds of vegetation cover. Among the most commonly applied functions are Ross and Li Kernels (Wanner et al., 1995, Lucht et al., 2000, Strugnell and Lucht, 2001) with the Ross kernels (Roujean et al., 1992) based on the radiative transfer theory of Ross (1981), whereas the Li kernels are geometric-optically based (Li and Strahler, 1986). Both types of kernels are examples of physical reflectance models. In temperate climatic zones and when observing discontinuous, stacked canopies (e.g. conifer stands), the bi-directional reflectance distribution is most commonly represented by the Li-sparse (LS) and Ross-thick (RT) kernels, yielding the LSRT BRDF model as (Roujean et al., 1992, Lucht et al., 2000, Los et al., 2005),

$$\rho(\theta_v,\theta_s,\Delta\phi) = k_i + k_g K_L(\theta_v,\theta_s,\Delta\phi,\tfrac{h}{b},\tfrac{b}{r}) + k_v K_R(\theta_v,\theta_s,\Delta\phi) \qquad (5)$$

where

k_i	isotropic scattering component
k_g	geometric scattering component
K_L	Li-Sparse kernel
k_v	volumetric scattering component
K_R	Ross-Thick kernel
θ_v	view zenith angle
θ_s	solar zenith angle
$\Delta\phi$	azimuth angle
$\frac{h}{b}$	crown relative height =1 (Wanner et al., 1995, Justice et al., 1998)
$\frac{b}{r}$	crown relative shape =2 (Wanner et al., 1995, Justice et al., 1998)

k_i, k_g and k_v are the empirical components (kernel weights) derived from mathematical inversion of the linear model using multi-angular radiation observations. For a surface that behaves in a more Lambertian manner (e.g. a smooth non-layered surface), the magnitude of the isotropic kernel coefficient k_i of equation (5) should be larger than k_g and k_v. For a continuous layered canopy, k_i and k_v should dominate, since the RT function will better describe the directional observations. For a discontinuous coniferous canopy the LS function will better match the observations, hence k_g is expected to be the larger component. The LSRT model as shown in (5) has been applied to global satellite reflectance observations for a range of vegetation canopy structures thereby permitting a semi-empirical reconstruction of the full canopy BRDF from satellite acquisitions for a limited number of view and illumination angles (Wanner et al., 1995).

When utilizing a normalized difference reflectance index (NDRI) such as the PRI that uses reflectance in two spectral wavelengths, the BRDF of the NDRI can either be computed for each wavelength separately or by applying a mathematical inversion to the observed index directly. The latter approach has the advantage that the residual errors are directly minimized with respect to the NDRI (Los et al., 2005). Direct inversion of PRI can be achieved by substituting equation 5 into the general form of the NDRI, yielding (angular dependencies of the kernels are not stated):

$$\rho_{NDRI}(\theta_v,\theta_s,\Delta\phi)=\frac{\left(k_{i,\rho_d}-k_{i,\rho_r}\right)+\left(k_{g,\rho_d}-k_{g,\rho_r}\right)K_L+\left(k_{v,\rho_d}-k_{v,\rho_r}\right)K_R}{\left(k_{i,\rho_d}+k_{i,\rho_r}\right)+\left(k_{g,\rho_d}+k_{g,\rho_r}\right)K_L+\left(k_{v,\rho_d}+k_{v,\rho_r}\right)K_R} \tag{6}$$

where k_{ρ_d} and k_{ρ_r} are the kernel weights of detection and reference band, respectively. Los et al. (2005) concluded that if the isotropic kernel weights for both the reference and the detection band are somewhat larger than zero (which holds for most land surfaces with the exception of open surface water), the majority of the variability observed in equation (6) can be attributed to variations in the numerator and not to variations in the denominator. Therefore, equation (6) can be simplified by considering the denominator constant, reducing it to

$$\rho_{NDRI}(\theta_v,\theta_s,\Delta\phi)=k_i'+k_g'K_L+k_v'K_R \tag{7}$$

where the primes indicate that the kernel coefficients in equation (7) are a reformulation of the kernel coefficients in equation (5) (Los et al., 2005).

5.2.5.2 Classification of spectral observations and data analysis

Assuming a homogeneous stand structure, the BRDF of the PRI observed by AMSPEC is a function of three key factors: 1) the view-sun geometry, 2) the prevailing sky conditions at the time data was sampled and 3) the physiological status of the vegetation canopy observed (i.e. ε). Since modeling of the reflectance distribution using (7), assumes 2) and 3) to be constant, all PRI measurements were stratified on a half-hourly basis into subsets of homogeneous environmental conditions with respect to both sky conditions and ε and a separate BRDF was fitted to each stratum. First, reflectance measurements were grouped into classes of observations made under approximately homogeneous sky conditions, as determined by the ratio of direct to diffuse sky radiation (Q). These classes are hereafter referred to as Q_0 to Q_9, where Q_0 contains all spectra derived under sky conditions with $Q_0 \in [0..0.5], Q_1 \in [0.5..1.5], \ldots, Q_8 \in [7.5..8.5]$, $Q_9 \in [>8.5]$. Second, each of these classes was then further stratified into groups of measurements observed under homogenous values of ε as determined from flux tower instrumentation (named $\varepsilon_{0.1}$ to $\varepsilon_{3.5}$ where $\varepsilon_{0.1} \in [0..0.2], \varepsilon_{0.3} \in [0.2..0.4], \ldots, \varepsilon_{3.5} \in [3.4..3.6]$)

The model described in (7) was fitted separately for the observations contained in each class using a robust linear least squares algorithm (bi-square-weighted iterations) (Holland and Welsch 1997, DuMouchel and O'Brien 1989). Using k_i', k_g' and k_v', all PRI observations within each class were normalized to a constant view and illumination geometry (June 21st solar noon, looking north at a vertical zenith angle of 62°) to separate physiologically induced changes in PRI from those caused by other effects and permit the examination of changes in canopy NDRI strictly as a function of tower-measured ε. A subsequent analysis investigated the relationship between the BRDF scattering components and different physiological and atmospheric states as determined by ε and the ratio of direct to diffuse downwelling radiation, respectively. All BRDF kernel components can, under certain conditions, be related to tower-measured ε (Hall et al., 2008). The impact of the volumetric NDRI kernel component, however, is smaller for wavelengths with similar optical properties in stacked canopies and consequently, a focus was set on isotropic and geometric kernel weights. The isotropic kernel weight, representing Lambertian reflectance (Roujean et al., 1992, Wanner et al., 1995), was hypothesized to change as a function of ε as xanthophyll related pigment changes are closely related to PRI (Gamon et al., 1992, Peñuelas et al., 1995, Sims et al., 2005). Geometric BRDF scattering, representing crown shape and hence shading effects between tree crowns, was hypothesized to change as a function of the atmospheric conditions observed, as shading effects will be more distinct with increasingly clear sky conditions. Also, under clear conditions, the geometric component was expected to be correlated to ε across the different strata.

5.3 Results

5.3.1 Modeling the BRDF

Stratification of the flux tower observations of sky conditions and ε resulted in 31 unique physiological and atmospheric states identified for the one-year study period. Figure 5.2

shows an overview of the classes derived and number of observations made in each class (total number of observations: 246,276).

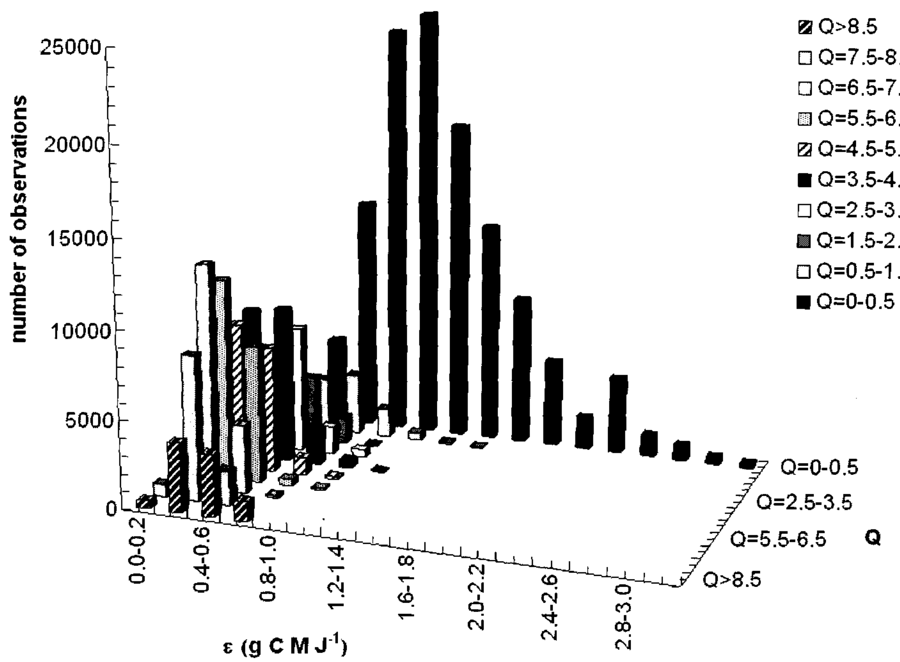

Figure 5.2: Number of observations made for classes of homogeneous sky conditions (ratio of direct to diffuse radiation, Q) and homogenous physiological states (ε). A total of 31 classes were derived with observations in it, n_{total}=246,276. The class width for ε is 0.2 g C MJ^{-1} and the class width for Q is 1.

Variations in ε were largest under diffuse radiation conditions, with values ranging from 0 to 3.6 g C MJ^{-1}, and ε was generally lower under clear sky conditions. Directional reflectance effects were smallest under overcast situations and increasing with increasingly clear skies. The BDRF models fitted separately for each class of observations were, on average, able to explain of 60% of variations in PRI (mean $\bar{r}^2 = 0.6, \sigma = 0.2,\ p < 0.05$) with the most significant results being achieved for clear sky observations. An overview of the amount of spectral variation explained under different sky conditions is given in Figure 5.3.

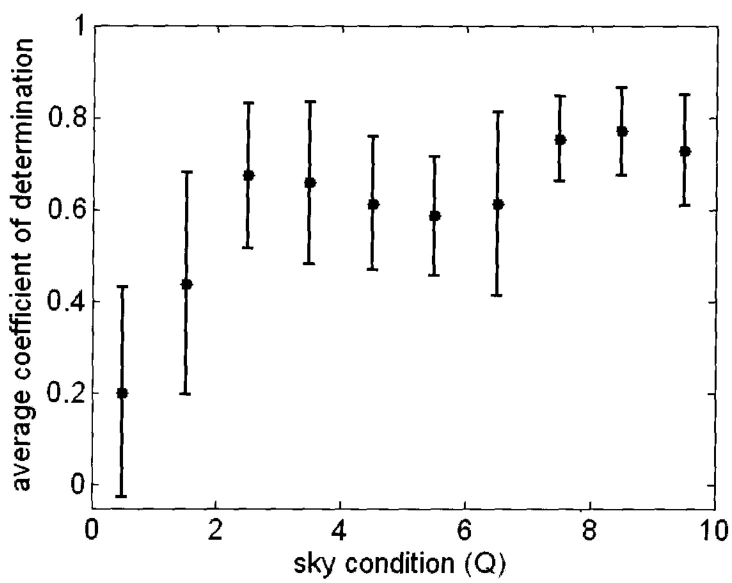

Figure 5.3: Average coefficient of determination for fitting the BRDF functions to observations made under different cloud conditions (Q_1- Q_9). The amount of variation explained by the BRDF increases with increasingly clear skies as directional reflectance effects under diffuse radiation conditions are minimal. The error-bars represent the deviation from the mean according to different classes of ε. No relations were found between the quality of BRDF fitting and different levels of ε.

BRDF surfaces modeled for different Q and ε strata are shown in Figure 5.4A-J. Each graph (5A-J) represents a different range of sky conditions (Q_0 to Q_9), from cases where almost all radiation is scattered, diffuse light (Figure 5.4A) to observations acquired under completely clear skies (Figure 5.4J). The different BRDF surfaces shown within each figure are the PRI surfaces for all ε strata, while sky conditions remain constant. The PRI values are plotted for each (x,y) location beneath the tower as defined by a Cartesian coordinate system whose origin is the tower, and whose positive y-axis is aligned with geodetic north (to the right in 5A-J). All reflectance surfaces shown are standardized to a constant sun geometry (June 21st, solar noon). The variability of PRI due to ε is most apparent under cloudy sky conditions (5A), showing the full range of ε values from 0-3.6 g C MJ^{-1}. Raw measured PRI values varied between -0.2 and 0, the BRDF corrected, normalized surface reflectance of PRI ranged between -0.1 and 0, respectively.

The difference between sunlit (~min) and shaded (~max) PRI (ΔPRI) within each strata shown in Figure 5.4 (=tilt of each BRDF surface) is depending on both directional reflectance effects (because of the amount of shadow cast seen by the observing probe) and ε induced changes in leaf level reflectance (because sunlit parts of the canopy are more likely to be exposed to excess light levels, causing a conversion of violaxanthin to zeaxanthin and resulting in a lowering of PRI) (Hall et al., 2008). As a result, ΔPRI is highest under clear skies and high stress levels (low ε) (Figure 5.5) and decreases with decreasing Q and increasing ε-values.

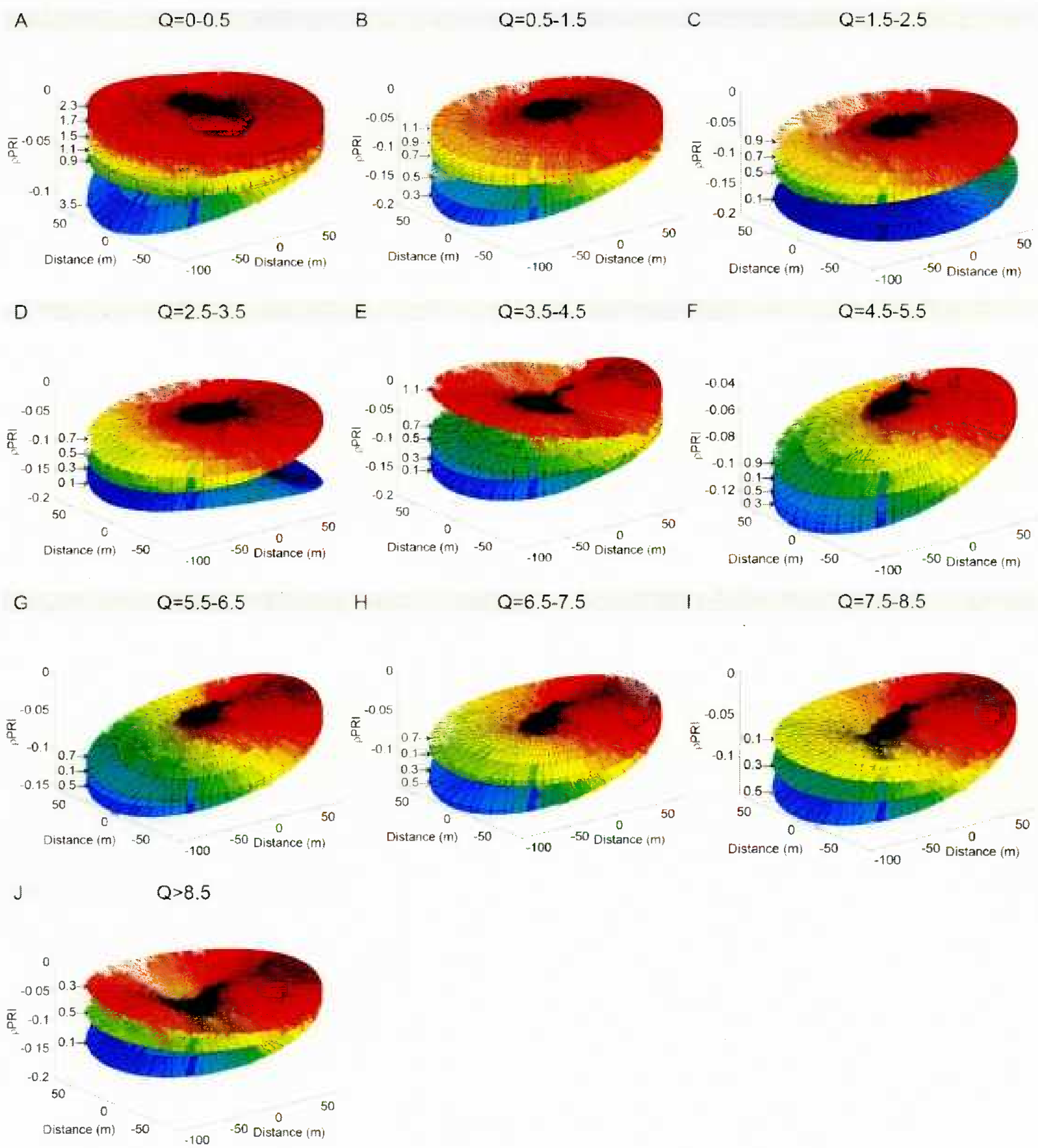

Figure 5.4 A-J: BRDF surfaces obtained for homogeneous sky and physiological condition. Each figure represents one state of cloudiness from overcast (A) to perfectly clear skies (J). The different BRDF surfaces within each figure represent different physiological states (ε) while the sky conditions for observations within each figure are constant. Low ε values result in low PRI measurements, while higher ε measurements result in PRI values up to 0. All BRDF surfaces are standardized to a common viewing geometry (June 21st, 2006, solar noon). The colors of the surfaces are used to emphasize the topographic properties of the surfaces. The labels within the figures represent the ε strata for each BRDF surface. The width in ε strata is 0.2, that is, a surface labelled "0.3" for instance, represents reflectance observations made under conditions where ε- values were between 0.2 and 0.4.

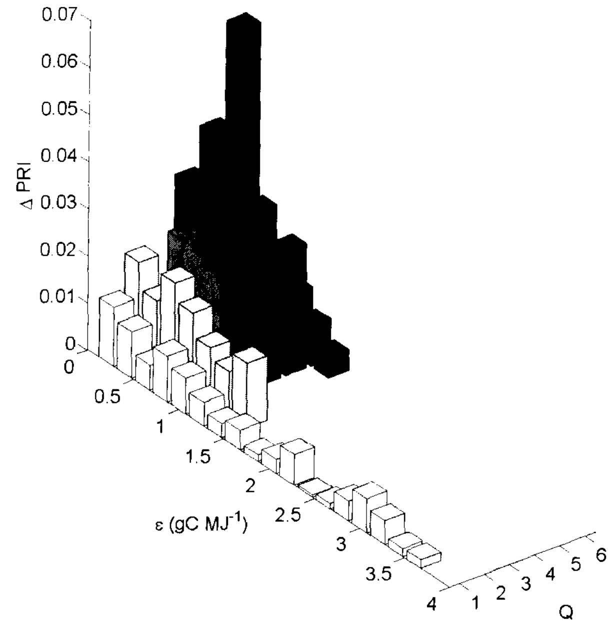

Figure 5.5: Difference between maximum (south) and minimum (north) PRI (ΔPRI) for different ε and Q strata for the directionally corrected case (zenith angle of 62°). Higher stress levels (low ε) cause differences between sunlit and shaded parts of the canopy to be more distinct. Also ΔPRI is increasing with increasingly clear skies.

5.3.2 Analysis of BRDF scattering

Figure 5.6 shows the relationship between ε and the isotropic kernel weight as given in Figure 5.4 for observations made under different sky conditions (Q_0 - Q_9). The data points in each figure show the value of the isotropic BRDF scattering component fitted as a function of ε using weighted least squares, the error-bars give the standard error of the BRDF estimate. Significant correlations were found between ε and the isotropic kernel weights ($\bar{r}^2 = 0.62, \sigma = 0.28$, $p < 0.05$) for all sky conditions (Q_0 - Q_9).

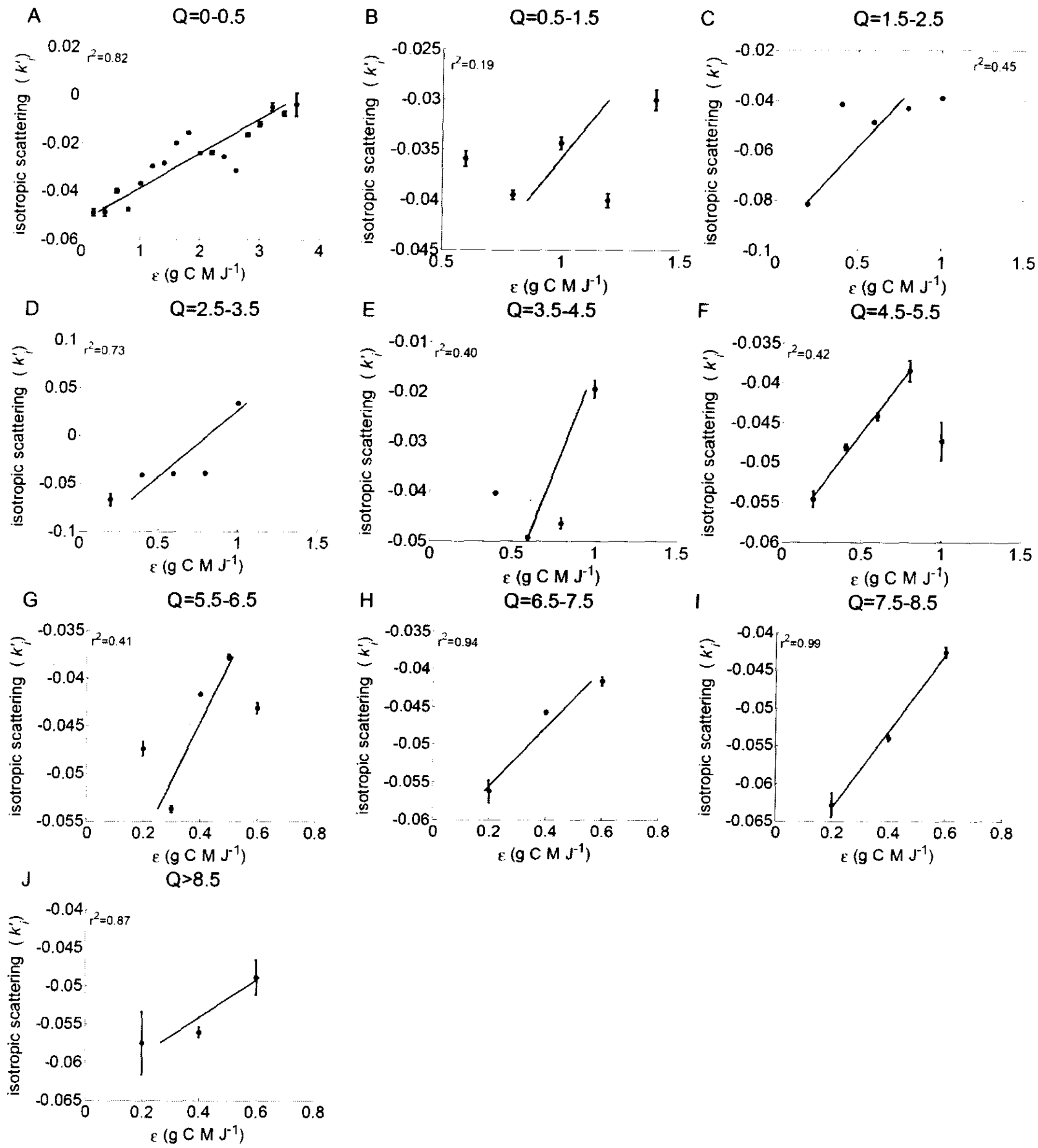

Figure 5.6A-J: Relationship between isotropic PRI scattering and ε for different sky conditions from overcast (A) to perfectly clear skies (J) (corresponding to Figure 4). Each figure represents one state of cloudiness, the data points show the isotropic BRDF scattering components derived for different classes of ε (corresponding to the surfaces in each Figure 5.3).

Figure 5.7 shows the relationship between Q and the geometric scattering component for different levels of ε. Data with ε>0.8 g C MJ^{-1} were excluded from this analysis as these data show no observations for clear sky conditions (Figure 5.4). Significant relationships were found between Q and the geometric scattering components for all observed classes of $\varepsilon(\varepsilon_{0.1}(r^2=0.5), \varepsilon_{0.3}(r^2=0.8), \varepsilon_{0.5}(r^2=0.7)$ and $\varepsilon_{0.7}(r^2=0.7)(p<0.05)$).

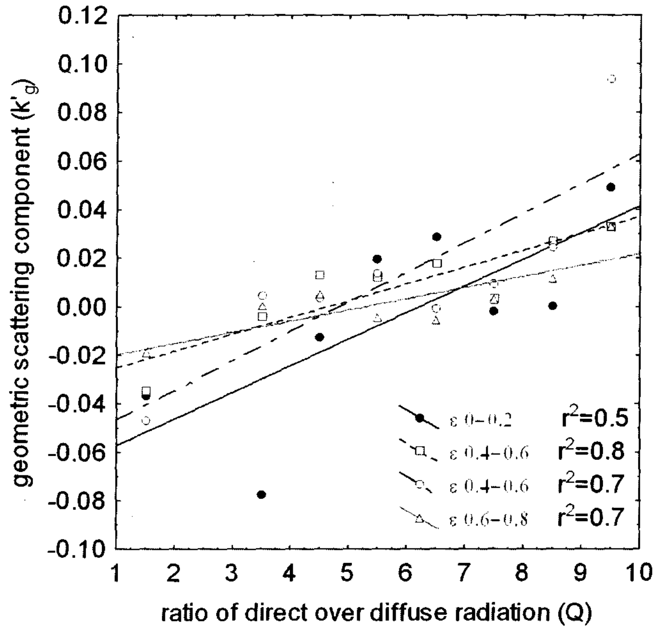

Figure 5.7: Relationship between geometric PRI scattering and state of cloudiness (Q) for $\varepsilon_{0.1}$, $\varepsilon_{0.3}$, $\varepsilon_{0.5}$ and $\varepsilon_{0.7}$. Higher classes of ε had no observations for clear sky conditions and were hence excluded from the analysis. The relationship is significant for all examined cases (p<0.05).

5.3.3 Using BRDF modeling to determine canopy level ε

Figure 5.8A-B shows the relationship between ε and PRI for the directionally uncorrected (Figure 5.8A) and directionally corrected case (Figure 5.8B). The directional effects on uncorrected PRI measurements are visible in Figure 8A, showing large variability of PRI compared to half-hourly flux based estimates of ε. As a result, only moderate relations exist between canopy level PRI and $\varepsilon(r^2=0.37, p<0.05)$. As shown in Figure 5.8B, the standardization of PRI to a common view- and solar illumination geometry (June 21[st] solar noon)) significantly enhances the PRI-ε relationship to $r^2 = 0.82$ ($p < 0.05$) as the vertical range of PRI values for a given ε is largely reduced.

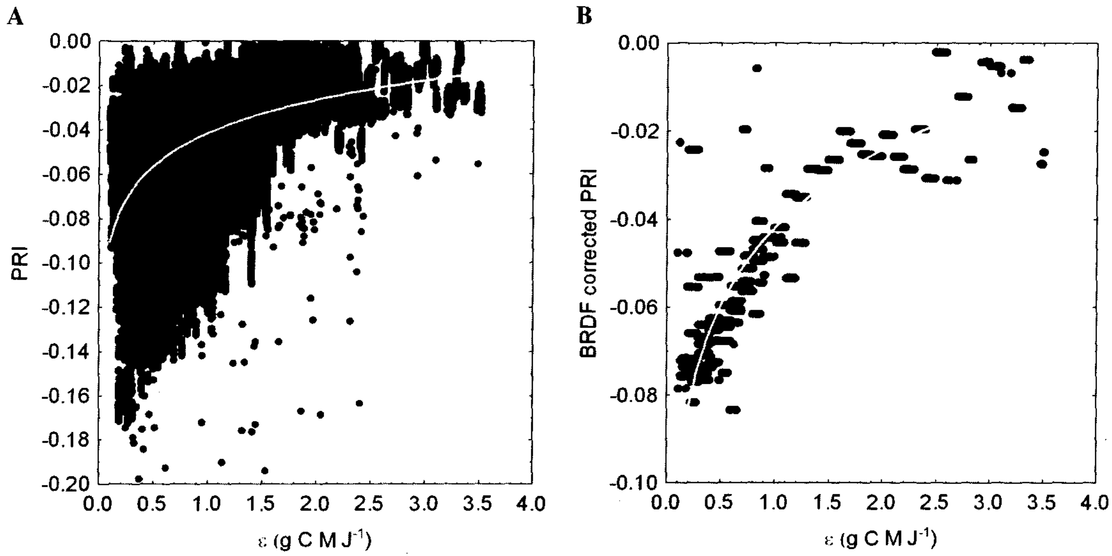

Figure 5.8 A-B A: Relationship between measured PRI and ε for all observations made between April 1st 2006 and March 31st 2007. The large variability in PRI is due to directional reflectance effects (r^2=0.37, p<0.05). Figure 5.8B: Relationship between directionally corrected PRI and ε for the vegetation period of 2006. The variability in PRI due to directional reflectance effects is largely reduced and the relationship between PRI and ε is significantly increased (r^2=0.82, p<0.05). Due to normalization of different view and sun angles, multiple points show identical values and are placed above each other. The absolute number of observations is not reduced with respect to Figure 5.8A.

Figure 5.9 demonstrates the ability of the directionally standardized canopy level PRI to track changes in ε over half-hourly (Figure 5.9A) and daily (Figure 5.9B) time steps. The upper line shows half-hourly and daily estimates of ε, respectively between April 1[st] 2006 and March 31[st] 2007, while the lower line shows the corresponding directionally corrected PRI measurements of this time period. Figure 5.9A represents the same data as Figure 5.8; Figure 5.9B represents the data aggregated over diurnal cycles. The directionally corrected PRI closely follows the pattern of ε as determined from EC flux measurements over half-hourly and daily time steps, thereby underlining the potential of directionally corrected canopy PRI to permanently track ε on a stand level. The figure also reveals the large amount of variability in stand level ε over the course of one year, with moderate patterns apparent due to seasonality or other regularities (i.e. ε is highest in early summer while it decreases during the dry period in late August and is also generally lower during the winter months).

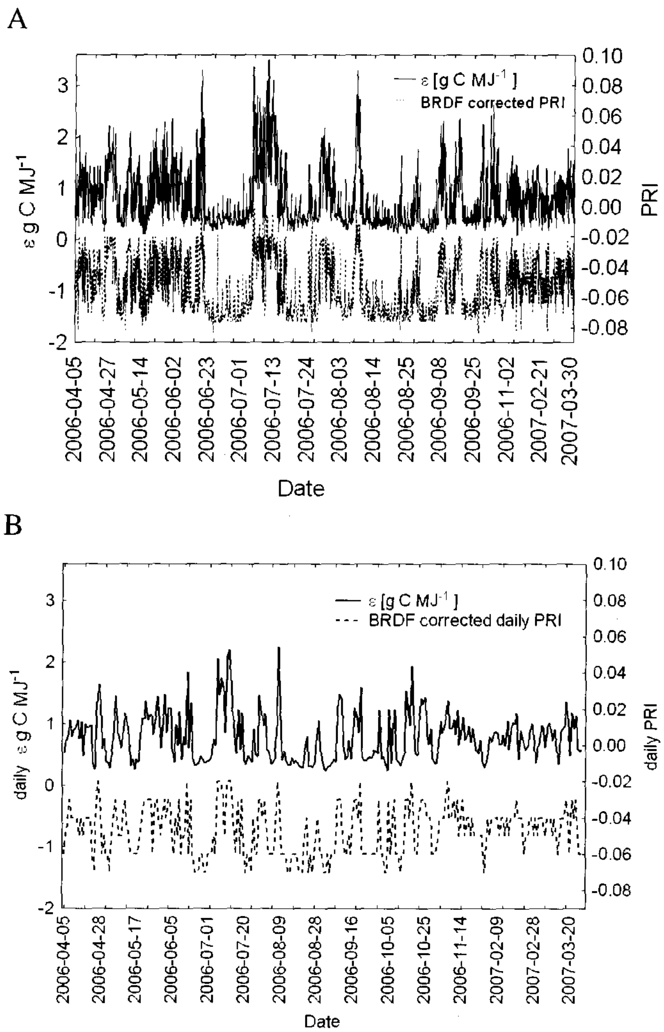

Figure 5.9A-B: Temporal variability of half hourly ε as determined from eddy flux measurements between April 1st 2006 and March 31st 2007 over half-hourly (A) and daily time steps (B). Values ranged between 0 and 3.6 g C M J^{-1}. Changes in canopy level ε can be tracked using a directionally corrected PRI, following its pattern closely.

5.4 Discussion and Conclusions

This study introduced an approach for predicting ε on the stand scale using high frequency multi-angular spectral reflectance measurements obtained from an automated, tower-based radiometer platform. A simple classification technique, clustering homogeneous atmospheric and physiological conditions, with separate semi-empirical kernel driven BRDF models being computed for each of these classes, successfully separated directional reflectance effects existing in year-round multi-angular PRI measurements from physiologically induced changes in canopy reflectance related to ε (Figure 5.4, Figure 5.8). Hall et al. (2008) demonstrated conclusively that the 531 nm signal associated with reductions in canopy ε was clearly detectable at stand scales and under a wide range of view and illumination conditions. The results of this study confirm these findings using high frequency year round observations thereby demonstrating the capacity of the PRI signal to track changes in ε over diurnal and seasonal cycles in a Douglas-fir forest (Figure 5.9).

The differences shown between the BRDF surfaces (Figure 5.4, 5.6) lead us to conclude that changes in the PRI signal seen by the instrument under homogeneous illumination conditions (see Figure 5.4a as an example) are mostly explained by changes in leaf-level reflectance. For instance, isotropic scattering was significantly related to changes in ε (Figure 5.6), which emphasizes its representativeness of bulk leaf reflectance in the tree crown. While the relationship between ε and isotropic scattering was significant (p<0.05) for all states of cloudiness, the restricted variability of ε under very clear sky conditions

(Q>6.5) yielded limited numbers of BRDF surfaces and, as a result, the coefficients of determination between cloudy and sunny data are not directly comparable.

This study also shows that changes in canopy level ε are related to both leaf-level reflectance changes and directional changes in canopy reflectance (Figure 5.5) as sunlit regions of the canopy are more likely to be exposed to excess light levels than shaded parts. This result is consistent with previous studies (e.g. Demmig Adams et al., 1996) and was also demonstrated by Hall et al. (2007). The dependency of the geometric scattering component on Q can be explained by the dependency of this component on shadow fractions, which become more distinct with increasingly clear skies. This result is consistent with Hall et al. (2008) finding that PRI can only depend on shadow fraction when the reflectance of the 531 nm band differs between the shaded and sunlit portions of the canopy. The selected modeling approach facilitates comparison of continuous spectral observations to half-hourly estimates of ε obtained using the eddy covariance technique (Figure 5.8b). The result is notably enhanced compared to the directionally uncorrected case (5.8A). The strong correlation was found between ε and directionally corrected PRI (Figure 5.8) is persistent throughout the year and can be used to accurately track ε over half hourly and daily time steps (Figure 5.9a and b). While the seasonal patterns were not very distinct, highest values for ε were found in early summer with the canopy undergoing only moderate stress levels, while photosynthetic efficiency was reduced during late August and early September, presumably due to drought conditions found at the site, and also during the winter months.

While the approach introduced in this chapter accounts for changes plant physiology related to ε, Barton and North (2001) showed that PRI reflectance may also dependent on other, longer term physiological processes influencing the pigment pool size (=carotenoid to chlorophyll ratio). The assumption that this variable is approximately constant over the study period can be justified for the evergreen forest by the favourable nutrient conditions found at the site and the distinct temperate climate allowing tree growth year round. Pigment pool size may, however, be a restriction to other, more variable sites or broad leaf forests and is also expected to change between sunlit and shaded leaves. Another assumption made in here is that the stand is uniform and no differences in canopy reflectance occurred due to differences in structure or species.

An important conclusion of this study is that multiple look angles are helpful for minimizing stand geometric effects, thereby enhancing the clarity of the physiological signal observed. The methodology shown in this study can be easily extended to investigate similar relationships in other forest types, but can possibly also be adapted for multi-angle satellite observations, which, when normalized to a common view- and illumination geometry and under cloud-free conditions, will allow geosynchronous satellites to monitor diurnal changes in ε by correcting for extraneous effects from a changing sun elevation throughout the day, and for varying view angles with latitude and longitude. A possible way to achieve this is by calibrating BRDF observations to canopies with higher levels of ε first (which can be measured for instance ground based instrumentation), and comparing these data to observations of more stressed canopies in the afternoon.

Permanently established canopy reflectance measurements are vital components of ongoing research aimed at up-scaling PRI based estimates of ε to landscape, regional and global scales. Airborne or satellite-based observations can only provide detection of spectral features as isolated temporal snapshots determined by the satellite's or aircraft's overpass (Sims et al., 2005) and, as a result, considerable gaps exist between these observations. Instruments and methodologies like the ones developed in this study can help to fill these gaps by identifying physiological cycles of the vegetation observed and serve as calibration for the broader band spectral observations available from satellite data. Ultimately, a comprehensive understanding of correlations between variations in ε and spectral reflectance in both xanthophyll and fluorescence related absorption features can help in developing models suitable for determination of global productivity from space.

5.5 References

Asner, G. (1998) Biophysical and Biochemical Sources of Variability in Canopy Reflectance. *Remote Sensing of Environment* **64**, 225-226.

Barton CVM, North PRJ (2001) Remote Sensing of Canopy Light-Use Efficiency Using the Photochemical Reflectance Index: Model and Sensitivity Analysis. *Remote Sensing of Environment* **78**, 264-273.

Baldocchi, D.D. (2003) Assessing the Eddy Covariance Technique for Evaluating Carbon Dioxide Exchange Rates of Ecosystems: Past, Present and Future. *Global Change Biology* **9**, 479-492.

Barnsley, M.J., Lewis, P., Sutherland, M. and Muller, J.P. (1997) Estimating Land Surface Albedo in the Hapex-Sahel Southern Super-Site: Inversion of Two Brdf Models Against Multiple Angle Asas Images. *Journal of Hydrology* **189**, 749-778.

Black, T.A., Den Hartog, G., Neumann, H.H., Blanken, P.D., Yang, P.C., Russell, C., Nesic, Z., Lee, X., Chen, S.G., Staebler, R. and Novak, M.D. (1996) Annual Cycles of Water Vapour and Carbon Dioxide Fluxes in and Above a Boreal Aspen Forest. *Global Change Biology* **2**, 219-229.

Blanken, P.D., Black, T.A., Neumann, H.H., Den Hartog, G., Yang, P.C., Nesic, Z. and Lee, X. (2001) The Seasonal Water and Energy Exchange Above and Within a Boreal Aspen Forest. *Journal of Hydrology* **245**, 118-136.

Chen, J. (1996) Evaluation of Vegetation Indices and a Modified Simple Ratio for Boreal Applications. *Canadian Journal of Remote Sensing* **22**, 229-242.

Chen, J. and Black, T. (1991) Measuring Leaf Area Index of Plant Canopies with Branch Architecture. *Agricultural and Forest Meteorology* **57**, 1-12.

Chen, J.M. and Leblanc, S.G. (1997) A Four-Scale Bi-directional Reflectance Model Based on Canopy Architecture. *IEEETransactions on Geoscience and Remote Sensing* **35**, 1316-1337.

Chen, J.M., Liu, J., Leblanc, S.G., Lacaze, R. and Roujean, J.L. (2003) Multi-angular Optical Remote Sensing For Assessing Vegetation Structure and Carbon Absorption. *Remote Sensing of Environment* **84**, 516-525.

Chen, J.M., Menges, C.H. and Leblanc, S.G. (2005) Global Mapping of Foliage Clumping Index Using Multi-Angular Satellite Data. *Remote Sensing of Environment* **97**, 447-457.

Chen, J.M., Govind, A., Sonnentag, O., Zhang, Y.Q., Barr, A. and Amiro, B. (2006) Leaf Area Index Measurements at Fluxnet-Canada Forest Sites. *Agricultural and Forest Meteorology* **140**, 257-268.

Demmig-Adams, B. and Adams, W.W. (1996) The Role of Xanthophyll Cycle Carotenoids in the Protection of Photosynthesis. *Trends in Plant Science* **1**, 21-26.

Demmig-Adams, B. and Adams, W.W. (2000) Photosynthesis - Harvesting Sunlight Safely. *Nature* **403**, 371-372

Demmig-Adams, B., Moeller, D.L., Logan, B.A. and Adams, W.W. (1998) Positive Correlation Between Levels of Retained Zeaxanthin Plus Antheraxanthin and Degree of Photoinhibition in Shade Leaves of Schefflera Arboricola (Hayata) Merrill. *Planta* **205**, 367-374.

Drewitt, G.B., Black, T.A., Nesic, Z., Humphreys, E.R., Jork, E.M., Swanson, R., Ethier, G.J., Griffis, T. and Morgenstern, K. (2002) Measuring Forest Floor CO_2 Fluxes in a Douglas-Fir Forest. *Agricultural and Forest Meteorology* **110**, 299-317.

Drolet, G.G., Huemmrich, K.F., Hall, F.G., Middleton, E.M., Black, T.A., Barr, A.G. and Margolis, H.A. (2005) A MODIS-Derived Photochemical Reflectance Index to Detect Inter-Annual Variations in the Photosynthetic Light-Use Efficiency of a Boreal Deciduous Forest. *Remote Sensing of Environment* **98**, 212-224.

DuMouchel, W.H., and F.L. O'Brien (1989) Integrating a Robust Option into a Multiple Regression Computing Environment. Computer Science and Statistics: *Proceedings of the 21st Symposium on the Interface*, Alexandria, VA: American Statistical Association.

Field C. and Mooney, H.A. (1986) The photosynthesis-nitrogen relationship in wild plants. In: T.Givnish, editor. *On the Economy of Plant Form and Function*. Cambridge Univ. Press, Cambridge, U.K. 22-55.

Field CB (1991) Ecological scaling of carbon gain to stress and resource availability. In: *Integrated Responses of Plants to Stress* (eds. Mooney, HA Winner, SE Pell, EJ) Academic Press, San Diego, CA. 28, 35-65.

Filella, I., Amaro, T., Araus, J.L. and Peñuelas, J. (1996) Relationship Between Photosynthetic Radiation-Use Efficiency of Barley Canopies and the Photochemical Reflectance Index (PRI). *Physiologia Plantarum* **96**, 211-216.

Gamon, J.A. and Surfus, J.S. (1999) Assessing Leaf Pigment Content and Activity With a Reflectometer. *New Phytologist* **143**, 105-117.

Gamon, J.A., Field, C.B., Bilger, W., Björkman, O., Fredeen, A.L. and Peñuelas, J. (1990) Remote-Sensing of the Xanthophyll Cycle and Chlorophyll Fluorescence in Sunflower Leaves and Canopies. *Oecologia* **85**, 1-7.

Gamon, J.A., Peñuelas, J. and Field, C.B. (1992) A Narrow-Waveband Spectral Index That Tracks Diurnal Changes in Photosynthetic Efficiency. *Remote Sensing of Environment* **41**, 35-44.

Gamon JA, Filella I, Peñuelas J (1993) The Dynamic 531-Nanometer Reflectance Signal: A Survey of Twenty Angiosperm Species. Yamamoto HY , Smith CM (Eds). Photosynthetic Responses to the Environment. *American Society of Plant Physiologists*, Rockville. pp. 172-177.

Gao, F., Schaaf, C.B., Strahler, A.H., Jin, Y. and Li, X. (2003) Detecting Vegetation Structure Using a Kernel-Based BRDF Model. *Remote Sensing of Environment* **86**, 198-205.

Goel, N.S. and Grier, T. (1988) Estimation of Canopy Parameters for Inhomogeneous Vegetation Canopies From Reflectance Data .3. Trim - a Model for Radiative-Transfer in Heterogeneous 3-Dimensional Canopies. *Remote Sensing of Environment* **25**, 255-293.

Goetz, S.J., Prince, S.D., Goward, S.N., Thawley, M.M., Small, J. and Johnston, A. (1999) Mapping Net Primary Production and Related Biophysical Variables With Remote Sensing: Application to the Boreas Region. *Journal of Geophysical Research-Atmospheres* **104**, 27719-27734.

Goodwin G Regeneration Study on the Logged-off Lands of the Comox Logging and Railway Company Oyster River Forest Survey No R 72 Survey file No 0124780 BC Forest Service 39p and Map

Goulden, M.L. and Crill, P.M. (1997) Automated Measurements of CO_2 Exchange at the Moss Surface of a Black Spruce Forest. *Tree Physiology* **17**, 537-542.

Hall, F.G., Townshend, J.R. and Engman, E.T. (1995) Status of Remote-Sensing Algorithms for Estimation of Land-Surface State Parameters. *Remote Sensing of Environment* **51**, 138-156.

Hall, F.G., Huemmrich, K.F., Goetz, S.J, Sellers, P.J., Nickeson, J.E. (1992) Satellite Remote-Sensing of Surface-Energy Balance-Success, Failures and Unresolved Issues in FIFE. *Journal of Geophysical Research-Atmospheres* **97**, 19061-19089.

Hall, F.G., Hilker, T., Coops, N.C., Lyapustin, A., Huemmrich, K.F., Middleton, E.M., Drolet, G.G., Margolis, H.A., Black, T.A. (2008) Can Light-Saturated Reductions in Canopy Photosynthetic Capacity Be Observed From Space? *Remote Sensing of Environment*, submitted

Holland, P.W., and R.E. Welsch (1977) Robust Regression Using Iteratively Reweighted Least-Squares. Communications in Statistics: Theory and Methods, A6, 813-827.

Humphreys, E.R., Black, T.A., Morgenstern, K., Cai, T.B., Drewitt, G.B., Nesic, Z. and Trofymow, J.A. (2006). Carbon Dioxide Fluxes in Coastal Douglas-Fir Stands at Different Stages of Development After Clearcut Harvesting. *Agricultural and Forest Meteorology* **140**, 6-22.

Jassal, R.S., Black, T.A., Cai, T.B., Morgenstern, K., Li, Z., Gaumont-Guay, D. and Nesic, Z. (2007) Components of Ecosystem Respiration and an Estimate of Net Primary Productivity of an Intermediate-Aged Douglas-Fir Stand. *Agricultural and Forest Meteorology* **144**, 44-57.

Jupp, D.L.B. (1998) Directional Radiance and Emissivity Measurement Models for Remote Sensing of the Surface Energy Balance. *Environmental Modelling & Software* **13**, 341-351.

Justice, C.O., Vermote, E., Townshend, J.R.G., Defries, R., Roy, D.P., Hall, D.K., Salomonson, V.V., Privette, J.L., Riggs, G., Strahler, A., Lucht, W., Myneni, R.B., Knyazikhin, Y., Running, S.W., Nemani, R.R., Wan, Z.M., Huete, A.R., Van Leeuwen, W., Wolfe, R.E., Giglio, L., Muller, J.P., Lewis, P. and Barnsley, M.J. (1998) The Moderate Resolution Imaging Spectroradiometer (MODIS): Land Remote Sensing for Global Change Research. *IEEE-Transactions on Geoscience and Remote Sensing* **36**, 1228-1249.

Kljun, N., Kastner-Klein, P., Fedorovich, E. and Rotach, M.W. (2004) Evaluation of Lagrangian Footprint Model Using Data From Wind Tunnel Convective Boundary Layer. *Agricultural and Forest Meteorology* **127**, 189-201.

Leclerc, M.Y. and Thurtell, G.W. (1990) Footprint Prediction of Scalar Fluxes Using a Markovian Analysis. *Boundary-Layer Meteorology* **52**, 247-258.

Leuning, R., Hughes, D., Daniel, P., Coops, N.C. and Newnham, G. (2006) A Multi-Angle Spectrometer for Automatic Measurement of Plant Canopy Reflectance Spectra. *Remote Sensing of Environment* **103**, 236-245.

Li, X.W. and Strahler, A.H. (1986) Geometric-Optical Bi-directional Reflectance Modeling of a Conifer Forest Canopy. *IEEE-Transactions on Geoscience and Remote Sensing* **24**, 906-919.

Liu, J., Chen, J.M., Cihlar, J. and Chen, W. (2002) Net Primary Productivity Mapped for Canada at 1-Km Resolution. *Global Ecology and Biogeography* **11**, 115-129.

Los, S.O., North, P.R.J., Grey, W.M.F. and Barnsley, M.J. (2005) A Method to Convert AVHRR Normalized Difference Vegetation Index Time Series to a Standard Viewing and Illumination Geometry. *Remote Sensing of Environment* **99**, 400-411.

Lucht, W., Schaaf, C.B. and Strahler, A.H. (2000) An Algorithm for the Retrieval of Albedo From Space Using Semiempirical Brdf Models. *IEEE-Transactions on Geoscience and Remote Sensing* **38**, 977-998.

Margolis, H.A., Flanagan, L.B. and Amiro, B.D. (2006) The Fluxnet-Canada Research Network: Influence of Climate and Disturbance on Carbon Cycling in Forests and Peatlands. *Agricultural and Forest Meteorology* **140**, 1-5.

Monteith, J.L. (1972) Solar-Radiation and Productivity in Tropical Ecosystems. *Journal of Applied Ecology* **9**, 747-766.

Monteith, J.L. (1977) Climate and Efficiency of Crop Production in Britain. *Philosophical Transactions of the Royal Society of London Series B-Biological Sciences* **281**, 277-294.

Morgenstern, K., Black, T.A., Humphreys, E.R., Griffis, T.J., Drewitt, G.B., Cai, T.B., Nesic, Z., Spittlehouse, D.L. and Livingstone, N.J. (2004) Sensitivity and Uncertainty of the Carbon Balance of a Pacific Northwest Douglas-Fir Forest During an El-Niño La-Niña Cycle. *Agricultural and Forest Meteorology* **123**, 201-219.

Myneni, R.B., Hoffman, S., Knyazikhin, Y., Privette, J.L., Glassy, J., Tian, Y., Wang, Y., Song, X., Zhang, Y., Smith, G.R., Lotsch, A., Friedl, M., Morisette, J.T., Votava, P., Nemani, R.R. and Running, S.W. (2002) Global Products of Vegetation Leaf Area and Fraction Absorbed PAR from Year One of MODIS Data. *Remote Sensing of Environment* **83**, 214-231.

Nichol, C.J., Huemmrich, K.F., Black, T.A., Jarvis, P.G., Walthall, C.L., Grace, J. and Hall, F.G. (2000) Remote Sensing of Photosynthetic-Light-Use Efficiency of Boreal Forest. *Agricultural and Forest Meteorology* **101**, 131-142.

Nichol, C.J., Lloyd, J., Shibistova, O., Arneth, A., Roser, C., Knohl, A., Matsubara, S. and Grace, J. (2002) Remote Sensing of Photosynthetic-Light-Use Efficiency of a Siberian Boreal Forest. *Tellus Series B-Chemical and Physical Meteorology* **54**, 677-687.

Peñuelas, J., Filella, I. and Gamon, J.A. (1995) Assessment of Photosynthetic Radiation-Use Efficiency With Spectral Reflectance. *New Phytologist* **131**, 291-296.

Peñuelas, J., Gamon, J.A., Fredeen, A.L., Merino, J. and Field, C.B. (1994) Reflectance Indexes Associated With Physiological-Changes in Nitrogen-Limited and Water-Limited Sunflower Leaves. *Remote Sensing of Environment* **48**, 135-146.

Peñuelas, J., Llusia, J., Pinol, J. and Filella, I. (1997) Photochemical Reflectance Index and Leaf Photosynthetic Radiation-Use-Efficiency Assessment in Mediterranean Trees. *International Journal of Remote Sensing* **18**, 2863-2868.

Peñuelas, J., Munne-Bosch, S., Llusia, J. and Filella, I. (2004) Leaf Reflectance and Photo- and Antioxidant Protection in Field-Grown Summer-Stressed Phillyrea Angustifolia. Optical Signals of Oxidative Stress? *New Phytologist* **162**, 115-124.

Prince, S. and Goward, S. (1995) Global primary production: a remote sensing approach. *Journal of Biogeography* **22**, 815-835.

Privette, J.L., Myneni, R.B., Tucker, C.J. and Emery, W.J. (1994) Invertibility of a 1-D Discrete Ordinates Canopy Reflectance Model. *Remote Sensing of Environment* **48**, 89-105.

Reda, I. and Andreas, A. (2004) Solar Position Algorithm for Solar Radiation Applications. *Solar Energy* **76**, 577-589.

Roujean, J.L., Leroy, M. and Deschamps, P.Y. (1992) A Bi-directional Reflectance Model of the Earths Surface for the Correction of Remote-Sensing Data. *Journal of Geophysical Research-Atmospheres* **97**, 20455-20468.

Ross, J.K. (1981) The Radiation Regime and Architecture of Plant Stands, Dr. W.Junk Publishers, The Hague, 392pp.

Schmid, H.P. and Lloyd, C.R. (1999) Spatial Representativeness and the Location Bias of Flux Footprints Over Inhomogeneous Areas. *Agricultural and Forest Meteorology* **93**, 195-209.

Sims, D.A., Rahman, A.F., Cordova, V.D., Baldocchi, D.D., Flanagan, L.B., Goldstein, A.H., Hollinger, D.Y., Misson, L., Monson, R.K., Schmid, H.P., Wofsy, S.C. and Xu, L.K. (2005) Midday Values of Gross CO_2 Flux and Light-use efficiency During Satellite Overpasses Can Be Used to Directly Estimate Eight-Day Mean Flux. *Agricultural and Forest Meteorology* **131**, 1-12.

Strahler, A.H. and Jupp, D.L.B. (1990) Modeling Bi-directional Reflectance of Forests and Woodlands Using Boolean Models and Geometric Optics. *Remote Sensing of Environment* **34**, 153-166.

Strugnell, N.C. and Lucht, W. (2001) An Algorithm to Infer Continental-Scale Albedo From AVHRR Data, Land Cover Class, and Field Observations of Typical BRDFs. *Journal of Climate* **14**, 1360-1376.

Turner, D.P., Urbanski, S., Bremer, D., Wofsy, S.C., Meyers, T., Gower, S.T. and Gregory, M. (2003) A Cross-Biome Comparison of Daily Light-use efficiency for Gross Primary Production. *Global Change Biology* **9**, 383-395.

Wang, Z., Zeng, X., Barlage, M., Dickinson, R.E., Gao, F. and Schaaf, C.B. (2004) Using MODIS BRDF and Albedo Data to Evaluate Global Model Land Surface Albedo. *Journal of Hydrometeorology* **5**, 3-14.

Wanner, W., Li, X. and Strahler, A.H. (1995) On the Derivation of Kernels for Kernel-Driven Models of Bi-directional Reflectance. *Journal of Geophysical Research-Atmospheres* **100**, 21077-21089.

Xiao, X.M., Zhang, Q.Y., Braswell, B., Urbanski, S., Boles, S., Wofsy, S., Berrien, M. and Ojima, D. (2004) Modeling Gross Primary Production of Temperate Deciduous Broadleaf Forest Using Satellite Images and Climate Data. *Remote Sensing of Environment* **91**, 256-270.

6 A MODELING APPROACH FOR UP-SCALING GROSS ECOSYSTEM PRODUCTION TO THE LANDSCAPE SCALE USING REMOTE SENSING DATA[7]

6.1 Introduction

Satellite data will be essential for driving spatially-continuous, global-scale carbon cycle models (Hall et al., 1995a). Satellite-derived estimates of primary production are based on the links between plant physiological properties, specifically the biochemical composition of plant foliage, and the optical properties of leaves. Whilst the remote sensing community has long been limited by the number and width of spectral wavebands available for detection of leave optical properties, the recent advent of high spectral resolution optical sensors, capable of detecting changes in leaf-spectral properties with a high temporal frequency, has encouraged a new phase in global carbon cycle modeling (Prince and Goward, 1995), with an eventual goal of forcing these models entirely with satellite data. (Running et al., 2004, Rahman et al., 2005). As one of the most widely applied concepts for estimating plant productivity (also known as gross ecosystem production, GEP[8]), the light-use efficiency approach of Monteith (1972, 1977) expresses GEP as the product of the incident photosynthetically active radiation (PAR) (μmol m^{-2} s^{-1}), defined as solar radiation between 400-700 nm wavelengths, the fraction

[7] A version of this paper has been submitted for publication. Hilker, T., Coops, N.C., Hall, F.G., Black, T.A., Chen, B., Krishnan, P.,Wulder, M.A., Sellers, P.J., Middleton, E.M., Huemmrich, K.F. (2008) A Modeling Approach for Up-scaling Gross Ecosystem Production to the Landscape Scale Using Remote Sensing Data. *Journal of Geophysical Research – Biogeosciences*, submitted
[8] In the previous chapters of this thesis, this was referred to as gross primary production, GPP

of PAR that is absorbed by the plant canopy (f_{par}) and the efficiency (ε), with which absorbed PAR can be converted into the chemical energy associated with it:

$$GEP = PAR \cdot f_{PAR} \cdot \varepsilon \qquad (1)$$

Remotely-sensed estimates of PAR are typically derived from top of the atmosphere solar radiances using satellite observations combined with optical modelling (Eck and Dye 1991, Sellers et al., 1995, Van Laake and Sanchez-Azofeifa, 2004), while f_{PAR} is regarded as a function of the leaf area index (Sellers, 1985) which in turn is closely related to top of the canopy reflectance measurements in the visible and near-infrared region (Tucker 1979, Daughtry et al., 1983, Asrar et al., 1984, Sellers, 1985, 1987). Since the mid-1980's, physical approaches have been developed to determine f_{PAR} globally, based on techniques using satellite data (Tucker and Sellers, 1986), plot scale field studies (Asrar et al., 1984, Tucker et al., 1981), large field experiments (Sellers and Hall, 1992, Hall et al, 1992, Sellers et al., 1997, Running et al., 1999) and theoretical work (Myneni et al, 1992, Hall et al, 1990, Sellers 1985, 1987, Sellers et al,. 1992, 1996).

Arguably, one of the most challenging components of the Monteith model to be inferred from remote sensing is ε, which is determined by any of a large number of environmental stress factors and as a result, is highly variable in space and time. Biochemically, ε is controlled by a group of leaf-pigments named xanthophylls, responsible for balancing absorption and utilization of light quanta in order to prevent oxidative damage to the photosynthetic apparatus in leaves (Demmig-Adams and Adams, 1998, Demmig-Adams and Adams, 2000). Gamon et al. (1990) demonstrated a principal relationship between the status of these pigments and a narrow waveband absorption feature at 531 nm, which led to the formulation of the photochemical reflectance index (PRI), comparing this absorption feature to a reference band at 570 nm (Gamon et al., 1992, 1993). Numerous studies demonstrated a logarithmic relationship between ε and PRI (maximum ε values correspond to minimum PRI values and vice versa, as PRI is negative) at the leaf and stand level and Chapter 5 and Hall et al. (2008) demonstrated that this signal is detectable over a wide range of view and illumination conditions throughout the year. However, up-scaling this relationship through space and time is difficult. A critical component in up-scaling PRI measurements is canopy structure (Rahman et al., 2001), as it not only alters the reflected signal by physically changing its strength depending on integrated leaf angle distribution and the sun-surface-sensor geometry (Barton and North, 2001), but also drives the photosynthetic output of individual leaves through its effect on canopy light transmittance (Forseth and Norman 1991). The capacity of passive remote sensing to investigate such structural dependencies is limited, since remotely-sensed reflectances are largely dependent on the properties of the top of the canopy, while the contributions of shaded leaves lower in the canopy are harder to quantify (Hall et al., 1992, Chen et al., 2003, Myneni et al., 2002, Gao et al., 2003). Further, optical remote sensing measures are typically asymptotic with respect to vertically distributed structural attributes such as leaf area, volume, or biomass (Wulder, 1998). As a result, satellite-derived predictions of primary production often model ε as a biome dependent constant, adjusted by simple meteorological variables such as surface temperature and vapor pressure deficit (Turner et al., 2003, Heinsch et al., 2006), rather than attempting to model directly. The inaccuracies inherent in this method are believed to account for many of the differences found between field measured and satellite-derived estimates of GEP (Running et al., 2004). While direct measurements of ε using satellite data hold promise for calculating more accurate estimates of carbon budgets from space (Hall et al., 2008), appropriate methods to facilitate up-scaling from leaf and canopy to landscape level will be required.

One way to investigate the interaction between photosynthesis, canopy radiation regime, and canopy structure is to combine high spectral resolution optical remote sensing data with structural information on the canopy obtained from airborne LiDAR. LiDAR is an active remote sensing technique that facilitates direct measurements of the three-dimensional distribution of vegetation canopy components as well as sub-canopy topography, thereby providing high spatial resolution topographic elevation, and accurate estimates of vegetation height, cover density, and other aspects of canopy structure (Lefsky et al., 2005). Measurement errors for individual tree heights (of a given species) are typically in the order of less than 1.0 m (Persson et al., 2002) and less than 0.5 m for plot-based estimates of maximum and mean canopy height with full canopy closure (Næsset 1997, 2002, Magnussen and Boudewyn 1998, Næsset and Økland 2002).

In this chapter, we investigate the potential of combining high spectral resolution optical remote sensing observations with small footprint LiDAR data to model ε and GEP vertically and horizontally a forest whose dominant species is Douglas-fir (*Pseudotsuga menziesii* var *menziesii* (Mirb.) Franco). ε was determined from remotely-sensed spectra acquired from a permanently established tower-based spectroradiometer (Chapter 4), allowing continuous observation of the canopy surface with high spatial and spectral resolution. First, year round tower-based measurements were decomposed into sunlit and shaded endmembers (Hall et al., 1995b, Asner et al., 1998, Peddle et al., 1999, Asner and

Warner, 2003) using a bi-directional reflectance distribution model (Roujean et al., 1992, Chapter 5). The physiological signal contained in these endmember reflectances was then spatially extrapolated using information about the canopy structure from LiDAR-based measures. Finally, GEP was calculated separately for sunlit and shaded canopies and compared to vertically and horizontally integrated measurements of GEP obtained from CO_2 exchange measurements using the eddy covariance (EC) technique. The goal of our approach was to investigate possibilities for up-scaling stand level observations to satellite scales thereby improving our understanding of interactions between canopy radiation regime and photosynthesis.

6.2 Methods

6.2.1 Research area

The study area is a Canadian Carbon Program flux tower site, located between Courtenay and Campbell River on Vancouver Island, British Columbia, Canada (49°52'7.8" N, 125°20'6.3" W, tower location) at 350 m mean above sea level. The coniferous forest consists of 80% Douglas-fir, 17% western red cedar (*Thuja plicata* Donn ex D. Don) and 3% western hemlock (*Tsuga heterophylla* (Raf.) Sarg.) (Morgenstern et al., 2004) and is considered to be second-growth stand, planted in 1949, after harvesting of the original stand (Goodwin, 1937). The understorey consists mainly of salal (*Gaultheria shallon* Pursh.), Oregon grape (*Berberis nervosa* Pursh.), vanilla-leaf deer foot (*Achlys triphylla* (Smith) DC), plus various ferns and mosses (Morgenstern et al., 2004). A 1998 site survey found that the stand density was 1100 stems ha^{-1}, tree height ranged between 30 and 35 m, with an average diameter at breast height (DBH) of 29 cm. Chen et al. (2006) found that the effective leaf area index (L_e) was 4.3 m^2 m^{-2} based on measurements using TRAC and LAI-2000 instruments.

6.2.2 Eddy flux measurements

Continuously since 1997, half-hourly fluxes of CO_2 and water vapor were measured at the site using the EC measurement technique (Morgenstern et al., 2004, Humphreys et al., 2006) and data were extracted between April 1st 2006 and March 31st 2007 for this study. EC-fluxes were measured with a three-axis sonic anemometer-thermometer (SAT, model R3, Gill Instruments Ltd., Lymington, UK) and a closed-path CO_2/H_2O infrared gas analyzer (IRGA) (model LI-6262, LI-COR Inc., Lincoln, NE, USA). Net ecosystem exchange (NEE) was calculated as the sum of the half-hourly fluxes of CO_2 and the rate of change in CO_2 storage in the air column between the ground and the EC-measurement level (42 m). Incident and reflected photosynthetically active radiation (PAR [μmol m^{-2} s^{-1}]), defined as the photon flux density for the 400-700 nm wavelength band, were measured using up and downward looking quantum sensors (model 190 SZ, LI-COR Inc.), installed above and below the canopy and diffuse PAR was measured using a "sunshine sensor" (model BF3, Delta-T Devices Ltd., Burwell, UK). Gaps in data collection of less than two hours were filled using linear interpolation. Half-hourly measurements of GEP were calculated using,

$$GEP = NEP + R_d \qquad (2)$$

where NEP is the daytime net ecosystem production (NEP = -NEE) and R_d is the daytime ecosystem respiration (Morgenstern et al., 2004), calculated using the annual exponential relationship between nighttime NEE and soil temperature at 5 cm depth. Gaps in GEP were filled using a Michaelis-Menten GEP versus PAR relationship fitted to daytime data when air temperature $T_{Air} > -1$ °C. A complete description of the EC data and processing methods applied can be found in Morgenstern et al. (2004), Humphreys et al. (2006), and Jassal et al. (2007).

6.2.3 Spectral measurements

Canopy reflectance measurements were obtained from an automated multi-angular spectroradiometer platform (AMSPEC) installed at a height of 45 m (≈10 m above the tree canopy) on the open-lattice 50-cm triangular flux tower (Chapter 4). The instrument features a motor-driven probe that allows observations in a 330° view area around the tower. The probe rotates in 11.5° intervals every 30 seconds, thereby completing a full rotation every 15 minutes. A potentiometer attached to the shaft of the motor facilitates exact measurement of the probe's position. At the end of each sweep, the sensor is returned to its original position. The spectroradiometer used is a Unispec-DC (PP Systems, Amesbury, MA, USA) featuring 256 contiguous bands with a nominal bandwidth of 3 nm and a nominal range of operation between 350 and 1200 nm. To allow sampling under varying sky conditions, canopy reflectance was obtained from simultaneous measurements of solar irradiance and radiance, sampled every 5 seconds from sunrise to sunset. The upward pointing probe was equipped with a cosine receptor (PP-Systems) to correct sky irradiance measurements for varying solar altitudes. The downward looking probe measured canopy reflectance at a zenith angle of 62° (Chen and Black, 1991). The probe's instantaneous field of view (IFOV) was 20°. The outer diameter of the instrument's footprint was approximately 62 m at canopy height, while the elliptic instantaneous view area of the probe had a major axis of about 17.9 m and a minor axis of about 3.5 m. No observations were made between an azimuth of 220° and 250° (defined from geodetic north) due to obstruction by the tower. Coinciding with the EC observations, reflectance measurements used for this analysis were collected continuously between April 1st 2006 and March 31st 2007. A complete technical description of the instrument and its setup can be found in Chapter 4.

6.2.4 LiDAR measurements

LiDAR data were acquired at the site on June 8th 2004, using a Mark II sensor (Terra Remote Sensing, Sidney, British Columbia, Canada) with a spacing density of 0.7 hits per m^2 and a footprint (spot size) of 0.19 m (with survey and system details in Table 6.1). Separation of vegetation and terrain was carried out using a software package (Terrascan v. 4.006, Terrasolid, Helsinki, Finland) which iteratively classifies LiDAR data into either ground or non-ground returns. Figure 6.1 provides an overview of the study area covered by LiDAR measurements.

Parameter	Performance
Sensor	Mark II
Laser scan frequency	25 Hz
Laser impulse frequency	40000 Hz
Laser power	< 4 Watt
Maximum scan angle	< 20°
Type of scanning mirror	oscillating
Laser beam divergence	<0.5 milliradians
Measurement density	0.5 – 0.8 hits per sq meter.
Geodetic datum	NAD83
Plotting projection	UTM Zone 10
Airborne platform	Bell 206 Jet Ranger helicopter
Flight altitude above ground	900 m
Flight speed	25-30ms^{-1}
Version of TerraScan used to classify data	Version 004.006

Table 6.1: LiDAR parameters

6.2.5 Modeling the eddy flux footprint

Interpretation of EC-flux measurements over heterogeneous surfaces is largely dependent on the area or flux footprint from which a measurement originates. The typical size of EC-flux footprints ranges from a few hectares to a few square-kilometres (Schmid and Lloyd, 1999) depending on atmospheric stability and meteorological conditions (Leclerc and Thurtell, 1990). As a result, the footprint spatial structure varies significantly over different time scales (half-hourly to multiple years) (Chen et al., 2007a,b). Exact knowledge of the EC-flux footprints is, however, critical when comparing flux tower measured GEP to spatially-integrated remote sensing observations over heterogeneous areas. In this study, a published flux footprint model (Chen et al., 2007b) was used to predict the EC-flux footprints for given half hour intervals. This algorithm is based on Eulerian advection diffusion (Kormann and Meixner, 2001) and defines the EC-flux footprint as the product of the crosswind-integrated footprint and a Gaussian crosswind concentration distribution function (Chen et al., 2007b). The flux footprint estimates were calculated at half-hourly time steps for the period from April 1st, 2006 to March 31st, 2007 with a spatial resolution of 10 m x 10 m covering the 12km^2 area around the tower. The output of the model yields the percent impact each 10 m x 10 m cell within the raster has on the EC-flux measurement per half hour time step.

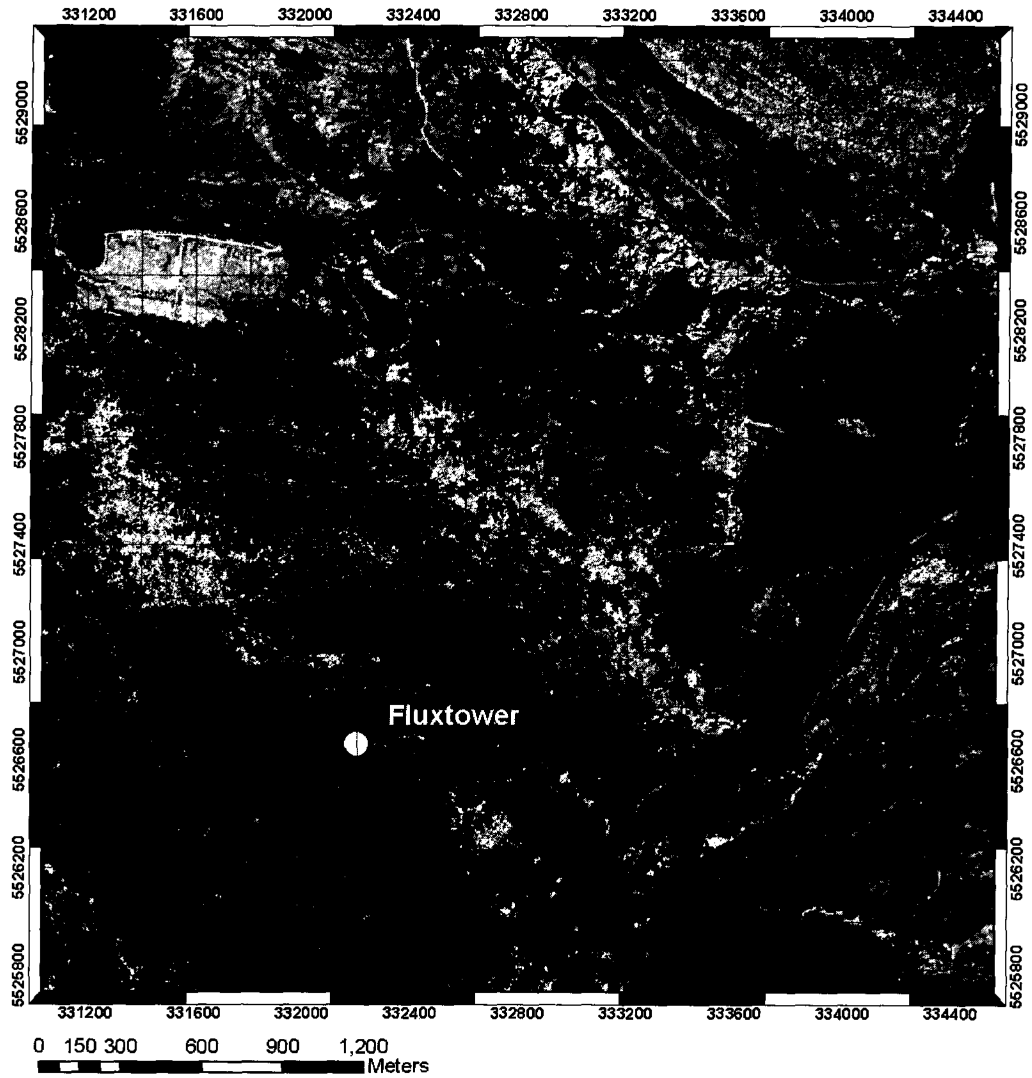

Figure 6.1: QuickBird satellite image of the study area covered by LiDAR. The total size of the area is approximately 12.5 km^2.

6.2.6 Endmember reflectance of PRI

Building upon the theoretical foundation of Li and Strahler (1985), Hall et al. (1995b), illustrated that multi-angular stand-level reflectance signals for a given species can be decomposed into spectral endmembers, namely sunlit crown, sunlit background, and shadow. The fraction of area occupied by each of these endmembers for a given observation varies as a function of the sun - observer geometry and can be determined using linear mixture modeling if the reflectance for totally sunlit and totally shaded crown and background are known (Hall et al., 1995b, Asner et al., 1998, Peddle et al., 1999, Asner and Warner, 2003). In this study, we simplified this concept by reducing the number of endmembers to sunlit and shaded crown components only, as the background reflectance was assumed to make a minimal contribution due to the high canopy density at the study site. Sunlit and shaded endmember reflectances can only be approximated from direct AMSPEC measurements, as the instrument, which has a field of view of approximately 60 m^2, will always observe a mixture of sunlit and shaded canopies. However, it is possible to accurately determine these endmembers using a bi-directional reflectance distribution function (BRDF) derived from the AMSPEC acquired spectra. A BRDF describes how land surface reflectance varies with view zenith, solar zenith and azimuth angle (Barnsley et al., 1997, Gao et al., 2003) and is often applied to standardize multi-angular reflectance measurements to common viewing geometries. Once a BRDF model is established for a series of multi-directional measurements, reflectance values can be estimated for any possible sun-observer geometry, including those for which no measurements were acquired. In terms of a BRDF, the sunlit endmember reflectance corresponds to a geometry where the probe is perfectly aligned with the sun being behind it (the BRDF hotspot) while the shaded endmember corresponds to a geometry where sun is located in front of the probe (BRDF darkspot) (Li and Strahler, 1985, Middleton et al., 1987, Li and Strahler, 1992, Wanner et al., 1995). The shaded PRI endmember then defines the highest possible photosynthetic performance for a given time interval, while the sunlit PRI endmember defines its lowest performance (Chapter 5). It was demonstrated in Chapter 5 that the PRI reflectance as observed by AMSPEC is a function not only of the sun-observer geometry, but also of the sky condition at the time of measurement and the physiological status of the vegetation canopy observed (i.e. ε). To facilitate accurate modeling of BRDF, geometric effects need to be separated from both leaf physiological effects as well as reflectance effects related to sky conditions. This can be achieved by stratifying spectra into homogeneous subsets of observations with respect to both sky conditions and tower-measured ε and subsequently fitting individual BRDF models to each of these strata (Chapter 5).

The time period for modeling BRDF needs to be chosen carefully, as on one hand a large enough set of spectral observations is required to establish a stable BRDF surface (Los et al., 2005, Chapter 5) and the time period should not be so long as to incorporate short-term changes in ε which may not adequately represent variations in photosynthetic performance over shorter time intervals. In this study, an 8-day period was chosen for calculation of PRI endmembers and thus also for calculating GEP, as this interval is also commonly used in satellite products such as the GPP product of the Moderate Resolution Imaging Spectroradiometer (MODIS) (Heinsch et al., 2006).

6.2.7 Determining stand structural parameters using LiDAR

LiDAR data were used to estimate forest stand attributes, including L_e and the probability of canopy gaps within different layers of the forest canopy (P_{gap}). Computation of P_{gap} from the top of the canopy to a given depth into the canopy (z) has been described in detail by Lovell et al. (2003) and Coops et al. (2007). For a given cell, P_{gap} can be estimated by summing the total number of LiDAR returns down to z and comparing them to the total number of independent LiDAR pulses (N):

$$P_{gap}(z) = \frac{1 - \sum_{z=j}^{z=z_{max}} \# z_j}{N} \tag{3}$$

where $\#z_j$ is the number of hits down to a height z above the ground. From P_{gap}, the cumulative projected foliage area index $L(z)$ from the top of the canopy down to a height z can be derived using,

$$L(z) = -\log\left(P_{gap}(z)\right) \tag{4}$$

where the first derivative of $L(z)$ is the apparent foliage density profile (Lovell et al., 2003, Coops et al., 2007). The effective P_{gap} of a clumped forest canopy at a given time of the day (P_e), can be calculated if $L(z)$ and the solar zenith angle (θ) are known (Chen, 1996):

$$P_e(\theta, z) = \exp\left[\frac{-G_t(\theta)L(z)}{\cos\theta}\right] \tag{5}$$

where $G_t(\theta)$ is the projection coefficient for total PAR transmission approximated as 0.5 (Chen, 1996, Chen et al., 2006). θ was calculated for each 30-minute interval using the timestamps from the flux measurements (Reda and Andreas, 2004). Estimates of canopy structure were based on a spatial resolution of 10 m x 10 m, corresponding to the flux-footprint model (Chen et al., 2007a,b).

6.2.8 Establishing a spatial GEP model

6.2.8.1 Modeling PAR as a function of θ and z

As a simplifying assumption, the forest canopy is herein modelled as two populations of sunlit and shaded leaves, with photosynthesis driven by the direct and diffuse radiation components, respectively (Norman 1980, Forseth and Norman, 1991). Following this concept, incident PAR at the top of the canopy (Q_{total0}) can be decomposed into direct and diffuse radiation components, measurable using total and diffuse PAR sensors.

$$Q_{total0} = Q_{b0} + Q_{d0} \tag{6}$$

where Q_{b0} is the direct radiation component and Q_{d0} is the diffuse component a the top of the canopy. The direct radiation penetrating the canopy will decrease exponentially as a function of $P_e(\theta,z)$:

$$Q_b(\theta, z) = Q_{b0} P_e(\theta, z) \tag{7}$$

The diffuse radiation component Q_d also extinguishes exponentially through the canopy but the extinction coefficient is assumed to be invariant with solar angle and much smaller than for direct PAR (Weiss and Norman, 1985, Brakke 1994, Smolander and

Stenberg, 2001). Diffuse radiation is therefore mostly a function of the canopy density (Annandale et al., 2003) and total PAR per canopy height layer can be calculated using

$$Q(\theta, z) = Q_{b0} P_e(\theta, z) + Q_d(z) \tag{8}$$

6.2.8.2 *Modeling f_{PAR}*

The fraction of PAR absorbed per canopy layer ($f_{PAR}(\theta, z)$) varies with the solar zenith angle and canopy depth and is a function of the foliage density profile. Consequently, the amount of foliage intercepted by a light beam at a specific height z can be calculated as

$$f_{PAR}(\theta, z) = f_{PAR0}(P_e(\theta,(z-1)) - P_e(\theta, z)) \tag{9}$$

where f_{PAR0} is the total fraction PAR absorbed, P_e (θ, z) is the effective probability of gap at a given height z and P_e (θ, z-1) is the effective probability of gap of the height above it.

6.2.8.3 *Modeling GEP*

Using (1), a direct and diffuse GEP component can be computed for each 10 x 10 m cell from the sunlit and shaded endmembers of PRI, if the ε-related response to a given amount of light is assumed to be constant throughout the canopy:

$$GEP_b(\theta, z) = f(PRI_b) \cdot f_{PAR}(z) \cdot Q_b(\theta, z) \tag{10a}$$

$$GEP_d(z) = f(PRI_d) \cdot f_{PAR}(z) \cdot Q_d(z) \tag{10b}$$

where PRI_d and PRI_b are the sunlit and shaded endmembers of measured PRI reflectance, respectively. A logarithmic transformation of PRI (f(PRI)) was introduced in the model to linearize the PRI - ε relationship (Chapter 5).

Integrating equations 10a-b over all height intervals (z) from 1 m to the maximum tree height (z_{max}) and over all 10 m x 10 m cells (c) within the study area, yields the total amount of photosynthesis for the direct and diffuse radiation component.

$$GEP_{Ib} = \int_{c=1}^{c=c_{max}} \left(\int_{z=1m}^{z=z_{max}} GEP_b(\theta, z) dz \right) dn \qquad (11a)$$

$$GEP_{Id} = \int_{c=1}^{c=c_{max}} \left(\int_{z=1m}^{z=z_{max}} GEP_d(z) dz \right) dn \qquad (11b)$$

where GEP_{Id} and GEP_{Ib} are the remotely-sensed estimates for the direct and diffuse GEP components, respectively.

6.2.9 Comparing EC determined to remotely-sensed GEP

Estimates of GEP provided by EC-flux data were compared with estimates derived from remotely-sensed data as follows: The integrated LiDAR and optical remotely-sensed outputs of (10a) and (10b) were weighted according to footprint of each 10 x 10 m cell. The EC-footprint weighted GEP components can be defined as

$$GEP_{Ibw} = \int_{c=1}^{c=c_{max}} \left(\int_{z=1m}^{z=z_{max}} GEP_b(\theta, z) dz \right) \phi(c) dc \qquad (12a)$$

$$GEP_{Idw} = \int_{c=1}^{c=c_{max}} \left(\int_{z=1m}^{z=z_{max}} GEP_d(z)dz \right) \phi(c)dc \qquad (12b)$$

where $\phi(c)$ describes the footprint per 10 m x 10 m cell (c) and GEP_{Idw} and GEP_{Ibw} are the footprint weighted estimates for the direct and diffuse GEP components, respectively.

6.3 Results

6.3.1 PRI endmembers

Figure 6.2A-D shows sunlit and shaded endmembers of PRI, averaged as 8-day values between April 1st, 2006 and March 31st 2007, as a function of time (Figure 6.2A), the ratio of direct to diffuse sky radiation above the canopy (*Q*) (Chapter 3) (Figure 6.2B), soil moisture (Figure 6.2C) and atmospheric pressure deficit (Figure 6.2D). As expected from previous studies conducted at this site (Chapter 5, Hall et al., 2008), the PRI of shaded leaves was generally larger than that of sunlit leaves, indicating that shaded leaves are exposed to less stress and thus have a higher ε than sunlit parts of the canopy. Chapter 5 showed that the canopy stress level is strongly related to the difference between sunlit and shaded PRI components (ΔPRI). These differences can largely be explained by meteorological variables. The ratio of direct to diffuse sky radiation above the canopy, representing the state of cloudiness, accounted for about 50% of variation in ΔPRI alone ($p<0.05$) (Figure 6.2B), while the atmospheric vapor pressure deficit (*D*) (Figure 6.2D) explained 39% of variations in ΔPRI ($p<0.05$). The soil-moisture content explained about 60% of variation in ΔPRI, except during the mid to late summer period (DOY 190-268) when soil moisture content was low. A linearized multiple regression revealed that these three meteorological variables together explained 79% of variation in ΔPRI ($p<0.05$) throughout the year. Differences between sunlit and shaded endmembers of PRI were largest in late summer when the canopy underwent significant drought and temperature stress, as well as in late winter, due to snowfall. Minimum differences were found through spring and early summer, when the canopy underwent only moderate stress.

6.3.2 Determining stand structural parameters using LiDAR

Figure 6.3 shows vertical profiles for L_e, P_{Gap} and the sunlit component of GEP for a mature (left column: A,C,E) and a young (right column: B,D,F) Douglas-fir dominated forest stand for August 28th 9:30 AM Pacific Standard Time (PST) (solar elevation = 36.4°). The mature stand is adjacent to the flux tower site, whilst the young stand is located in the north east of the 12 km^2 area and has a canopy height of 10 m (distance to tower: 1.5 km). L_e (Figures 6.3A-B) and P_e (Figures 6.3C-D) are shown for the mature and young stand respectively. A vertical profile of GEP is shown only for the sunlit GEP component (Figures 6.3E-F), as GEP_d was calculated for all canopy layers as a whole since it was assumed to be independent of within-canopy shading. The sunlit component of GEP diminishes quickly with decreasing height since PAR_b is largely absorbed within the top 10 m of the canopy (Figures 6.3E and F).

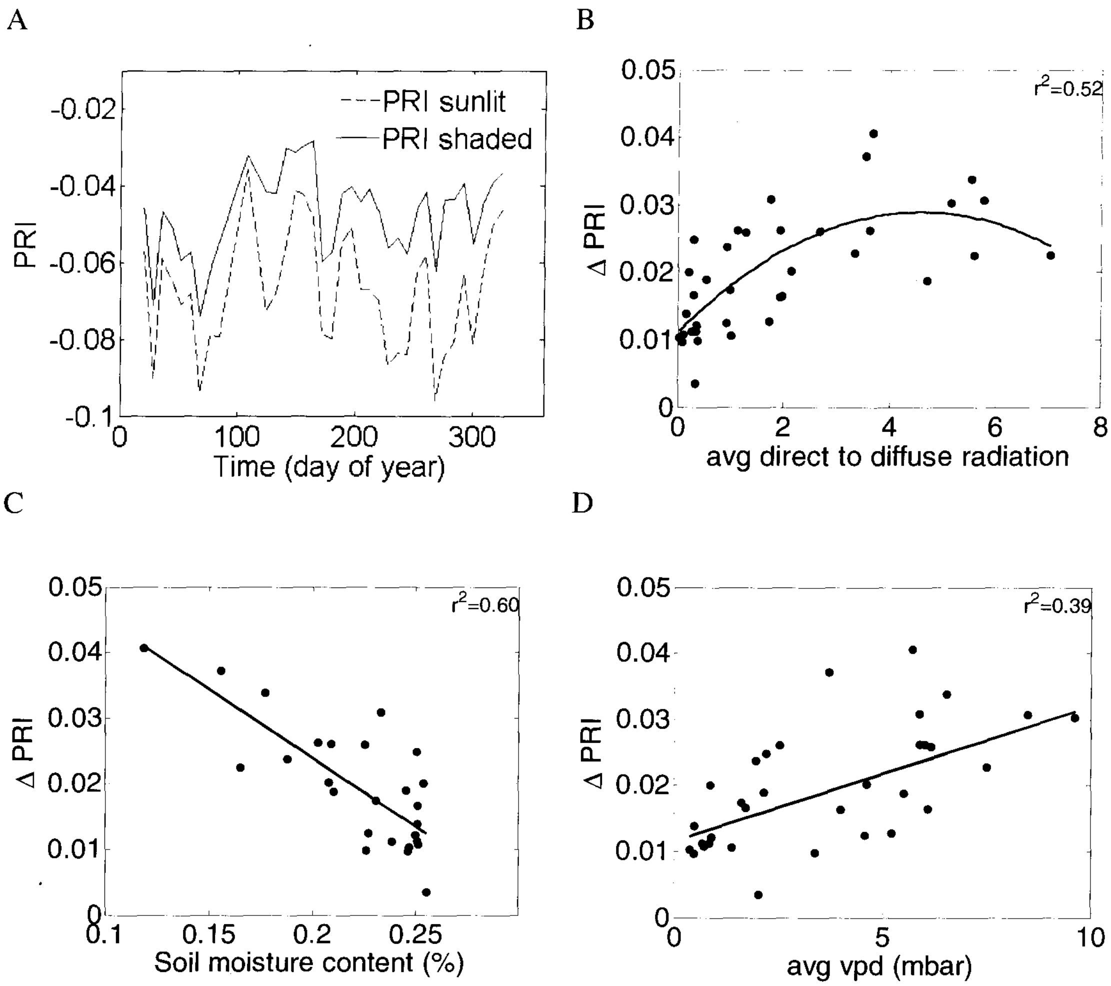

Figure 6.2A-D: Difference between sunlit and shaded PRI (ΔPRI) over a year computed as 8-day averaged datasets (A). Sunlit and shaded PRI were calculated using a kernel driven BRDF approach (Ross-Thick Li-Sparse Kernels). Relationship between Δ PRI and 8-day averaged state of cloudiness, expressed as ratio of direct to diffuse radiation (B), 8-day averaged soil moisture content (%/100 (vol.water content)) (C) (excluding DOY 190-268), and 8-day averaged vapour pressure deficit (in mbar) (D). Multiple regression analysis of all 3 components explained 77% of variation in ΔPRI. (all relationships where established for *p*<0.05)

6.3.3 Spatial modeling of GEP

Figure 6.4 shows the spatial distribution of sunlit GEP for a cloudy (A) and a sunny day (B). The figure shows the percent coverage of the sunlit GEP component for each 10 m x

10 m cell. The ratio of direct to diffuse radiation was 0.2 and 9, respectively. Differences between sunlit and shaded GEP coverage are most distinct for the sunny day and within younger stands with open spaced regeneration (compare Figure 6.1), dominated by direct sunlight due to the lack of canopy structure. Diffuse radiation played a larger role in mature forested areas where it dominates the radiation regime in the lower portions of the canopy. On overcast days, diffuse sky radiation provides the majority of incident PAR, and structure-related differences in percent cover as expressed in spectral descriptions using endmembers become more marginal.

Figure 6.5 shows the spatial distribution of remotely-sensed GEP for the study area surrounding the flux tower site as eight-day averaged values for the examples of DOY 26-33 (February, A), DOY 98-106 (April, B), 24-248 (August, C) and 288-296 (October, D). The highest GEP values were found for the mature forest stands with higher L_e values, while young regeneration sites (following harvesting) had the lowest rates of photosynthesis. Maximum GEP values in February obtained up to 9 μmol $m^{-2}s^{-1}$, while maximum values in August reached 30 μmol $m^{-2}s^{-1}$. Structure-related differences in GEP were persistent throughout the year, and were most distinct for higher levels of productivity (i.e. during the summer) with mature stands absorbing significantly more carbon than younger stands. The productivity of non-forested areas estimated from this model is close to zero throughout the year, as the LiDAR derived leaf area for these areas is nearly zero.

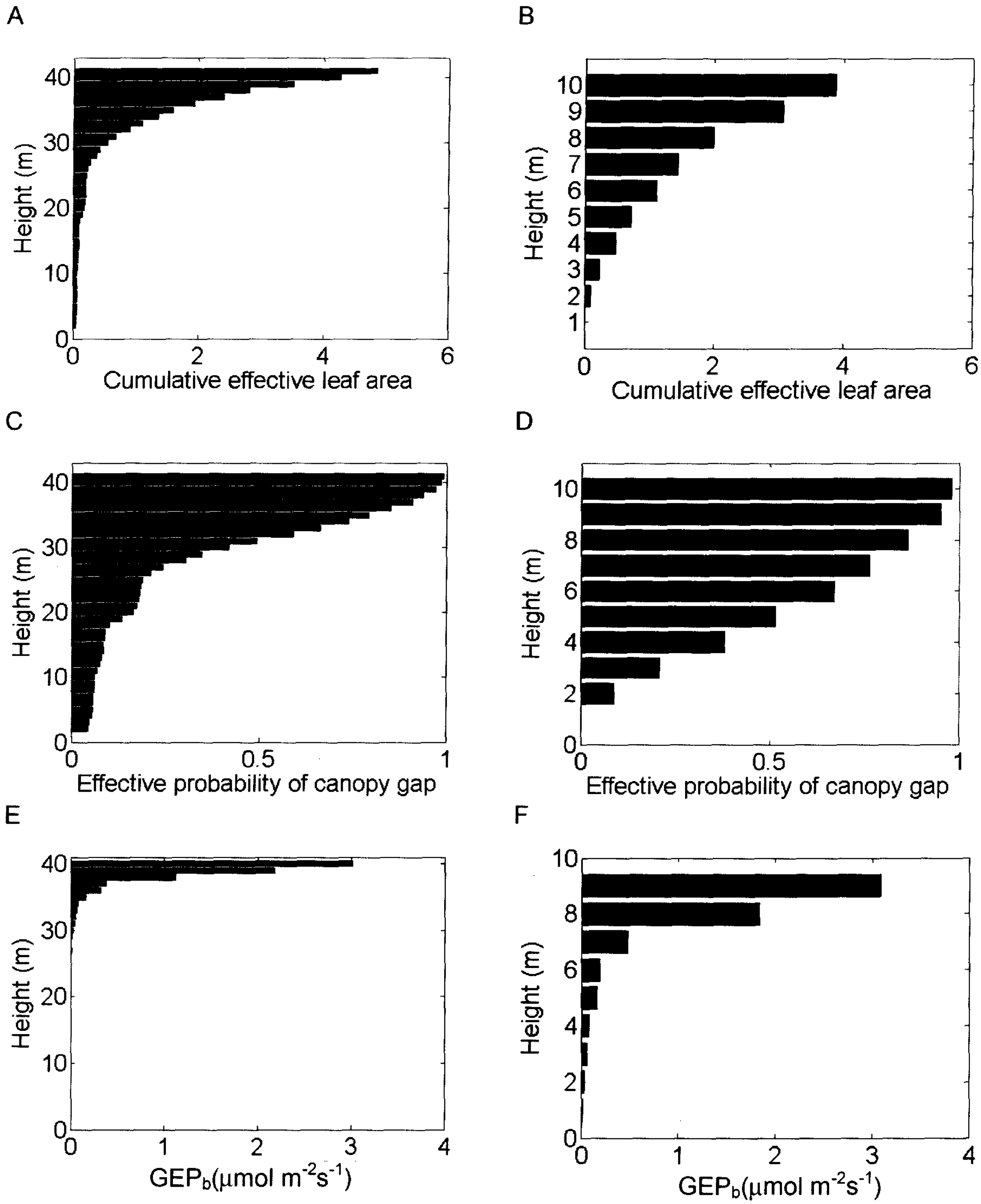

Figure 6.3A-F: Vertical profile of cumulative leaf area, effective probability of canopy gap and sunlit components of GEP for a mature (A,C,E) and a young (B,D,F) Douglas-fir stand as derived from spectral and LiDAR measurements for a given θ (25°). The shaded GEP components have been derived as integrated measurements over all heights.

A B

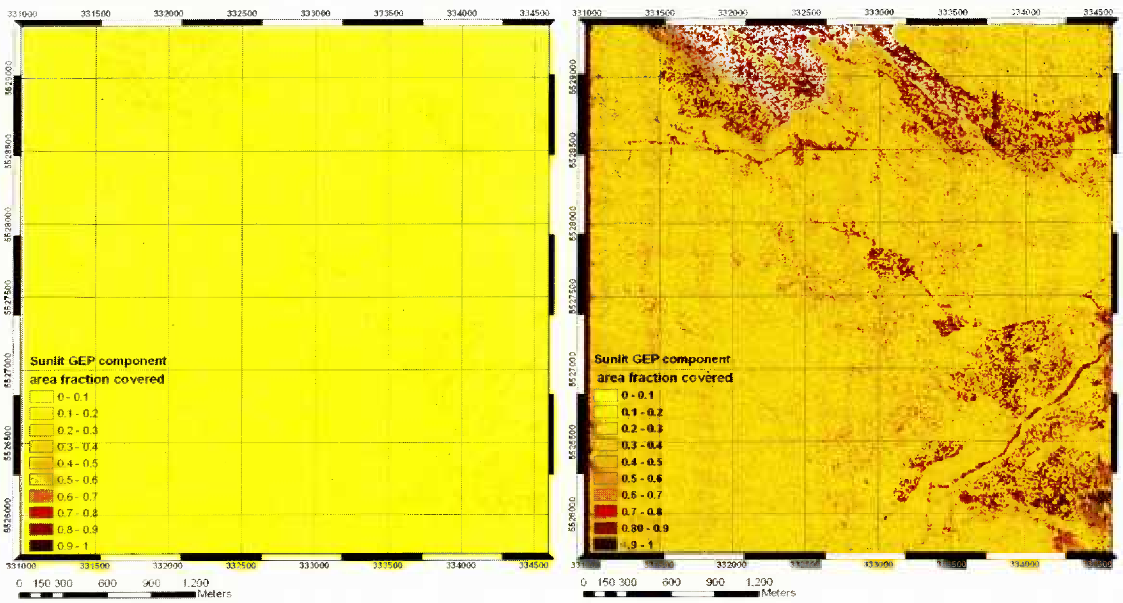

Figure 6.4: Spatial distribution of sunlit GEP components for a cloudy (A) and a sunny day (B). The ratio of direct to diffuse radiation was 0.2 and 9, respectively. The different colors the percent coverage of the sunlit GEP component per 10x10 m cell. The coverage of shaded GEP component is the complement of the images.

6.3.4 Comparing EC measured and remote sensed GEP

Figure 6.6 shows the yearly averaged footprint of daytime EC-flux measurements as modeled using Chen et al. (2007a, 2007b), overlaid over the footprint of the radiometer instrument installed at the flux-tower. The contour lines show the time-averaged impact (in percent) each 10 m x 10 m cell has on the EC-determined GEP values. The area with a daytime EC-footprint of greater than 0.1% had a diameter of approximately 150 m x 200 m (downwind and crosswind, respectively). As expected, the area with the largest impact was located closest to the tower.

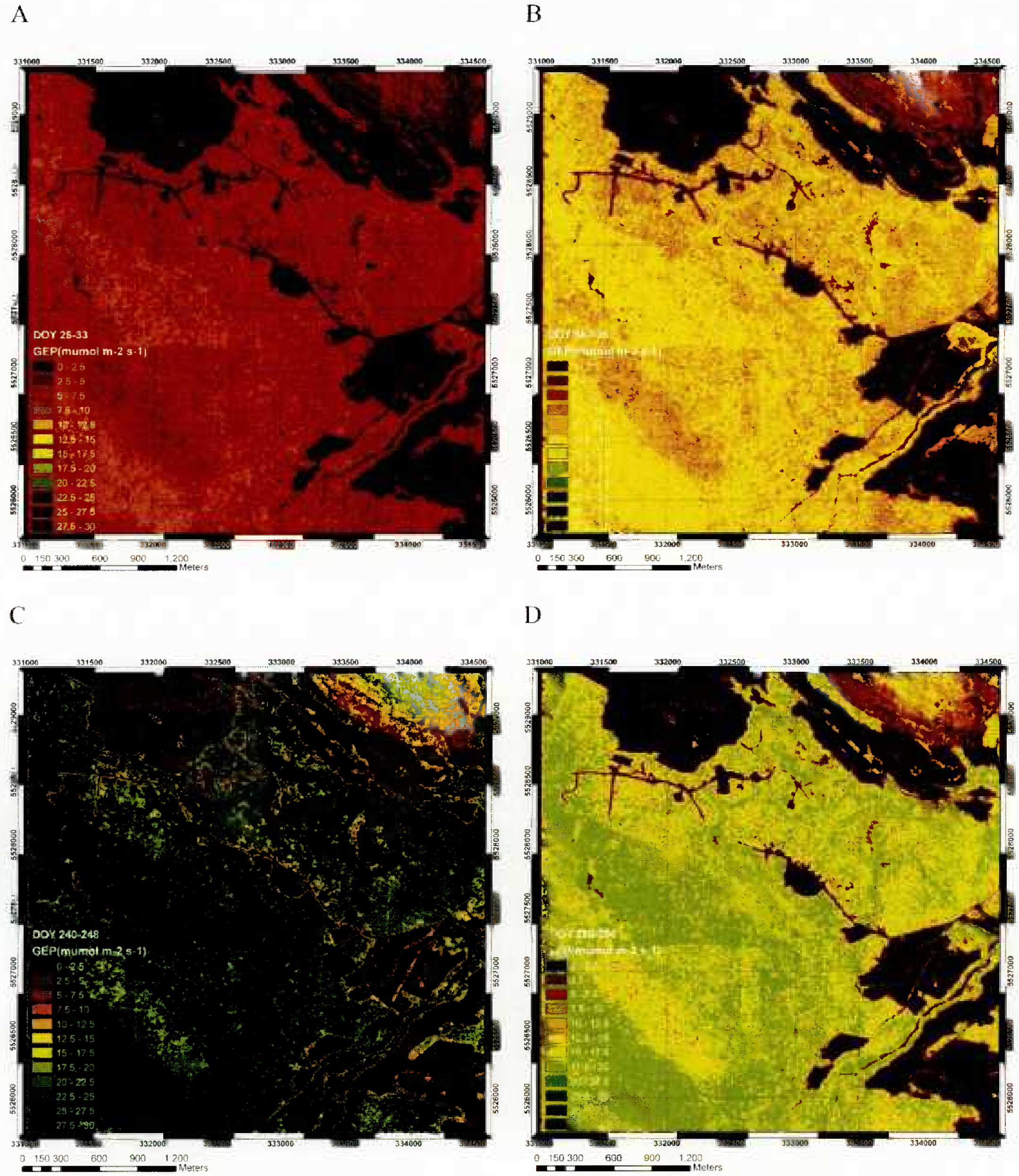

Figure 6.5A-D: Spatial distribution of GEP (sunlit + shaded) as a function of canopy structure for the study area, estimated as 8-day averages for the examples of a 8-day time period in late winter (February) (A), early spring (April) (B), late summer (August) (C) and fall (October) (D). The moderate climate conditions allow vegetation to photosynthesize almost year round (Morgenstern et al., 2004).

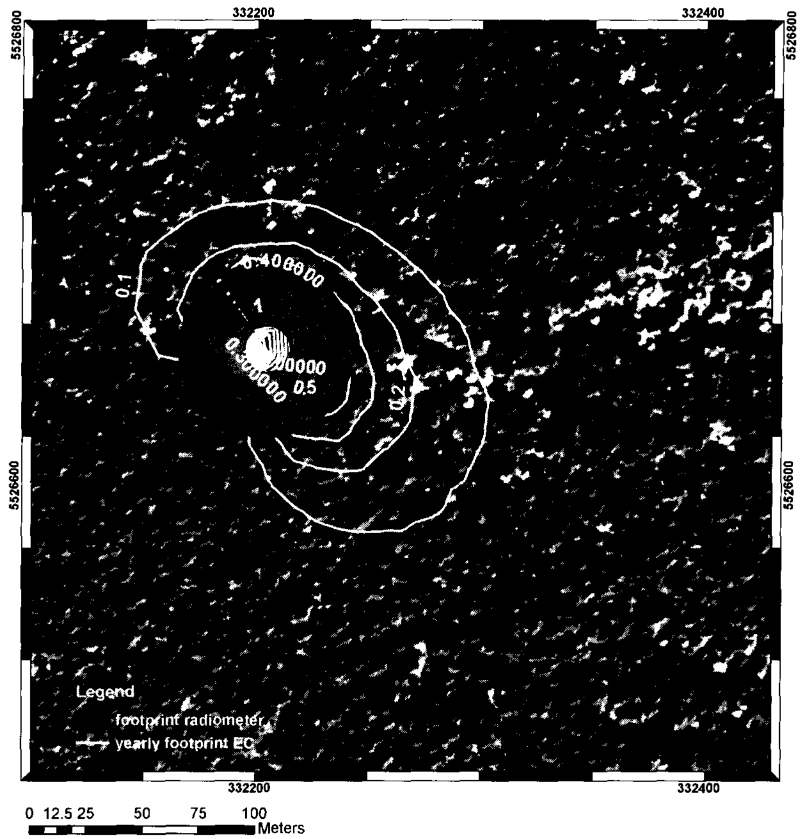

Figure 6.6: Footprint of the spectroradiometer (gray) and eddy covariance (EC) data (yearly average between March 31st 2006 and April 1st 2007). While the radiometer footprint is constant, the EC footprint varies throughout the year. The contour lines show the different levels of impact (in percent) an area had on the EC measurement over the study period. The figure shows daytime averages only.

Figure 6.7 shows a comparison between remotely-sensed GEP weighted by the EC footprint (ϕ) vs. EC-determined GEP over four 8-day time intervals between March 31st, 2006 and April 1st, 2007; DOY 26-33 (February, A), DOY 98-106 (April, B), 24-248 (August, C) and 288-296 (October, D), in correspondence with Figure 6.4. All graphs show a high correlation between remotely-sensed (predicted) and EC-determined GEP (r^2=0.85, 0.91, 0.75 and 0.81, respectively, p<0.05) for the time intervals observed.

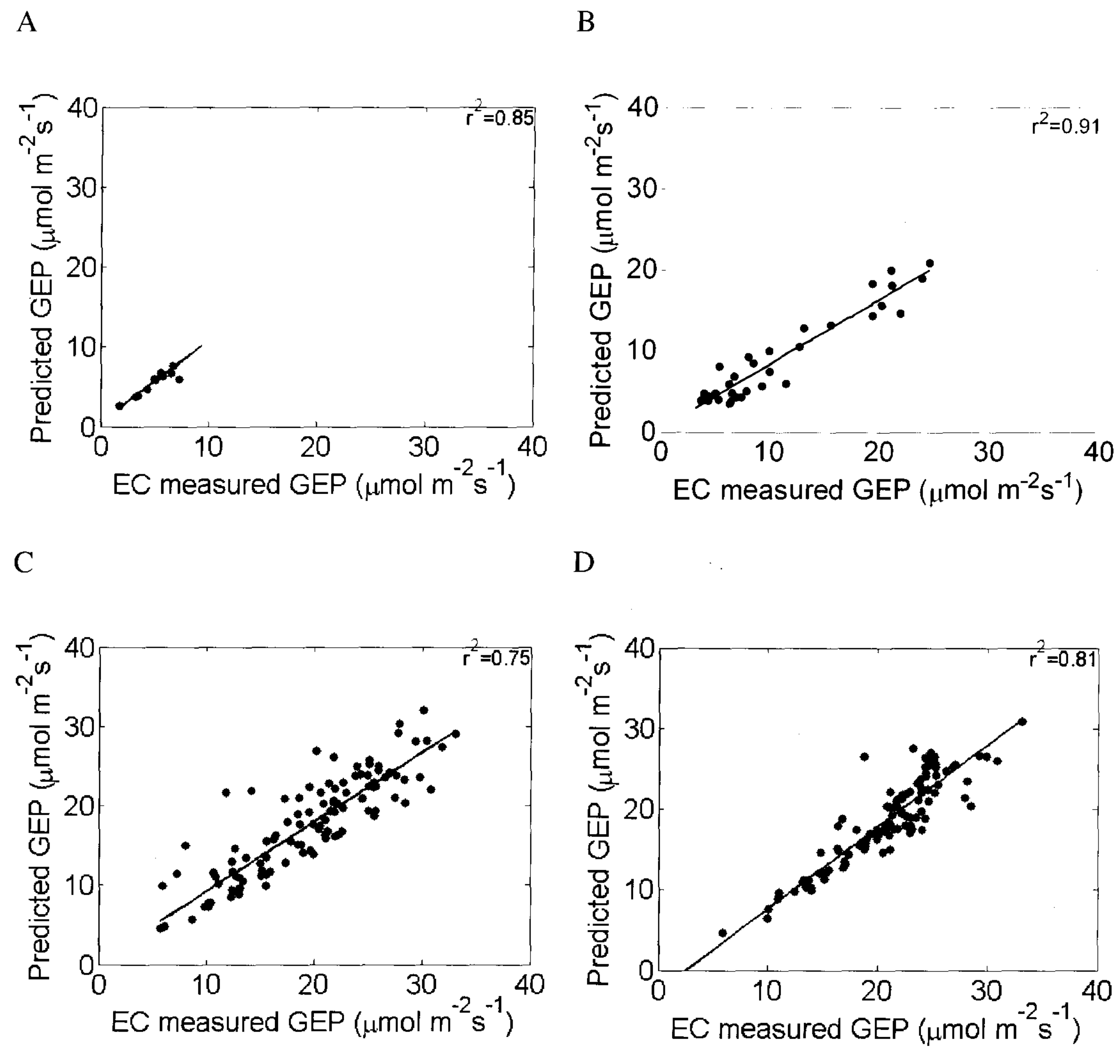

Figure 6.7: Relationship between remotely-sensed GEP, computed using PAR measurements, endmember reflectance of PRI and LiDAR derived information about the canopy structure and GEP measured as using eddy covariance technique. Both datasets are computed over an 8-day period for the examples of late winter (February) (A), early spring (April) (B), late summer (August) (C) and fall (October) (D). (corresponding to Figure 6.5).

6.4 Discussion and Conclusions

This study demonstrates an approach for up-scaling stand based on *in situ* spectrally determined GEP to obtain landscape level predictions for remote sensing to be expected from aircraft or satellite platforms. This was accomplished using structural information of the canopy derived from airborne laser scanning, combined with multi-angular high spectral-resolution PRI measurements decomposed into sunlit and shaded values. GEP was predicted vertically and horizontally over a 12 km^2 area at eight-day time steps.

The BRDF approach of Chapter 5 was successfully used to derive minimal and optimal photosynthetic performance for a given time interval throughout the year. We undertook our analysis at an eight-day time step, comparable to that used by the MODIS GEP product, as it not only provided enough spectral observations for establishing stable reflectance models, but was also flexible enough to account for changing environmental conditions at the research site (Figure 6.5, Figure 6.7). Differences between sunlit and shaded PRI were largely determined by environmental conditions, suggesting that canopy level PRI is a useful indicator for plant stress and thus photosynthetic efficiency. This result is consistent with Hall et al. (2008) and Chapter 5, which showed that ε can be detected at stand scales and under a wide range of view and illumination conditions throughout the year from spectral observations and that changes in ε are largely a result of changes in meteorological conditions.

The approaches of Lovell et al. (2003) and Coops et al. (2007) were successfully used for modeling the vertical and horizontal distribution of foliage and light interception within the tree canopy over two different-aged forest stands and thus allowed useful predictions of light interception at a landscape level with a high spatial resolution. Largest values for GEP were found in the older stands throughout the year, largely due to a bigger canopy surface, which led to greater absorption of PAR. Our results also demonstrate that diffuse sky radiation plays an important role in forest productivity, even on sunny days, as the diffuse radiation component largely dominates the radiation regime below the top of the canopy. This result is consistent with Alton et al. (2007) and Kotchenova (2004) finding that within canopy foliage can contribute significantly to stand level GEP. While spectral measurements alone often fail to account for within canopy productivity (Hall et al., 1992), LiDAR has been successfully used for extrapolating top of canopy level reflectance throughout different height levels of the canopy. The LiDAR based model yielded accurate results for forested areas throughout the year (Figure 6.5, Figure 6.7) the approach, however, is likely to underestimate the productivity of new regeneration areas as the leaf area is only assessed with a vertical resolution of 1 m and LiDAR returns below this threshold are considered ground returns rather than shrub or herbal vegetation. A possible way to mitigate this false estimation is to estimate GEP from surface reflectance directly within these areas.

The spectroradiometer installed at the site was able to capture the majority of the top of canopy reflectance for the EC-footprint area as estimated using the flux footprint model of Chen et al. (2007 a, b). Daytime GEP originated from a relatively restricted area around the tower, but due to the nature of EC-flux measurements, was vertically integrated throughout the canopy. The approach of modeling the within-canopy light regime using LiDAR combined with estimates of ε derived from multi-angular top of canopy reflectance measurements yielded accurate predictions of stand level photosynthesis for the time periods observed (Figure 6.7). Remotely-sensed data did however, slightly underestimated GEP throughout the year (Figure 6.7) due to the simple logarithmic conversion of PRI (Chapter 5), which was linearly scaled according to the maximum of the EC-determined ε.

The approach described in this study assumes that vegetation stress factors other than light are spatially constant and that the xanthophyll related response to light is constant, which is only reasonable over smaller areas within homogenous environmental conditions. Another assumption is that changes in the pigment pool size (=carotenoid to chlorophyll ratio), were small within each eight-day period and over the study area (Barton and North 2001) and possible age related biochemical differences in foliage composition had only minor effects on PRI. As a result, the area to which spectral measurements can be extrapolated is limited as (1) the empirical relationship between ε and PRI will change with species composition and (2) light independent stress factors such as soil-water or nutrition supply are likely to change with slope soil type and water table thereby affecting PRI. More research will be required to investigate the interactions between of these factors and stand level ε. A further simplifying assumption made in here is that the diffuse radiation component is independent of both mutual shading effects and θ (lambertian leaf surfaces) and thus approximately uniformly distributed within the canopy. This assumption is valid to a first approximation, as the magnitude of the scattering effect of direct radiation within the canopy is small (Norman 1980, Forseth and Norman, 1991).

The modeling approach using LiDAR data is suitable for up-scaling canopy level (or even leaf level) observations to small scaled satellite measures, such as $1km^2$ MODIS pixels. Approaches like the one demonstrated in this chapter could therefore aid current efforts trying to relate stand-based GEP measurements to globally available satellite data (Heinsch et al., 2006, Running et al., 2004, Drolet et al., 2005, 2007).

6.5 References

Adams, W.W., Demmig-Adams, B., Logan, B.A., Barker, D.H. and Osmond, C.B. (1999) Rapid Changes in Xanthophyll Cycle-Dependent Energy Dissipation and Photosystem Ii Efficiency in Two Vines, Stephania Japonica and Smilax Australis, Growing in the Understory of an Open Eucalyptus Forest. *Plant Cell and Environment* **22**, 125-136.

Alton, P.B., North, P.R. and Los, S.O. (2007) The Impact of Diffuse Sunlight on Canopy Light-Use Efficiency, Gross Photosynthetic Product and Net Ecosystem Exchange in Three Forest Biomes. *Global Change Biology* **13**, 776-787.

Annandale J.G., Jovanovic N.Z., Campbell G.S., Du Sautoy N., Lobit P. (2002) Two-Dimensional Solar Radiation Interception Model for Hedgerow Fruit Trees. *Agricultural and Forest Meteorology* **121**, 207-225

Asner, G.P. and Warner, A.S. (2003) Canopy Shadow in Ikonos Satellite Observations of Tropical Forests and Savannas. *Remote Sensing of Environment* **87**, 521-533.

Asner, G.P., Bateson, C.A., Privette, J.L., El Saleous, N. and Wessman, C.A. (1998) Estimating Vegetation Structural Effects on Carbon Uptake Using Satellite Data Fusion and Inverse Modeling. *Journal of Geophysical Research-Atmospheres* **103**, 28839-28853.

Asrar, G., Fuchs, M., Kanemasu, E. and Hatfield, J. (1984) Estimating absorbed photosynthetic radiation and leaf area index from spectral reflectance in wheat. *Agronomy Journal* **76**, 300-306.

Barnsley, M.J., Lewis, P., Sutherland, M. and Muller, J.P. (1997). Estimating Land Surface Albedo in the Hapex-Sahel Southern Super-Site: Inversion of Two BRDF Models Against Multiple Angle ASAS Images. *Journal of Hydrology* **189**, 749-778.

Barton, C.V.M. and North, P.R.J. (2001) Remote Sensing of Canopy Light-use efficiency Using the Photochemical Reflectance Index - Model and Sensitivity Analysis. *Remote Sensing of Environment* **78**, 264-273.

Brakke, T.W. (1994). Specular and Diffuse Components of Radiation Scattered by Leaves. *Agricultural and Forest Meteorology* **71**, 283-295.

Chen B., Black T.A. and Morgenstern K. (2007b) Intra- and Inter- Annual Variability of EC-Flux Footprint and its Implications in Carbon Balance Analysis, *Boundary-Layer Meteorology* (submitted).

Chen B., Chen, J. M., Mo, G. and Black T. A. (2007a) Comparison of Regional Carbon Flux Estimates from CO_2 Concentration Measurements and Remote Sensing-based Footprint Integration. *Global Biogeochemical Cycle*, (*accepted*).

Chen, J. and Black, T. (1991) Measuring Leaf Area Index of Plant Canopies with Branch Architecture. *Agricultural and Forest Meteorology* **57**, 1-12.

Chen, J.M. (1996) Canopy Architecture and Remote Sensing of the Fraction of Photosynthetically Active Radiation Absorbed by Boreal Conifer Forests. *IEEE-Transactions on Geoscience and Remote Sensing* **34**, 1353-1368.

Chen, J.M., Govind, A., Sonnentag, O., Zhang, Y.Q., Barr, A. and Amiro, B. (2006) Leaf Area Index Measurements at Fluxnet-Canada Forest Sites. *Agricultural and Forest Meteorology* **140**, 257-268.

Chen, J.M., Liu, J., Leblanc, S.G., Lacaze, R. and Roujean, J.L. (2003) Multi-Angular Optical Remote Sensing for Assessing Vegetation Structure and Carbon Absorption. *Remote Sensing of Environment* **84**, 516-525.

Coops, N.C., Hilker, T., Wulder, M.A., St-Onge, B., Newnham, G., Siggins, A. and Trofymow, J.A. (2007) Estimating Canopy Structure of Douglas-Fir Forest Stands From Discrete-Return LiDAR. *Trees-Structure and Function* **21**, 295-310.

Daughtry, C.S.T., Gallo, K.P. and Bauer, M.E. (1983) Spectral Estimates of Solar-Radiation Intercepted by Corn Canopies. *Agronomy Journal* **75**, 527-531.

Demmig-Adams, B. and Adams, W.W. (2000) Photosynthesis - Harvesting Sunlight Safely. *Nature* **403**, 371-372

Demmig-Adams, B., Moeller, D.L., Logan, B.A. and Adams, W.W. (1998) Positive Correlation Between Levels of Retained Zeaxanthin Plus Antheraxanthin and Degree of Photoinhibition in Shade Leaves of Schefflera Arboricola (Hayata) Merrill. *Planta* **205**, 367-374.

Drolet, G.G., Huemmrich, K.F., Hall, F.G., Middleton, E.M., Black, T.A., Barr, A.G. and Margolis, H.A. (2005) A MODIS-Derived Photochemical Reflectance Index to Detect Inter-Annual Variations in the Photosynthetic Light-Use Efficiency of a Boreal Deciduous Forest. *Remote Sensing of Environment* **98**, 212-224.

Eck, T.F. and Dye, D.G. (1991) Satellite Estimation of Incident Photosynthetically Active Radiation Using Ultraviolet Reflectance. *Remote Sensing of Environment* **38**, 135-146.

Forseth, I.N. & Norman, J.M. (1991) Modelling of Solar Irradiance, Leaf Energy Budget, and Canopy Photosynthesis. In Hall, D.O., Scurlock, J.M.O., Bolhar-Nordenkampf, R.C., Leegood, R.C. & Long, S.P. (eds). *Techniques in Photosynthesis and Productivity Research for a Changing Environment.* Chapman & Hall. London.

Gamon JA, Filella I, Peñuelas J (1993) The dynamic 531-nanometer Reflectance Signal: A Survey of Twenty Angiosperm Species. Yamamoto HY , Smith CM (Eds). *Photosynthetic Responses to the Environment.* American Society of Plant Physiologists, Rockville. pp. 172-177.

Gamon, J.A., Field, C.B., Bilger, W., Björkman, O., Fredeen, A.L. and Peñuelas, J. (1990) Remote-Sensing of the Xanthophyll Cycle and Chlorophyll Fluorescence in Sunflower Leaves and Canopies. *Oecologia* **85**, 1-7.

Gamon, J.A., Peñuelas, J. and Field, C.B. (1992) A Narrow-Waveband Spectral Index That Tracks Diurnal Changes in Photosynthetic Efficiency. *Remote Sensing of Environment* **41**, 35-44.

Gamon, J.A., Rahman, A.F., Dungan, J.L., Schildhauer, M. and Huemmrich, K.F. (2006) Spectral Network (SpecNet) - What Is It and Why Do We Need It? *Remote Sensing of Environment* **103**, 227-235.

Gao, F., Schaaf, C.B., Strahler, A.H., Jin, Y. and Li, X. (2003) Detecting Vegetation Structure Using a Kernel-Based BRDF Model. *Remote Sensing of Environment* **86**, 198-205.

Goodwin G (1937) Regeneration Study on the logged-off lands of the Comox Logging and Railway Company Oyster River Forest Survey No R 72 Survey file No 0124780 BC Forest Service 39p and Map

Hall, F.G., Hilker, T., Coops, N.C., Lyapustin, A., Huemmrich, K.F., Middleton, E.M., Drolet, G.G., Margolis, H.A., Black, T.A. (2008). Can Light-Saturated Reductions in Canopy Photosynthetic Capacity Be Observed From Space? *Remote Sensing of Environment* , accepted

Hall, F.G., Huemmrich, K.F. and Goward, S.N. (1990) Use of Narrow-Band Spectra to Estimate the Fraction of Absorbed Photosynthetically Active Radiation. *Remote Sensing of Environment* **32**, 47-54.

Hall, F.G., Huemmrich, K.F., Goetz, S.J., Sellers, P.J. and Nickeson, J.E. (1992) Satellite Remote-Sensing of Surface-Energy Balance - Success, Failures, and Unresolved Issues in FIFE. *Journal of Geophysical Research-Atmospheres* **97**, 19061-19089.

Hall, F.G., Shimabukuro, Y. E., Huemmrich, K.F., (1995b) Remote Sensing of Forest Biophysical Structure Using Mixture Decomposition and Geometric Reflectance Models. *Ecologocial Applications* **5**, 993-1013.

Hall, F.G., Townshend, J.R. and Engman, E.T. (1995a). Status of Remote-Sensing Algorithms for Estimation of Land-Surface State Parameters. *Remote Sensing of Environment* **51**, 138-156.

Heinsch, F.A., Zhao, M.S., Running, S.W., Kimball, J.S., Nemani, R.R., Davis, K.J., Bolstad, P.V., Cook, B.D., Desai, A.R., Ricciuto, D.M., Law, B.E., Oechel, W.C., Kwon, H., Luo, H.Y., Wofsy, S.C., Dunn, A.L., Munger, J.W., Baldocchi, D.D., Xu, L.K., Hollinger, D.Y., Richardson, A.D., Stoy, P.C., Siqueira, M.B.S., Monson, R.K., Burns, S.P. and Flanagan, L.B. (2006) Evaluation of Remote Sensing Based Terrestrial Productivity From MODIS Using Regional Tower Eddy Flux Network Observations. *IEEE-Transactions on Geoscience and Remote Sensing* **44**, 1908-1925.

Humphreys, E.R., Black, T.A., Morgenstern, K., Cai, T.B., Drewitt, G.B., Nesic, Z. and Trofymow, J.A. (2006) Carbon Dioxide Fluxes in Coastal Douglas-Fir Stands at Different Stages of Development After Clearcut Harvesting. *Agricultural and Forest Meteorology* **140**, 6-22.

Jassal, R.S., Black, T.A., Cai, T.B., Morgenstern, K., Li, Z., Gaumont-Guay, D. and Nesic, Z. (2007). Components of Ecosystem Respiration and an Estimate of Net Primary Productivity of an Intermediate-Aged Douglas-Fir Stand. *Agricultural and Forest Meteorology* **144**, 44-57.

Kormann R., Meixner F.X. (2001) An Analytical Footprint Model for Non-Neutral Stratification. *Boundary Layer Meteorology* **99**, 207-224

Kotchenova, S.Y., Song, X.D., Shabanova, N.V., Potter, C.S., Knyazikhin, Y. and Myneni, R.B. (2004) Lidar Remote Sensing for Modeling Gross Primary Production of Deciduous Forests. *Remote Sensing of Environment* **92**, 158-172.

Leclerc, M.Y. and Thurtell, G.W. (1990) Footprint Prediction of Scalar Fluxes Using a Markovian Analysis. *Boundary-Layer Meteorology* **52**, 247-258.

Lefsky, M.A., Turner, D.P., Guzy, M. and Cohen, W.B. (2005) Combining LiDAR Estimates of Aboveground Biomass and Landsat Estimates of Stand Age for Spatially Extensive Validation of Modeled Forest Productivity. *Remote Sensing of Environment* **95**, 549-558.

Li, X. and Strahler, A. (1985) Geometric-optical modeling of a conifer forest canopy. *IEEE-Transactions on Geoscience and Remote Sensing* GE **23**, 705-721.

Li, X. and Strahler, A. (1992) Geometric-optical Bi-directional Reflectance Modeling of the Discrete Crown Vegetation Canopy – Effect of Crown Shape and Mutual Shadowing. *IEEE-Transactions on Geoscience and Remote Sensing*, **30**, 276-292

Los, S.O., North, P.R.J., Grey, W.M.F. and Barnsley, M.J. (2005) A Method to Convert AVHRR Normalized Difference Vegetation Index Time Series to a Standard Viewing and Illumination Geometry. *Remote Sensing of Environment* **99**, 400-411.

Lovell, J.L., Jupp, D.L.B., Culvenor, D.S. and Coops, N.C. (2003) Using Airborne and Ground-Based Ranging LiDAR to Measure Canopy Structure in Australian Forests. *Canadian Journal of Remote Sensing* **29**, 607-622.

Magnussen, S. and Boudewyn, P. (1998) Derivations of Stand Heights from Airborne Laser Scanner Data with Canopy-Based Quantile Estimators. *Canadian Journal of Forest Research* **28**, 1016-1031.

Middleton, E.M., D.W. Deering and S.P. Ahmad (1987) Surface Anisotropy and Hemispheric Reflectance for a Semiarid Ecosystem, *Rem. Sens. Environ.* **23**, 193-212.

Monteith, J.L. (1972) Solar-Radiation and Productivity in Tropical Ecosystems. *Journal of Applied Ecology* **9**, 747-766.

Monteith, J.L. (1977) Climate and Efficiency of Crop Production in Britain. *Philosophical Transactions of the Royal Society of London Series B-Biological Sciences* **281**, 277-294.

Morgenstern, K., Black, T.A., Humphreys, E.R., Griffis, T.J., Drewitt, G.B., Cai, T.B., Nesic, Z., Spittlehouse, D.L. and Livingstone, N.J. (2004) Sensitivity and Uncertainty of the Carbon Balance of a Pacific Northwest Douglas-Fir Forest During an El-Niño La-Niña Cycle. *Agricultural and Forest Meteorology* **123**, 201-219.

Myneni RB, Hoffman S, Knyazikhin Y, Privette JL, Glassy J, Tian Y, Wang Y, Song X, Zhang Y, Smith GR, Lotsch A, Friedl M, Morisette JT, Votava P, Nemani RR, Running SW (2002). Global Products of Vegetation Leaf Area and Fraction Absorbed PAR from Year One of MODIS Data. *Remote Sensing of Environment* **83**, 214-231.

Myneni RB, Williams DL (1994) On the Relationship Between F_{APAR} and NDVI. *Remote Sensing of Environment* **49**, 200-211.

Næsset, E. (1997) Determination of mean tree height of forest stands using airborne laser scanner data. *ISPRS Journal of Photogrammetry & Remote Sensing* **52**, 49-56.

Næsset, E. (2002) Predicting Forest Stand Characteristics with Airborne Scanning Laser Using a Practical Two-Stage Procedure and Field Data. *Remote Sensing of Environment* **80**, 88-99.

Næsset, E. and Okland, T. (2002) Estimating tree height and tree crown properties using airborne scanning laser in a boreal nature reserve. *Remote Sensing of Environment* **79**, 105-115.

Norman, J.M. (1980) Interfacing leaf and canopy light interception models. In Hesketh, J.D. & Jones, J.W. (eds). *Predicting Photosynthesis for Ecosystem Models.* CRC Press. Boca Raton, Florida. pp.49-67.

Peddle, D.R., Hall, F.G. and Ledrew, E.F. (1999) Spectral Mixture Analysis and Geometric-Optical Reflectance Modeling of Boreal Forest Biophysical Structure. *Remote Sensing of Environment* **67**, 288-297.

Persson, A., Holmgren, J. and Soderman, U. (2002) Detecting and measuring individual trees using an airborne laser scanner. *Photogrammetric Engineering & Remote Sensing* **68**, 925-932.

Prince, S.D. and Goward, S.N. (1995) Global Primary Production: a Remote Sensing Approach. *Journal of Biogeography* **22**, 815-835.

Rahman, A.F., Gamon, J.A., Fuentes, D.A., Roberts, D.A. and Prentiss, D. (2001) Modeling Spatially Distributed Ecosystem Flux of Boreal Forest Using Hyperspectral Indices From AVIRIS Imagery. *Journal of Geophysical Research-Atmospheres* **106**, 33579-33591.

Rahman, A.F., Sims, D.A., Cordova, V.D. and El-Masri, B.Z. (2005) Potential of MODIS EVI and Surface Temperature for Directly Estimating Per-Pixel Ecosystem C Fluxes. *Geophysical Research Letters*, **32,** (19): Art. No. L19404

Reda, I. and Andreas, A. (2004) Solar Position Algorithm for Solar Radiation Applications. *Solar Energy* **76**, 577-589.

Roujean, J.L., Leroy, M. and Deschamps, P.Y. (1992) A Bi-directional Reflectance Model of the Earths Surface for the Correction of Remote-Sensing Data. *Journal of Geophysical Research-Atmospheres* **97**, 20455-20468.

Running SW, Baldocchi DD, Turner DP, Gower ST, Bakwin PS, Hibbard KA (1999) A Global Terrestrial Monitoring Network Integrating Tower Fluxes, Flask Sampling, Ecosystem Modeling and Eos Satellite Data. *Remote Sensing of Environment* **70**, 108-27.

Running, S.W., Nemani, R.R., Heinsch, F.A., Zhao, M.S., Reeves, M. and Hashimoto, H. (2004) A Continuous Satellite-Derived Measure of Global Terrestrial Primary Production. *Bioscience* **54**, 547-560.

Schmid, H.P. and Lloyd, C.R. (1999) Spatial Representativeness and the Location Bias of Flux Footprints Over Inhomogeneous Areas. *Agricultural and Forest Meteorology* **93**, 195-209.

Sellers PJ, Hall FG (1992). FIFE in 1992 - Results, Scientific Gains, and Future-Research Directions. Journal of Geophysical Research-Atmospheres **97**,19091-19109.

Sellers, P. (1985) Canopy reflectance, Photosynthesis and Transpiration. *International Journal of Remote Sensing* **6**, 1335-1372.

Sellers, P.J. (1987) Canopy Reflectance, Photosynthesis, and Transpiration .2. The Role of Biophysics in the Linearity of Their Interdependence. *Remote Sensing of Environment* **21**, 143-183.

Sellers, P.J., Hall, F.G., Kelly, R.D., Black, A., Baldocchi, D., Berry, J., Ryan, M., Ranson, K.J., Crill, P.M., Lettenmaier, D.P., Margolis, H., Cihlar, J., Newcomer, J., Fitzjarrald, D., Jarvis, P.G., Gower, S.T., Halliwell, D., Williams, D., Goodison, B., Wickland, D.E. and Guertin, F.E. (1997) Boreas in 1997: Experiment Overview, Scientific Results, and Future Directions. *Journal of Geophysical Research-Atmospheres* **102**, 28731-28769.

Sellers, P.J., Los, S.O., Tucker, C.J., Justice, C.O., Dazlich, D.A., Collatz, G.J. and Randall, D.A. (1996) A Revised Land Surface Parameterization (SiB2) for Atmospheric GCMs .2. The Generation of Global Fields of Terrestrial Biophysical Parameters From Satellite Data. *Journal of Climate* **9**, 706-737.

Sellers, P.J., Meeson, B.W., Hall, F.G., Asrar, G., Murphy, R.E., Schiffer, R.A., Bretherton, F.P., Dickinson, R.E., Ellingson, R.G., Field, C.B., Huemmrich, K.F., Justice, C.O., Melack, J.M., Roulet, N.T., Schimel, D.S. and Try, P.D. (1995) Remote-Sensing of the Land-Surface for

Studies of Global Change - Models, Algorithms, Experiments. *Remote Sensing of Environment* **51**, 3-26.

Sellers, P.J., Randall, D.A., Collatz, G.J., Berry, J.A., Field, C.B., Dazlich, D.A., Zhang, C., Collelo, G.D. and Bounoua, L. (1996) A Revised Land Surface Parameterization (SiB2) for Atmospheric GCMs .1. Model Formulation. *Journal of Climate* **9**, 676-705.

Smolander, S. and Stenberg, P. (2001) A Method for Estimating Light Interception by a Conifer Shoot. *Tree Physiology* **21**, 797-803.

Tucker, C. (1979) Red and photographic infrared linear combinations for monitoring vegetation. *Remote Sensing of Environment* **8**, 127-150.

Tucker, C. and Sellers, P. (1986) Satellite remote sensing of primary production. *International Journal of Remote Sensing* **7**, 1395-1416.

Tucker, C.J., Jones, W.H., Kley, W.A. and Sundstrom, G.J. (1981) A 3-Band Hand-Held Radiometer for Field Use. *Science* **211**, 281-283.

Turner DP, Urbanski S, Bremer D, Wofsy SC, Meyers T, Gower ST, Gregory M. (2003) A Cross-Biome Comparison of Daily Light-use efficiency for Gross Primary Production. *Global Change Biology* **9**, 383-395.

Van Laake, P.E. and Sanchez-Azofeifa, G.A. (2004) Simplified Atmospheric Radiative Transfer Modelling for Estimating Incident Par Using MODIS Atmosphere Products. *Remote Sensing of Environment* **91**, 98-113.

Wanner, W., Li, X. and Strahler, A. (1995) On the derivation of kernels for kernel-driven models of bi-directional reflectance. *Journal of Geophysical Research* **100**, 21 077-21 089

Weiss, A. and Norman, J.M. (1985) Partitioning Solar-Radiation Into Direct and Diffuse, Visible and Near-Infrared Components. *Agricultural and Forest Meteorology* **34**, 205-213.

Wulder, M. (1998) Optical Remote Sensing Techniques for the Assessment of Forest Inventory and Biophysical Parameters. *Progress in Physical Geography* **22**, 449-476.

7 ASSESSING UNCERTAINTIES IN MODIS LIGHT-USE EFFICIENCY IN A DOUGLAS-FIR STAND USING MULTI-ANGULAR SPECTRAL OBSERVATIONS AND EDDY COVARIANCE DATA[9]

7.1 Introduction

The "Net Photosynthesis 8-Day L4 Global 1 km" product (MOD17) of NASA's moderate resolution imaging spectroradiometer (MODIS) provides eight-day averages of gross primary production (GPP) at a 1 km spatial resolution for the entire vegetated land surface of the Earth computed as the product of incident photosynthetically active radiation (PAR), the fraction of it being absorbed by the plant canopy (f_{par}) and the light-use efficiency (ε), with which absorbed PAR is used in the production of biomass (Monteith 1972, 1977). Input parameters for MOD17 are derived from a combination of satellite observations, describing canopy characteristics from visible and near-infrared spectral reflectance, globally derived meteorological variables, and a set of biome-specific look-up parameters. Despite the widespread use of this model, a number of recent studies have highlighted its limitations (Heinsch et al., 2006, Turner et al., 2003, 2005, Yuan et al., 2007, Zhao et al., 2006) and, as a result, the usefulness of MODIS predictions depends on our ability to quantify and explain these uncertainties (Coops et al., 2007).

Arguably, one of the biggest limitations to MOD17 is its approach of modeling ε as a biome specific constant (ε_{max}), adjusted through daily measurements of minimum air

[9] A version of this chapter has been submitted for publication. Hilker, T., Coops, N.C., Black, T.A. (2008) Assessing Uncertainties in MODIS Light-Use Efficiency in a Douglas-Fir Stand Using Multi-Angular Spectral Observations and Eddy Covariance Data. *Geophysical Research letters* (submitted)

temperature (S_{Tmin}) and mean daytime atmospheric water vapour pressure deficit (S_D) (Running et al., 2004, Heinsch et al., 2006), obtained from NASA's data assimilation office (DAO) at a 1° x 1.25° spatial resolution (Heinsch et al., 2003). This simple look-up technique distinguishes between 11 different vegetation types (Turner et al., 2003, Heinsch et al., 2006) and therefore greatly simplifies the existing species dependent variability of ε (Running et al., 2000, Heinsch et al., 2006, Turner et al., 2003). Additionally, the parameters down-regulating ε often fail to account for its spatial and temporal variability, which is determined by any of a large number of environmental stresses reducing the photosynthetic capacity at a given time and at fine spatial scales (Prince and Goward 1995, Goetz and Prince, 1996, Landsberg and Warring, 1997).

In this study, we assess the spatial and temporal uncertainties of the two MODIS-ε modifiers, S_{Tmin} and S_D, for describing ε in a Douglas-fir (*Pseudotsuga menziesii* var *menziesii* (Mirb.) Franco) dominated forest stand in British Columbia, Canada over one year. Eight-day averages of S_{Tmin} and S_D were derived from flux tower measurements and compared to eddy covariance (EC) derived ε and a number of alternative stress indicators identified in previous studies (Schwalm et al., 2006, Chapter 3). Variability of ε was assessed from remote sensing data using a tower-based spectroradiometer, observing the canopy surface at multiple view and sun angles (Chapter 5). The objective of this study was to develop an improved modeling of the spatial and temporal variability in ε at landscape and global scales.

7.2 Methods

7.2.1 Eddy-covariance-based determination of ε

The study area is a Canadian Carbon Program flux-tower site on Vancouver Island, British Columbia, Canada at 300 m above sea level (49°52'7.8" N, 125°20'6.3" W). The 58-year-old second-growth coniferous forest consists of 80% Douglas-fir, 17% western red cedar (*Thuja plicata* Donn *ex* D. Don) and 3% western hemlock (*Tsuga heterophylla* (Raf.) Sarg.) and is highly productive with rotation cycles as short as 60 years (Morgenstern et al., 2004).

Continuous, half-hourly fluxes of CO_2 were measured using the EC method (Morgenstern et al., 2004) between April 2006 and March 2007. Net ecosystem exchange (NEE) was determined as the sum of the half-hourly fluxes of CO_2 (positive upward) and the rate of change in CO_2 storage in the air column between ground and EC measurement level (42 m), using a three-axis sonic anemometer-thermometer (model R3, Gill Instruments Ltd., Lymington, UK) and a closed-path CO_2/H_2O infrared gas analyzer (model LI-6262, LI-COR Inc., Lincoln, NE, USA) (Humphreys et al., 2006, Jassal et al., 2007). Incident and reflected PAR [μmol m^{-2} s^{-1}] was measured from upward and downward facing quantum sensors (model 190 SZ, LI-COR Inc.) above and below the canopy. GPP was calculated as daytime ecosystem respiration minus daytime NEE. EC-ε (ε_{EC}) was determined from GPP, incident PAR and f_{PAR} (Schwalm et al., 2006), where f_{PAR} was calculated following Chen and Black (1991) and Chen (1996). Latent heat fluxes (λE) were calculated following Humphreys et al. (2006) and half-hourly means of volumetric soil water content at 0.3 m depth (θ_{30}) were derived from water content reflectometers (Model CS-615, Campbell Scientific Inc., Logan, UT, USA) (Coops et al., 2007).

7.2.2 Determining ε from remote sensing

Canopy reflectance was obtained from AMSPEC, an automated tower-based, multi-angular spectroradiometer platform (Chapter 4) installed 10 m above the canopy. This instrument features a motor-driven probe rotating in 11.5° intervals every 30 seconds, thereby allowing observations in a 330° view area around the tower every 15 minutes. The spectroradiometer used is a Unispec-DC (PP Systems, Amesbury, MA, USA) featuring 256 contiguous 3-nm bands between the wavelengths of 350 and 1200 nm (Chapter 4). Canopy spectra was obtained from simultaneous measurements of radiance and cosine corrected solar irradiance (Chapter 4), sampled every 5 seconds from sunrise to sunset with the downward looking probe pointing at a vertical zenith angle of 62° to account for canopy clumping effects (Chen and Black, 1991).

Light-use efficiency was determined using the photochemical reflectance index (PRI) (Gamon et al., 1992, 1993, Peñuelas et al., 1995), which had previously been used for prediction of instantaneous ε at the site over the one-year period (Chapter 5). PRI was defined as (Gamon et al., 1992, 1993)

$$\mathrm{PRI} = \frac{\rho_{531} - \rho_{570}}{\rho_{531} + \rho_{570}} \qquad (1)$$

where ρ_{531} and ρ_{570} is the reflectance at 531 and 570 nm, respectively. Remotely-sensed ε (ε_{RS}) (g C MJ^{-1}) was obtained from a log-normal transformation of PRI, derived from ε_{EC} (Chapter 5).

7.2.3 Determining MODIS-ε

Eight-day MODIS-ε (ε_{MODIS}) was calculated using ε_{max} obtained from the MODIS biome properties look-up table (BPLUT), and eight-day means of scaled daily minimum air temperature (T_{Air}) and atmospheric water vapour pressure deficit (D) (Heinsch et al., 2003), derived from air temperature and relative humidity measured above the canopy (Buck, 1981, Humphreys et al., 2006) and scaled according to the MODIS user guide (Heinsch et al., 2003).

7.2.4 Temporal variablity

MODIS modifiers were compared to a range of temperature and moisture related stress indicators, including T_{Air}, measured above the canopy, soil temperature (T_{soil}), measured at 30cm depth, and λE and θ_{30}, for S_{Tmin} and S_D, respectively. Time periods were identified in which the two MODIS modifiers were able to describe changes in each of these additional stress indicators more or less accurately and eight-day ε_{MODIS} was compared to eight-day averages of ε_{EC} and ε_{RS} over four seasonal windows defined as early summer, late summer, late fall and spring (DOY 96-209, 209-297, 297-9, 9-96).

7.2.5 Spatial variability

The spatial variability within the radiometer footprint was assessed using AMSPEC. The instrument samples data under a wide range of view and illumination conditions, hence the PRI observations made are a function of not only the physiological status of the canopy (i.e. ε), but also the sun-observer geometry, the prevailing sky conditions (Chapter 5) and, when comparing multi-directional observations to one another, canopy and leaf structural differences. Reflectance changes due to the physiological status of the plant can be extracted when stratifying data into homogeneous subsets of observations with respect to both sky conditions and EC-determined ε, with individual bi-directional reflectance (BRDF) models being fitted to each strata (Chapter 5). BRDF can, however, also be obtained separately for individual constant viewing directions (as defined by the angular deviation from geodetic north) provided that observations are obtained for multiple sun angles, that is, during different times of the day and year. Once a BRDF surface is developed for a given viewing direction, state of cloudiness and ε-stratum, all reflectance data can be transformed to one common sun-observer geometry and differences found between these standardized observations can be ascribed to structural differences in leaves and canopies. The state of cloudiness was determined using the ratio (q) of direct to diffuse incident PAR measured using a "sunshine sensor" (model BF3, Delta-T Devices Ltd., Burwell, UK) and BRDF models were established from year-round observations using 10 q and 16 ε-strata separately for all 34 different viewing directions. No observations were made between an azimuth of 220° and 250° due to obstruction by the tower and data were linearly interpolated from adjacent observations.

7.3 Results

Figure 7.1A shows the annual eight-day pattern of the MODIS temperature modifier (S_{TMin}) plotted as a time series together with the corresponding means of T_{Air} and T_{soil}. S_{TMin} reduces photosynthesis throughout the year with the exception of mid to late summer (DOY 190-270) thereby closely following the patterns of both T_{Air} and T_{soil} (r^2 = 0.86 and r^2 = 0.88, respectively; $p < 0.05$). During the late winter and early spring period (DOY 9-90) the agreement between S_{TMin} and T_{Air} and S_{TMin} and T_{soil} was less significant (r^2 = 0.49 and 0.60, respectively; $p < 0.05$). Figure 7.1B shows a time series of the eight-day MODIS water vapour pressure deficit modifier (S_D) plotted together with eight-day averages of λE and θ_{30}. This modifier reduces ε_{MODIS} for a shorter period of time during the late summer months (DOY 109 to 290) by up to 70%. The relationship between S_D and θ_{30} and S_D and λE is weak (r^2 = 0.19 and r^2 = 0.16, respectively) with changes in θ_{30} not being well described by this modifier. Additionally, annual changes in evaporation, especially during early spring (DOY 9-90), are not being well captured by S_D. Figure 7.1C and D show the annual relationship between ε_{EC} and S_{Tmin} and ε_{EC} and S_D. Both stress modifiers explained little variability in ε_{EC} (r^2= 0.03 and r^2 = 0.13) with the relationship between ε_{EC} and S_D being non-linear.

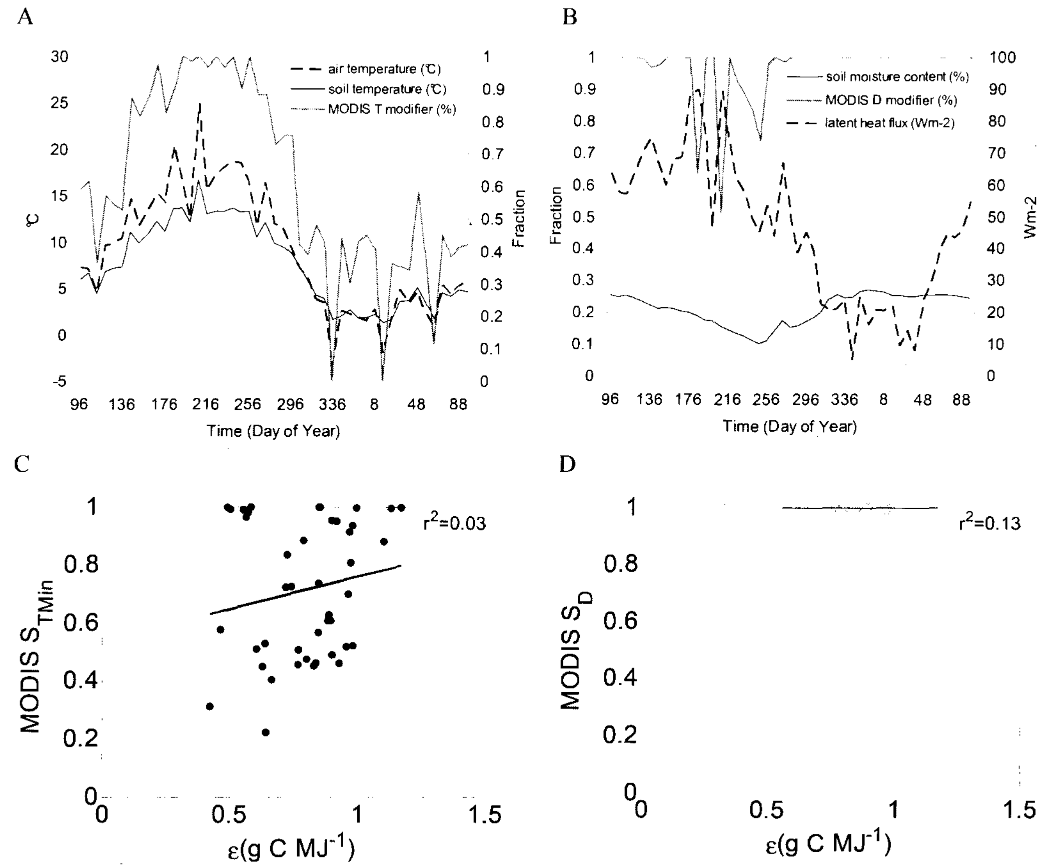

Figure 7.1 A-D. A: Time series of the MODIS temperature modifier S_{TMin}, daily mean air temperature and daily mean soil temperature between April 2006 and March 2007. The MODIS temperature modifier follows the patterns of air and soil temperature well, thereby constraining photosynthesis almost throughout the year. Figure 7.1B: Time series of the MODIS vapour pressure deficit modifier S_D, latent heat flux and soil moisture content between April 2006 and March 2007. The MODIS vapour pressure deficit modifier does not well describe changes in soil water availability and evaporation and limits photosynthesis only during early summer. Figure 7.1C and D: Relationship between ε_{EC} and S_{TMin} and ε_{EC} and S_D. The yearly relationship is moderate with $r^2 = 0.03$ and $r^2 = 0.13$ ($p < 0.05$) for S_{TMin} and S_D, respectively.

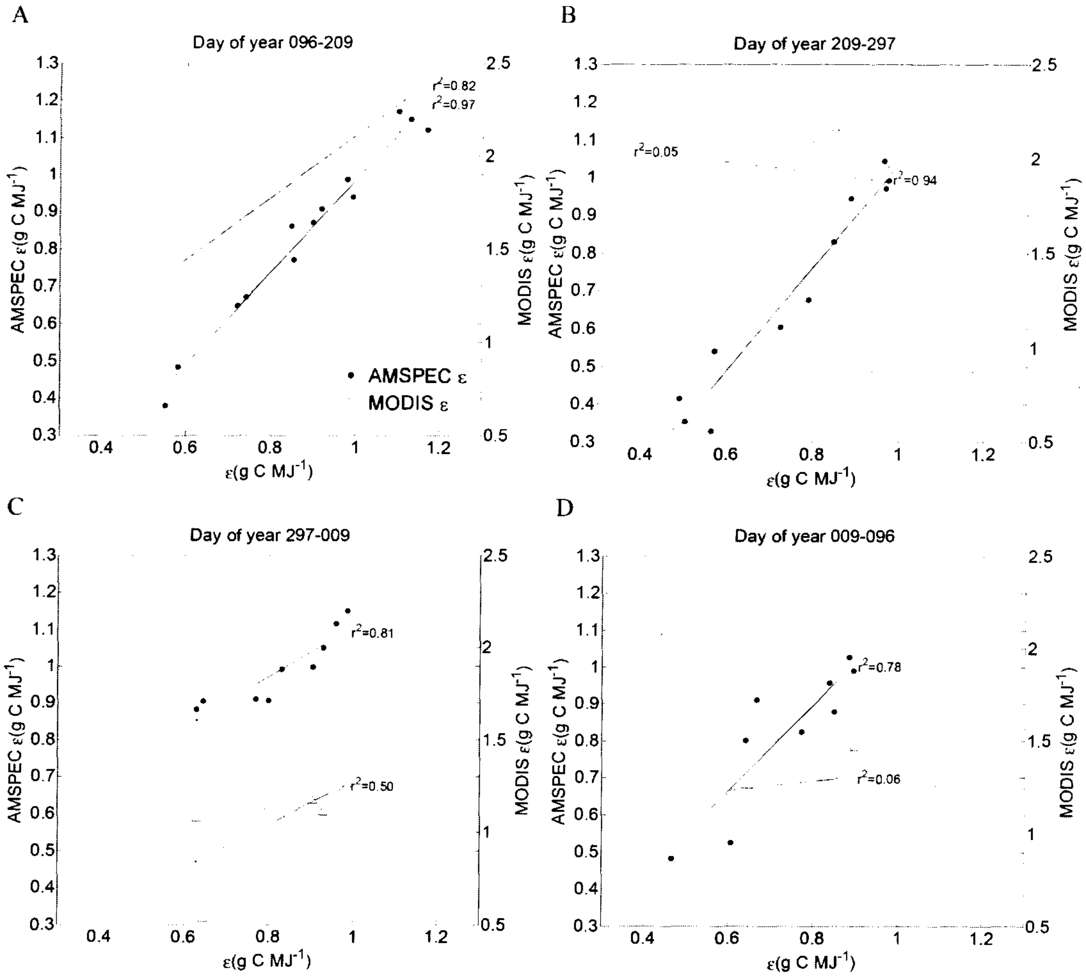

Figure 7.2 A-D: Eight-day averaged eddy covariance determined ε plotted against ε_{MODIS} derived from S_{TMin} and S_D and radiometer measured ε using PRI. The relationship between ε and ε_{MODIS} is highly significant ($p < 0.05$) during the beginning of the summer (A), while it is insignificant during late summer (B). Likewise, the fall and early winter period shows a significant relationship at ($p <$ 0.05) (C), while ε_{MODIS} fails to describe ε during the late winter and spring period (*D*). Remotely-sensed ε measured from spectral reflectance shows a high correlation to ε_{EC} throughout the year ($p<0.05$).

Figure 7.2A-D shows the correlation between ε_{EC} and ε_{MODIS}, and ε_{EC} and ε_{RS} during the early summer, late summer, winter and early spring. During early summer, when canopy drought stress is moderate, ε_{EC}, is highly correlated to both ε_{MODIS} (r^2 = 0.82 p < 0.05), and ε_{RS} (rr^2 = 0.97, p < 0.05). During the late summer months (DOY 209-297), when θ_{30} was below 20%, the relationship between ε and ε_{MODIS} is non-significant at $p < 0.05$, while ε_{EC} is still strongly correlated to remotely-sensed data ($r^2 = 0.94$, $p < 0.05$). Figures 7.2C and 7.2D show the winter and early spring periods, respectively (DOY 297-009 and DOY 009-96). While during winter, the relationship between ε_{EC} and ε_{MODIS} is significant ($r^2 = 0.50$, $p < 0.05$) the MODIS modifiers fail to describe ε_{EC} during the early spring period (DOY 009-96). The relationship between ε_{EC} and ε_{RS} is highly significant during both of these observation periods with r^2 being 0.82 and 0.78 ($p < 0.05$), respectively.

Figure 7.3 shows the spatial variability of ε_{RS} within the AMSPEC-footprint as yearly averaged values. The x and y coordinates are showing the distance from the tower in meters, while the z axis illustrates the yearly averaged ε_{RS} value as calculated from standardized BRDF observations (June 21 solar noon, looking north at a vertical zenith angle of 62°). Light-use efficiency was, on average lowest at an azimuth of about 20° measured from geodetic north (0.8 g CMJ^{-1}). Highest ε values were found south and south-east of the tower (azimuth about 200°) with the canopy facing north and north-west (1.4 g CMJ^{-1}).

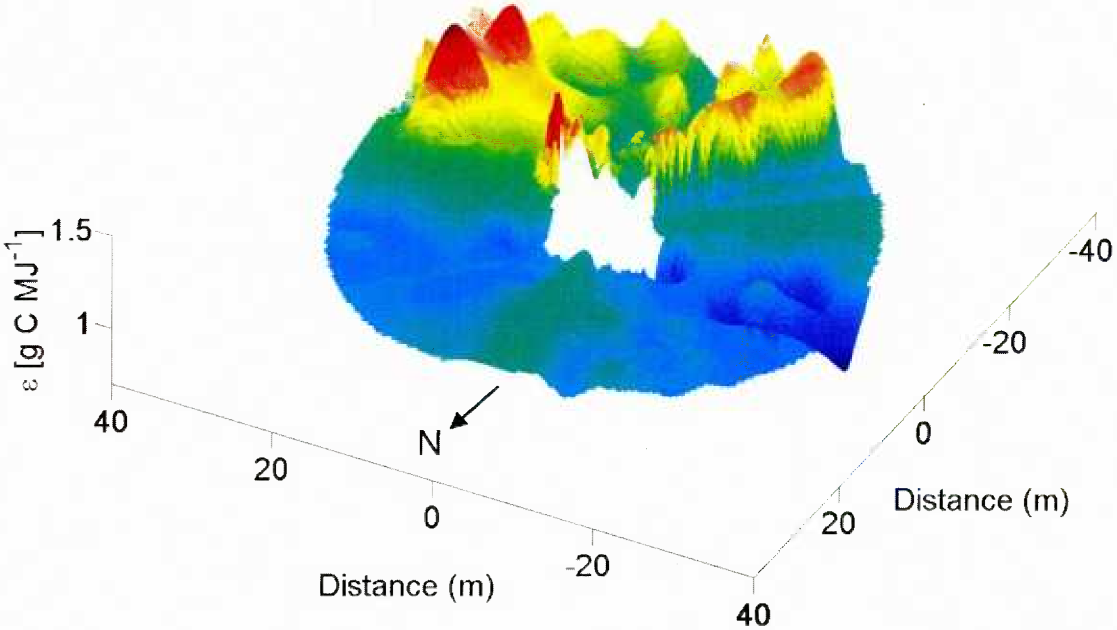

Figure 7.3: Spatial variability of ε assessed from AMSPEC. ε-values are lowest at the north site with the observed canopy facing south, while generally higher values are achieved south of the tower with the observed canopy facing north. Local differences between two adjacent angles are a result of tree species composition and health status.

7.4 Discussion and Conclusions

The comparison of the MODIS temperature modifier to T_{Air} and T_{soil} showed high correlations, with eight-day patterns in T_{Air} and T_{soil} being well described by S_{Tmin}. A similar result was also reported by Turner et al. (2006), finding good correlations between S_{Tmin} and temperature related reductions in photosynthesis at a boreal forest site. In contrast, the relationship between S_D and alternative moisture related stress indicators was much weaker (Figure 7.1B). For example, the significant decrease in θ_{30} towards the end of the summer (DOY 216-296) was not as well described by S_D as by D, most likely due to increasing temperatures (Figure 7.1A) and decreasing solar irradiance after summer solstice. This is especially important as drought related canopy stress is expected to show an additional time lag of several days following θ_{30} due to transport and storage of water in plants (Grant et al., 2006). Schwalm et al. (2006) and Chapter 3 found λE to be an important indicator of soil moisture related stress; however, changes in λE have almost no effect on S_D and as a result, S_D fails to describe evaporation and tree water use. Consequently, little agreement was found between ε_{MODIS} and ε_{EC} during some parts of the year; however, highly significant relationships were observed during other times of the year, when photosynthesis was largely driven by changes in temperature (DOY 96-209 and DOY 297-009, Figure 7.2). Similar results were reported by Running et al. (2004), Heinsch et al. (2006) and Nightingale et al. (2007), who found that photosynthesis is not sufficiently constrained by S_D during dry periods. Also, Plummer (2006) found that ε_{MODIS} describes well during non-stress periods, but fails to account for photosynthetic down-regulation when the canopy is stressed, which can be confirmed by this study. ε_{MODIS} overestimated ε_{EC} by around 30% throughout the year (Figure 7.2 and 7.3). A similar result was found by Heinsch et al. (2006) reporting an overestimation of between 20-30% for various flux tower sites in North America. For other sites however, MODIS was found to underestimate ε and GPP (Turner et al., 2003).

In contrast to the poor estimates of ε using the two MODIS modifiers, eight-day averages of ε_{RS} were able to predict ε_{EC} during the entire study period with the strongest relationships found in the early summer (Figure 7.2A-D). This result confirms the findings of Chapter 5 and Hall et al. (2008), who found that PRI was a powerful indicator of stand level ε throughout the year. These findings suggest that global estimates of ε can be improved if measured directly using a remote sensing technique (Hall et al., 2008). AMSPEC slightly underestimates ε_{EC} throughout the year, due to the logarithmic transformation function used (Chapters 5, 6).

The spatial variability of ε_{RS} as estimated from AMSPEC largely reflects leaf structural adaptations to the shading conditions within the canopy (Chapter 3). Although immediate directional reflectance effects resulting from the sun-observer geometry were eliminated using BRDF, notable differences were still found in canopy reflectance corresponding the viewing angles of AMSPEC. The north-facing part of the canopy experiences, on average, a much lower level of incident PAR and, as a result, will show higher levels of ε than the south facing part, because sunlit parts of the canopy are more likely to be exposed to excessive light levels (Demmig-Adams and Adams, 1998). This result is confirmed by Chapter 3 reporting mutual crown shading to be an important factor in canopy-level ε. Another possible factor contributing to the spatial variability in ε is the pigment pool size, defined as the ratio of carotenoids to chlorophyll pigment concentrations, which affects both, photosynthesis and PRI reflectance (Barton and North, 2001). Although these directional differences may be relatively spatially constant within a homogenous forest stands, thus being somewhat accounted for by a spatially averaged estimate of water vapor pressure deficit (which also depends on solar irradiance), the coarse spatial resolution of S_D and S_{Tmin} does not account for differences in ε related to stand age and canopy structure (such as canopy crown closure), both of which have an impact on mutual canopy shading (Chapter 3) and thus ε. Spatial resolution is therefore a crucial factor in current efforts seeking to improve global level estimates of photosynthetic light-use efficiency. Directly estimates of ε using remote sensing revealed a constantly more significant relationship to ε_{EC} than indirect estimates using climate data and may therefore help improving global modeling of GPP.

7.5 References

Barton CVM, North PRJ (2001) Remote Sensing of Canopy Light-Use Efficiency Using the Photochemical Reflectance Index: Model and Sensitivity analysis. *Remote Sensing of Environment* **78**, 264-273.

Buck, A. L. (1981) New equations for Computing Vapor Pressure and Enhancement Factor, *J. Appl. Meteorol.* **20**: 1527-1532.

Chen, J. (1996) Evaluation of Vegetation Indices and a Modified Simple Ratio for Boreal Applications. *Canadian Journal of Remote Sensing* **22**, 229-242.

Chen, J. and Black, T. (1991) Measuring Leaf Area Index of Plant Canopies with Branch Architecture. *Agricultural and Forest Meteorology* **57**, 1-12.

Coops, N.C., Black, T.A., Jassal, R.P.S., Trofymow, J.A.T. and Morgenstern, K. (2007) Comparison of MODIS, Eddy Covariance Determined and Physiologically Modelled Gross Primary Production (GPP) in a Douglas-Fir Forest Stand. *Remote Sensing of Environment* **107**, 385-401.

Demmig-Adams, B. 1998. Survey of Thermal Energy Dissipation and Pigment Composition in Sun and Shade Leaves. *Plant and Cell Physiology* **39**, 474-482.

Gamon JA, Filella I, Peñuelas J (1993) The Dynamic 531-Nanometer Reflectance Signal: A Survey of Twenty Angiosperm Species. Yamamoto HY , Smith CM (Eds). Photosynthetic Responses to the Environment. *American Society of Plant Physiologists*, Rockville. pp. 172-177.

Gamon, J.A., Peñuelas, J. and Field, C.B. (1992) A Narrow-Waveband Spectral Index That Tracks Diurnal Changes in Photosynthetic Efficiency. *Remote Sensing of Environment* **41**, 35-44.

Goetz, S.J. and Prince, S.D. (1996) Remote Sensing of Net Primary Production in Boreal Forest Stands. *Agricultural and Forest Meteorology* **78**, 149-179.

Grant, R.F., Zhang, Y., Yuan, F., Wang, S., Hanson, P.J., Gaumont-Guay, D., Chen, J., Black, T.A., Barr, A., Baldocchi, D.D. and Arain, A. (2006) Intercomparison of Techniques to Model Water Stress Effects on CO_2 and Energy Exchange in Temperate and Boreal Deciduous Forests. *Ecological Modelling* **196**, 289-312.

Hall, F.G., Hilker, T., Coops, N.C., Lyapustin, A., Huemmrich, K.F., Middleton, E.M., Drolet, G.G., Margolis, H.A., Black, T.A. (2008) Can Light-Saturated Reductions in Canopy Photosynthetic Capacity Be Observed From Space? *Remote Sensing of Environment*, accepted

Heinsch, F.A., M. Reeves, C.F. Bowker, P. Votava, S. Kang and C. Milesi (2003) User's Guide: GPP and NPP (MOD17A2/A3) Products. NASA MODIS Land Algorithm. Version 2.0. Available Online at: http://www.ntsg.umt.edu/modis/MOD17UsersGuide.pdf. Accessed 11/2007.

Heinsch, F.A., Zhao, M.S., Running, S.W., Kimball, J.S., Nemani, R.R., Davis, K.J., Bolstad, P.V., Cook, B.D., Desai, A.R., Ricciuto, D.M., Law, B.E., Oechel, W.C., Kwon, H., Luo, H.Y., Wofsy, S.C., Dunn, A.L., Munger, J.W., Baldocchi, D.D., Xu, L.K., Hollinger, D.Y., Richardson, A.D., Stoy, P.C., Siqueira, M.B.S., Monson, R.K., Burns, S.P. and Flanagan, L.B. (2006) Evaluation of Remote Sensing Based Terrestrial Productivity From MODIS Using Regional Tower Eddy Flux Network Observations. *IEEE-Transactions on Geoscience and Remote Sensing* **44**, 1908-1925.

Holmgren, J., Nilsson, M. and Olsson, H. (2003) Simulating the Effects of LiDAR Scanning Angle for Estimation of Mean Tree Height and Canopy Closure. *Canadian Journal of Remote Sensing* **29**, 623-632.

Humphreys, E.R., Black, T.A., Morgenstern, K., Cai, T.B., Drewitt, G.B., Nesic, Z. and Trofymow, J.A. (2006) Carbon Dioxide Fluxes in Coastal Douglas-Fir Stands at Different Stages of Development After Clearcut Harvesting. *Agricultural and Forest Meteorology* **140**, 6-22.

Hyde, P., Nelson, R., Kimes, D. and Levine, E. (2007) Exploring LiDAR-Radar Synergy - Predicting Aboveground Biomass in a Southwestern Ponderosa Pine Forest Using LiDAR, SAR and INSAR. *Remote Sensing of Environment* **106**, 28-38.

Jassal, R. S., Black, T.A., Cai, T.B., Morgenstern, K., Li, Z., Gaumont-Guay, D., Nesic, Z. (2007) Components of ecosystem respiration and an estimate of net primary productivity of an intermediate-aged Douglas-Fir stand. *Agricultural and Forest Meteorology* ***144***, 44-57

Landsberg, J.J. and Waring, R.H. (1997) A Generalised Model of Forest Productivity Using Simplified Concepts of Radiation-Use Efficiency, Carbon Balance and Partitioning. *Forest Ecology and Management* **95**, 209-228.

Monteith, J.L. (1972) Solar-Radiation and Productivity in Tropical Ecosystems. *Journal of Applied Ecology* **9**, 747-766.

Monteith, J.L. (1977) Climate and Efficiency of Crop Production in Britain. *Philosophical Transactions of the Royal Society of London Series B-Biological Sciences* **281**, 277-294.

Morgenstern, K., Black, T.A., Humphreys, E.R., Griffis, T.J., Drewitt, G.B., Cai, T.B., Nesic, Z., Spittlehouse, D.L. and Livingstone, N.J. (2004) Sensitivity and Uncertainty of the Carbon Balance of a Pacific Northwest Douglas-Fir Forest During an El-Niño La-Niña Cycle. *Agricultural and Forest Meteorology* **123**, 201-219.

Nightingale, J.M., Hill, M.J., Phinn, S.R. and Held, A.A. (2007) Comparison of Satellite-Derived Estimates of Gross Primary Production for Australian Old-Growth Tropical Rainforest. *Canadian Journal of Remote Sensing* **33**, 278-288.

Peñuelas, J., Filella, I. and Gamon, J.A. (1995) Assessment of Photosynthetic Radiation-Use Efficiency With Spectral Reflectance. *New Phytologist* **131**, 291-296.

Prince, S. and Goward, S. (1995) Global Primary Production: A Remote Sensing Approach. *Journal of Biogeography* **22**, 815-835.

Running, S.W., Nemani, R.R., Heinsch, F.A., Zhao, M.S., Reeves, M. and Hashimoto, H. (2004) A Continuous Satellite-Derived Measure of Global Terrestrial Primary Production. *Bioscience* **54**, 547-560.

Running, S.W., Queen, L. and Thornton, M. (2000) The Earth Observing System and Forest Management. *Journal of Forestry* **98**, 29-31.

Schwalm, C.R., Black, T.A., Arniro, B.D., Arain, M.A., Barr, A.G., Bourque, C.P.A., Dunn, A.L., Flanagan, L.B., Giasson, M.A., Lafleur, P.M., Margolis, H.A., Mccaughey, J.H., Orchansky, A.L. and Wofsy, S.C. (2006) Photosynthetic Light-use efficiency of Three Biomes Across an East-West Continental-Scale Transect in Canada. *Agricultural and Forest Meteorology* **140**, 269-286.

Thomas, V., Treitz, P., Mccaughey, J.H. and Morrison, I. (2006) Mapping Stand-Level Forest Biophysical Variables for a Mixedwood Boreal Forest Using LiDAR: An Examination of Scanning Density. *Canadian Journal of Forest Research-Revue Canadienne De Recherche Forestiere* **36**, 34-47.

Turner, D.P., Ollinger, S., Smith, M.-L., Krankina, O. and Gregory, M. (2004) Scaling net primary production to a MODIS footprint in support of Earth observing system product validation. *International Journal of Remote Sensing* **25**, 1961-1979.

Turner, D.P., Ritts, W.D., Cohen, W.B., Maeirsperger, T.K., Gower, S.T., Kirschbaum, A.A., Running, S.W., Zhao, M.S., Wofsy, S.C., Dunn, A.L., Law, B.E., Campbell, J.L., Oechel, W.C., Kwon, H.J., Meyers, T.P., Small, E.E., Kurc, S.A. and Gamon, J.A. (2005) Site-Level Evaluation of Satellite-Based Global Terrestrial Gross Primary Production and Net Primary Production Monitoring. *Global Change Biology* **11**, 666-684.

Turner, D.P., Ritts, W.D., Zhao, M.S., Kurc, S.A., Dunn, A.L., Wofsy, S.C., Small, E.E. and Running, S.W. (2006) Assessing Interannual Variation in MODIS-Based Estimates of Gross Primary Production. *IEEE-Transactions on Geoscience and Remote Sensing* **44**, 1899-1907.

Turner, D.P., Urbanski, S., Bremer, D., Wofsy, S.C., Meyers, T., Gower, S.T. and Gregory, M. (2003) A Cross-Biome Comparison of Daily Light-use efficiency for Gross Primary Production. *Global Change Biology* **9**, 383-395.

Wagner, W., Ullrich, A., Ducic, V., Melzer, T. and Studnicka, N. (2006) Gaussian Decomposition and Calibration of a Novel Small-Footprint Full-Waveform Digitising Airborne Laser Scanner. *ISPRS Journal of Photogrammetry and Remote Sensing* **60**, 100-112.

Yuan, W.P., Liu, S., Zhou, G.S., Zhou, G.Y., Tieszen, L.L., Baldocchi, D., Bernhofer, C., Gholz, H., Goldstein, A.H., Goulden, M.L., Hollinger, D.Y., Hu, Y., Law, B.E., Stoy, P.C., Vesala, T. and Wofsy, S.C. (2007) Deriving a Light-use efficiency Model From Eddy Covariance Flux Data for Predicting Daily Gross Primary Production Across Biomes. *Agricultural and Forest Meteorology* **143**, 189-207.

Zhao, M., Running, S.W. and Nemani, R.R. (2006) Sensitivity of Moderate Resolution Imaging Spectroradiometer (MODIS) Terrestrial Primary Production to the Accuracy of Meteorological Reanalyses. *Journal of Geophysical Research-Biogeosciences* **111**, (G1): Art. No. G01002

8 CONCLUSIONS

This work investigated the potential of using PRI reflectance to sense photosynthetic light-use efficiency (ε) over a one-year period at the stand level from multi-angular tower-based reflectance measurements of a Douglas-fir (*Pseudotsuga menziesii* var *menziesii* (Mirb.) Franco) dominated forest stand, with the aim of modeling stand and landscape level GPP from spectral reflectance.

Remote sensing of GPP, often expressed as a product of globally inferred estimates of PAR, f_{par} and ε (Monteith 1972, 1977), holds promise to significantly improve our understanding of global carbon cycling thereby allowing the study of interactions between changes in CO_2 levels and the terrestrial biosphere (Chapter 2). While our ability to estimate PAR and f_{par} using satellite remote sensing has increased significantly over the last few decades, global determination of ε is difficult. From the reviewed literature, it becomes apparent that direct measurements of ε using an empirical relationship to PRI can help overcome some of the issues existing with indirect approaches that estimate ε from globally-measured meteorological variables (Chapter 2, Chapter 6). Up-scaling the PRI-ε relationship to landscape and global levels, however, requires comprehensive understanding of the spatial and temporal contributions altering spectral reflectance in the PRI wavebands at the leaf, stand, and landscape scales (Nichol et al., 2000, Zarco-Tejada et al., 2001). One of the most important requirements for remote sensing of ε in a spatially and temporally continuous mode is the separation of physiologically and directionally induced changes in PRI reflectance (Chapter 5). This analysis requires not only a comprehensive understanding of plant physiological processes, but also knowledge about canopy structure and canopy radiation regime (Chapter 5). Stand-level data play a key role in this regard as they facilitate detailed studies of many of the factors that alter satellite-observed reflectance using comprehensive ground and tower-based measurements. Importantly, stand-level spectral observations can directly be related to tower-based eddy covariance measurements (Chapter 4) and as a result, physiologically induced changes in canopy reflectance can be identified by combining spectral observations with the understanding of stand-level physiology obtained from EC measurements (Chapter 5).

Regression tree analysis showed that in the temporal domain, sensible (H) and latent heat fluxes (λE), vapour pressure deficit (D), longwave radiation ($L\downarrow$) and the state of cloudiness (Q), altering downwelling PAR, played a significant role in downregulating photosynthesis at the research site (Chapter 3). In the spatial domain, this study was among the first to document the importance of mutual canopy shading (σ_c) for modeling variations in stand level ε (Chapters 3, 5 and 6) LiDAR data were successfully used to model the canopy structure (Coops et al., 2007, Chapter 6). The LiDAR-derived canopy-hillshade approach was able to describe shading within the tree canopy with a high level of detail (Chapter 3). An additional finding of Chapter 3 is that the relative contribution of individual factors downregulating photosynthesis changes with the time scale of observation (i.e. half hourly, daily or weekly observations).

In order to facilitate investigations of the interactions between spatial and temporal changes in stand-level ε and canopy reflectance, AMSPEC, a high spectral, spatial and temporal resolution radiometer platform was developed and installed at the research site

(Chapter 4). The system proved suitable for unattended, high-frequency measurements of canopy reflectance, allowing observations of the entire canopy around the tower every 15 minutes to track diurnal and seasonal variations of plant physiological processes under various weather and illumination conditions. Additionally, the motor-driven probe allowed observations of canopy spectra under different view and sun-angles thereby facilitating the observation of spatial differences in PRI (Chapter 5, Hall et al., 2008). Over a one-year period, AMSPEC generated a unique dataset consisting of over 4 million multi-angular spectral observations which allowed studying the interactions between stand level reflectance and ε with a high level of detail (Chapters 5 and 6). The novel approach introduced in Chapter 5 successfully isolated physiologically induced changes in canopy reflectance for the first time by stratifying observations into homogenous classes with respect to the physiological plant status (ε) and state of cloudiness (Q) with separate BRDF models being fitted to each strata. Importantly, this approach managed to significantly enhance the PRI-ε relationship throughout the one-year observation period. These are key findings of this dissertation as they allowed changes in ε to be continuously tracked at the stand level for the first time and with high accuracy (Figure 5.8).

A unique finding of this study is that not only PRI, but also photosynthetic downregulation itself was dependent on the view-observer geometry, as sunlit regions of the canopy were more often exposed to excess light levels than shaded parts (Chapter 5). This result is consistent with the findings of Chapter 3, and confirms mutual shadowing as a major factor driving canopy-level ε (Chapter 5, Hall et al., 2008). Importantly, this study has also demonstrated that a multi-angular radiometer setup is able to detect these shadow-dependent changes in canopy-level ε (Chapters 5 and 6, Middleton et al., 2008), since directionally-corrected PRI measurements still exhibited different values for sunlit and shaded canopy parts (Figure 6.5). This allowed us to determine ε separately for entirely sunlit and shaded canopy elements by modeling the BRDF of PRI reflectance with the PRI hotspot representing ε for a 0% shaded canopy and the PRI darkspot representing ε at 100% shading (Chapter 6). These are unique and important results of this dissertation, as they facilitate modeling of bulk canopy ε and GPP from top-of-canopy remote sensing by describing the within-canopy radiation regime using vertical foliage profiles derived from LiDAR.

LiDAR data were also successfully used to extrapolate spectrally derived predictions of sunlit and shaded ε horizontally throughout the landscape by modeling the distribution of sunlit and shaded canopy elements within a 12 km^2 study area (Chapter 6). The high correlation between remotely-sensed bulk-canopy GPP and estimates of GPP obtained from EC measurements in combination with a flux-footprint model underlined the potential of remote sensing to accurately measure stand level GPP continuously throughout the year (Chapter 6). The combination of EC measurements with tower-based remote sensing data therefore provide a means for up-scaling stand based findings to the landscape level where they can be directly compared to satellite-based observations (Chapters 6 and 7). Approaches like the one demonstrated in this study should therefore be helpful in future efforts seeking to validate satellite-derived estimates of GPP from tower-based reflectance.

Comparison between directly and indirectly derived values of ε shows that direct measurements of ε using PRI yields more accurate results of GPP than those modeling ε from vegetation stresses (Chapter 7). These findings underline the results found in Chapters 2 and 3, and suggest that during certain times of the year ε was driven by stress factors other than vapour pressure deficit and air temperature. However, another possible interpretation is that the same stresses did not automatically yield the same response in canopy-level ε (for instance, early- and late-summer period). As a result, further investigation will be required to assess the impact of single stress factors on ε throughout the year. A possible way to achieve this is to use other, stress related spectral indices, such as the plant water related indices Water Band Index, (WBI; Peñuelas et al., 1994, 1997) and investigate its relationship to both MODIS ε modifiers and the actual ε value derived from either EC or spectral measurements.

While this research has generated valuable insights to many of the scaling issues related to stand, landscape, and global level estimates of GPP from remotely-sensed inputs, further investigation is also required to confirm the existing findings across different biomes and vegetation types. Possible limitations may be faced especially in deciduous forests which show much more distinct phenological patterns during the year.

Separation of physiologically- and directionally-induced changes in canopy reflectance relies on EC and meteorological measurements to identify the physiological status of the plant canopy for modeling the BRDF of PRI reflectance. Remote sensing of ε using the approach described in this work will therefore still require flux-tower networks, however, tower-based radiometer observations combined with LiDAR provide a means by which stand level GPP can be extrapolated to the landscape level where it is easily comparable to satellite observations. Radiometer equipped flux-tower sites can then be used to calibrate satellite observations thereby facilitating up-scaling of spatially discrete spectra in a continuous mode across the landscape and the globe. While the relationship between PRI and ε has been confirmed over a wide range of species (Peñuelas et al., 1994, 1995, Filella et al., 1996, Gamon et al., 1997, Gamon and Surfus, 1999), its shape is likely to change as a function of species. Differences in the ε-PRI relationship, however, may be accounted for by identifying landcover classes for instance using a satellite-based landcover classification product and fitting different ε-PRI models for each of these classes. High spatial resolution land cover products are becoming increasingly available over large areas (Wulder et al, 2003, Homer et al., 2004, 2007) and may be helpful for future fine scale, global classification of vegetation cover. While LiDAR data are helpful for extrapolating information about the physiological status of the canopy, the limited availability of this data source at landscape and global scales can be a restriction to the approach demonstrated in here. Spatially continuous landscape level information of stand structure may, however, be obtained when combining transect based LiDAR samples with high spatial resolution satellite imagery, such as from Landsat or Quickbird satellites (Hudak et al., 2002, Hilker et al., 2008), thereby overcoming the need for providing full spatial LiDAR coverage.

A challenge for estimating ε globally from remotely-sensed inputs is the current lack of appropriate spaceborne narrow-waveband sensors with a sufficiently high spatial, spectral, and temporal resolution. EO-1 Hyperion was the first hyperspectral sensor in space with a contiguous spectral bandwidth of 10 nm and a spatial resolution of 30 m.

However, being designed as a demonstration instrument, this sensor was limited in its signal to noise ratio and calibration accuracy (Datt et al., 2003, Khurshid et al., 2006, White et al., 2007). While the Moderate Resolution Imaging Spectroradiometer (MODIS) on board NASA's spacecrafts Terra and Aqua features a 10 nm band in the 531 nm region (band 11) with daily global coverage, an appropriate reference band is missing at 570 nm; additionally, the spatial resolution of this band is likely too low to adequately describe ε in heterogeneous landscapes. As a result, a new generation of earth observing satellites will be required to obtain accurate estimates of ε globally from PRI reflectance.

While not being investigated in this thesis, chlorophyll fluorescence holds promise to also allow satellite-derived measures of ε (Bilger et al., 1990, Ananyev et al., 2005, Hall et al., 2008). As demonstrated in Chapter 2, the progress in existing remote-sensing instrumentation may likely overcome the restrictions currently faced in satellite-based predictions of fluorescence measurements in the near future (Chapter 2). Furthermore, a companion paper to Chapter 5, Hall et al. (2008) which also uses AMSPEC observations acquired at the DF49 site suggests that the fluorescence signal is visible by AMSPEC through a narrow waveband feature in the 705 nm region. Further investigation will be required to confirm these findings; however, fluorescence measurements can be a valuable addition to current efforts seeking global determination of ε from space thereby offering a second source of measurements which may be used for mutual validation of satellite-derived findings from PRI and fluorescence index.

The findings introduced in this thesis are an important step in current efforts seeking to up-scale the relationship between ε and PRI to landscape and global levels thereby trying to improve the accuracy of globally derived estimates of GPP. Based on the findings provided in this thesis, future studies will need to address differences in stand level PRI reflectance across biomes and specify the requirements for a potential future satellite designed to measure global-level photosynthesis from space.

8.1 References

Ananyev, G., Kolber, Z.S., Klimov, D., Falkowski, P.G., Berry, J.A., Rascher, U., Martin, R. and Osmond, B. (2005) Remote Sensing of Heterogeneity in Photosynthetic Efficiency, Electron Transport and Dissipation of Excess Light in Populus Deltoides Stands Under Ambient and Elevated CO_2 Concentrations, and in a Tropical Forest Canopy, Using a New Laser-Induced Fluorescence Transient Device. *Global Change Biology* **11**, 1195-1206.

Bilger, W. and Björkman, O. (1990) Role of the Xanthophyll Cycle in Photoprotection Elucidated by Measurements of Light-Induced Absorbency Changes, Fluorescence and Photosynthesis in Leaves of Hedera-Canariensis. *Photosynthesis Research* **25**, 173-185.

Coops, N.C., Hilker, T., Wulder, M.A., St-Onge, B., Newnham, G., Siggins, A. and Trofymow, J.A. (2007) Estimating Canopy Structure of Douglas-Fir Forest Stands From Discrete-Return LiDAR. *Trees-Structure and Function* **21**, 295-310.

Datt, B., Mcvicar, T.R., Van Niel, T.G., Jupp, D.L.B. and Pearlman, J.S. (2003) Preprocessing EO-1 Hyperion Hyperspectral Data to Support the Application of Agricultural Indexes. *IEEE-Transactions on Geoscience and Remote Sensing* **41**, 1246-1259.

Filella, I., Amaro, T., Araus, J.L. and Peñuelas, J. (1996) Relationship Between Photosynthetic Radiation-Use Efficiency of Barley Canopies and the Photochemical Reflectance Index (PRI). *Physiologia Plantarum* **96**, 211-216.

Gamon, J.A. and Surfus, J.S. (1999) Assessing Leaf Pigment Content and Activity With a Reflectometer. *New Phytologist* **143**, 105-117.

Gamon, J.A., Serrano, L. and Surfus, J.S. (1997) The Photochemical Reflectance Index: an Optical Indicator of Photosynthetic Radiation Use Efficiency Across Species, Functional Types, and Nutrient Levels. *Oecologia* **112**, 492-501.

Hall, F.G., Hilker, T., Coops, N.C., Lyapustin, A., Huemmrich, K.F., Middleton, E.M., Drolet, G.G., Margolis, H.A., Black, T.A. (2008) Can Light-Saturated Reductions in Canopy Photosynthetic Capacity Be Observed From Space? *Remote Sensing of Environment*, accepted

Hilker, T. Wulder, M.A., Coops, N.C. (2008) Update of Forest Inventory Data with LiDAR and High Spatial Resolution Satellite Imagery. *Canadian Journal of Remote Sensing*, in press

Hudak, A. T., Lefsky, M. A., Cohen, W. B., and Berterretche, M (2002) Integration of LiDAR and Landsat-TM Data for Estimating and Mapping Forest Canopy Height. *Remote Sensing of Environment* **82**, 397-416.

Homer, C., Dewitz, J., Fry, J., Coan, M., Hossain, N., Larson, C., Herold, N., McKerrow, A., Vandriel, J.N. and Wickham, J. (2007) Completion of the 2001 National Land Cover Database for the Conterminous United States. *Photogrammetric Engineering and Remote Sensing* **73**, 337-341.

Homer, C., Huang, C.Q., Yang, L.M., Wylie, B. and Coan, M. (2004) Development of a 2001 National Land-Cover Database for the United States. *Photogrammetric Engineering and Remote Sensing* **70**, 829-840.

Khurshid, K.S., Staenz, K., Sun, L.X., Neville, R., White, H.P., Bannari, A., Champagne, C.M. and Hitchcock, R. (2006) Preprocessing of EO-1 Hyperion Data. *Canadian Journal of Remote Sensing* **32**, 84-97.

Middleton, E.M., Cheng, Y.B., Hilker, T., Huemmrich, K.F., Black, T.A., Krishnan, P., Coops, N.C. (2008) Linking Canopy Level and MODIS Ecosystem Photosynthetic Light-Use Efficiency at a Douglas-Fir Forest in Canada, *Canadian Journal of Remote Sensing*, in prep.

Peñuelas, J., Filella, I. and Gamon, J.A. (1995) Assessment of Photosynthetic Radiation-Use Efficiency With Spectral Reflectance. *New Phytologist* **131**, 291-296.

Peñuelas, J., Gamon, J.A., Fredeen, A.L., Merino, J. and Field, C.B. (1994) Reflectance Indexes Associated With Physiological-Changes in Nitrogen-Limited and Water-Limited Sunflower Leaves. *Remote Sensing of Environment* **48**, 135-146.

Peñuelas, J., Gamon, J.A., Fredeen, A.L., Merino, J. and Field, C.B. (1994) Reflectance Indexes Associated With Physiological-Changes in Nitrogen-Limited and Water-Limited Sunflower Leaves. *Remote Sensing of Environment* **48**, 135-146.

Peñuelas, J., Pinol, J., Ogaya, R. and Filella, I. (1997) Estimation of Plant Water Concentration by the Reflectance Water Index WI (R900/R970). *International Journal of Remote Sensing* **18**, 2869-2875.

White, J.C., Coops, N.C., Hilker, T., Wulder, M.A. and Carroll, A.L. (2007) Detecting Mountain Pine Beetle Red Attack Damage With EO-1 Hyperion Moisture Indices. *International Journal of Remote Sensing* **28**, 2111-2121.

Wulder, M.A., Dechka, J.A., Gillis, M.A., Luther, J.E., Hall, R.J. and Beaudoin, A. (2003) Operational Mapping of the Land Cover of the Forested Area of Canada With Landsat Data: EOSD Land Cover Program. *Forestry Chronicle* **79** , 1075-1083.